Hydrodynamic Interactions between a Solitary Wave and a Partially Submerged Structure of Either a Thin Porous Wall or a 2-D Finite-Length Body with Attached Dual Porous Walls

A Dissertation

Presented to

the Faculty of the Department of Civil and Environmental Engineering

University of Houston

In Partial Fulfillment

of the Requirements for the Degree

Doctor of Philosophy

in Civil Engineering

by

Yan Miao

August 2017

Hydrodynamic Interactions between a Solitary Wave and a Partially Submerged Structure of Either a Thin Porous Wall or a 2-D Finite-Length Body with Attached Dual Porous Walls

Yan Miao

Approved:

Chair of the Committee
Keh-Han Wang, Professor,
Civil and Environmental Engineering

Committee Members:

Yi-Lung Mo, Professor,
Civil and Environmental Engineering

Arturo S. Leon, Associate Professor,
Civil and Environmental Engineering

Ali K. Kamrani, Associate Professor,
Industrial Engineering

Di Yang, Assistant Professor,
Mechanical Engineering

Suresh K. Khator, Associate Dean,
Cullen College of Engineering

Roberto Ballarini, Professor and Chair
Civil and Environmental Engineering

Acknowledgments

I would like to appreciate my advisor, Dr. K.H. Wang for his suggestions, support and guidance throughout, not only the research and the writing of my dissertation, but also my entire Ph.D study. I would like to express my gratitude to him for giving me the chance to start my Ph.D study in such an interesting and wonderful research area.

I would also like to thank Dr. Yi-Lung Mo, Dr. Arturo S. Leon, Dr. Ali K. Kamrani, and Dr. Di Yang for serving on my dissertation committee. I appreciate their time and suggestions on my dissertation.

I must thank the GAANN (Graduate Assistance in Areas of National Need) program and Dr. Abdeldjelil Belarbi for the financial support during my Ph.D study at UH.

I would like to express my gratitude to my colleagues, Dr. Ted Chu, Fong-Shu Jao, and Jassim Jaf for their support and assistance to carry out the experiments. I would also like to thank my other colleagues and friends who provided the encouragements and suggestions during my Ph.D studies.

Finally, I want to express my deepest gratitude to my family, especially my mom and little brother, who have provided constant encouragements, support, care and love, not only during my Ph.D studies but also my whole life.

Hydrodynamic Interactions between a Solitary Wave and a Partially Submerged Structure of Either a Thin Porous Wall or a 2-D Finite-Length Body with Attached Dual Porous Walls

An Abstract

of a

Dissertation

Presented to

the Faculty of the Department of Civil and Environmental Engineering

University of Houston

In Partial Fulfillment

of the Requirements for the Degree

Doctor of Philosophy

in Civil Engineering

by

Yan Miao

August 2017

Abstract

This dissertation presents the development of analytical models for the investigation of the hydrodynamic interactions between a solitary wave and either a partially submerged porous wall or a 2-D finite-length body with attached dual porous walls. Analytical solutions to describe the propagation of an incident wave and the associated reflected and transmitted waves after the interaction are derived by solving the governing equations. The solutions of reflection and transmission related unknown coefficients, as functions of wave number components and other physical parameters, are formulated by applying the matching conditions of the continuous velocities and velocity potentials at the interfaces of the fluid domains to evaluate the reflection and transmission of a solitary wave. The pressures according to the Bernoulli equation are calculated and the hydrodynamic forces are computed by integrating the pressure distributions on the structural surfaces.

A series of laboratory experiments were carried out to collect the free-surface elevations for the verification of the derived analytical solutions under various cases of interest. The comparisons of the incident, reflected and transmitted wave profiles predicted by the present analytical solutions with the experimental data and other published results are presented and discussed. It is demonstrated through result comparisons that the present analytical solutions for a given incident solitary wave can provide reliable predications on the time varying transmitted waves including wave peak and slightly overestimate the reflected wave height. For the topic of a partially submerged porous wall, the horizontal hydrodynamic forces from the present analytical solutions are found to agree reasonably

well with other published experimental data when a special case of non-porous wall is considered.

The physical parameters that affect the hydrodynamic forces on structures are investigated. More importantly, for the evaluation of the performance of the proposed partially submerged body systems, the parametric studies with results showing the effects of the incident wave height, submerged depth of porous structures, draft of 2-D partially submerged body, porous-effect parameter, and structural length on wave run-up, time variations of the free-surface elevations, and the overall reflection and transmission coefficients are presented and discussed.

Table of Contents

List of Figures

List of Tables

List of Symbols

A_j	Coefficient
b	2-D body draft
b_0^*, b_0	Dimensional and dimensionless material constant of porous wall
b_1, b_2	Dimensionless material constants of the attached dual porous walls
B_j	Coefficient
c^*, c	Dimensional and dimensionless phase velocity
c_0	Reference phase velocity
C	Coefficient
C_R	Overall reflection coefficient
C_T	Overall transmission coefficient
d^*, d	Dimensional and dimensionless submerged structural depth
D	Coefficient
F_x	Dimensionless horizontal hydrodynamic force
F_z	Dimensionless vertical hydrodynamic force
h^*, h	Dimensional and dimensionless water depth
H^*, H	Dimensional and dimensionless wave height
L	Structural length

k^*, k	Dimensional and dimensionless wave number
p^*, p	Dimensional and dimensionless hydrodynamic pressure
R_0, R_1	Reflection related coefficients
R_e	Constant of the fluid condition
t^*, t	Dimensional and dimensionless time
T_0, T_1	Transmission related coefficient
x^*, z^*	Dimensional coordinates in 2-D Cartesian system
x, z	Dimensionless coordinates in 2-D Cartesian system
x_1^*, x_1	Dimensional and dimensionless value of half of the length of the 2-D structure
α	Dimensionless wave amplitude
μ^*	Dimensional dynamic viscosity
ρ^*	Dimensional density
η^*, η	Dimensional and dimensionless free-surface elevation
ϕ^*, ϕ	Dimensional and dimensionless velocity potential
$\overline{\phi}$	Dimensionless depth-averaged velocity potential

Chapter 1 Introduction

1.1 Problem Statement

Water waves are one of the most common forms through which energy and materials are transmitted between oceans and continents in nature, and are usually caused by tectonic activities, wind, vessel movement, and so on. Enormous energy can be carried and transmitted from the ocean into shorelines or coastal/offshore structures by these water waves, especially high nonlinearity waves, and in extreme cases, tsunami like solitary waves. This phenomenon significantly influences the coastal and offshore protections and associated structural designs, as underestimating energy transmitted by water waves can cause severe damage to the protective areas. Studying the interactions between water waves and structures and the feasibility and effectiveness of the methods of reducing the impacts of the transmitted energy carried by water waves have become important aspects of the coastal and offshore engineering.

In the past decades, researchers have studied the characteristics of the interaction between water waves and structures through multiple approaches including numerical, analytical and experimental methods. Understanding the properties such as flow velocity, free-surface elevation, and pressure distribution during and after a water wave encounters a structure is essential for offshore and coastal structural design. When a water wave propagates through a structure, part of the wave are reflected back while the rest continues the process of wave transmission. By solving the velocity potential of the interested flow field, researchers can estimate the percentage of the energy the water wave transmitted after interacting with structure and understand the impact of this interaction.

Placing breakwaters is one of the most practical methods to reduce the impact of the energy of transmitted waves. Economically, a submerged breakwater can be a better choice, but its efficiency is generally less than a partially submerged breakwater, since the dynamic energy of a water wave concentrates near the water surface. Researchers have also observed that the energy can be dissipated when a water wave passes through a porous structure. Applying a partially submerged porous breakwater may become a practical way to effectively reduce the impact of the transmitted wave as well as keep the ecological harmony in that region by allowing the material passing through the porous breakwater and increasing the flushing capability.

Although many studies have been done to model the characteristics of interactions between water waves and structures, it is still a significant challenge for researchers to study the interaction between a nonlinear shallow-water wave, such as a solitary wave, and a partially submerged porous breakwater. Because of the nonlinear free surface boundary conditions of the water waves and the complex behavior of porous media, modeling a solitary wave interacting with a partially submerged porous structure becomes limited in both analytical and experimental approaches. It would be beneficial to develop a model to describe the behavior of the interactions between solitary waves and a partially submerged thin porous breakwater, especially for the purpose of analytically deriving the reflection and transmission coefficients and experimentally proving them.

Another challenging aspect of the interaction between a nonlinear shallow-water wave and a fixed partially submerged structure is that the effect of its thickness or structural length on the wave transformation in general cannot be ignored. Because of the inclusion of the structural dimension, the structure will introduce another velocity potential field underneath and vertically separate the flow regions. As a result, finding the practical approaches to solve the velocity potentials in the interested areas becomes much harder as accurately determining the velocity potential field underneath the structure becomes a challenging task, especially in coastal/offshore engineering applications. For instance, performing the analysis for the design of a ship or a bridge deck, the calculation of uplift forces generated by nonlinear waves, such as solitary waves, are critical. Reducing wave loads on those partially submerged structures is as important as reducing the wave transmission. A fixed dual porous-wall attached partially submerged body system may be a potential solution to this problem. Modeling the behaviors of such system will help engineers to develop more practical and effective methods to reduce the impact of transmitted waves and design the offshore and coastal structure properly.

In this study, coastal or offshore structures including either a partially submerged porous wall or a fixed dual porous-wall attached partially submerged body system are considered for the analytical and experimental investigations of their hydrodynamic performances in terms of wave reflection and transmission and induced wave loads after the interaction by an incident solitary wave. This study contains two major aspects.

(1) Modeling the hydrodynamic behavior of a solitary wave interacting with a partially submerged porous wall as a breakwater. An analytical approach is used to derive the reflection and transmission related unknown coefficients. With those two coefficients, the

velocity potentials and the wave elevations of the interested regions including both reflected and transmitted wave region can be obtained. The relationships between the effectiveness of reducing the impact of the transmitted solitary waves and the properties such as the ratio of the draft of the porous wall to the water depth and the porous property are investigated. Additionally, laboratory experiments were conducted to verify the analytical solutions.

(2) Investigating the interaction between a solitary wave and a fixed dual porous-wall attached partially submerged body system that combines a partially submerged 2-dimensional (2-D) structure of finite length and two vertically attached porous walls. This system could be used as an improved partially submerged breakwater system for reducing the impact of wave loads on the structure and the elevation level of the transmitted waves. Again, an analytical approach is carried out to determine the velocity potentials in all flow regions including that beneath the partially submerged structure and to evaluate the effectiveness of the two porous walls in reducing not only the impact of the incident wave but also the transmitted wave height by using the obtained wave elevations and wave forces. Experiments were also performed to verify the present analytical model. The relationships between variables, such as the body draft to water depth ratios, porous wall draft to water depth ratios, and the length of the partially submerged body, and the reflection and transmission coefficients are investigated based on the derived analytical solutions and measured data.

1.2 Literature Review

1.2.1 Nonlinear Shallow Water Wave

The study of nonlinear shallow water waves can be traced back to the observation of solitary wave. John Scott Russell (1838, 1845) discovered the “wave of translation” by observing the motion of a boat rapidly drawn along a narrow channel that was then suddenly stopped, after which a “large solitary elevation, a rounded, smooth and well-defined heap of water” was created and continued along the narrow channel without any significant changes of form and velocity for a certain distance before gradually diminishing. Following Russell’s laboratory experiments, researchers were eager to formulate the profile of such nonlinear shallow water waves. The development of the Korteweg and de Vries (KdV) equation by Korteweg and de Vries (1895) and the original depth-averaged Boussinesq equation by Boussinesq (1871) are two common pioneer formulations that were developed to describe nonlinear shallow water waves. These pioneer equations created a new path to discover the behavior of nonlinear shallow water waves.

In the past decades, an intense amount of studies were conducted to refine and expand the nonlinear shallow water wave theories. Zabusky and Kruskal (1965) discovered that with the numerical solution of the KdV equation, a solitary wave pulse propagating in a nonlinear dispersive media can be observed. However, the KdV equation assumes that the wave is unidirectional with negligible higher-order nonlinear disturbances. It can be used to describe cnoidal waves, which are the nonlinear periodic solutions to the KdV equation in terms of a Jacobian elliptic function. Friedrichs (1948) improved the study of high-order shallow water waves by considering the effects of perturbation, and Laitone (1960, 1962, 1965) proposed a second order solution for cnoidal waves and compared the results with

Stokes' higher order waves (De, 1955). Later, Isaacson (1977, 1978) modeled the incident velocity potential of cnoidal waves with a Fourier series and investigated the interactions between cnoidal waves and structures. His approximated nonlinear solutions were also compared with the results from linear wave theories and experimental measurements. In the end, since the key assumption of deriving the KdV equation is that the wave is unidirectional, the KdV equation is restricted to unidirectional waves or waves propagating in a predominant direction. On the other hand, the KdV equation is not able to model the cases of a nonlinear shallow water wave encountering a structure where a reflected wave is generated after the interaction process.

In contrast to the KdV equation, Boussinesq-class equations can be applied to describe the propagation of a nonlinear shallow water wave in multiple directions. The original Boussinesq equations (Boussinesq, 1871) were limited to horizontal bottom conditions. Later, Mei and LeMehaute (1966) and Peregrine (1967) expanded the set of Boussinesq equations to be applicable for variable depths to model shallow water waves. Because of the inaccurate representation of the frequency related dispersion of wave propagation in deep water, the standard Boussinesq equations (Peregrine, 1967) are only valid in shallow water. In order to improve the dispersion characteristics, a new set of Boussinesq equations with an additional third-order term were derived by Madsen (1991). The extended formulations was then tested to simulate the propagation of a nonlinear wave from deep water to shallow water. For intermediate water depth, Nwogu (1993) improved the linear dispersive properties of the long-wave model without adding higher order terms into the equation. Later, Liu (1994) and Wei et al. (1995) developed highly nonlinear Boussinesq-class equations to simulate highly nonlinear unsteady waves propagating from deep water to shallow water. Based on the research conducted by Nwogu (1993) and Wei and Kirby (1995), a high-order fully nonlinear Boussinesq model was developed by Gobbi et al. (2000).

In order to model a three-dimensional nonlinear shallow water wave with less limitations, Wu (1981) proposed a new set of Boussinesq-class equations, known as the generalized Boussinesq (gB) model, to determine the free-surface elevation and depth-averaged velocity potential. Since the gB model is based on the principles of mass and momentum conservation and expressed with depth averaged velocity potential, it is easier for the researchers to carry out 3-dimensional (3-D) wave simulation than the KdV equation. Later, Wu (2001) improved the theory by developing a model that can be applied to unsteady, fully nonlinear and dispersive 3-D waves within variable water depth in a single water layer. Thus, as the ability to model the propagation of nonlinear shallow-water waves has improved, researchers can continue the development of better perceptions and methods for studying the interactions between propagating nonlinear shallow-water waves and the different structures they come into encounter with.

1.2.2 Solitary Wave Interacting with Structures

In nature, solitary waves are translatory waves and usually contain tremendous energy. As a solitary wave propagates toward a structure, the impact caused by the interaction between the solitary wave and the structure can be substantial. An extreme case of the solitary wave is tsunami, which can result in the deaths of people living near the coastal regions and inflict severe damage to coastal and offshore structures. Understanding the impact of a solitary wave on structures is essential for coastal protection and offshore structure design. Over the past decades, the interaction between solitary waves and various types of structures has become an active topic in coastal and ocean engineering.

In the past decades, a significant amount of research has been conducted to study the interaction between water waves and structures. MacCamy and Fuchs (1954) presented one of the first analytical studies on wave diffraction on a cylinder. For partially submerged bodies, Mei and Black (1969) developed a numerical model to determine the wave transformation and forces related to waves interacting with rectangular structures. McCartney (1985) studied the performances of various types of floating breakwaters used in floating breakwater design. Later, Drimer et al. (1992), Williams et al. (2000) and Zheng et al. (2004) developed analytical models for linear waves propagating through different types of floating bodies. Others such as Murali and Mani (1997), Koutandos et al. (2005) and Dong et al. (2008) have conducted laboratory experiments to investigate the reflection and transmission characteristics and the effectiveness of different types of floating breakwaters. For submerged structures, Ursell (1947) started the study of the effect of a fixed vertical barrier on surface waves, and Dick and Brebner (1968) conducted experiments to test the performances of solid and permeable submerged breakwaters. Later, through analytical approaches, Abul-Azm (1993), Xie et al. (2011), Liu and Li (2012) and Liu et al. (2013) examined the performance of submerged breakwaters in reducing the transmitted wave energy. Beji and Battjes (1993), Stephan et al. (1994), and Losada et al. (1996) also conducted laboratory experiments to record the reflected and transmitted waves.

Most of researches mentioned above were conducted by using the linear waves or sinusoidal waves. As a result, there was significantly less focus on nonlinear waves, such as solitary waves, and their interactions with structures. For solitary waves, Goring (1978) started to look at the propagation of a tsunami that can be considered as an extreme case of a solitary wave. Another of the few people focusing on solitary waves interacting with structures at that time, Isaacson (1982) developed an integral equation method to solve the nonlinear diffraction problems regarding to the interaction between a solitary wave and a vertical cylinder. A year later, he presented an analytical solution using the Fourier integral approach and a linear diffraction solution to estimate the behavior of a solitary wave interacting with a solid vertical cylinder (Isaacson, 1983).

Other researchers have also focused on the studies of solitary waves interacting with cylindrical structures. Ohyama (1991) adopted a boundary element approach to estimate the resultant forces of a solitary wave on a vertical cylinder. In order to improve the results on the nonlinear effects such as scattering, Wang et al. (1992) proposed a generalized Boussinesq (gB) model to investigate the behavior of a solitary wave encountering a vertical cylinder. Later, an experimental study of the scattering of a solitary wave after interacting with a vertical cylinder was carried out by Yates and Wang (1994). Based on the gB model, Wang and Jiang (1994) presented a numerical method to model the interaction between solitary waves and cylinder arrays, and later cnoidal waves and multiple cylinders (Wang and Ren, 1994). To improve the accuracy to fully-nonlinear shallow water waves, a numerical model was developed by Zhong and Wang (2009). With this model, the behavior of a fully nonlinear wave interacting with cylindrical structures can be evaluated. Continuing Isaacson's (1983) work, Zhong and Wang (2006) investigated the behavior of a solitary wave interacting with a concentric porous cylinder system, and the Fourier integrals solutions of free surface elevations and velocity potentials were presented.

To study of the hydrodynamic interactions between a solitary wave and a vertical wall or plate, Power and Chwang (1984) used both analytical and numerical approaches to examine the reflection process of a planar solitary wave from an impermeable vertical wall. Sugimoto et al. (1987) adopted a matched-asymptotic expansion method to derive analytical solutions to estimate the behavior of the interaction between a solitary wave and a submerged thin plate. They presented a solution by separately solving the KdV equations of the incident, reflected and transmitted waves which may not perform well in term of wave transmission. Patarapanich and Cheong (1989) studied a solitary wave propagating through a submerged plate in terms of reflection and transmission coefficients to evaluate the effect of a submerged plate on the wave transmission. The wave scattering effect caused by a submerged disk was analyzed by Yu and Chwang (1993). The reflection of a solitary wave after impinging with a vertical wall was also studied by Wu et al. (1998). Later, Hu and Wang (2005) investigated the damping effect on solitary waves propagating though a submerged horizontal plate and a vertical porous wall. Recently, Jaf and Wang (2015), by combining Isaacson's (1983) and Zhong and Wang's (2006) researches, developed an analytical solution in terms of reflection and transmission related coefficients for the interaction between a solitary wave and a completely submerged impermeable breakwater. Their analytical solutions were found to agree fairly well with the experimental data.

When studying the reflection and transmission characteristics of the interaction between solitary waves and rectangular structures of finite length, the longitudinal dimension and submergence of the structure become critical variables to be included in the analysis. Considering tsunami-level solitary waves, Silva et al. (2000) used an inverse Fourier transformation to estimate the reflection and transmission coefficients of tsunami waves interacting with a surface-piercing permeable finite-thickness breakwater. Also, in terms of reflection, transmission and dissipation coefficients, Lin (2004) studied the characteristics of the interaction between solitary waves and rectangular structures with various heights and thicknesses. Later, Lin (2006) developed a 2-D numerical model to simulate the transformation of a solitary wave after encountering a 2-D body placed at various vertical locations, including completely submerged or partially submerged positions. Used an integrated experimental and numerical method, Wu et al. (2012) studied the interaction between a solitary wave and a bottom-mounted barrier and evaluated the reflection and transmission coefficients. Recently, Lu and Wang (2015) developed an integrated analytical and numerical model to simulate the interaction between a solitary wave and a fixed floating structure. The velocity potential of the region beneath the structure was evaluated analytically and the propagation of wave including incident, reflected and transmitted waves were evaluated numerically by solving the gB equations. Laboratory experiments were also conducted to verify their modeling results.

1.2.3 Water Wave Interacting with Porous Structure

Porous structures, such as porous breakwaters, are widely used in coastal and ocean engineering design consideration. It has been observed that when water wave propagates through a porous structure, parts of energy from both the reflected and transmitted waves are dissipated and the resultant forces on the structure are reduced. Because of this phenomena, researchers started to investigate the usage of porous structures in terms of reducing wave energy impacts and protecting coastal and offshore structures. However, the complexities of the behavior of porous structures and the flow passing through it are the major challenges hindering the investigation of using porous structures to solve water wave problems.

Starting with linear waves, Sollitt and Cross (1972) presented a solution of flow propagating through a finite-thickness porous breakwater, while Madsen (1974) analyzed the reflected and transmitted waves far away from the porous structures. Chwang (1983) developed a porous wavemaker theory to avoid the complexity of flow propagating though a porous media by applying Taylor's (1956) revised Darcy's flow concept of a porous screen. Later, following Chwang's (1983) work, Chwang and Li (1983) investigated a piston-type porous wavemaker and evaluated the interaction between surface waves and a porous screen. By neglecting the thickness of the structure, the problem of water waves interacting with a porous structure is simplified and the velocity inside the porous structure depends on the pressure difference across the structure. Extending Chwang's (1983) theory, Wang and Ren (1993) presented a study of water waves interacting with flexible porous breakwaters. The interaction between water waves and a floating porous breakwater on mooring lines connected to the structure was also investigated by Ren and Wang (1994). Using linear wave theory, Yu and Chwang (1994) studied the transformation of a water wave as it propagates thought a horizontally orientated submerged porous plate. Wang and Ren (1994) also derived analytical solutions to describe wave interactions with a concentric porous cylinder system. Later, William and Li (2000) developed a semi-analytical model for water wave interactions with a porous cylinder system. Recently, a new analytical solution to wave reflection and transmission caused by porous breakwaters was presented by Liu and Li (2013) to avoid difficult procedures of traditional numerical solutions. Although a considerable number of studies have been conducted on the interaction between water waves and porous structures, however, most of the research mentioned above focused on a linear periodic wave. The studies concerning the interaction between a nonlinear long wave, such as a solitary wave, and a porous structure have been very limited.

In terms of interaction between solitary wave and porous structures, Vidal et al. (1988) presented experimental data of solitary waves transmitted through a porous breakwater. The wave scattering caused by a submerged porous disk was investigated by Chwang and Wu (1994). Liu (1997) simulated solitary waves propagating through a finite-thickness porous breakwater with a model using the Runge-Kutta integration method. Also, Li (1999) and Lynett et al. (2000) developed numerical solvers to model solitary waves propagating through a porous breakwater. Wu et al. (1998) considered a structure system composed of a vertical end wall and a submerged horizontal porous plate and studied the wave reflection caused by this structural system. Considering the wave height reducing effect on long waves, Hu and Wang (2005) proposed a structural system composed of a submerged horizontal plate and a vertical porous wall and investigated the performance of the breakwater system analytically. Zhong and Wang (2006) investigated the interaction between solitary waves and a concentric porous cylinder system by following Isaacson's (1983) and Wang and Ren's (1994) work. Recently, Wu et al. (2014) developed a 3-D numerical model to simulate the interaction between a solitary wave and a porous breakwater.

Based on the literature review mentioned above, studies involving the interactions between a solitary wave and either a partially submerged porous structure, especially a thin structure, or a partially submerged 2-D body with attached porous walls have been extremely limited. Most of the research proposed numerical methods to solve the complex behavior of the solitary wave propagating through a porous media. The experimental data necessary to validate those models are also limited. In the present study, analytical solutions are developed to investigate the performance of a partially submerged porous barrier subject to an encountering of an incident solitary wave. Theoretical solutions for a solitary wave interacting with a fixed floating structure with attached two porous walls are also derived. Additionally, a series of experimental measurements were carried out to verify the derived analytical solutions.

1.3 Dissertation Outline

This study is composed of two topics. The first topic focuses on the study of the interactions between a solitary wave and a partially submerged porous wall by analytically deriving the solutions of velocity potentials and wave elevations in terms of reflection and transmission related coefficients, while also conducting laboratory experiments to make direct measurements of reflected and transmitted wave elevations for such interactions. The experimental measurements are used for the validations of the derived analytical solutions. Instead of a single thin porous structure, the second part of this research extends the analytical and experimental approaches to investigate a solitary wave interacting with a more complex partially submerged breakwater or an offshore floater that consists of a 2-D finite-length body with attached dual porous walls. Solutions of the velocity potentials and wave elevations in the flow regions outside and underneath of the body are analytically derived. The reflection and transmission associated wave elevations and coefficients are derived and compared with the experimental measurements. The aims of this study is to not only develop analytical solutions for solving the hydrodynamic problems of a solitary wave interacting with these two types of structures but also provide experimental data through laboratory tests to verify the developed solutions or predictive models in terms of the wave reflection and transmission during the interaction process. Furthermore, based on the analytical solutions, the parametric studies are conducted to evaluate the effects of physical parameters on the reflection and transmission of a solitary wave while interacting with the two partially submerged structures described above. Hydrodynamic forces on these structures are also examined.

Chapter 1 includes the problem statement, literature review and the outline of the dissertation. Chapter 2 presents the analytical model of the interaction between a solitary wave and a partially submerged porous wall. The analytical solutions for the velocity potentials of the interested flow fields are derived based on the combined Fourier integral and solution superposition method proposed by Isaacson (1983) and Zhong and Wang (2006). The porous effect is included by using the Darcy's law where Chwang's (1983) porous wavemaker theory and Zhong and Wang's (2006) work are followed for formulations of boundary conditions. The unknown coefficients related to the reflected and transmitted waves are derived by applying the least squares method (Sneddon, 1966; Dalrymple and Martin, 1990) to the mixed boundary condition. By substituting the derived coefficients back to the equations of velocity potentials and free-surface elevations in both regions, the water surface profiles for both reflected and transmitted waves and their corresponding velocity potentials can be determined. Using the nonlinear Bernoulli equation, the pressure can be calculated and the hydrodynamic forces acting on the porous wall can be estimated by integrating the pressure distribution on the wall surfaces.

To extend the study to a more complex partially submerged body system, Chapter 3 presents the analytical model for describing the interaction between a solitary wave and a 2-D finite length body with attached dual porous walls. The analytical solutions of the velocity potentials outside of the 2-D body are similar to those given in Chapter 2 and for the flow domain underneath the partially submerged body, the velocity potential is derived by solving the Laplace equation with the specified boundary (or matching) conditions at the interfaces. By applying the matching conditions and the orthogonality property of solution based eigenfunctions at the interfaces of the inner and outer domains, the unknown coefficients can be derived. Similar formulations as shown in Chapter 2 can be used to obtain the free-surface elevations and the hydrodynamic forces on the partially submerged body system.

In order to verify the analytical solutions presented in Chapter 2 and Chapter 3, a series of laboratory experiments were conducted to collect the free-surface elevations at locations of upstream (for incident and reflected waves) and downstream (for transmitted waves) of a partially submerged structure mentioned above under various conditions. The setups of experiments including the wave tank, partially submerged body systems, wave gauges and the parameters like the incident wave heights, porous wall conditions and 2-D body conditions are summarized in Chapter 4.

Chapter 5 presents the results of the derived analytical solutions for various cases of solitary waves interacting with a partially submerged porous wall. First, the comparisons between analytical solutions and experimental data on the time-variations of the free-surface elevations are carried out to verify the analytical solutions. Then, the parametric studies of the effects of incident wave height, depth (draft) of a submerged porous wall, porous-effect parameter on the physical variables of the wave run-ups on the porous wall, time-variations of the free-surface elevation, and the overall transmission coefficients are presented in this chapter. Furthermore, the induced hydrodynamic forces under different cases of varying incident wave height, submerged depth, and porous property of the wall structure are examined.

Similarly, Chapter 6 presents the results of hydrodynamic interaction between a solitary wave and a partially submerged body system that consists of a partially submerged 2-D rectangular structure with two attached porous walls. Experimental data collected in the present wavetank tests and those of special cases from Lu and Wang's (2015) work are used to verify the derived analytical solutions given in Chapter 3. The effects of various parameters, such as incident wave height, draft of 2-D body, property of porous walls, and structural length on the reflection and transmission of the incident wave are examined. Results of the wave run-up on the front face of the partially submerged body system, the horizontal forces, and the vertical forces acting on the bottom of the 2-D body are also presented and discussed in this chapter.

Finally, in Chapter 7, the key results and conclusions of this study are summarized and the future studies on the extension of the present study are also presented.

Chapter 2 Analytical Model of Interactions between a Solitary Wave and a Partially Submerged Porous Wall

In this study, the velocity potentials of the interested field for a solitary wave interacting with a partially submerged porous wall (barrier) is derived analytically based on the Fourier integral method proposed by Isaacson (1983) and Zhong and Wang (2006). The porous effect included in the wall boundary conditions follows Chwang's (1983) formulation that was based on the Darcy's law. Also, the least squares minimization procedure (Sneddon, 1966; Dalrymple and Martin, 1990; Jassim and Wang, 2015) is applied for the mixed matching conditions defined at the wall location to determine the unknown coefficients. A schematic diagram showing the problem statement is given in Figure 2-1. Due to the existence of a porous wall, the fluid domain is separated into two regions. As defined in Figure 2-1, region 1 ($x^* \leq 0, -h^* \leq z^* \leq \eta^*$) denotes the fluid domain on the left side of the porous wall and region 3 ($x^* \geq 0, -h^* \leq z^* \leq \eta^*$) stands for the fluid domain on the right side of the porous wall. The notations with superscript "*" represent the dimensional physical variables. A two-dimensional (2-D) Cartesian coordinate system (x^*, z^*) is applied for this study. The x^* axis represents the horizontal axis where the $\mathrm{x}^* = 0$ is at the location of the partially submerged porous wall, and the z^* axis points vertically upwards with the undisturbed water surface set as $z^* = 0$. η^* and h^* denote respectively the wave elevation and constant water depth. The draft of the partially submerged porous wall is set as d^* beneath the water surface. It is assumed that the partially submerged porous wall is a rigid thin structure. Additionally, the fluid is assumed to be inviscid and incompressible and the flow is irrotational. The governing equation, boundary conditions, and derived analytical solutions of the velocity potentials and free-surface elevations are summarized in the following sub-sections. Detailed derivations of the solution formulations given in this chapter can be found in Appendix A.

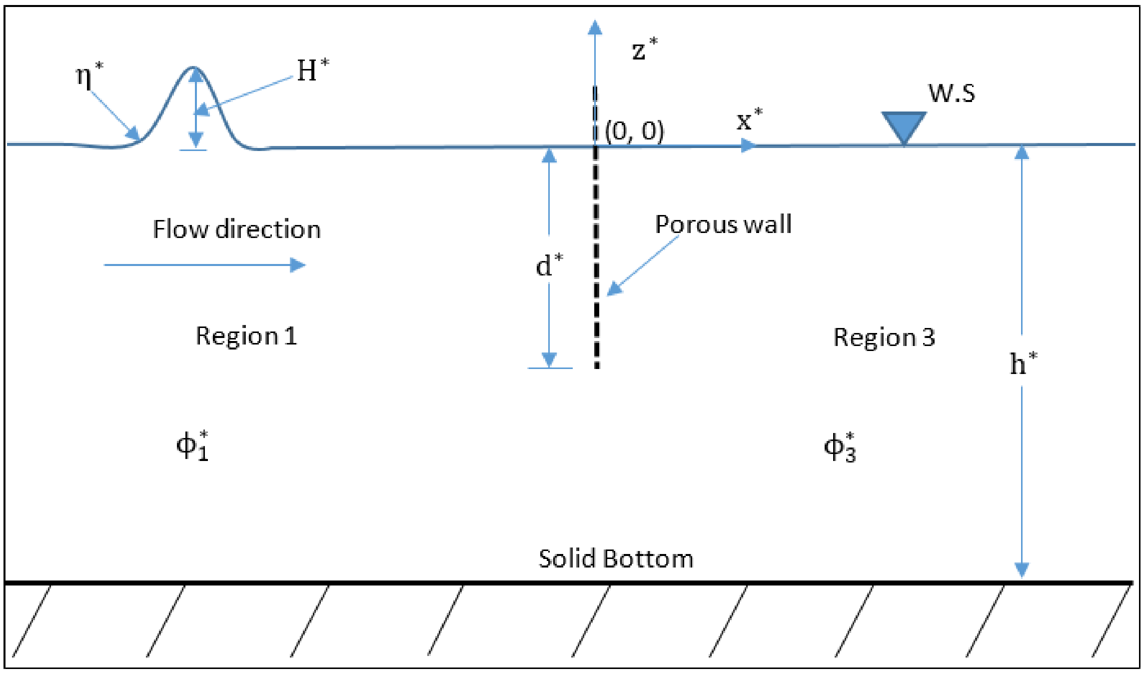

Figure 2-1: Schematic of a solitary wave interacting with a partially submerged porous wall.

2.1 Governing Equations

In order to derive the analytical solution for a solitary wave interacting with a partially submerged porous wall, the free-surface elevation $\eta_I^*(x^*, t^*)$ of an incident right-going (propagating along the positive x^* direction) solitary wave, according to the solitary wav theory, can be expressed as

$$\eta_I^* = H^* sech^2\left[\sqrt{\frac{3H^*}{4(h^*)^3}}(x^* - c^*t^*)\right], \tag{2-1}$$

where H^* stands for the incident wave height and c^* and t^* represent respectively the wave celerity and time. In Eqn. (2-1), the variable with subscript, I, represents that of an incident wave. $c^* = \sqrt{gh^*}$ where g is the gravitational acceleration and $\alpha = H^*/h^*$ is the dimensionless wave height.

Based on the Fourier integral method presented by Isaacson (1983) and later extended by Zhong and Wang (2006), the velocity potential of the incident wave can be expressed as

$$\phi_I^* = \frac{H^*}{2\pi\sqrt{\frac{h^*}{g^*}}}\int_{-\infty}^{\infty}\frac{A(k^*)}{ik^*}e^{ik^*(x^*-c^*t^*)}dk^*, \quad (2\text{-}2)$$

and the corresponding equation for the free-surface elevation becomes

$$\eta_I^* = \frac{H^*}{2\pi}\int_{-\infty}^{\infty}A(k^*)e^{ik^*(x^*-c^*t^*)}dk^*, \quad (2\text{-}3)$$

where k^* indicates the wave number. For the mathematical convenience, Eqns. (2-2) and (2-3) have the complex expressions where the real part of the equations represent the true physical variables. From Eqns. (2-1) and (2-3), the coefficient of the Fourier integral $A(k^*)$ can be derived as

$$A(k^*) = \frac{4\pi(h^*)^3k^*}{3H^*}csch(\pi k^*\sqrt{\frac{(h^*)^3}{3H^*}}). \quad (2\text{-}4)$$

As the fluid domain is separated by a porous wall, ϕ_1^* and ϕ_3^* are introduced to represent the velocity potentials in region 1 ($x^* \le 0, -h^* \le z^* \le \eta^*$) and region 3 ($x^* \ge 0, -h^* \le z^* \le \eta^*$), respectively. For a solitary wave, the velocity potential ϕ_j ($j = 1{,}3$) in a dimensionless form satisfies the Laplace equation

$$\frac{\partial^2\phi_j}{\partial x^2}+\frac{\partial^2\phi_j}{\partial z^2}=0 \qquad (j=1,3), \tag{2-5}$$

where $\phi_j=\phi_j^*/c_0h^*$, $x=x^*/h^*$, $z=z^*/h^*$ and $c_0=\sqrt{g^*h^*}$. All the physical variables without superscript "*" are nondimensionalized by using h^* as length scale, c_0 as velocity scale and $\sqrt{h^*/g^*}$ as time scale. A variable with subscript *j* denotes that variable in region *j*.

For a weakly nonlinear and weakly dispersive wave, α, where $\alpha=O(\mu^2)$, can be used as the order of the governing equations of this study. Following the classical expansion method presented by Wu (1981), Wang et al. (1992) proposed an expression of the original velocity potential in term of the depth-averaged velocity potential shown as

$$\phi_j(x,z,t)=\overline{\phi}_j(x,t)-\alpha\left(\frac{1}{3}+z+\frac{z^2}{2}\right)\nabla^2\overline{\phi}_j+O(\mu^5) \quad (j=1,3), \tag{2-6}$$

where $\overline{\phi}_j(x,t)$ $(j=1,3)$ denote the depth-averaged velocity potential either in region 1 or in region 3. Other variables can be transferred into dimensionless forms shown as $k=k^*h^*$,$\eta=\eta^*/h^*$, $d=d^*/h^*$, $H=H^*/h^*$, and $c=c^*/c_0$.

Following the approaches proposed by Zhong and Wang's (2006) and Jaf and Wang (2015), the depth-averaged velocity potential of region 1, including both incident and reflected waves, can be written as

$$\overline{\phi}_1=\int_{-\infty}^{\infty}\{(-iq)[e^{ikx}+R_0e^{-ikx}]\}e^{-ikct}dk, \tag{2-7}$$

whereas the depth-averaged velocity potential of region 3 can be expressed as

$$\overline{\phi}_3=\int_{-\infty}^{\infty}\{(-iq)[T_0e^{ikx}]\}e^{-ikct}dk, \tag{2-8}$$

where R_0 and T_0 are the reflection and transmission related coefficients respectively, and

$$q = \frac{2}{3} csch\left(\pi k \sqrt{\frac{1}{3H}}\right). \tag{2-9}$$

Substituting Eqn. (2-7) into Eqn. (2-6) leads the original velocity potential for region 1 as

$$\phi_1 = \int_{-\infty}^{\infty} \{(-iq)[e^{ikx} + R_0 e^{-ikx}] + \alpha k^2 \left(\frac{1}{3} + z + \frac{z^2}{2}\right)(-iq)[e^{ikx} + R_0 e^{-ikx}]\} e^{-ikct} dk. \tag{2-10}$$

Similarly, the velocity potential for region 3 can be formulated from Eqns. (2-6) and (2-8) as

$$\phi_3 = \int_{-\infty}^{\infty} \{(-iq)[T_0 e^{ikx}] + \alpha k^2 \left(\frac{1}{3} + z + \frac{z^2}{2}\right)(-iq)[T_0 e^{ikx}]\} e^{-ikct} dk. \tag{2-11}$$

In Eqns. (2-10) and (2-11), R_0 and T_0 are unknown coefficients required to be determined from the matching conditions. In this integral method, the corresponding R_0 and T_0 for each wave number component k are determined to describe their contributions to the wave reflection and transmission. With the integration, the overall reflection and transmission coefficients can be estimated. Velocity potentials of region 1 and region 3 as shown in Eqns. (2-10) and (2-11) satisfy the far field condition.

2.2 Boundary and Matching Conditions

In order to describe the behavior of a porous plate at the interface of region 1 and region 3, Darcy's law is applied, so that the velocity of fluids flows through the porous plate is linearly proportional to the pressure difference between two sides of the porous wall (Chwang, 1983), which gives

$$\frac{\partial \phi_1^*}{\partial x^*} = \frac{\partial \phi_3^*}{\partial x^*} = \frac{b_0^*}{\mu}(p_1 - p_3), \tag{2-12}$$

where μ is the dynamic viscosity, b_0^* is a specific material constant for the porous wall, and p is the pressure. In combination with the linearized dynamic free-surface boundary condition, the velocity of the fluid at the interface of region 1 and region 3 can be derived as

$$\frac{\partial \phi_1^*}{\partial x^*} = \frac{\partial \phi_3^*}{\partial x^*} = \frac{-b_0^* \rho}{\mu}\left(\frac{\partial \phi_1^*}{\partial t^*} - \frac{\partial \phi_3^*}{\partial t^*}\right). \tag{2-13}$$

Let $b_0 = b_0^*/h^*$, the dimensionless form of Eq. (2-13) can be expressed as

$$(\frac{\partial \phi_1}{\partial x})_{x=0} = (\frac{\partial \phi_3}{\partial x})_{x=0} = (ikc)R_e b_0(\phi_1 - \phi_3), \tag{2-14}$$

where $R_e = \rho h^* \sqrt{g^* h^*}/\mu$ is a Reynolds number like parameter describing the flow condition passing through the porous wall. In order to solve R_0 and T_0, the matching boundary conditions at the interface $x = 0$ are applied. They are

$$(\frac{\partial \phi_1}{\partial x})_{x=0} = (\frac{\partial \phi_3}{\partial x})_{x=0} \quad @ -1 \le z \le 0, \tag{2-15}$$

$$(\phi_1)_{x=0} = (\phi_3)_{x=0} \quad @ -1 \le z \le -d, \text{and} \tag{2-16}$$

$$\left(\frac{\partial \phi_1}{\partial x}\right)_{x=0} = \left(\frac{\partial \phi_3}{\partial x}\right)_{x=0} = (ikc)R_e b_0(\phi_1 - \phi_3) \quad @ -d \le z \le 0. \tag{2-17}$$

Eqn. (2-15) indicates the continuity of the fluid velocity at the interface while Eqn. (2-16) describes the continuity of the velocity potential for the opening part of the interface. The porous effect is added into the mixing matching boundary condition with the application of Eqn. (2-17) where the normal velocity passing through the porous plate is found to be associated with the difference between the velocity potentials in region 1 and region 3.

By substituting Eqns. (2-10) and (2-11) into Eqn. (2-15), we can get the relationship between R_0 and T_0 as

$$T_0 = 1 - R_0. \tag{2-18}$$

Also, substituting Eqns. (2-10) and (2-11) into Eqn. (2-16), we have

$$2R_0 + \alpha k^2 \left(\frac{1}{3} + z + \frac{z^2}{2}\right)(2R_0) = 0 \quad -1 \le z \le -d. \tag{2-19}$$

Furthermore, from Eq. (2-17), we can acquire

$$1 - R_0 - 2GR_0 + \alpha k^2 \left(\frac{1}{3} + z + \frac{z^2}{2}\right)[1 - R_0 - 2GR_0] = 0 \quad @-d \le z \le 0, \tag{2-20}$$

where $G = R_e b_0 c$ is a dimensionless porous effect parameter.

2.3 Analytical Solutions

Eqns. (2-19) and (2-20) form a system of mixed matching conditions at the interface (*x=0*) between region 1 and region 3. A function describing the errors between the left-hand sides and right-hand-sides of Eqns. (2-20) and (2-19) is defined as

$$H_0 = \begin{cases} 1 + (-1 - 2G)R_0 + \alpha k^2 \left(\frac{1}{3} + z + \frac{z^2}{2}\right)[1 + (-1 - 2G)R_0] & -d \le z \le 0 \\ 2R_0 + \alpha k^2 \left(\frac{1}{3} + z + \frac{z^2}{2}\right)(2R_0) & -1 \le z \le -d \end{cases}. \tag{2-21}$$

The least squares method (Sneddon, 1966; Dalrymple and Martin, 1990) by minimizing $\int_{-1}^{0} \left|{H_0}^2\right| dz$ is applied to determine the unknown coefficient R_0. The minimizing condition is given as

$$\int_{-1}^{0} H_0(z) \frac{\partial H_0}{\partial R_0} dz = 0. \tag{2-22}$$

The derivative of H_0 versus R_0 leads

$$\frac{\partial H_0}{\partial R_0} = \begin{cases} (-1-2G) + \alpha k^2 \left(\frac{1}{3} + z + \frac{z^2}{2}\right)[(-1-2G)] & -d \le z \le 0 \\ 2 + \alpha k^2 \left(\frac{1}{3} + z + \frac{z^2}{2}\right)(2) & -1 \le z \le -d \end{cases} . \tag{2-23}$$

Substituting Eqns. (2-21) and (2-23) into Eqn. (2-22), we have

$$\begin{aligned} &\int_{-1}^{0} H_0(z) \frac{\partial H_0}{\partial R_0} dz \\ &= \int_{-d}^{0} \left\{1 + BR_0 + C\left(\frac{1}{3} + z + \frac{z^2}{2}\right)[1 + BR_0]\right\}\left\{B + C\left(\frac{1}{3} + z + \frac{z^2}{2}\right)[B]\right\} dz \\ &+ \int_{-1}^{-d} \left\{2R_0 + C\left(\frac{1}{3} + z + \frac{z^2}{2}\right)(2R_0)\right\}\left\{2 + C\left(\frac{1}{3} + z + \frac{z^2}{2}\right)(2)\right\} dz \\ &= 0, \end{aligned} \tag{2-24}$$

where

$$B = -1 - 2G \text{ and} \tag{2-25}$$

$$C = \alpha k^2. \tag{2-26}$$

The reflection coefficient R_0 can be derived from Eqn. (2-24) as

$$R_0 = \frac{-BE}{B^2 E - 4(E - 4C^2 - 180)}, \tag{2-27}$$

where

$$\begin{aligned} E &= 9C^2 d^5 - 45C^2 d^4 + (80C^2 + 60C)d^3 + (-60C^2 - 180C)d^2 \\ &\quad + (20C^2 + 120C + 180)d. \end{aligned} \tag{2-28}$$

Based on the determined R_0 and T_0 from Eqns. (2-27) and (2-18), the velocity potentials (Eqns. (2-10) and (2-11)) in both region 1 and region 3 can be calculated. As an approximation, the linearized dynamic free-surface boundary condition is applied separately in region1 and region 3 to obtain the free surface profiles. In region 1, we have the dimensionless wave elevation as

$$\eta_1 = -\frac{\partial \overline{\phi}_1}{\partial t} = -\int_{-\infty}^{\infty} \{-(q)(kc)[e^{ikx} + R_0 e^{-ikx}]\} e^{-ikct} dk. \qquad (2\text{-}29)$$

Similarly, the free-surface elevation of the transmitted wave in region 3 can be derived as

$$\eta_3 = -\frac{\partial \overline{\phi}_3}{\partial t} = -\int_{-\infty}^{\infty} \{-(q)(kc)[T_0 e^{ikx}]\} e^{-ikct} dk. \qquad (2\text{-}30)$$

The real parts of Eqns. (2-29) and (2-30) can be calculated to give the physical values of the free-surface elevations in region 1 and region 3, respectively.

To determine the maximum hydrodynamic forces on the partially submerged porous wall, the pressure distribution along the wall needs to be computed. According to the Bernoulli equation, the dimensionless form of the pressure can be expressed as

$$p = -(\frac{\partial \phi}{\partial t} + \frac{1}{2}(\phi_x^2 + \phi_z^2)), \qquad (2\text{-}31)$$

where p= $p^*/\rho g h^*$. Due to the assumption of a thin wall (zero thickness), only the horizontal hydrodynamic force is considered in this study. Through the linearization procedure, the horizontal hydrodynamic force can be computed by integrating the pressure acting on the front face of the porous wall as

$$F_x = (\int_{-d}^{0} p_1 dz + \frac{1}{2}\eta_1|\eta_1|) - (\int_{-d}^{0} p_3 dz + \frac{1}{2}\eta_3|\eta_3|), \qquad (2\text{-}32)$$

where p_1 and p_2 are the respective pressures acting on the front and rear faces of the porous wall. It should be noted that the maximum force happens at the time $(t = t_F)$ when the maximum wave run-up reaching the front face of the porous wall.

Chapter 3 Analytical Model of Interactions between a Solitary Wave and a 2-D Finite-Length Partially Submerged Body with Attached Dual Porous Walls

To include the effect of structural dimension, a 2-D finite-length partially submerged body with two porous walls attached separately with one on the front face and the other on the back face of the structure is considered in the second part of study. The analytical solutions for a solitary wave interacting with this partially submerged body system are derived by extending some of the solution procedures presented in Chapter 2 to include the applications of additional matching conditions and use of the orthogonality property of the solution eigenfunctions. The schematic diagram of the partially submerged body system is shown in Figure 3-1, where the region 1 ($x^* \leq -x_1^*, -h^* \leq z^* \leq \eta^*$) represents the fluid domain on the left side of the structural system, the region 3 ($x^* \geq x_1^*, -h^* \leq z^* \leq \eta^*$) stands for the fluid domain on the right side of the system and the region 2 ($x_1^* \geq x^* \geq -x_1^*, -h^* \leq z^* \leq b^*$) denotes the fluid domain underneath the partially submerged body. The solution procedure for formulating the velocity potentials in region 1 and region 3 are similar to those presented in Chapter 2 while the velocity potential in region 2 is derived by solving the Laplace equation with the kinematic boundary conditions underneath the partially submerged structure (Lu and Wang, 2015). With the assumption of thin porous walls, the conditions for flows passing through them again follow the Darcy's law (Chwang, 1983; Zhong and Wang, 2006). It should be noted that the symbols of physical variables defined in Chapter 2 appear also in the formulations of the analytical derivations given in this chapter. Additional variables, such as b^* and x_1^*, represent respectively the draft and half length of the fixed partially submerged body. The solution procedure and derived analytical solutions of the velocity potentials and free-surface elevations for the second part of the present study are given in the following sub-sections. The detailed derivations of the solution formulations can be found in Appendix B.

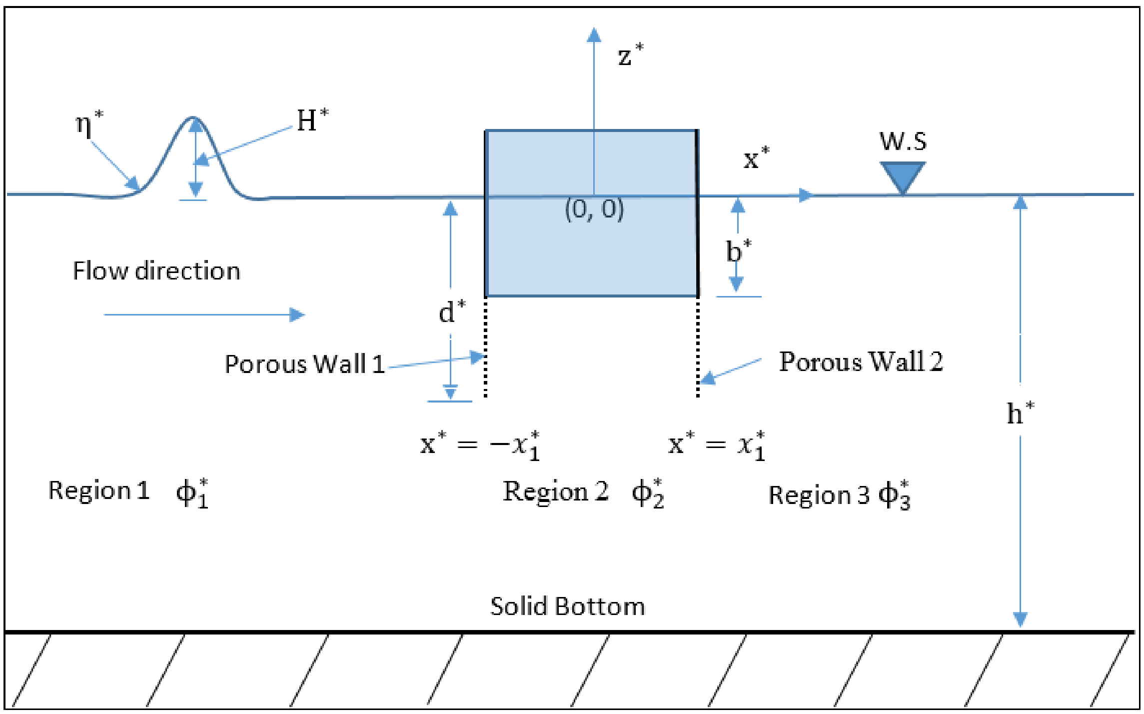

Figure 3-1: Schematic of a solitary wave interacting with a 2-D finite-length partially submerged body with attached dual porous walls.

3.1 Governing Equations

In this case, the region 1 and region 3 are corresponding to the domains with the velocity potentials of incident/reflected waves and transmitted waves, respectively. The analytical solutions for the velocity potentials of the region 1 and region 3 are similar to those derived based on the Fourier integral method as presented in Chapter 2. However, the velocity potential of region 2 requires to be re-derived and the boundary conditions due to the additional fluid domain (region 2) are also changed. Let R_1 and T_1 be the unknown coefficients for the velocity potentials of reflected and transmitted waves, respectively. Similar to Eqns. (2-10) and (2-11), the velocity potentials in region 1 and region 3 are expressed as

$$\phi_1 = \int_{-\infty}^{\infty} \{(-iq)[e^{ikx} + R_1 e^{-ikx}] + \alpha k^2 \left(\frac{1}{3} + z + \frac{z^2}{2}\right)(-iq)[e^{ikx} + R_1 e^{-ikx}]\} e^{-ikct} dk \; and \tag{3-1}$$

$$\phi_3 = \int_{-\infty}^{\infty} \{(-iq)[T_1 e^{ikx}] + \alpha k^2 \left(\frac{1}{3} + z + \frac{z^2}{2}\right)(-iq)[T_1 e^{ikx}]\} e^{-ikct} dk. \tag{3-2}$$

For the additional fluid domain, region 2, the velocity potential should satisfy the Laplace equation

$$\nabla^2 \phi_2 = 0 \quad @ \; -1 \le z \le -b, \tag{3-3}$$

and the kinematic boundary conditions applied at the bottom of the fluid domain and the bottom of the partially submerged body, i.e.,

$$\frac{\partial \phi_2}{\partial z} = 0 \quad @z = -1 \; \& \; z = -b. \tag{3-4}$$

Based on Lu and Wang (2015), the velocity potential in region 2 is derived as

$$\phi_2 = \int_{-\infty}^{\infty} \left\{ \sum_{j=1}^{\infty} \left(A_j \, cosh(m_j x) + B_j \, sinh(m_j x)\right) cos\left(m_j (z+1)\right) + Cx + D \right\} e^{-ikct} \, dk, \tag{3-5}$$

where m_j can be expressed as

$$m_j = \frac{j\pi}{1-b} \qquad j = 1,2, \dots . n. \tag{3-6}$$

It should be noted that the dimensionless forms of Eqns. (3-3), (3-4) and (3-5) are shown to be in consistency with the nondimensional approach given in Chapter 2, where h^* is selected as the length scale, c_0 as the velocity scale and $\sqrt{h^*/g^*}$ as the time scale). $A_{j,}$ ($j = 1,2, \dots .$), B_j, ($j = 1,2, \dots .$), C, and D are unknown coefficients to be determined by using the matching conditions at the interfaces.

3.2 Boundary and Matching Conditions

The existence of fluid region described as region 2 underneath the partially submerged body add additional boundary and matching conditions to be utilized for solving the problem. The matching conditions are expanded to be applied at the interfaces on both side of the partially submerged body, which are the interface between region 1 and region 2 and the interface between region 2 and region 3, for determining the unknown coefficients.

The boundary conditions on the submerged structural surfaces ($-b \leq z \leq 0$) at the interfacial locations ($x = -x_1$ and $x = x_1$) require that the normal velocities of fluids in regions 1 and 3 equal to zero. We have

$$\frac{\partial \phi_1}{\partial x} = 0 \quad @x = -x_1, -b \leq z \leq 0 \; and \tag{3-7}$$

$$\frac{\partial \phi_3}{\partial x} = 0 \quad @x = x_1, -b \leq z \leq 0. \tag{3-8}$$

Following the similar procedure as given in Chapter 2, the boundary conditions on the porous walls by following the Darcy's law can be expressed as

$$\frac{\partial \phi_1}{\partial x} = \frac{\partial \phi_2}{\partial x} - R_e b_1 \left(\frac{\partial \phi_1}{\partial t} - \frac{\partial \phi_2}{\partial t} \right) \;\; @\; x = -x_1, -d \le z \le -b \; and \tag{3-9}$$

$$\frac{\partial \phi_3}{\partial x} = \frac{\partial \phi_2}{\partial x} = -R_e b_2 \left(\frac{\partial \phi_2}{\partial t} - \frac{\partial \phi_3}{\partial t} \right) \;\; @x = x_1, -d \le z \le -b. \tag{3-10}$$

Similar to b_0 defined in Chapter 2, b_1 and b_2 are the dimensionless forms of the specific material constants for the porous walls 1 and 2, respectively. Again, $R_e = \rho h^* \sqrt{g^* h^*}/\mu$.

At the opening interfaces ($-1 \le z \le -d \; @ \; x = -x_1$ and $x = x_1$), the continuous velocities and velocity potentials are set to be satisfied. Now, adding the conditions given in Eqns. (3-9) and (3-10), the overall matching conditions at the interfaces can be expressed as

$$\frac{\partial \phi_1}{\partial x} = \frac{\partial \phi_2}{\partial x} \;\; @x = -x_1, -1 \le z \le -b, \tag{3-11}$$

$$\frac{\partial \phi_2}{\partial x} = \frac{\partial \phi_3}{\partial x} \;\; @x = x_1\,, -1 \le z \le -b, \tag{3-12}$$

$$\phi_1 = \phi_2 \;\; @\; x = -x_1, -1 \le z \le -d, and \tag{3-13}$$

$$\phi_2 = \phi_3 \;\; @\; x = x_1, -1 \le z \le -d. \tag{3-14}$$

3.3 Analytical Solutions

Considering the determination of the unknown coefficients R_1 and T_1 for a particular *k* value, we temporarily remove the effect of the integral form by letting the integrand of a given k satisfying the boundary conditions. Here, the terms in integration for the velocity potentials in regions 1, 2, and 3 (Eqns. (3-1), (3-2) and (3-5)) are specified as

$$\phi_1^p = \left\{(-iq)\left[e^{ikx} + R_1 e^{-ikx}\right]\right.$$

$$\left. + \alpha k^2 \left(\frac{1}{3} + z + \frac{z^2}{2}\right)(-iq)\left[e^{ikx} + R_1 e^{-ikx}\right]\right\} e^{-ikct}, \tag{3-15}$$

$$\phi_3^p = \left\{(-iq)\left[T_1 e^{ikx}\right] + \alpha k^2 \left(\frac{1}{3} + z + \frac{z^2}{2}\right)(-iq)\left[T_1 e^{ikx}\right]\right\} e^{-ikct}, and \tag{3-16}$$

$$\phi_2^p = \left\{\sum_{j=1}^{\infty}\left(A_j\, cosh\left(m_j x\right) + B_j\, sinh\left(m_j x\right)\right) cos\left(m_j (z+1)\right) + Cx + D\right\} e^{-ikct}, \tag{3-17}$$

where the terms with superscript "*p*" reflect the equations for a particular *k* value.

In order to relate the unknown coefficients $A_{j,}$ $(j = 1,2, \ldots .)$, B_j, $(j = 1,2, \ldots .)$, *C*, and *D* with R_1 and T_1, the matching conditions shown in Eqns. (3-13) and (3-14) combining with the porous boundary conditions shown as Eqns. (3-9) and (3-10) and the orthogonality property of eigenfunctions, $cos\left(k_j (z+1)\right)$, we have

$$\int_{-1}^{-d} \phi_1^p\, dz + \int_{-d}^{-b} \tilde{\phi}_2 dz = \int_{-1}^{-b} \phi_2^p\, dz \quad @\, x = -x_1, \tag{3-18}$$

$$\int_{-1}^{-d} \phi_3^p\, dz + \int_{-d}^{-b} \hat{\phi}_2 dz = \int_{-1}^{-b} \phi_2^p dz \quad @\, x = x_1, \tag{3-19}$$

$$\int_{-1}^{-d} \phi_1^p\; cos\left(m_j (z+1)\right) dz + \int_{-d}^{-b} \tilde{\phi}_2\, cos\left(m_j (z+1)\right) dz$$

$$= \int_{-1}^{-b} \phi_2^p\, cos\left(m_j (z+1)\right)\, dz \qquad @\, x = -x_1, j = 1,2, \ldots . n, and \tag{3-20}$$

$$\int_{-1}^{-d} \phi_3^p \ \cos\left(m_j(z+1)\right) dz + \int_{-d}^{-b} \hat{\phi}_2 \cos\left(m_j(z+1)\right) dz$$

$$= \int_{-1}^{-b} \phi_2^p \cos\left(m_j(z+1)\right) \ dz \qquad @\ x = x_1, j = 1,2, \dots . n, \qquad (3\text{-}21)$$

where

$$\tilde{\phi}_2 = \phi_1^p + \left(\frac{1}{R_e b_1}\right)\left(\frac{-1}{c}\right)\tilde{\phi}_1, \qquad (3\text{-}22)$$

$$\hat{\phi}_2 = \phi_3^p - \left(\frac{1}{R_e b_2}\right)\left(\frac{-1}{c}\right)\phi_3^p, and \qquad (3\text{-}23)$$

$$\tilde{\phi}_1 = \left\{(-iq)\left[e^{ikx} - R_1 e^{-ikx}\right]\right.$$

$$\left. + \alpha k^2 \left(\frac{1}{3} + z + \frac{z^2}{2}\right)(-iq)\left[e^{ikx} - R_1 e^{-ikx}\right]\right\} e^{-ikct}. \qquad (3\text{-}24)$$

Substituting Eqns. (3-15), (3-16) and (3-17) into Eqns. (3-18) and (3-19) we can derive the unknown coefficients C, and D, in terms of R_1 and T_1 as

$$C = \frac{1}{-2x_1(1-b)}\{\{(-iq)[I_2 + R_1 I_1 - T_1 I_3](1-b) + C_1(-iq)[I_2 + R_1 I_1 - T_1 I_3]\}$$

$$+ \{(-iq)[G_1(I_2 - R_1 I_1) + G_2 T_1 I_3](d-b)$$

$$+ C_2(-iq)[G_1(I_2 - R_1 I_1) + G_2 T_1 I_3]\}\} \ and \qquad (3\text{-}25)$$

$$D = \frac{1}{2(1-b)}\{\{(-iq)[I_2 + R_1 I_1 + T_1 I_3](1-b) + C_1(-iq)[I_2 + R_1 I_1 + T_1 I_3]\}$$

$$+ \{(-iq)[G_1(I_2 - R_1 I_1) - G_2 T_1 I_3](d-b)$$

$$+ C_2(-iq)[G_1(I_2 - R_1 I_1) - G_2 T_1 I_3]\}\}. \qquad (3\text{-}26)$$

where

$$G_1 = \left(\frac{1}{R_e b_1}\right)\left(\frac{-1}{c}\right), \quad (3\text{-}27)$$

$$G_2 = \left(\frac{1}{R_e b_2}\right)\left(\frac{-1}{c}\right), \quad (3\text{-}28)$$

$$C_1 = \alpha k^2 \left(-\frac{b^3 - 3b^2 + 2b}{6}\right), \quad (3\text{-}29)$$

$$C_2 = \alpha k^2 \left(\frac{(d^3 - b^3) - 3(d^2 - b^2) + 2(d - b)}{6}\right), \quad (3\text{-}30)$$

$$I_1 = I_3 = e^{ik(x_1)}, and \quad (3\text{-}31)$$

$$I_2 = e^{ik(-x_1)}. \quad (3\text{-}32)$$

For the unknown coefficients, $A_{j,}$ (j $= 1,2, \dots .$) and B_j, (j $= 1,2, \dots .$), similarly, by substituting Eqs. (3-15), (3-16) and (3-17) into Eqns. (3-20) and (3-21), we have

$$A_j = \frac{\{C_a(-iq)\alpha k^2 + G_1\left\{(-iq)\left(1 + \frac{1}{3}\alpha k^2\right) C_b + (-iq)(\alpha k^2)C_c\right\}\}[I_2]}{(1-b)\cosh\left(m_j(x_1)\right)} + \frac{\{C_a(-iq)\alpha k^2 + G_1\left\{(-iq)\left(1 + \frac{1}{3}\alpha k^2\right)[-]C_b + (-iq)(\alpha k^2)[-]C_c\right\}\}R_1[I_1]}{(1-b)\cosh\left(m_j(x_1)\right)} + \frac{\{\alpha k^2(C_a)(-iq) - G_2\left\{(-iq)\left(1 + \frac{1}{3}\alpha k^2\right)(C_b) + \alpha k^2(-iq)(C_c)\right\}\}T_1[I_3]}{(1-b)\cosh\left(m_j(x_1)\right)} \; and \quad (3\text{-}33)$$

B_j

$$= \frac{\{\alpha k^2(C_a)(-iq) - G_2\left\{(-iq)\left(1+\frac{1}{3}\alpha k^2\right)(C_b) + \alpha k^2(-iq)(C_c)\right\}T_1[I_3]}{(1-b)sinh\left(m_j(x_1)\right)}$$

$$- \frac{\{C_a(-iq)\alpha k^2 + G_1\left\{(-iq)\left(1+\frac{1}{3}\alpha k^2\right)C_b + (-iq)(\alpha k^2)C_c\right\}\}I_2}{(1-b)sinh\left(m_j(x_1)\right)}$$

$$- \frac{\{C_a(-iq)\alpha k^2 + G_1\left\{(-iq)\left(1+\frac{1}{3}\alpha k^2\right)(-C_b) + (-iq)(\alpha k^2)(-C_c)\right\}\}R_1 I_1}{(1-b)sinh\left(m_j(x_1)\right)}, \qquad (3\text{-}34)$$

where

$$C_a = \frac{(1-b)cos(j\pi)}{(m_j)^2}, \qquad (3\text{-}35)$$

$$C_b = -\frac{1}{m_j} sin\left(m_j(1-d)\right), and \qquad (3\text{-}36)$$

$$C_c = \frac{\left((d^2-2d){m_j}^2 - 2\right) sin\left(m_j(d-1)\right) + (2d-2)m_j\, cos\left(m_j(d-1)\right)}{2\left(m_j\right)^3} + \frac{(-2b+2)\, cos\left(m_j(b-1)\right)}{2\left(m_j\right)^2}. \qquad (3\text{-}37)$$

Furthermore, the integrations of the remaining velocity related boundary conditions at the interfaces (Eqns. (39), (40), (43) and (44)) along the vertical flow domains in regions 1 and 2 give

$$\int_{-1}^{0} \frac{\partial \phi_1^p}{\partial x}\, dz = \int_{-1}^{-b} \frac{\partial \phi_2^p}{\partial x}\, dz \quad @\, x = -x_1\, and \qquad (3\text{-}38)$$

$$\int_{-1}^{0} \frac{\partial \phi_3^p}{\partial x}\, dz = \int_{-1}^{-b} \frac{\partial \phi_2^p}{\partial x}\, dz \quad @\, x = x_1. \tag{3-39}$$

By substituting Eqns. (3-15, 3-16 and 3-17) into Eqns. (3-38) and (3-39), we have

$$T_1 = \frac{I_2}{I_3} - \frac{R_1 I_1}{I_3}\ and \tag{3-40}$$

$$R_1 = \frac{2x_1(ik)I_2 + (G_1 + G_2)I_2(K_2)}{\{(ik)I_1 2x_1 - [2I_1](K_1) + \{(G_1 + G_2)I_1(K_2)\}\}}, \tag{3-41}$$

where

$$K_1 = 1 - b + C_1\ and \tag{3-42}$$

$$K_2 = d - b + C_2 \tag{3-43}$$

After T_1 and R_1 are determined from Eqs. (3-40) and (3-41), Eqns. (3-1) and (3-2) can be applied to calculate analytically the velocity potentials in regions 1 and 3. Also, according to the obtained unknown coefficients $A_{j,}$ (j $= 1,2, \ldots.$), B_j, (j $= 1,2, \ldots.$), C, and D from Eqns. (3-33)-(3-34) and (3-25)-(3-26), the velocity potentials in region 2 can be evaluated from Eqn. (3-5). Again, based on the linearized kinematic free-surface boundary condition, the free-surface elevations in regions including both region 1 and 3 are linearly proportional to the derivative of depth-averaged velocity potentials with respect to time as

$$\eta_1 = -\frac{\partial \overline{\phi}_1}{\partial t} = -\int_{-\infty}^{\infty} \{-(q)(kc)[e^{ik(x)} + R_1 e^{-ik(x)}]\} e^{-ikct} dk\ and \tag{3-44}$$

$$\eta_3 = -\frac{\partial \overline{\phi}_2}{\partial t} = -\int_{-\infty}^{\infty} \{-(q)(kc)[T_1 e^{ik(x)}]\} e^{-ikct} dk. \tag{3-45}$$

It should be noted that the real part of the Eqns. (3-44) and (3-45) represent the physical values of the free-surface elevations in regions 1 and 3.

The Bernoulli equation (Eqn. (2-31)) is applied again to determine the pressure field in the fluid domain. Once the pressure is calculated, the horizontal wave force on the partially submerged body system can be determined by integrating the pressure acting on the submerged left and right faces of the structure, including the porous walls, to have

$$F_x = (\int_{-d}^{0} p_1 dz + \frac{1}{2}\eta_1|\eta_1|) - (\int_{-d}^{0} p_3 dz + \frac{1}{2}\eta_3|\eta_3|), \tag{3-46}$$

where p_1 is the pressure acting on the structural surface at $x = -x_1$ in region 1 whereas p_3 is the pressure acting on the structural surface at $x = x_1$ in region 3. The vertical uplifting force acting on the partially submerged body can be calculated by integrating the pressure acting on the bottom of the structure from the left to the right interfaces to have

$$F_z = \int_{-x_1}^{x_1} p dx. \tag{3-47}$$

Chapter 4 Experimental Measurements

In order to verify the derived analytical solutions for a solitary wave interactions with either a partially submerged porous wall (Chapter 2) or a partially submerged body system with attached dual porous walls (Chapter 3), laboratory tests were carried out to measure the free-surface elevations of the incident, reflected and transmitted waves for comparisons. The experiments were conducted in a 762-cm (25-ft) long, 30.48-cm (1-ft) wide and 91.44-cm (3-ft) high glass-walled section of a 12.5-m (41-ft) long wave tank in the Hydraulic Lab of the University of Houston. Various setting parameters including the incident wave height, porous wall condition, and the draft of test structures were selected for the wavetank tests.

4.1 Experimental Setup for a Solitary Wave Interacting with a Partially Submerged Porous Wall

4.1.1 Wave Gauge Setup and Calibration

A side-view of the schematic diagram of the wavetank setup is shown in Figure 4-1. By controlling the motions of a Tolomatic linear actuator, a solitary wave of a given wave height can be generated from a piston-type wavemaker at one end of the tank. At the other end of the tank, energy dissipaters were used to eliminate the reflections of the waves after encountering the end wall. Two resistance-type wave gauges were installed along the wavetank to measure the free-surface elevations of the incident, reflected and transmitted waves. Gauge 1 was placed at a distance 76.2 cm upstream of the partially submerged porous wall to measure the incident and reflected waves. Meanwhile, gauge 2 is set at a distance 63.5 cm downstream of the porous wall to capture the transmitted waves.

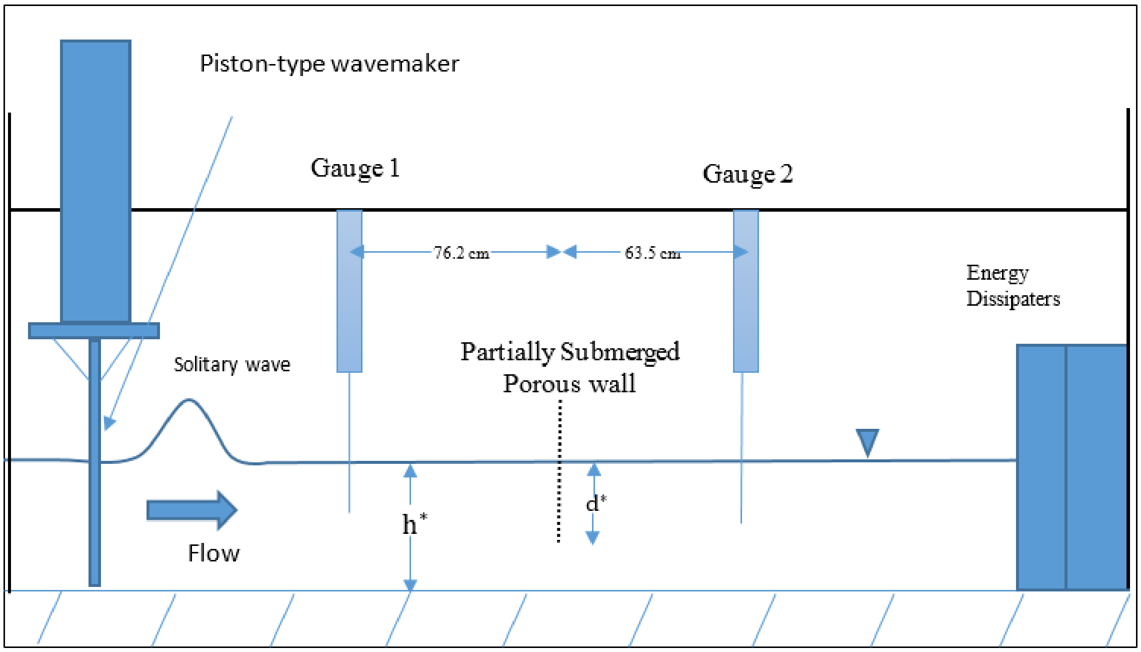

Figure 4-1: Side view of the schematic of the experimental setup in the study of solitary wave interacting with a partially submerged porous wall.

Before recording the wave elevations, calibration of wave gauges was performed to ensure the accuracy of the measurements. The linear regressions were applied to demonstrate the linear relationships between the water depths and the voltages for both gauges and the results are shown in Figure 4-2. All the wave elevations measured from the gauges were collected and recorded by the LabVIEW data acquisition system.

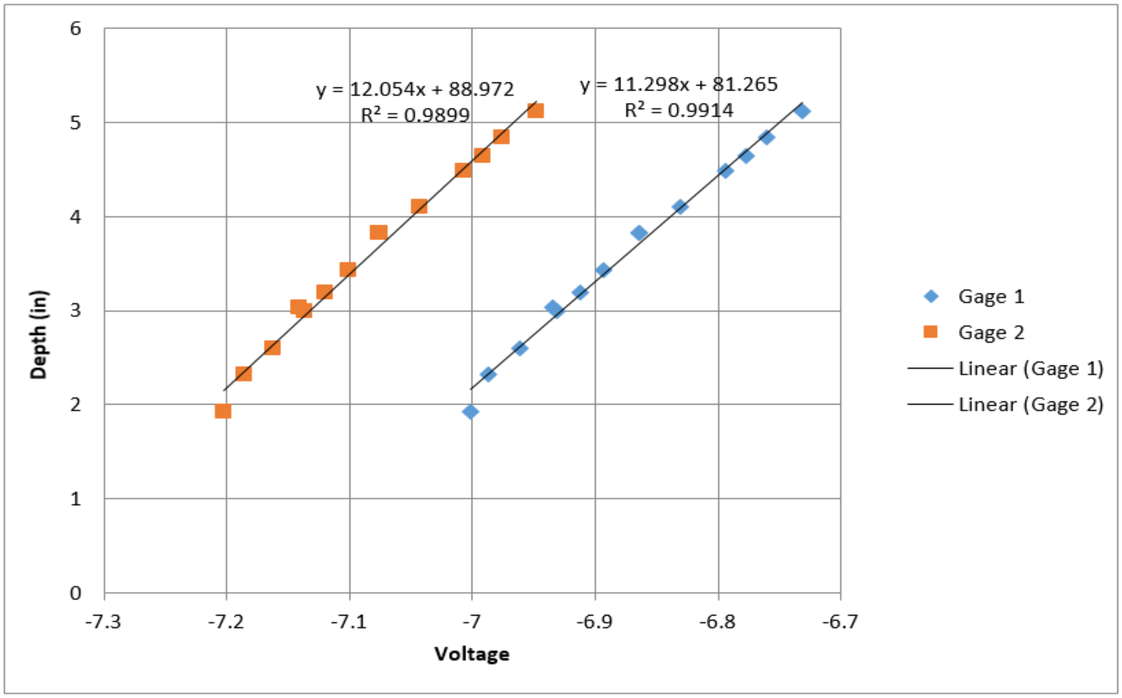

Figure 4-2: Calibrations of gauge 1 and gauge 2.

4.1.2 Parameters set for the experiments

Two different values of the depth of water in the channel, h^*, as 3 in (7.62 cm) and 4.5 in (11.43 cm) were set for the experiments. By altering the submerged depth of the fixed porous wall, d^*, the effect of the draft of the porous wall as a ratio to the depth of water, d^*/h^*, on the reflected and transmitted waves can be investigated. In this study, two predetermined values of d^*/h^*, i.e. $d^*/h^* = 0.5$ and $d^*/h^* = 1$, are utilized. It should be noticed that the dimensionless form of d^*, d, represents the same value as d^*/h^*. Various solitary waves with predetermined incident wave heights are generated to test the effect of the wave height on the reflected and transmitted waves. The incident wave heights, $\alpha = H = H^*/h^*$, which describes the original condition of the incident wave, vary from about 0.1 to 0.4 in this study.

For the porous wall, thin porous plates are utilized as the substitutes. Each porous plate was made of 11 gauge galvanized steel and the pore pattern was the standard round 60 degree staggered pattern. The properties of the four tested porous plates with various porosities, pore diameters, and calibrated b_0^* values as defined in Section 2.2 are shown in Table 4-1 (Chu, 2014).

Table 4-1: Properties of the porous plates.

Porosity (%)	Pore Diameter (in)	b_0^*(ft)
16.08	1/4	2.5 x 10^{-6}
22.67	1/4	4.0 x 10^{-6}
16.08	1/8	2.0 x 10^{-6}
22.67	1/8	2.5 x 10^{-6}

After knowing the water depth, we can calculate the corresponding constant value of R_e ($R_e = \rho h^* \sqrt{g^* h^*}/\mu$) for describing the flow condition passing through the porous wall. By adding the effect of b_0 ($b_0 = b_0^*/h^*$), the value of $R_e b_0$ as an input parameter of the experimental setup can be obtained. The $R_e b_0$ values are summarized in Table 4-2. Table 4-3 shows the setups and properties for three selected cases for the comparisons between the analytically obtained and experimentally recorded wave elevations in chapter 5.

Table 4-2: Values of $R_e b_0$.

h (in)	R_e	b_0	$R_e b_0$
3	65882	8.00E-06	0.527
3	65882	1.00E-05	0.659
3	65882	1.60E-05	1.054
4.5	121033	5.33E-06	0.646
4.5	121033	6.67E-06	0.807
4.5	121033	1.07E-05	1.291

Table 4-3: The setups and properties for each cases of experiments.

Case	h (in)	R_e	b_0	$R_e b_0$	d
1	3	65882	1.00E-05	0.659	0.5
2	3	65882	1.00E-05	0.659	1
3	3	65882	1.60E-05	1.054	0.5

4.2 Experimental Setup for a Solitary Wave Interacting with a 2-D Finite-Length Partially Submerged Body with Attached Dual Porous Walls

4.2.1 Setup of Wavetank and Wave Gauge Calibration

To enhance the verification of the analytical solutions for a solitary wave interacting with a 2-D finite-length partially submerged body with attached two porous walls, again, laboratory tests were carried out at the 12.5-m (41-ft) long wave tank as described above. The setup of the wave tank for the tests of the second topic is illustrated in Figure 4-3. A plastic solid rectangular box with two porous walls attached separately on its front and back sides was mounted at a partially submerged position in the wavetank as the defined partially submerged body system. The first gauge (Gauge 1) was placed at a distance (91.44 cm) upstream of the centerline of the partially submerged body to measure the incident and reflected waves. Meanwhile, the second gauge (Gauge 2) was set at a distance (134.62 cm) downstream of the partially submerged body to capture the transmitted waves. The wave gauges were calibrated again to confirm the linear variations between the voltages and the recorded water levels.

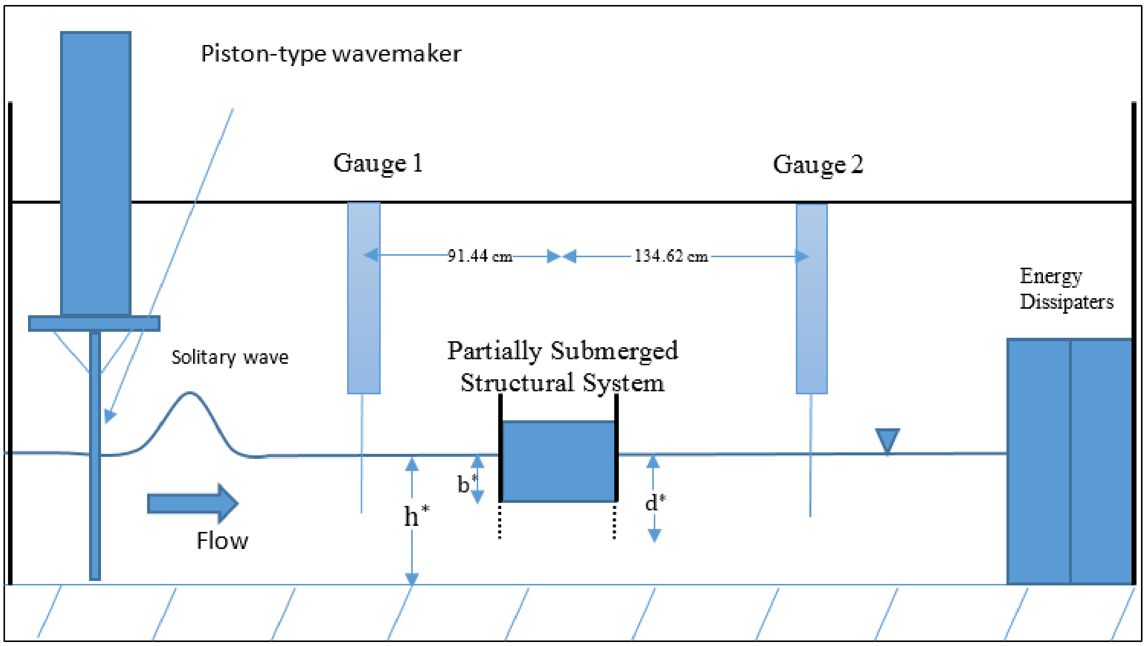

Figure 4-3: Side view of the schematic of the experimental setup in the study of solitary wave interacting with a 2-D finite-length partially submerged body with attached dual porous walls.

4.2.2 Parameters

The still water surface is set as a constant value of 3 inches. A series of measurements were conducted based on two predetermined values of d (or d^*/h^*), i.e. d=0 and d=1. When d equals to 0, there will be no porous wall effect. By modifying the draft of the body under the still water level, b^*, the effect of the ratio of the draft of structure to the water depth on the reflection and transmission of a solitary wave interaction with the partially submerged body can be investigated. Three different values of b, which is the dimensionless form of the draft of the partially submerged body, 0.3, 0.4 and 0.6, were set separately for the experiments. Also, by altering the length of the attached porous walls, the effect of the dual porous walls on reducing the transmitted waves can be studied. Two dimensionless values of L ($L = L^*/h^*$), i.e. L=4 and L=6, were selected to test the structural length effect. Again, as described in Section 4.1.2, the properties of the porous plates selected in the experiments were predetermined by Chu (2014). The porous properties in terms of either b_1^* or b_2^* are summarized in Table 4-4. With various porous plates applied, in all, 6 experimental settings as shown in Table 4-5 for their corresponding parameters in dimensionless forms were considered to use for comparisons of free-surface elevations obtained from experiments and the analytical results. For each experimental setting, solitary waves with incident wave heights ranging from about 0.2 to 0.4 were generated for the experiments and data collections.

Table 4-4: The material constant for each porous wall.

Porosity (%)	Pore Diameter (in)	b_1^* or b_2^* (ft)
40.31	1/8	6.00E-06
29.31	1/4	6.20E-06
16.08	1/8	2.00E-06
16.08	1/4	2.50E-06

Table 4-5: The setups and properties for each set of experiments.

Set #	Porous wall 1	Porous wall 2	b_1	b_2	h	d	b	L
1	N/A	N/A	N/A	N/A	3	0	0.6	4
2	N/A	N/A	N/A	N/A	3	0	0.6	6
3	N/A	N/A	N/A	N/A	3	0	0.3	6
4	1/4in,29.61%	1/8in,40.31%	2.48E-05	2.40E-05	3	1	0.4	6
5	1/4in,16.08%	1/8in,40.31%	1.00E-05	2.40E-05	3	1	0.4	6
6	1/8in,16.08%	1/8in,40.31%	8.00E-06	2.40E-05	3	1	0.4	6

Chapter 5 Results for the Study of the Hydrodynamic Interactions between a Solitary Wave and a Partially Submerged Porous Wall

In this chapter, the results for the study of the hydrodynamic interactions between a solitary wave and a partially submerged porous wall are presented. By applying the analytical solutions in Chapter 2, we can acquire the analytical results of the time-variations of the free-surface elevations of the incident, reflected and transmitted waves during the process of wave-structure interactions. The comparisons of the predicted free-surface elevations obtaining from the analytical solutions with the experimental data are conducted. By utilizing the analytical solutions, the effects of the physical variables, such as wave height, submerged structural depth of the wall, and $R_\mathrm{e} b_0$ (all the cases or plots in this chapter use the same R_e value of 65882), on the reflection and transmission of an incident wave are also investigated. Horizontal forces acting on the partially submerged wall surfaces under various wave and porous wall conditions are examined. All the results in this chapter are dimensionless.

5.1 Comparisons between the Analytical Results and Experimental Data

To verify the derived analytical solutions for the interactions of a solitary wave with a partially submerged porous wall, the free-surface elevations obtained by applying Eqns. (2-29) and (2-30) are compared with the experimental measurements that were recorded by gauge 1 (incident wave and reflected waves) and gauge 2 (transmitted waves) in each experiment. In this validation study, cases with various values of the incident wave height,

H, the submerged structural depth, d, and the material constant of the porous wall, b_0, are included in the comparison plots.

For the case with $h^* = 3$ inches, d = 0.5 (submerged depth=50% of the water depth), and $b_0 = 10^{-5}$ (case 1), Figure 5-1, Figure 5-2, and Figure 5-3 present the comparisons between the analytically obtained and experimentally recorded wave elevations considering the incident wave height of 0.09, 0.21, and 0.33, respectively. The upper plot of each of these three figures (Figure 5-1(a)-Figure 5-3(a)) shows the comparisons of incident and reflected waves from both the analytical and experimental results while the lower plots (Figure 5-1(b)-Figure 5-3(b)) reveal the comparisons of transmitted waves. All the cases in this chapter use the same R_e value of 65882. As can be seen from Figure 5-1 to Figure 5-3, the incident and transmitted waves predicted by the present analytical solutions in magnitudes and phases match well with the experimental data, and for the reflected waves, in general, the variation trend including the phase from the analytical solutions agree reasonably well with the measurements, however, with slightly over-predicted wave peaks. As expected, since the analytical solutions neglect the energy dissipations, the experimentally measured reflected and transmitted waves, especially the reflected waves, due to their run-up, run down, and backward propagation, are shown to have smaller wave amplitudes than those from the analytical solutions. Also, by comparing Figure 5-1 through Figure 5-3, the errors of predicted amplitudes of reflected waves increase when the incident wave height increases due to partly the increased energy dissipation and partly the nonlinear effect of the solitary wave as the linearized approximation of the kinematic free-surface boundary condition is applied for the determination of the free surface elevations. For instance, Figure 5-2 presents the case of

$H = 0.21$ and the difference in the predication of reflected wave amplitude is slightly smaller than the difference shown in Figure 5-3, which presents the case of $H = 0.33$. Also, the linearized approximation approach misses the predictions of the oscillatory tails observed in the recorded reflected waves (Figure 5-2 and Figure 5-3).

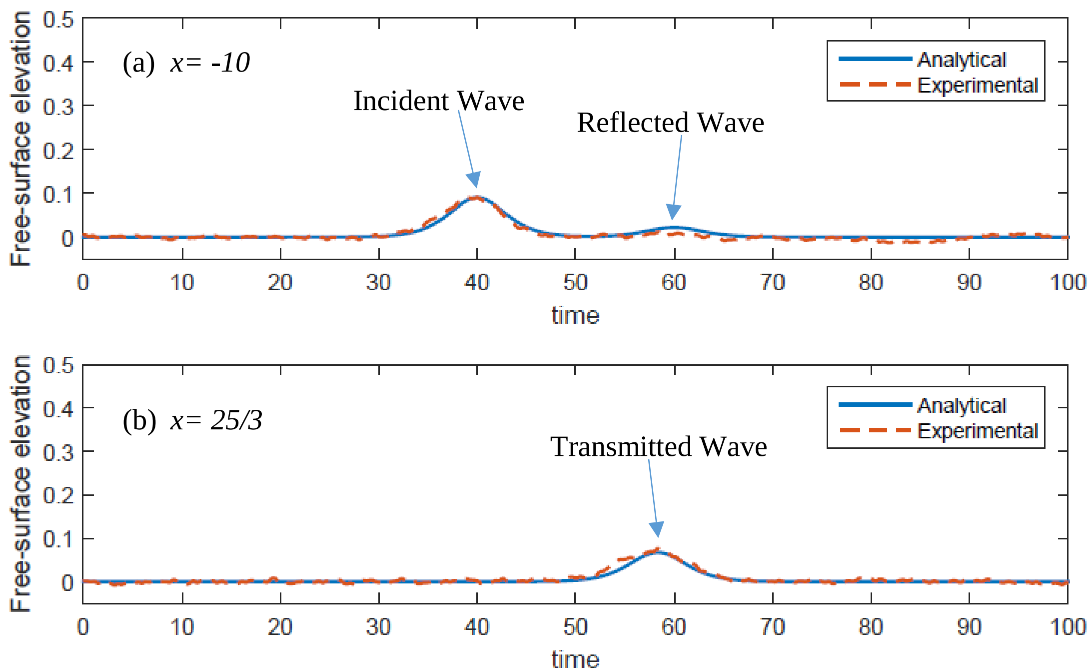

Figure 5-1: Comparisons of free-surface elevation obtained from analytical solutions and experimental measurements for $H = 0.09$, $d = 0.5$ and $b_0 = 10^{-5}$: (a) incident and reflected wave; (b) transmitted wave.

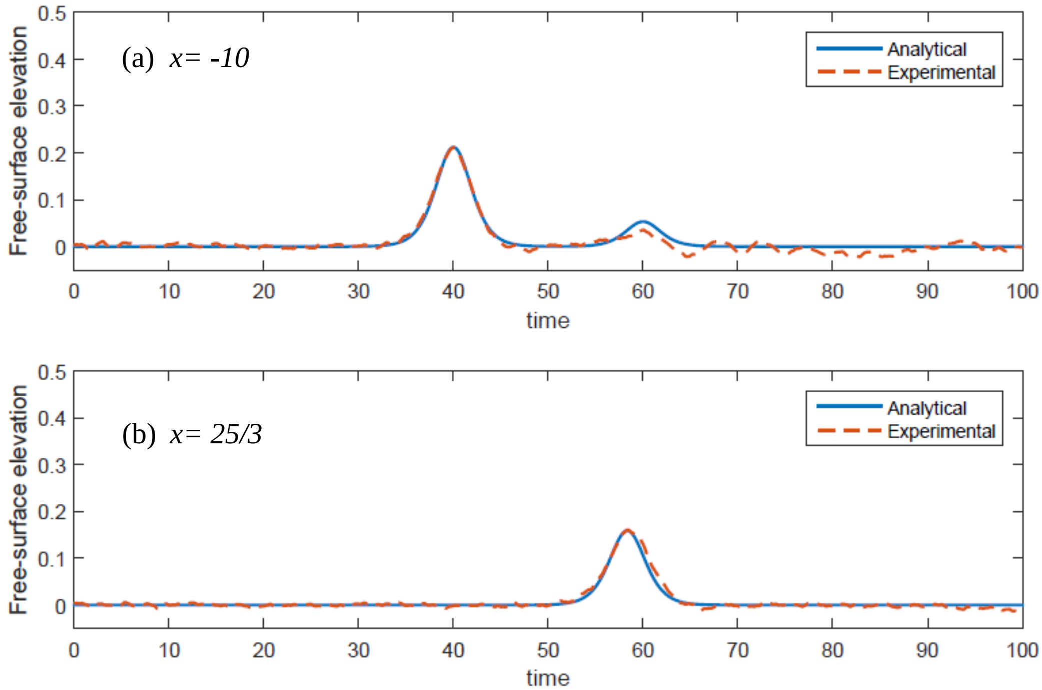

Figure 5-2: Comparisons of free-surface elevation obtained from analytical solutions and experimental measurements for $H = 0.21$, $d = 0.5$ and $b_0 = 10^{-5}$: (a) incident and reflected wave; (b) transmitted wave.

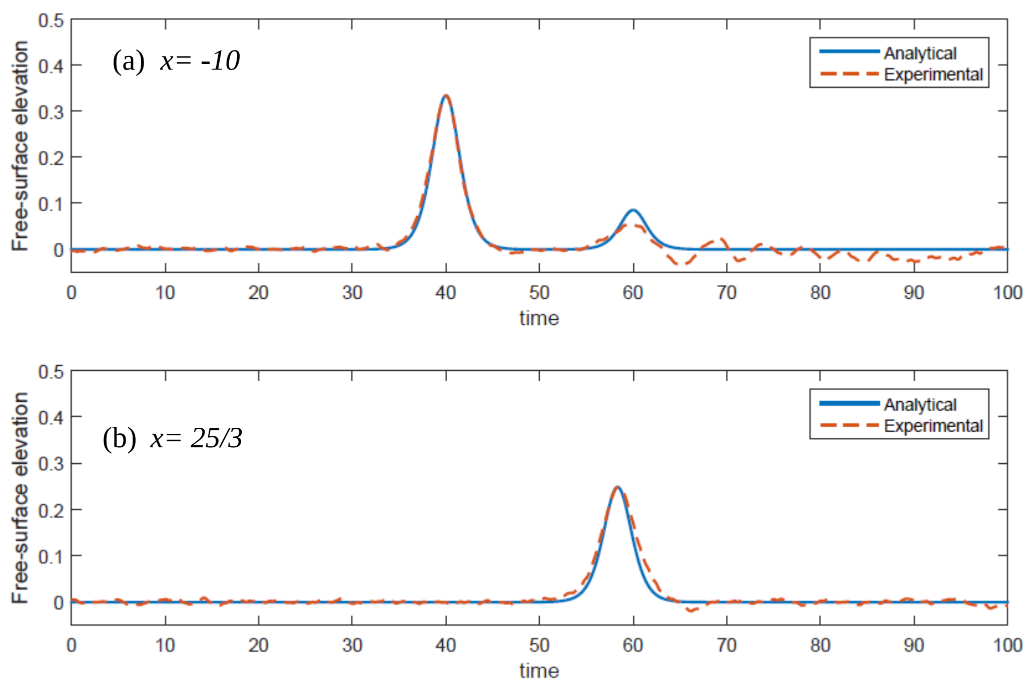

Figure 5-3: Comparisons of free-surface elevation obtained from analytical solutions and experimental measurements for $H = 0.33$, $d = 0.5$ and $b_0 = 10^{-5}$: (a) incident and reflected wave; (b) transmitted wave.

In terms of validations of the results for cases using different depths of submergence of the porous wall and its corresponding porous conditions, Figure 5-4 shows the comparisons of measurements from the gauge1 and gauge 2 with analytical solutions for the case (case 2) of a $H = 0.09$ solitary wave interacting with a porous wall, which is completely submerged (d=1) with a material constant of b_0 being equal to 10^{-5}. When comparing to the results presented in Figure 5-1 for the case of d=0.5 and $H = 0.09$, a greater reflected wave height for the case of d=1 (Figure 5-4) is noticed, which reflects that an increase in the submerged depth of the wall results in an increase in the reflected wave height. Considering the effect of porous wall property, Figure 5-5 illustrates the comparison results for the case (case 3) of a solitary wave with incident wave height $H = 0.33$ interacting with a partially submerged porous wall (d=0.5) having material constant b_0 being increased to 1.6×10^{-5}. Comparing the results shown in Figure 5-3 and Figure 5-5, it clearly indicates that by increasing b_0 the reflected wave height decreases slightly. As physically suggested when the opening of the porous wall increase (b_0 increases), the reflected wave height decreases and accordingly the transmitted wave height increases. Considering the comparisons shown in Figure 5-1 through Figure 5-5, the analytical solutions are demonstrated to be able to predict the transmitted waves well and tend to overestimate the reflected wave height for the study of interactions between a solitary wave and a partially submerged porous wall.

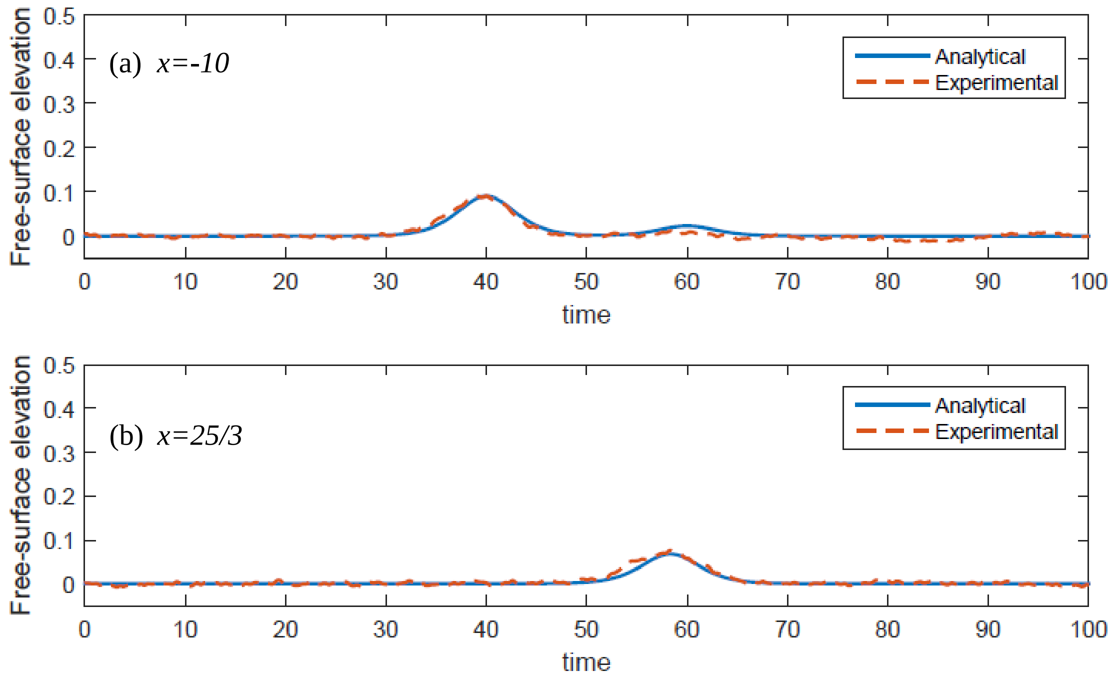

Figure 5-4: Comparisons of free-surface elevation obtained from analytical solutions and experimental measurements for $H = 0.09$, $d = 1$ and $b_0 = 10^{-5}$: (a) incident and reflected wave; (b) transmitted wave.

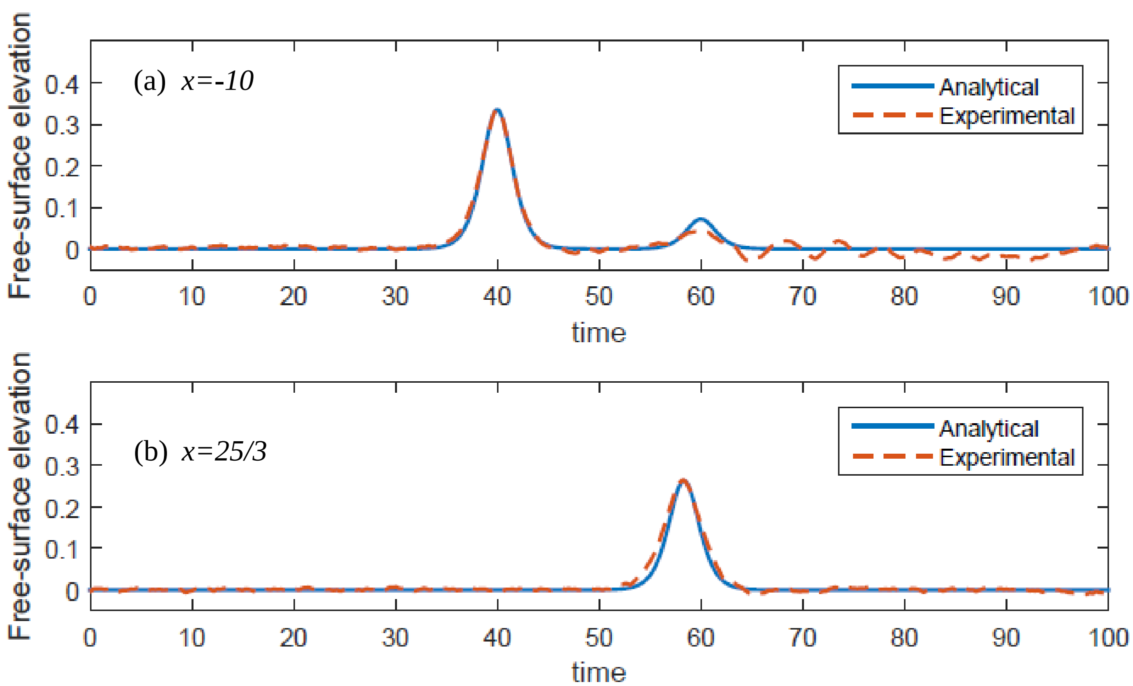

Figure 5-5: Comparisons of free-surface elevation obtained from analytical solutions and experimental measurements for $H = 0.33$, $d = 0.5$ and $b_0 = 1.6\times10^{-5}$: (a) incident and reflected wave; (b) transmitted wave.

To further the verification of the analytical results for other incident wave height conditions, Figure 5-6 plots the comparisons of analytical results of the overall transmission coefficient (transmitted wave height/incident wave height) versus incident wave height with experiment data for the cases of d=0.5 and d=1 with $b_0 = 10^{-5}$. In general, the analytical solutions and the experimental data agree reasonably well with each other especially at the setting of d=0.5. When d=1, the analytical solutions of the overall transmission coefficients are slightly higher than the experimental data. Again, this may be caused by the increased energy dissipation during the experiments which is not included in the analytical formulations.

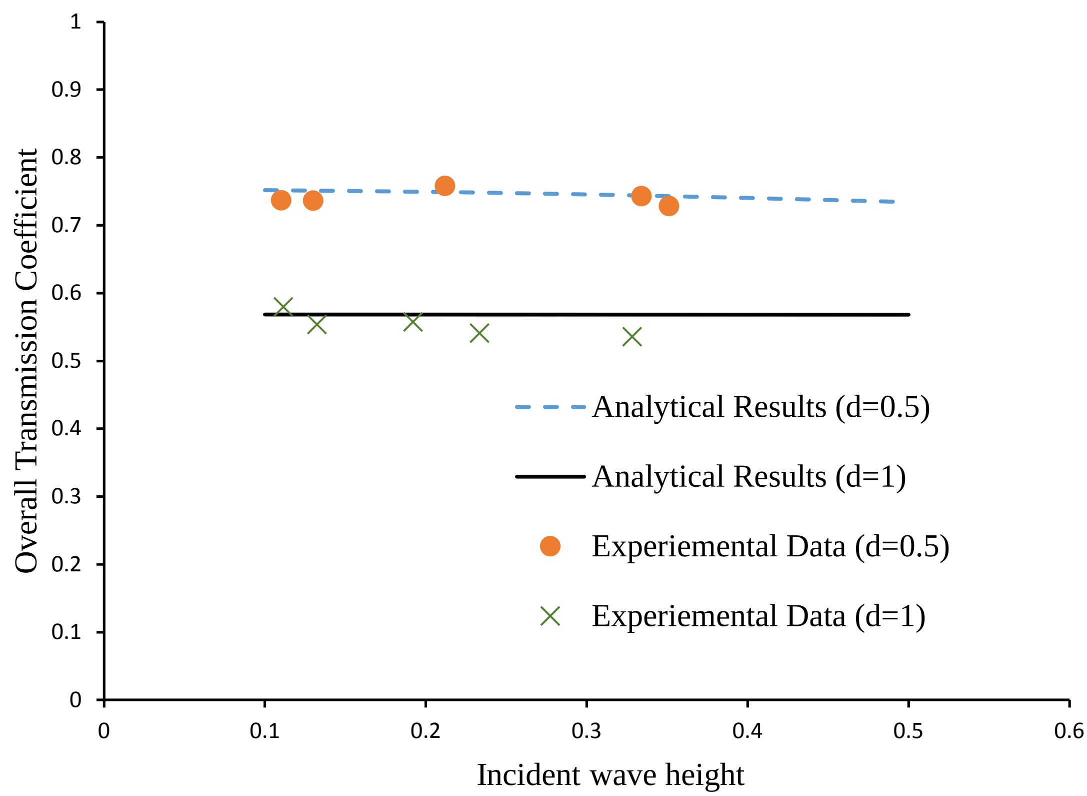

Figure 5-6: Comparisons of analytical results of the overall transmission coefficient versus incident wave height with experiment data for the cases of d=0.5 and d=1 with $b_0 = 10^{-5}$.

5.2 Parametric Study of the Effects of the Physical Variables on the Reflection and Transmission of a Solitary Wave Interacting with a Partially Submerged Porous Wall

Before carrying out the procedures of examining the effects of various physical variables on the outcomes of the reflection and transmission of a solitary wave interacting with a partially submerged porous wall, the variation behaviors of the reflection and transmission related coefficients R_0 and T_0 are discussed first. As described in Eqns. (2-27) and (2-18), the derived R_0 and T_0 are functions of the following dimensionless parameters: the submerged structural depth (draft) of the porous wall, d, the incident wave height, H, the material constant of the porous plate, b_0, and the wave number like parameter, k. Here, every specific value of k has its associated R_0 and T_0 values. Even though the physical variables for describing the interactions between a solitary wave and a partially submerged porous wall require the integration of the derived solutions through wave number k from $k = -\infty$ to $k = \infty$, the variations of the R_0 (or T_0) versus the draft of porous wall, d , or wave number k for a constant incident wave height would be interesting to examine for their effects on the eventual reflection (or transmission) coefficient. Also, through the study of the variations of the R_0 and T_0 versus d or k with and without porous effect, we can estimate the influences of the porous properties on the reflection and transmission of an incident solitary wave after interacting with a partially submerged porous wall.

For a case of a solitary wave with $H = 0.21$ interacting with a solid wall, it can be considered as a special case of the present solutions by setting the material constant of the porous plate b_0 to be equal to 0. Figure 5-7(a) and Figure 5-8(a) respectively illustrate the variations of R_0 versus d for different k values and the variations of R_0 versus k for different d values when $b_0 = 0$. The correspondingly variations for T_0 are shown in Figure

5-7(b) and Figure 5-8(b). The results indicate that when the wave number component *k* increases, the reflection related coefficient R_0 increases (or T_0 decreases). Physically, it suggests that for a given submerged wall depth the effect of R_0 on wave reflection increases (or T_0 on wave transmission decreases) when the value of *k* increases. Meanwhile, for a fixed wave number component *k*, as expected, when the submerged depth of the solid wall increases, the coefficient R_0 increases (or T_0 decreases).

It is also interesting to note for the case of larger k value, the increasing rate of coefficient R_0 is more significant in the range of small d when compare the case of smaller k value where the increasing rate is more significant when *d* is large. Reversely, the decreasing rate of coefficient T_0 for larger *k* values is more significant when the values of *d* are small. However, for the cases with smaller k value the decreasing rate of T_0 is more significant when d is large. For instance, for a case with $k = 0.5$ in Figure 5-8(b), the change of T_0 between cases of d=0.8 and d=1 is greater than that between cases of d=0.2 and d=0.4, however, for a case with k = 4, the smaller change of T_0 between conditions of d=0.8 and d=1 than that of d=0.2 and d=0.4 can be observed. Physically speaking, for a solid wall case, the initial increase of the draft of the wall tends to have more significant effect on decreasing the components of transmitted waves with higher wave number than the later increase of the submerged depth when it is already large. For the components with smaller wave number (like low frequency wave components), it is opposite, the change at the cases with larger draft has a stronger effect on decreasing those transmitted wave components. In terms of this limiting case of a partially submerged solid wall, the results in Figure 5-8 agree with the analytical solutions of a special case presented by Jaf and Wang (2015).

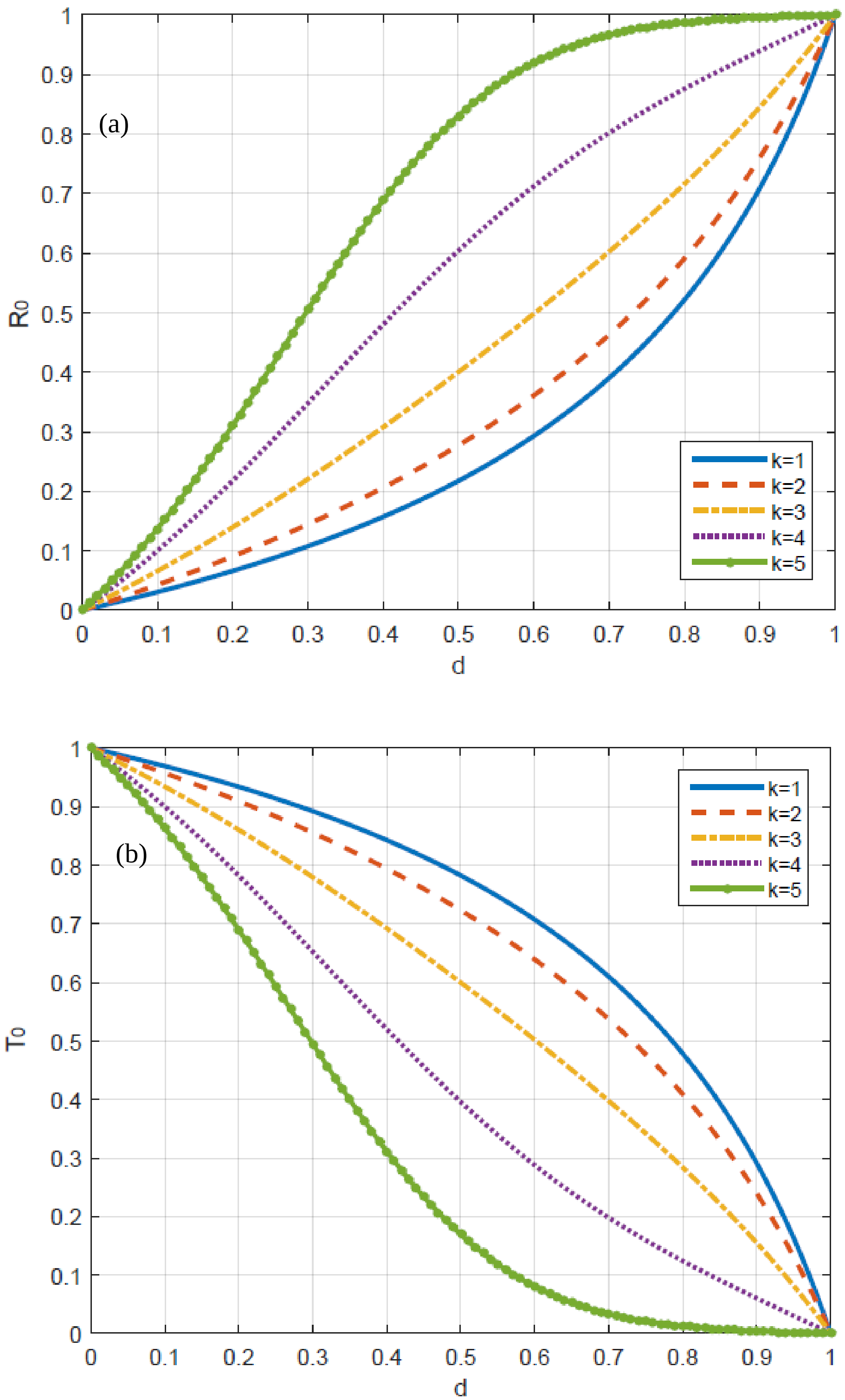

Figure 5-7: Variations of reflection and transmission related coefficients versus d for various k for a solitary wave $H = 0.21$ interacts with a solid wall: (a) R_0; (b) T_0.

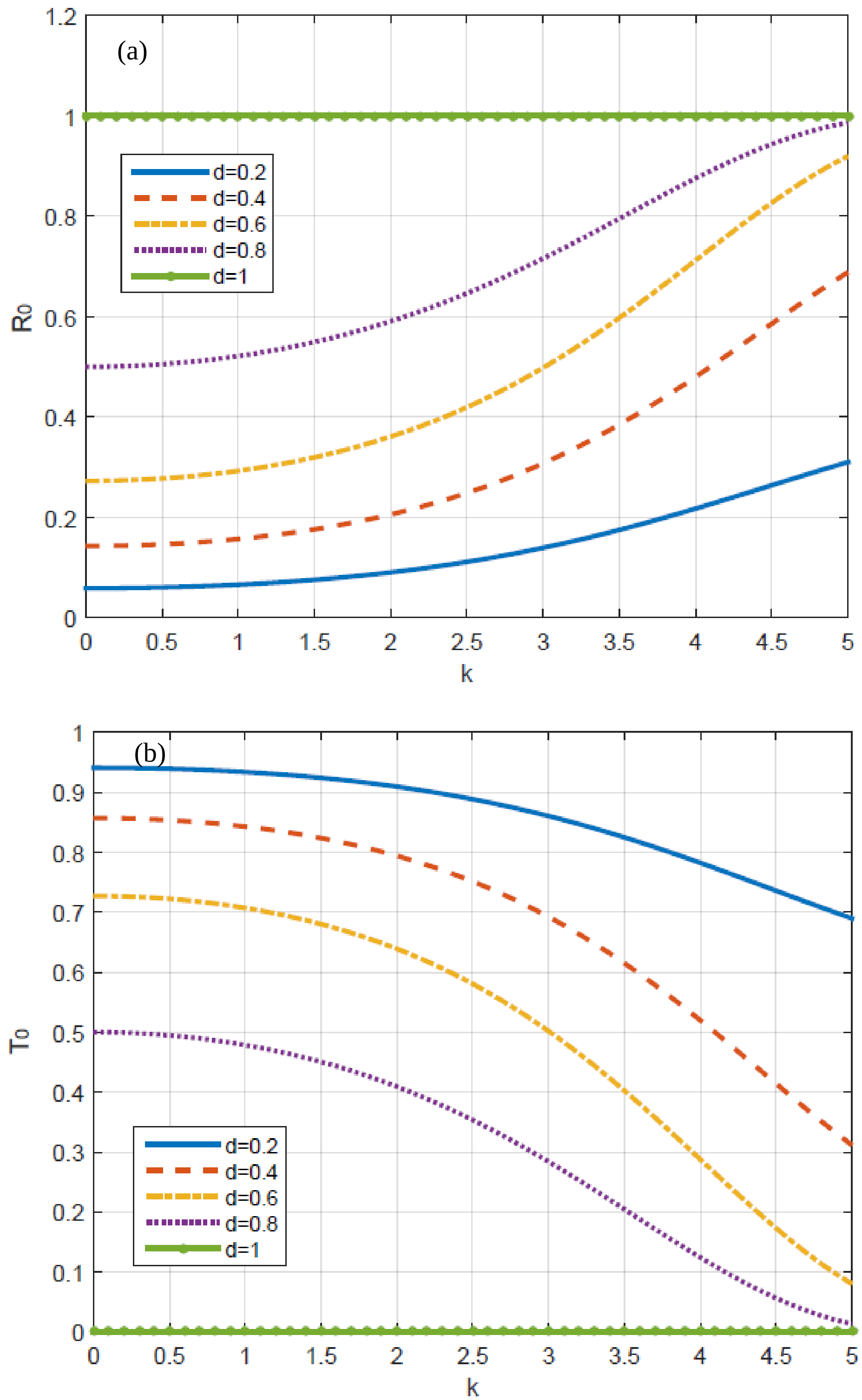

Figure 5-8: Variations of reflection and transmission related coefficients versus k for various d for a solitary wave $H = 0.21$ interacts with a solid wall: (a) R_0; (b) T_0.

In addition to the solid wall cases discussed above, the varying trend of T_0 (or R_0) for a solitary wave encountering a porous wall is also investigated. Let the incident wave height and material constant of porous wall be set as $H = 0.21$ and $b_0 = 10^{-5}$, respectively. Here, only the results of T_0 are presented. The variations of T_0 versus d for different k values and the variations of T_0 versus k for different d values are illustrated in Figure 5-9 and Figure 5-10, respectively. Since a porous structure is considered, the minimum T_0 for all k values, different from a solid wall case, reaches a constant of 0.57 when d=1. Certainly, the minimum T_0 depends on the material constant of the porous wall, b_0. Similar to the solid wall cases, for a constant k, an increase in submerged structural depth, d, the transmission related coefficient T_0 decreases. And for a constant d, when the wave number k increases, the value of T_0 decreases. However, for a porous wall case, with any given k's, the effect of pore opening makes the changes of T_0 to be more significant in the ranges of smaller d than those when d becomes large. It should be noted, for a given k, there is a corresponding transmission (or reflection) related coefficient T_0 (or R_0) and for the determination of the overall transmission (or reflection) coefficient, which is the ratio of the transmitted wave height (or reflected wave height) to the incident wave height, the integration of wave elevation solutions versus k from $k = -\infty$ to $k = \infty$ is required.

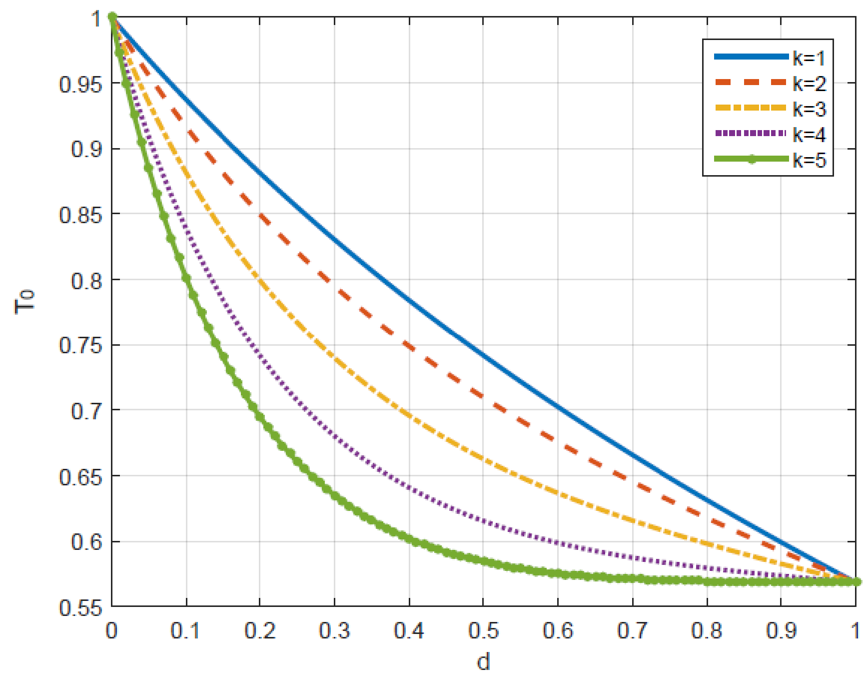

Figure 5-9: Variations of transmission coefficients versus *d* for various *k* for a solitary wave $H = 0.21$ interacts with a porous wall with $b_0 = 10^{-5}$.

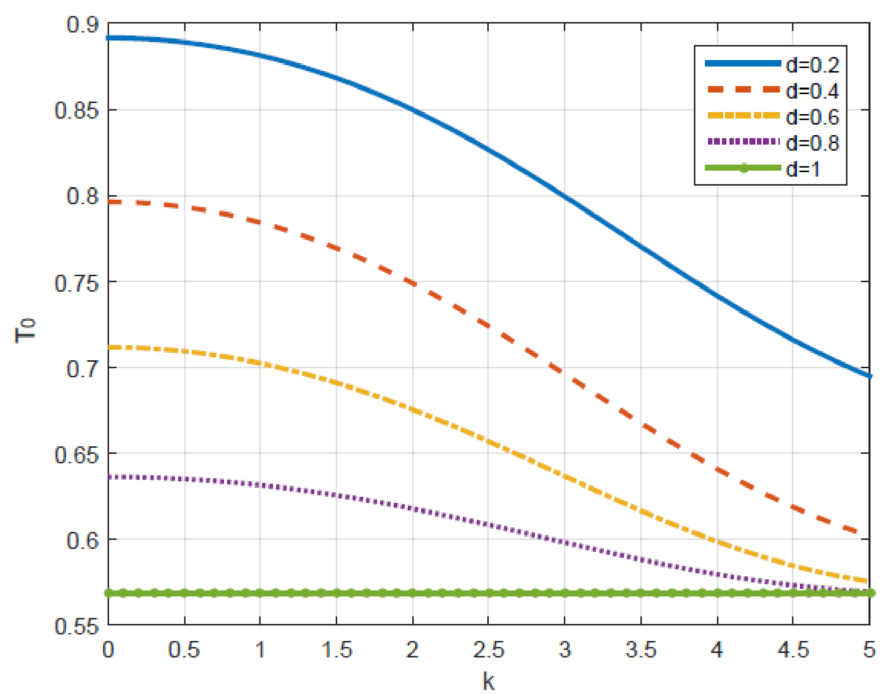

Figure 5-10: Variations of transmission coefficients versus *k* for various *d* for a solitary wave $H = 0.21$ interacts with a porous wall with $b_0 = 10^{-5}$.

5.2.1 Effect of Incident Wave Height

As noticed, the incident wave height or wave amplitude is one of the important parameters in affecting the reflection and transmission of a solitary wave interacting with a partially submerged porous wall. Results of examining the effect of incident wave height on various physical variables including the wave run-up on the porous wall, time-variation of the free-surface elevation in regions 1 and 3, and the overall transmission coefficients are presented in this section.

Figure 5-11 shows the maximum wave elevations (run-ups) of the incident wave on a solid wall of different submerged depths versus the incident wave height. The maximum crest is found to be twice of the incident wave height when the wave is subject to a complete reflection as d=1, which is slightly underestimated when comparing to those predicted by fully nonlinear approaches. It is clearly indicated that the wave run-up on the wall increases when the wave height of the incident wave increases. Also, as the submerged depth increases, the wave run-ups on the wall increase. It should be noticed that in Figure 5-11, the slope of the "d=1" line (as the increasing rate of the run-up) is greater than the slope of the "d=0.75" line. Physically speaking, for a solid wall case, the effect of incident wave height on the wave run-up increases when the submerged depth of the wall becomes larger.

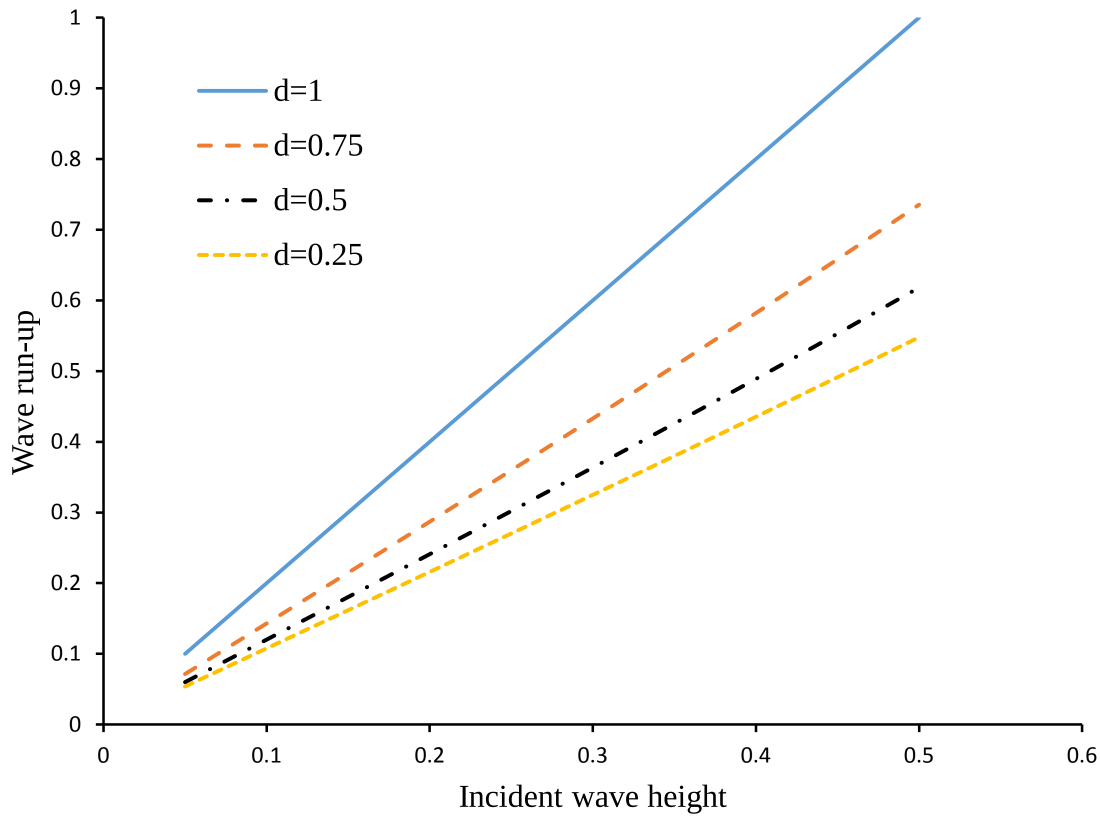

Figure 5-11: Wave run-up vs. incident wave height for solid walls with various *d*.

Now extending to porous wall cases, Figure 5-12 presents the variations of wave run-ups versus the incident wave height for various submerged depths of a porous wall with $b_0 = 10^{-5}$. Again, as expected, when the incident wave height or the submerged depth increases, the wave run-up on the wall increases. However, due to the porous effect, the values of wave run-ups for the case of *d*=1 are less than those for the cases of solid walls. Certainly, the level of decrease of the wave run-ups for a porous wall case depends on the combined wave and porous wall condition defined by the dimensionless parameter of $R_e b_0$. For both solid wall and porous wall cases, the linearly increased trend of the wave run-up as the incident wave height increases is observed.

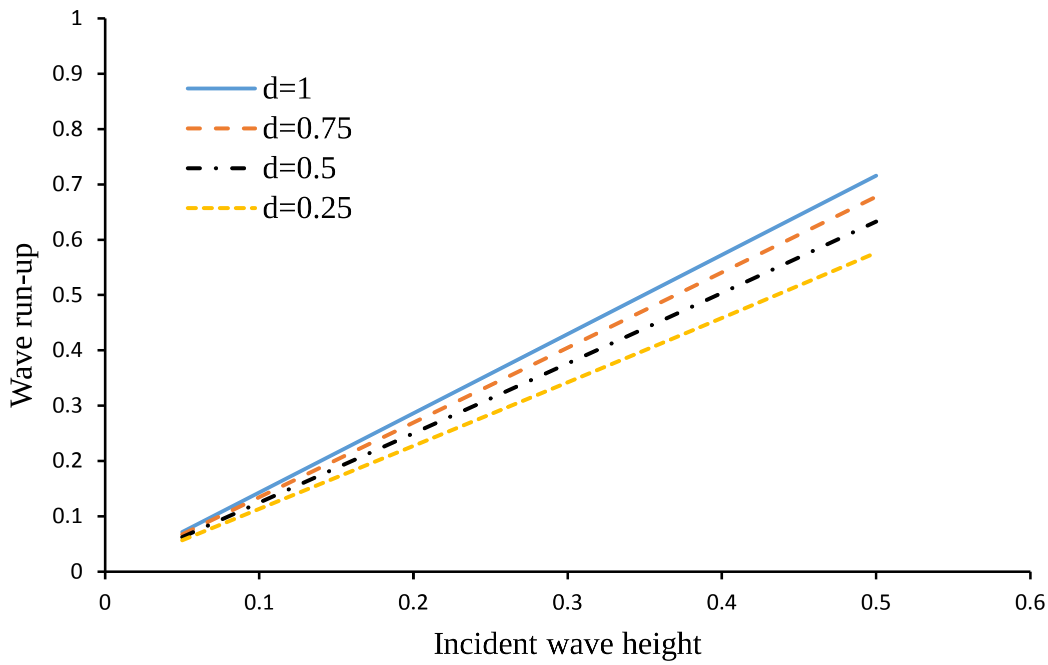

Figure 5-12: Wave run-up vs. incident wave height for porous wall with $b_0 = 10^{-5}$ with various *d*.

Figure 5-13 and Figure 5-14 display, under cases of various incident wave heights, the time variations of the free-surface elevations in regions 1 and 3 for a solid wall with two different submerged wall depths, i.e. *d*=1 and *d*=0.5, respectively. A complete reflection case can be seen in Figure 5-13 where the transmitted wave elevation equals to 0. Figure 5-14 shows the case of solitary waves interacting with a partially submerged solid wall (*d*=0.5). Both reflected and transmitted wave heights increase when the incident wave height increases. When the wall is in a partially submerged position, as expected, waves are transmitted to the region behind the wall and the reflected wave height is found to be less than that when the wall is extended to the bottom. It is interesting to note a wall with 50% opening (*d*=0.5) can allow a large portion (more than 50%) of the incident long solitary wave to be transmitted towards downstream while allows only a small wave-height wave to be reflected back.

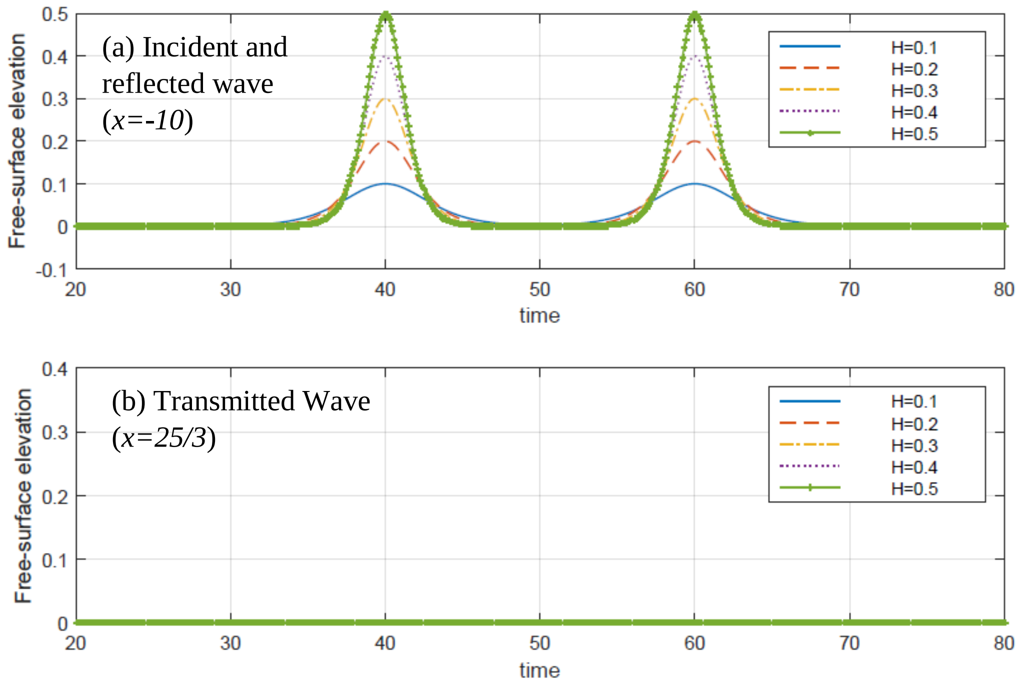

Figure 5-13: Time variations of derived analytical solutions of free-surface elevation for solitary waves with various H interact with a solid wall (d=1): (a) incident and reflected wave; (b) transmitted wave.

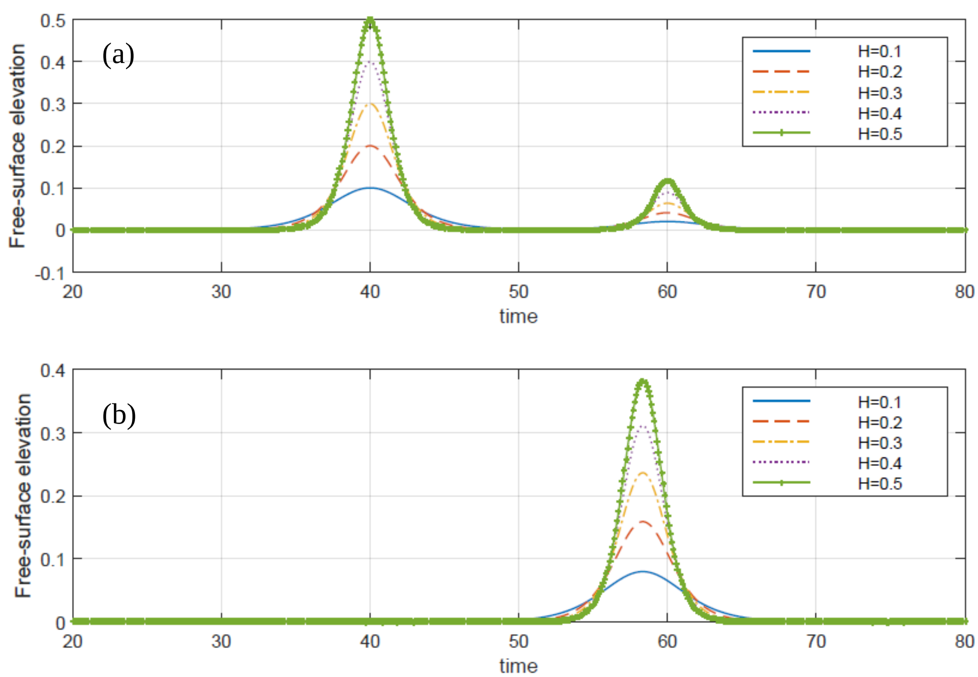

Figure 5-14: Time variations of derived analytical solutions of free-surface elevation for solitary waves with various H interact with a partially submerged solid wall (d=0.5): (a) incident and reflected wave; (b) transmitted wave.

Figure 5-15 and Figure 5-16 show the effect of incident wave height on the time variations of the free-surface elevations in regions 1 and 3 for a porous wall case of $b_0 = 10^{-5}$ with two wall heights which are d=1 and d=0.5 respectively. Similar to the solid wall cases by setting *d*=1 or *d*=0.5, however, considering a porous wall of $b_0 = 10^{-5}$, the time-variations of the free-surface elevations in regions 1 and 3 shown in Figure 5-15 and Figure 5-16, respectively suggest that when the incident wave height or the submerged structural depth increases, the reflected wave height increases and the transmitted wave height decreases. Comparing Figure 5-15 and Figure 5-16 with Figure 5-13 and Figure 5-14, generally the values of reflected wave profiles for a case with a porous wall are smaller than those using a solid wall. However, from Figure 5-14 and Figure 5-16, we notice that the values of transmitted wave profiles are larger when a partially submerged porous wall is considered. Again, the overall reflection coefficient varies according to the value of $R_e b_0$.

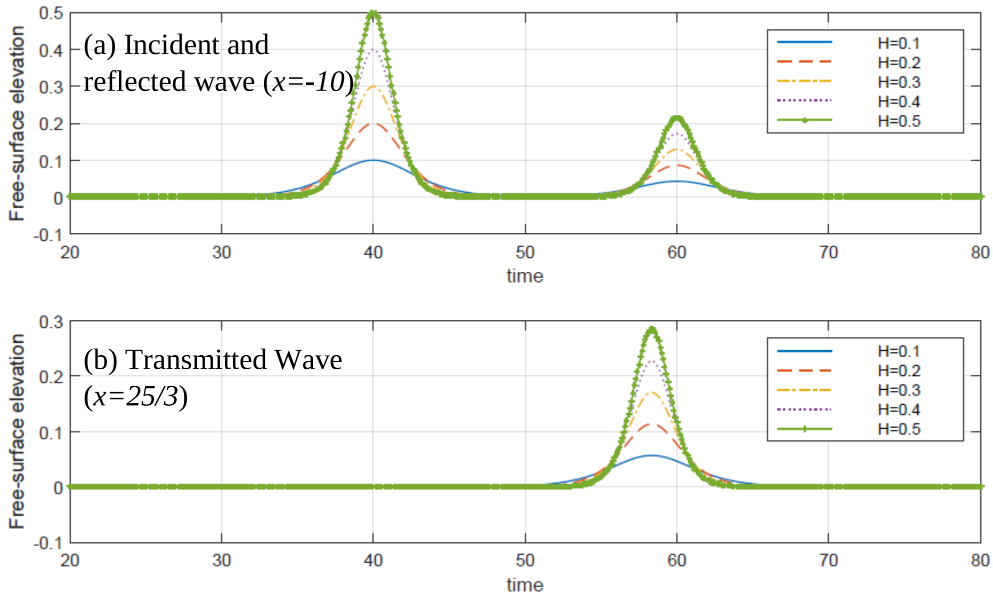

Figure 5-15: Time variations of derived analytical solutions of free-surface elevation for solitary waves with various H interact with a porous wall (d=1 and b_0 = 10^{-5}): (a) incident and reflected wave; (b) transmitted wave.

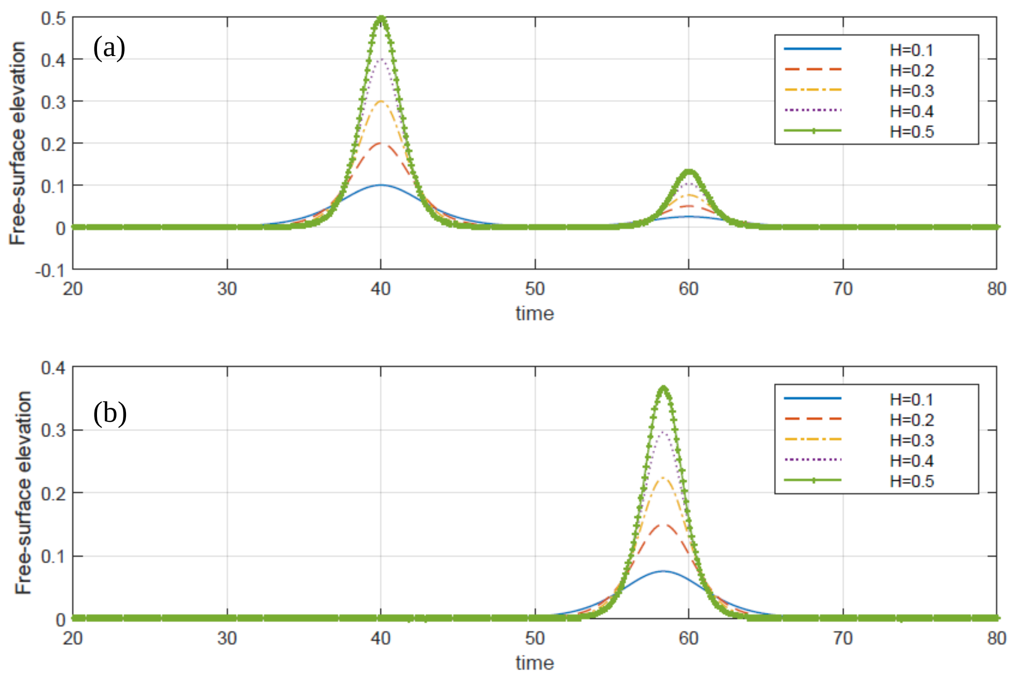

Figure 5-16: Time variations of derived analytical solutions of free-surface elevation for solitary waves with various H interact with a partially submerged porous wall (d=0.5 and b_0 = 10^{-5}): (a) incident and reflected wave; (b) transmitted wave.

In order to further the investigation of the effect of the incident wave height on the levels of reflection and transmission of a solitary wave interacting with a partially submerged porous wall, the results of overall transmission coefficients (transmitted wave height/incident wave height) are presented. For a solid wall case, Figure 5-17 shows the variations of overall transmission coefficient versus incident wave height for various submerged depth. For a submerged porous wall with $b_0 = 10^{-5}$, the transmission coefficients versus incident wave height are presented in Figure 5-18. It is can be concluded that, for either a solid or a porous wall, the observed downstream transmitted wave height when referenced to the incident wave height for any given incident wave condition is similar. This conclusion can also applied for any specified submergence of a porous or solid wall. Clearly, with an increase in submergence of either a porous or solid wall, the overall transmission coefficient decrease. Comparing results shown in Figure 5-18 and Figure 5-17, for cases with smaller submerged depths (e.g., d=0.1 or d=0.3 and d=0.5), the overall transmission coefficients for porous walls with $b_0 = 10^{-5}$ are slightly less than those for solid wall cases. However, when the submerged depth of porous wall increases, due to the additional pore areas introduced on porous walls, the transmission coefficients become much larger when compared to those under the solid wall conditions.

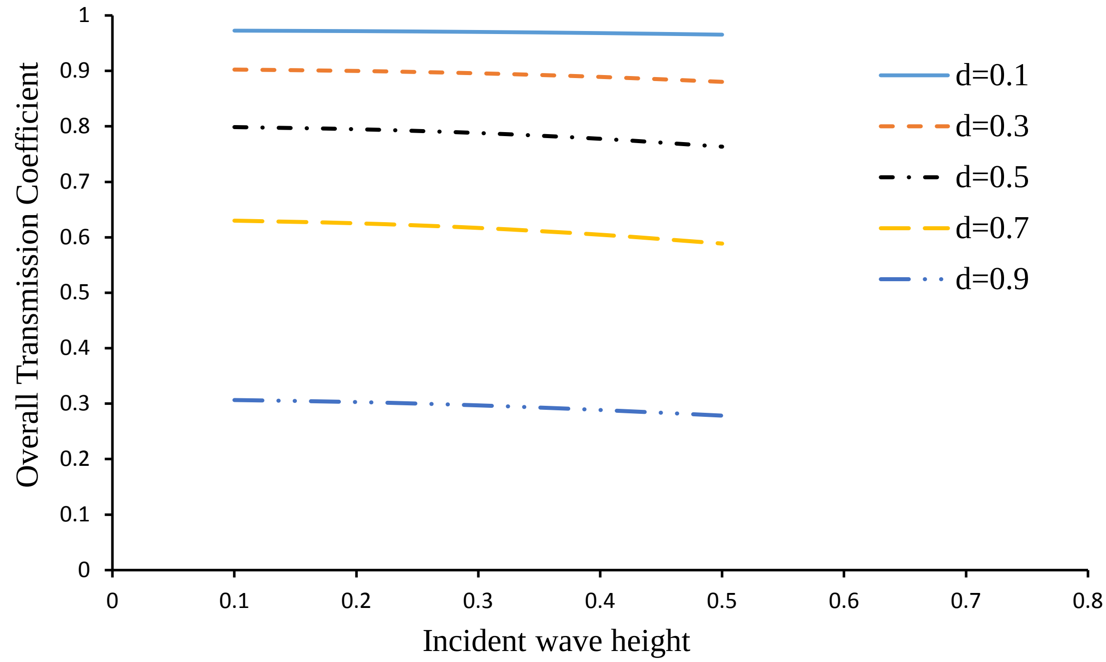

Figure 5-17: The overall transmission coefficient vs. incident wave height for various d for a solid wall case.

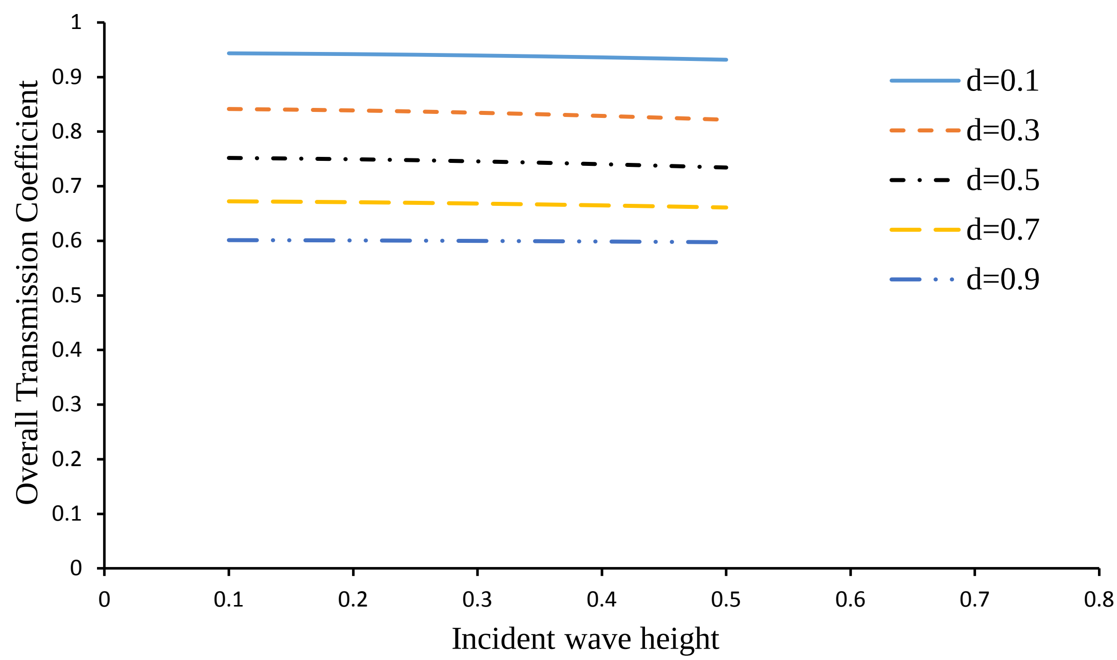

Figure 5-18: The overall transmission coefficient vs. incident wave height for various d for a porous wall case with $b_0 = 10^{-5}$.

5.2.2 Effect of the Submerged Structural Depth

The submerged structural depth d is a very critical parameter in the study of the reflection and transmission of a solitary wave interacting with a partially submerged porous wall. Similar physical variables including the wave run-ups on the porous wall, time variations of the free-surface elevations in regions 1 and 3, and the overall transmission coefficients are selected for the analyses.

A limiting case of $b_0 = 0$ (solid wall) is examined first. Figure 5-19 displays the variations of wave run-ups versus the submerged depth for various incident wave heights encountering a solid wall. It can be found that as the submerged depth increases the wave run-up increases, and clearly the relationship between the wave run-ups and the submerged depth is non-linear. Accordingly, when the submerged depth is small its effect on wave run-up is not as significant as that when the submerged depth is large. It should also be noticed that as the incident wave height become larger, the non-linear increasing trend of the wave run-up becomes more obvious. For the case of a porous wall with $b_0 = 10^{-5}$, the results of wave run-up versus the submerged depth with various inputs of incident wave heights are illustrated in Figure 5-20. Similar conclusions as for the case of a sold wall can be made that the wave run-up increases with an increase in submerged depth. However, in terms of the variation trend of the wave run-up by increasing the submerged depth, different from the solid wall case, for a porous wall with $b_0 = 10^{-5}$, the wave run-up shows a gradual increase and gives a relatively linear response with the submerged depth, especially for cases with $H \leq 0.3$. Comparing results shown in Figure 5-19 and Figure 5-20, clearly, we can notice that by extending a porous wall to near the sea bottom, the wave run-up can be substantially reduced.

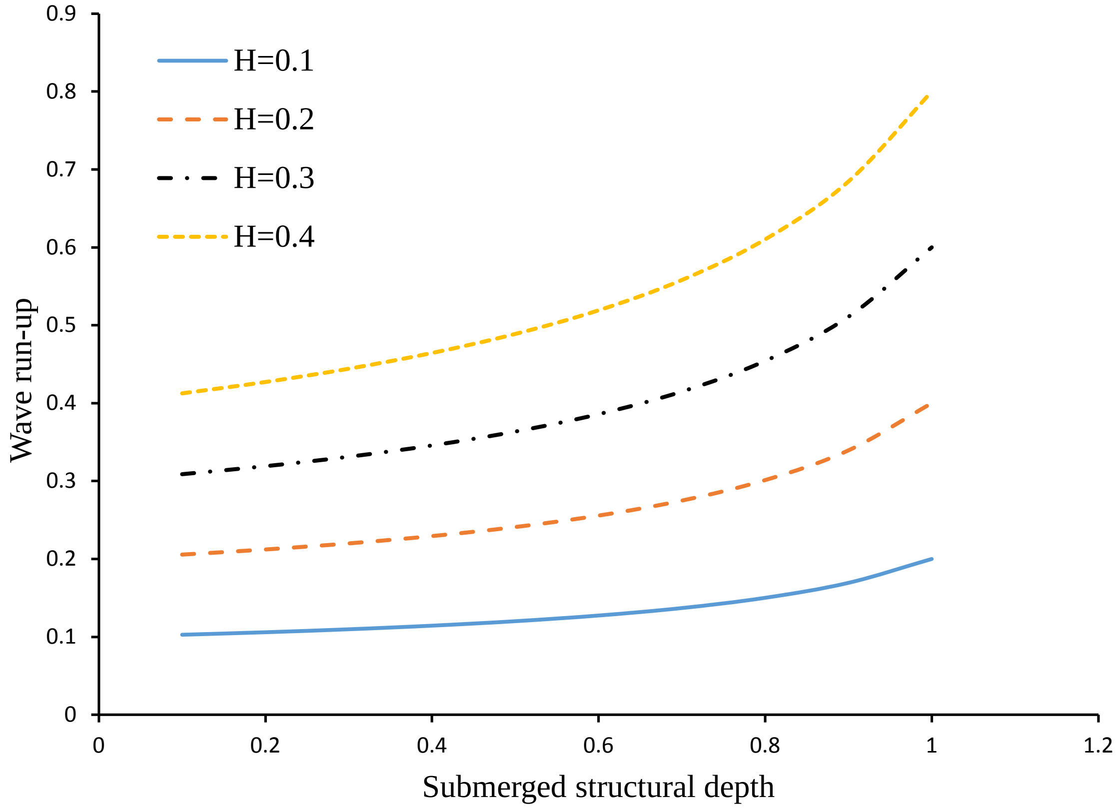

Figure 5-19: Wave run-up vs. submerged structural depth of solid walls with various *H*.

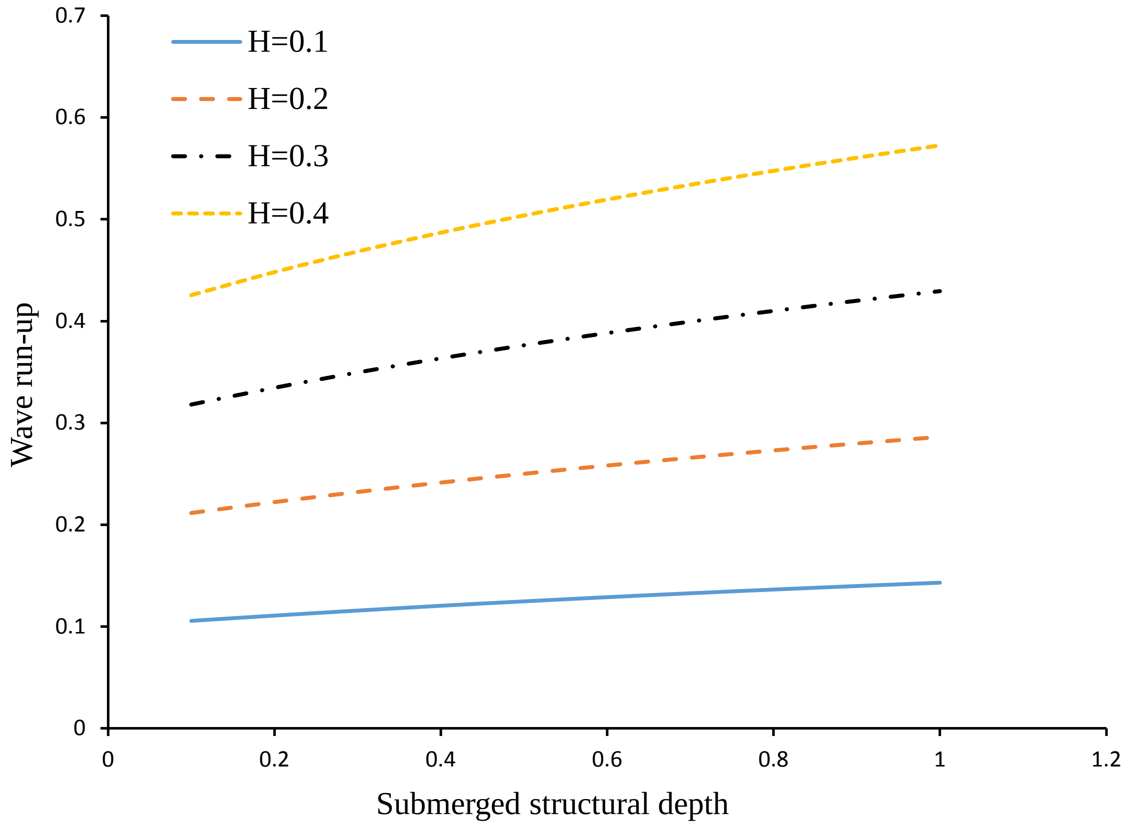

Figure 5-20: Wave run-up vs. submerged structural depth of porous wall with various H.

Figure 5-21 shows the time-variations of the free-surface elevations in regions 1 and region 3 for various submerged depths under the condition of a giving wave height $H = 0.3$ when the limiting case of a solid wall case is considered. Again, the complete reflection is observed when the solid wall is extended to the sea bottom (d=1). In general, when the submerged depth increases, the level of reflected waves increases whereas the transmitted waves decrease. As mentioned in previous section, it can also be noticed from Figure 5-21 that when the submerged depth become larger, its influence on the reflected (or transmitted) waves becomes more significant. It is also an indicator of the nonlinear varying trends of reflected and transmitted wave heights under the changes of submerged depth of a partially submerged solid wall.

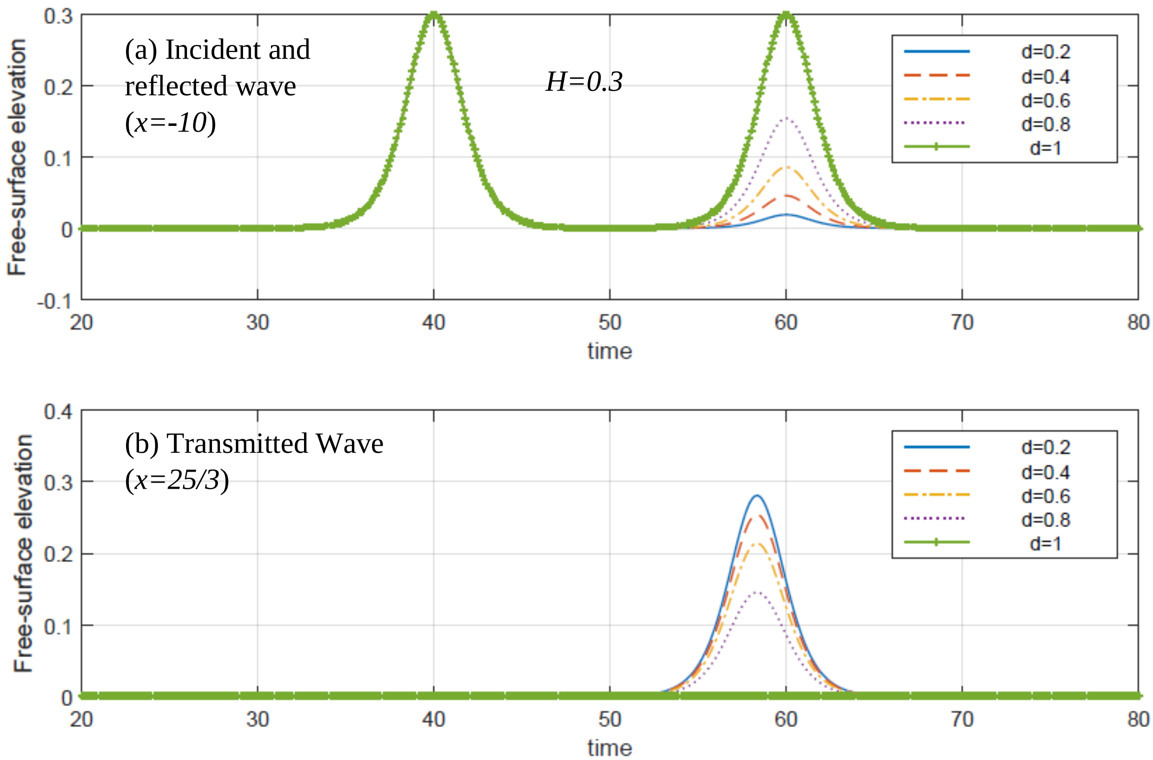

Figure 5-21: Time variations of derived analytical solutions of free-surface elevation for solitary waves with a constant *H* of 0.3 interact with solid walls with various *d*: (a) incident and reflected wave; (b) transmitted wave.

For a partially submerged porous wall case, Figure 5-22 illustrates the time-variations of the free-surface elevations in regions 1 and region 3 for $b_0 = 10^{-5}$, $H = 0.3$, and various submerged depths. The reflected wave height increases and the transmitted wave height decreases as the submerged depth increases. It can be seen when a completely submerged porous wall is used, both the reflected and transmitted wave heights can be effectively reduced.

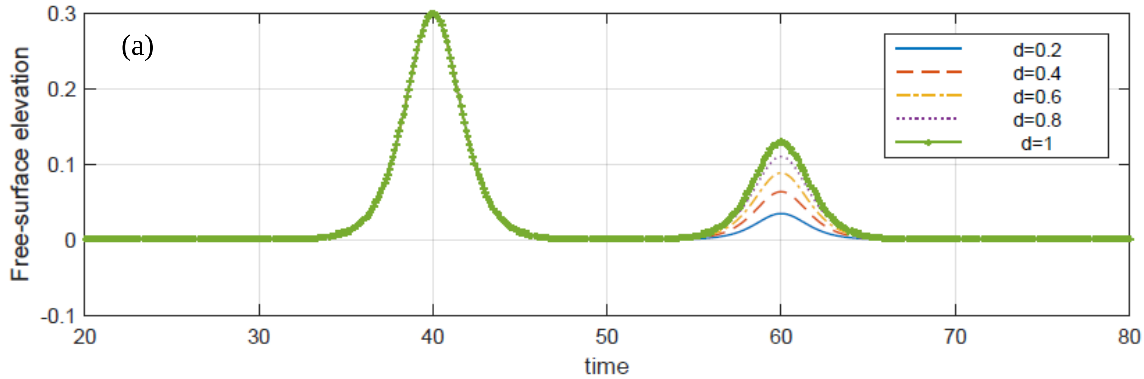

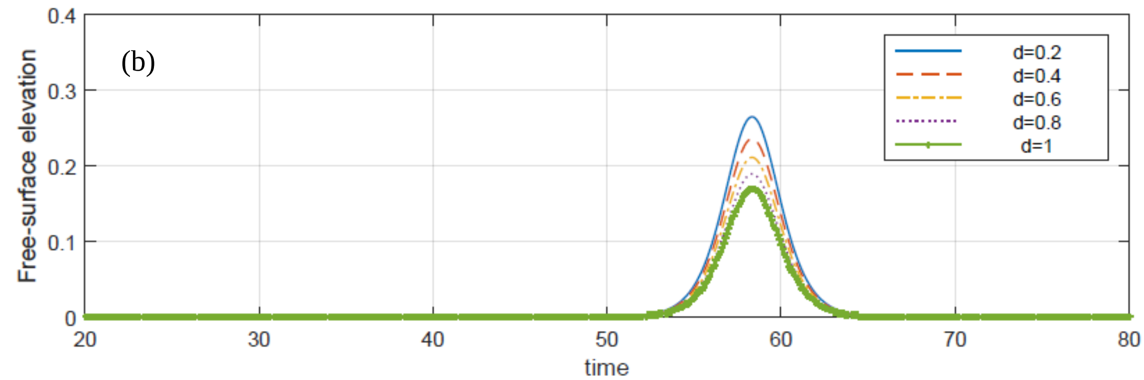

Figure 5-22: Time variations of derived analytical solutions of free-surface elevation for solitary waves with a constant H of 0.3 interact with porous walls with various d ($b_0 = 10^{-5}$): (a) incident and reflected wave; (b) transmitted wave.

In terms of the overall reflection coefficient (C_R = reflected wave height/incident wave height) or transmission coefficient (C_T = transmitted wave height/incident wave height) under the influence of submerged depth of a solid wall ($b_0 = 0$), Figure 5-23 presents the variations of C_T versus the submerged depth for cases with H = 0.3 and various incident wave heights. It is clearly shown that the submerged depth d is a dominant parameter on affecting the variations of the overall transmission coefficient while the incident wave height has an insignificant effect on the overall transmission coefficient. As the submerged depth increases, the overall transmission coefficient decreases, and the decreasing rate of C_T increases when the submerged depth becomes larger.

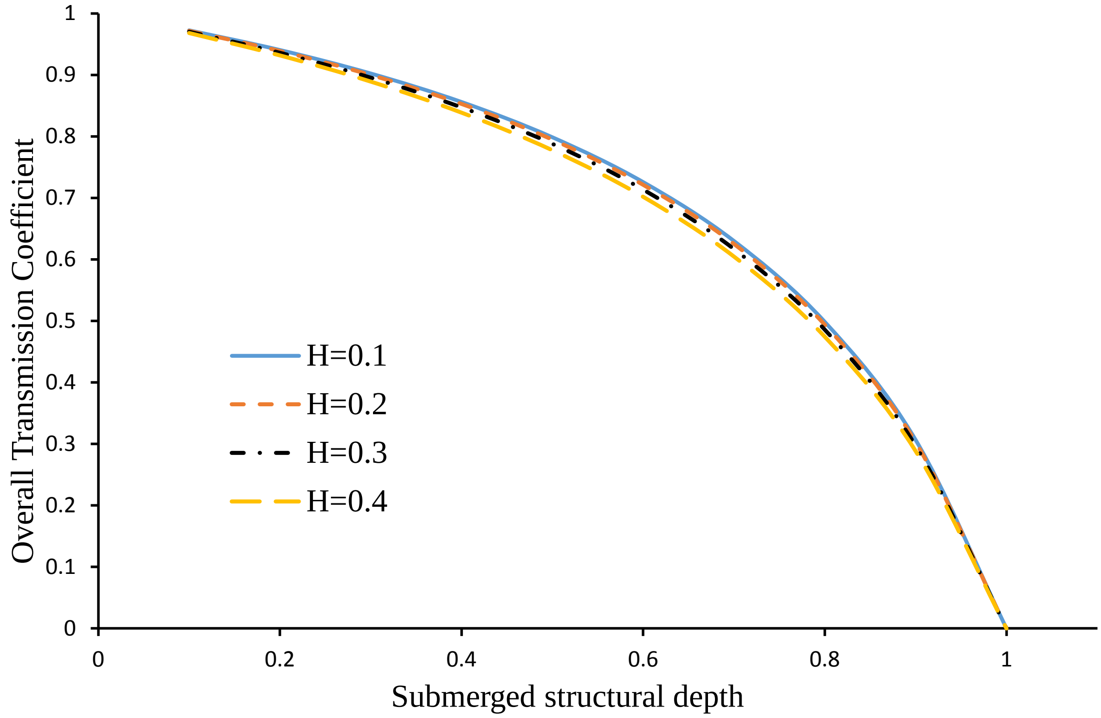

Figure 5-23: The overall transmission coefficient vs. submerged structural depth for various H for a solid wall case.

For a H = 0.3 incident solitary wave, Figure 5-24 presents the overall transmission coefficient, C_T, versus the submerged depth for a porous wall having $b_0 = 10^{-5}$. It is also concluded that the overall transmission coefficient decreases when the submerged depth of the porous wall increases. Different from the results shown in solid wall cases, a nearly linear decreasing trend of C_T when increasing the submerged depth can be observed. The other important controlling factor, porous property of a porous wall, needs to be examined to further the understanding of the varying trend of the overall transmission (or reflection) coefficient.

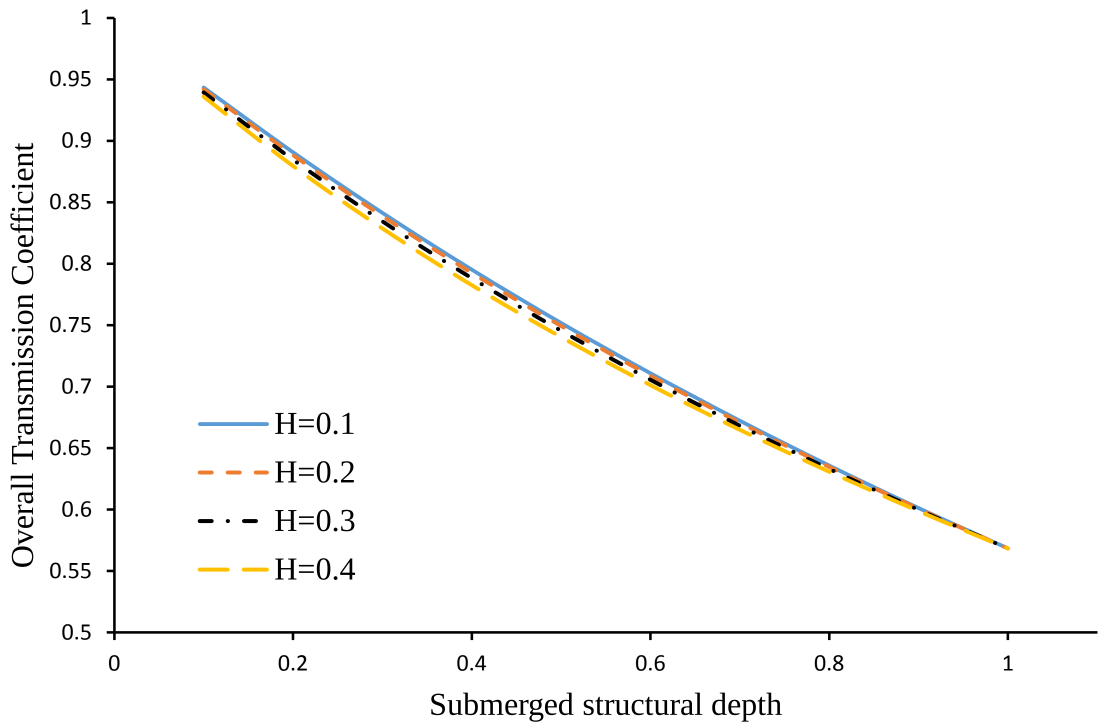

Figure 5-24: The overall transmission coefficient vs. submerged structural depth for various H for a porous wall case with $b_0 = 10^{-5}$.

5.2.3 Effect of the Porous-Effect Parameter

As the dissertation title suggested, this study focuses on the interactions between a solitary wave and a partially submerged porous wall, so it is critically important to examine the effects of the porous wall and fluid flow conditions on the reflection and transmission properties of an incident solitary wave. The $R_e b_0$ defined in Chapter 3 can be used as a dimensionless parameter representing the combined porous and fluid flow condition since b_0 is the material constant of the porous wall describing the porous condition while R_e is a Reynolds number like constant expressing the fluid flow condition. When R_e is set to be a constant, then $R_e b_0$ can be viewed as a porous-effect parameter. In this Section, the effect of $R_e b_0$ on the physical variables of wave run-ups on the porous wall, time variations of the free-surface elevations in regions 1 and 3, and the overall transmission coefficients are discussed.

First, the variations of wave run-up versus $R_e b_0$ for various incident wave heights under the setting of a completely submerged porous wall (d=1) are presented in Figure 5-25. It is found that for a completely submerged wall, the wave run-up reflects a nonlinear decreasing trend when $R_e b_0$ increases. For smaller values of $R_e b_0$, more apparent variations of wave run-ups are observed , however, when $R_e b_0$ becomes larger, its effect on wave run-up becomes insignificant. Also, as the incident wave height increases, stronger nonlinear decreasing trends of the wave run-up as $R_e b_0$ increases can be noticed.

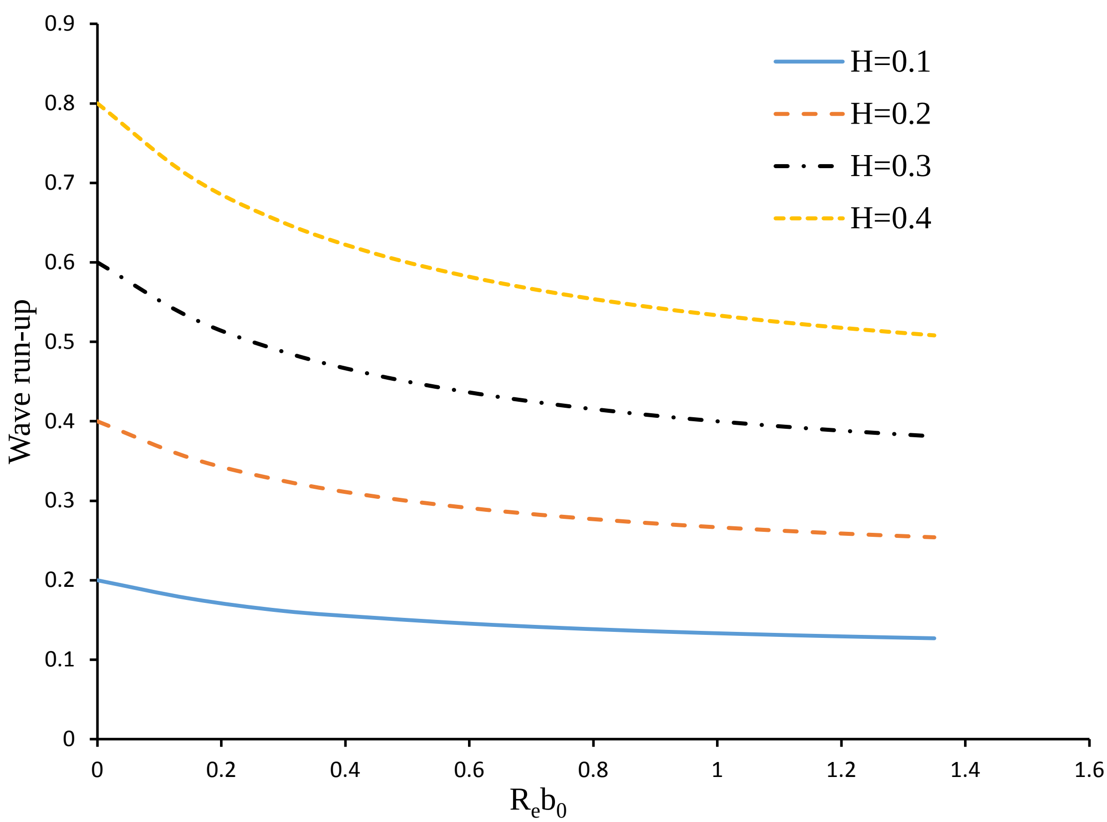

Figure 5-25: Wave run-up vs. the $R_e b_0$ with various H for a complete submerged wall (d=1).

Figure 5-26 shows the wave run-ups versus $R_e b_0$ for various incident wave heights when a porous wall is set at partially submerged position with *d*=0.5. It is found that for a partially submerged porous wall with a 50% opening, the effect of $R_e b_0$ on the wave run-ups is not significant, and the variation trend of wave run-up is close to linear when the incident wave height is small. This suggests that the 50% opening beneath the porous wall overtakes the effect of the porous-effect parameter.

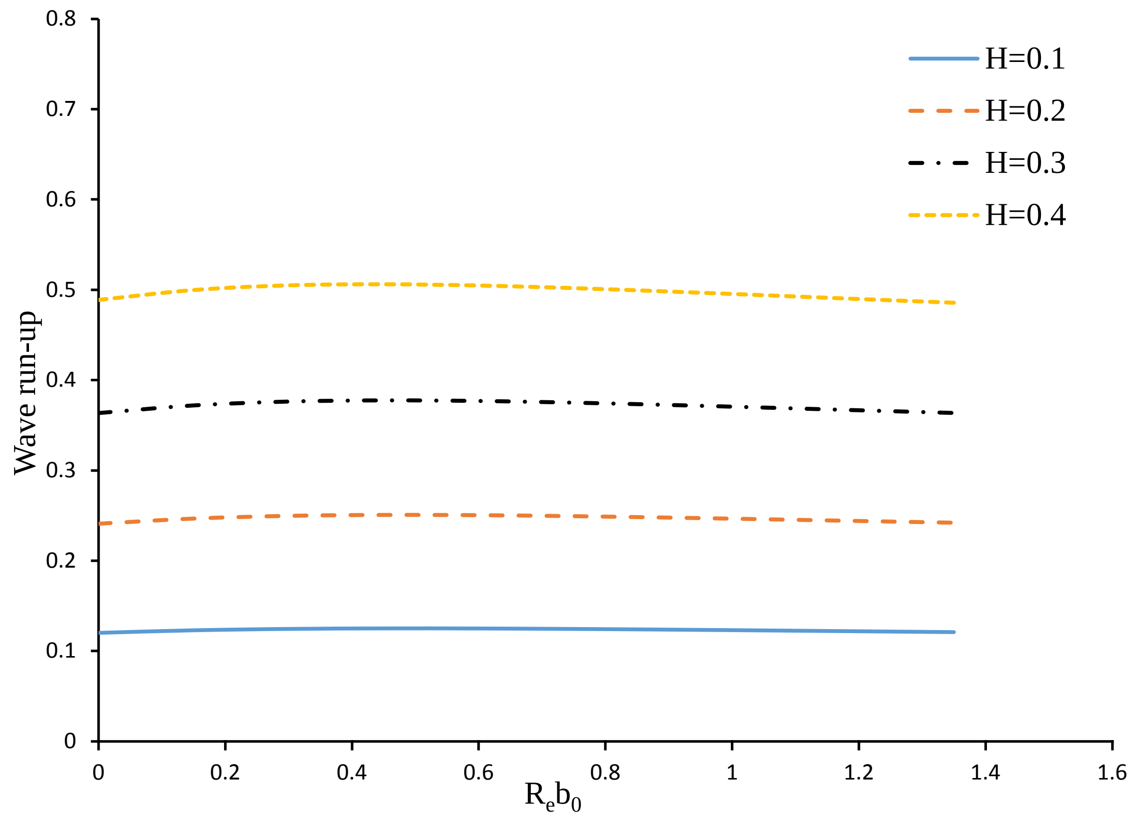

Figure 5-26: Wave run-up vs. the $R_e b_0$ with various *H* for a partially submerged wall (*d*=0.5).

In order to further the investigation of the effect of the $R_e b_0$ on the wave run-ups for the partially submerged conditions, Figure 5-27 show the plots of wave run-ups versus $R_e b_0$ with various submerged depths and a giving constant incident wave height of 0.2. It can be clearly noticed that when the submerged depth of wall is small the effect of $R_e b_0$ on the wave run-ups is insignificant and as the submerged depth become large, the effect of $R_e b_0$ on wave run-ups become more apparent. Also, for cases with smaller submerged depths (e.g. *d*=0.2 or *d*=0.4), it is interesting to note the overall maximum wave run-up in each case, although is not much different from the value under a solid wall case ($R_e b_0 = 0$), take place under a porous wall condition with an associated value of $R_e b_0$. This may be a result of the reduction of transmitted waves under a porous wall and large opening (or smaller *d*) condition that enhances slightly the wave run-up for later development of the reflected waves.

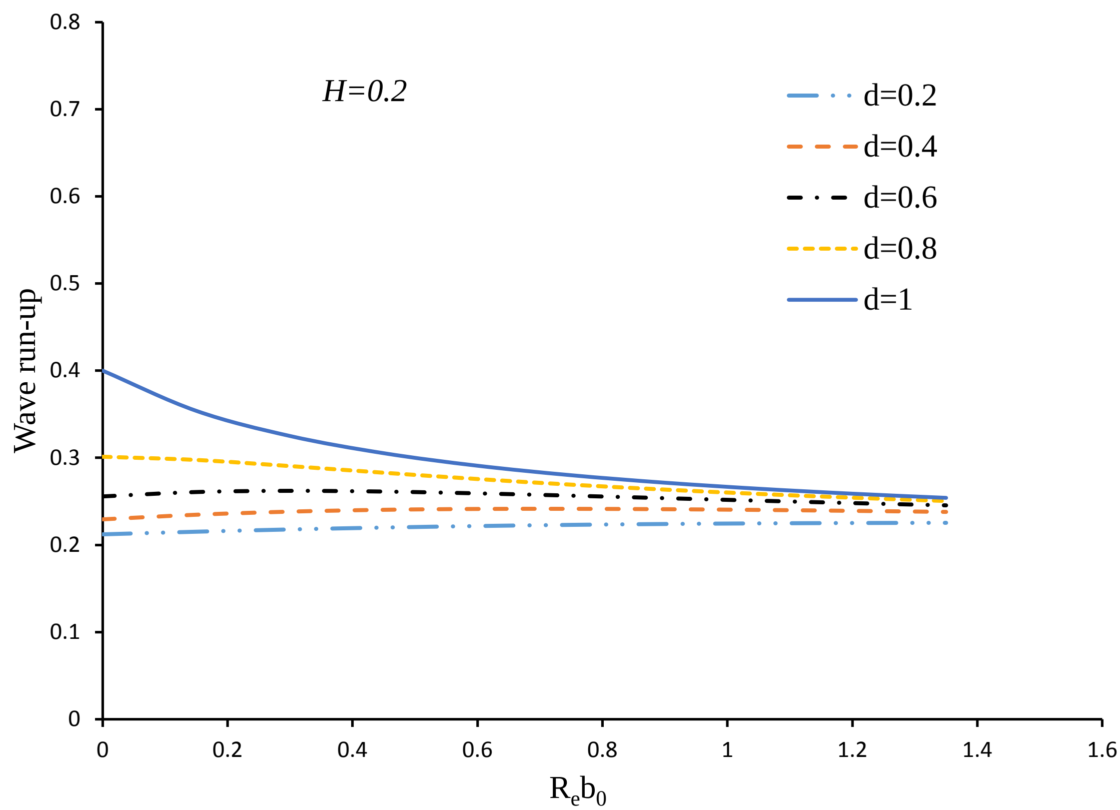

Figure 5-27: Wave run-up vs. the $R_e b_0$ with various *d* for a case of *H*= 0.2.

The time variations of free-surface elevations in regions 1 and region 3 with varying $R_e b_0$ for cases of a constant incident wave height of 0.3 and submerged depths of 1 and 0.5 are respectively illustrated in Figure 5-28 and Figure 5-29. Comparing these two figures, we notice when the wall is completely submerged (i.e., *d*=1), the effect of $R_e b_0$ on both reflected and transmitted wave heights is significant, and when the level of submergence becomes smaller (e.g., *d=0.5*), the effect become less significant. When comparing results for a solid wall and a porous wall cases with *d*=0.5, it appears that the reflected wave height from a solid wall case is slightly less than that from each of porous wall cases while the transmitted wave height are slightly larger for a solid wall case.

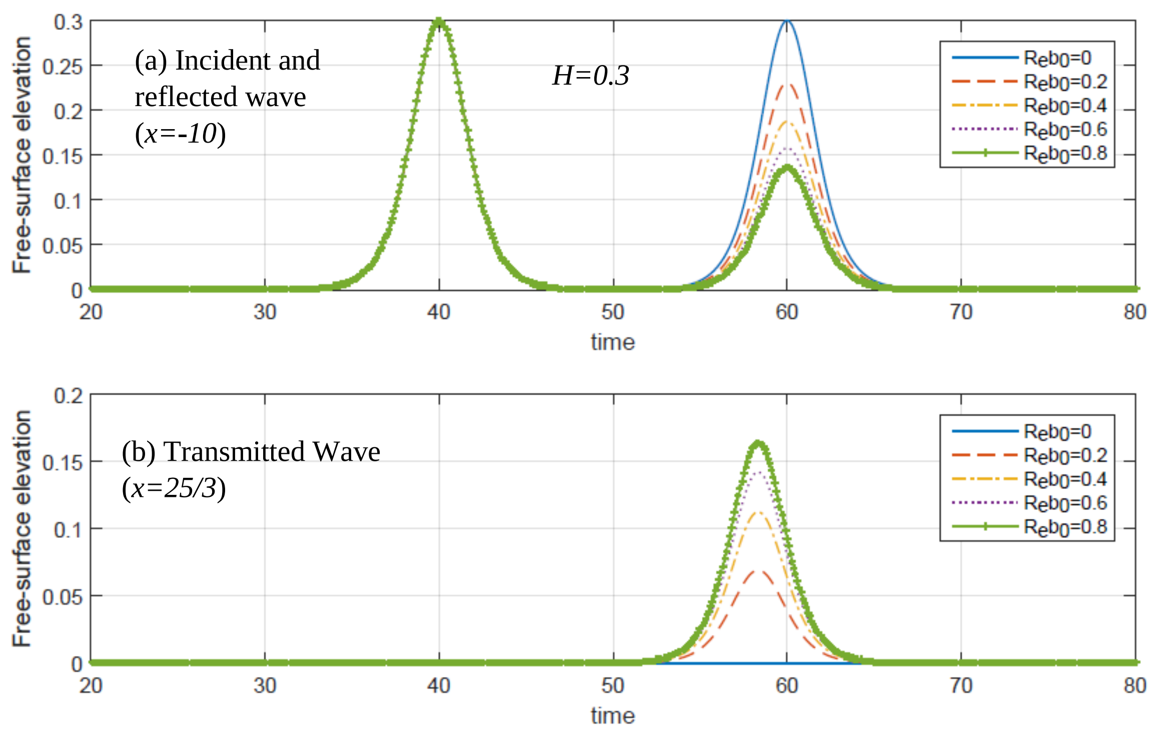

Figure 5-28: Time variations of derived analytical solutions of free-surface elevation for solitary waves with a constant *H*=0.3 interacts with porous walls (*d=1*) with various $R_e b_0$: (a) incident and reflected wave; (b) transmitted wave.

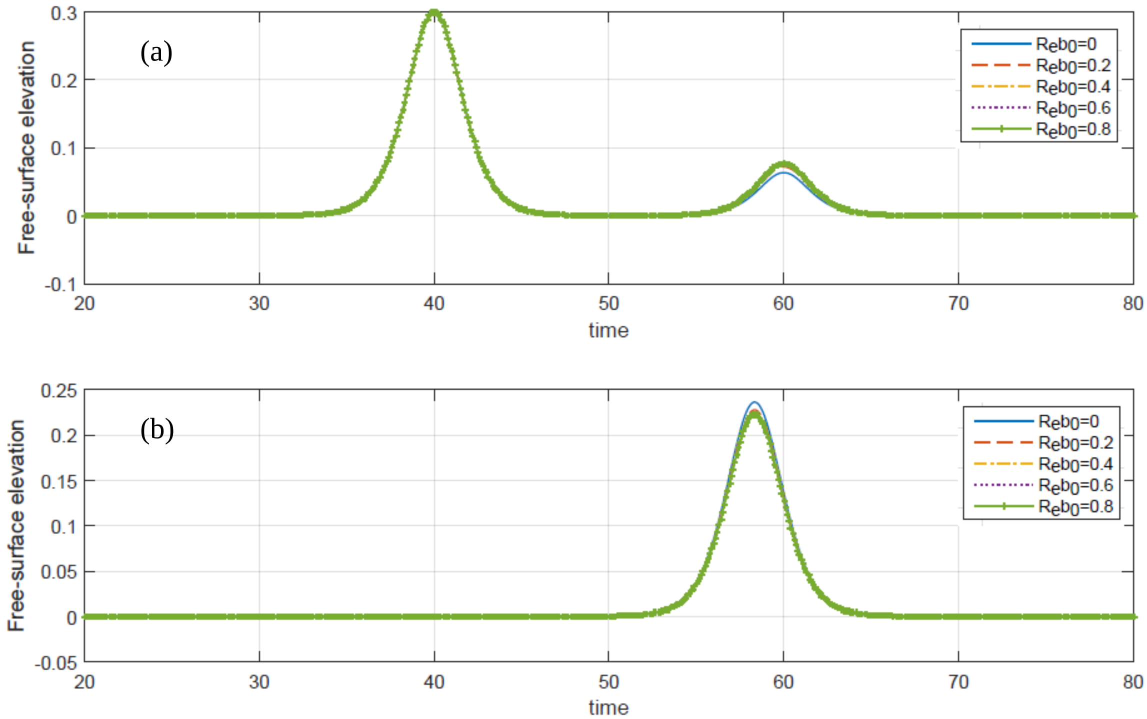

Figure 5-29: Time variations of derived analytical solutions of free-surface elevation for solitary waves with a constant *H=0.3* interacts with porous walls with various the $R_e b_0$: (a) incident and reflected wave; (b) transmitted wave.

The overall transmission coefficient is plotted versus $R_e b_0$ for a completely submerged wall case in Figure 5-30. It is found that the overall transmission coefficient increases when $R_e b_0$ increases for a completely submerged wall. The increasing trend of the overall transmission coefficient versus $R_e b_0$ is nonlinear. Meanwhile, no difference in terms of the variation trend of the overall transmission coefficient by varying incident wave height is noticed. As a result, we can conclude that for a completely submerged wall, the $R_e b_0$ is a dominant affecting parameter on the variations of the overall transmission coefficient.

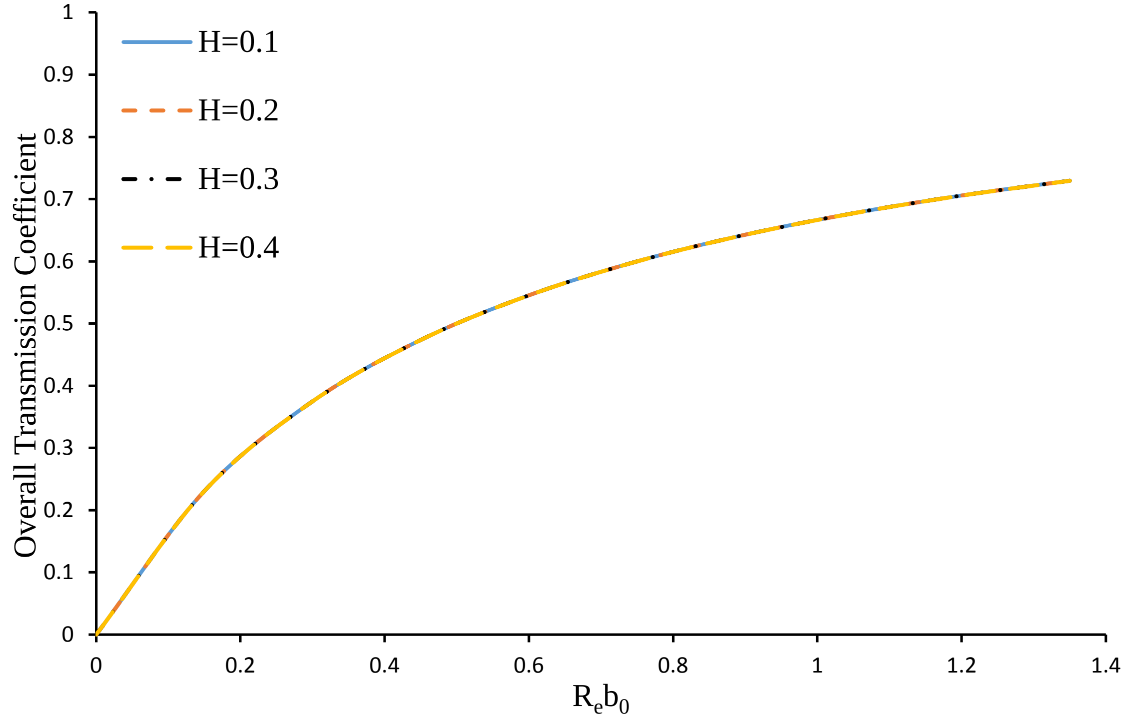

Figure 5-30: The overall transmission coefficient vs. the R_eb_0 with various H for a completely submerged wall ($d=1$).

Figure 5-31 shows the overall transmission coefficient varied versus $R_e b_0$ for various incident wave heights under the consideration of a partially submerged porous wall with d=0.5. Similar to Figure 5-30, the changing wave height is not shown to have a great influence on the overall transmission coefficient. Also, for this partially submerged wall case, the variation of $R_e b_0$ has a limit effect on the overall transmission coefficient. When $R_e b_0$ is small, the larger the wave height is, the slightly smaller overall transmission coefficient is observed. When $R_e b_0$ increases, the influence of incident wave height on the overall transmission coefficient decreases as shown in Figure 5-32. As the $R_e b_0$ increases towards a larger value, the overall transmission coefficient increases towards 1. Basically, the overall transmission coefficient for a partially submerged porous wall is less than that of a partially submerged solid wall due to the induced energy dissipation from the porous wall.

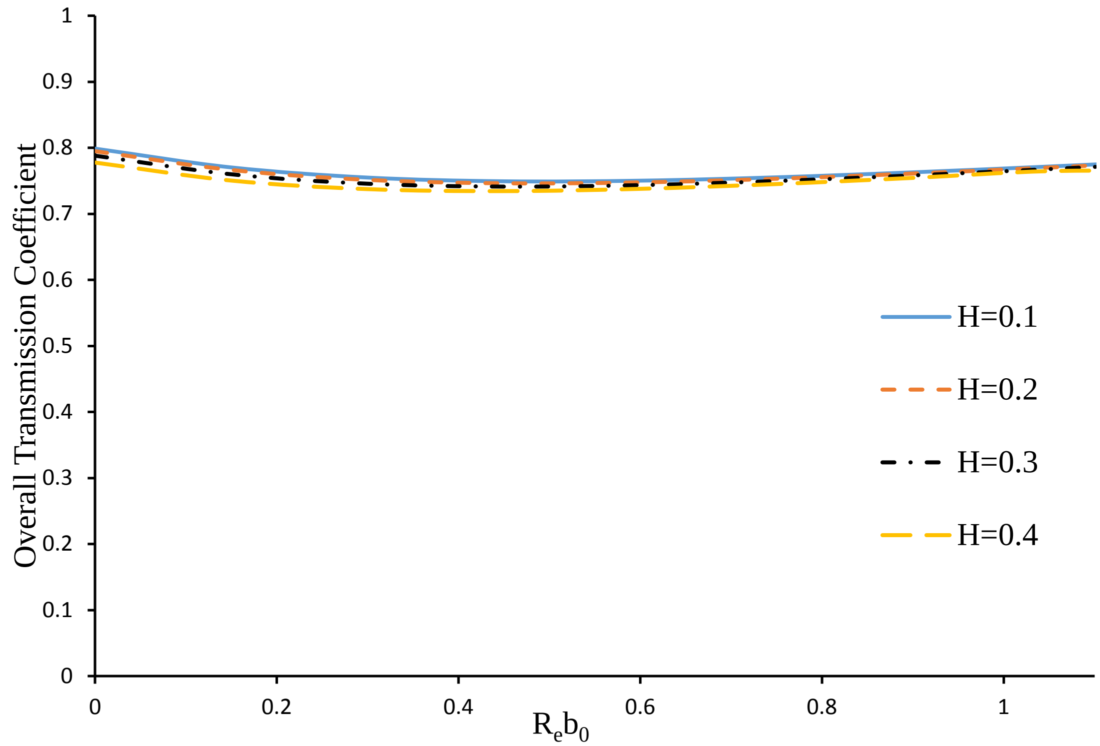

Figure 5-31: The overall transmission coefficient vs. the R_eb_0 with various H for a partially submerged wall (d=0.5).

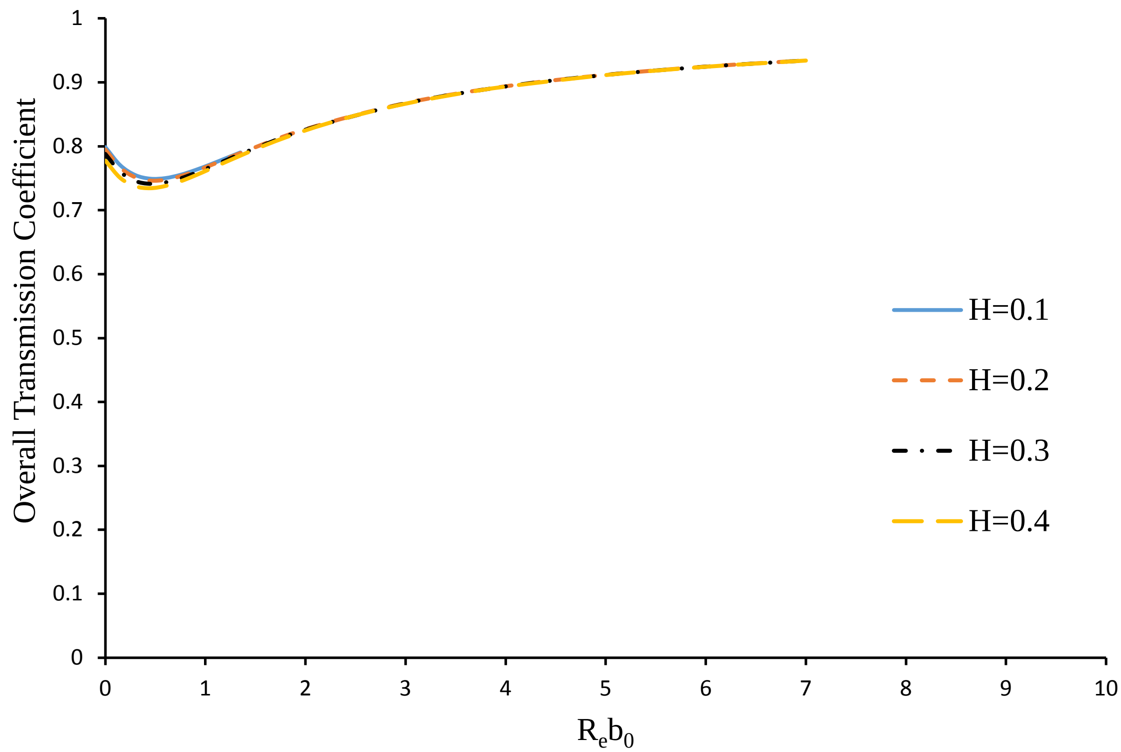

Figure 5-32: The overall transmission coefficient vs. the $R_e b_0$ (extend to 7) with various H for a partially submerged wall (d=0.5).

To further the analyses of the influences of the submerged depth and $R_e b_0$ on the overall transmission coefficient, Figure 5-33 illustrates the variations of the overall transmission coefficient (C_T) versus $R_e b_0$ for cases of various submerged depths and a fixed incident wave height of 0.2. It is found that when the submerged depth is large (e.g. d=1 or d=0.8), the overall transmission coefficient is shown to have a nonlinear increasing trend as $R_e b_0$ increases, and when the submerged depth becomes smaller (e.g. d=0.2 or d=0.4), the increase of $R_e b_0$ has an insignificant effect on the variation of the overall transmission coefficient. From Figure 5-33, it can be noted that the role played by the submerged depth of wall on the overall transmission coefficient becomes important when the values of porous-effect parameter $R_e b_0$ is small. When $R_e b_0$ approaches to 2, the effect of submerged depth on C_T is reduced.

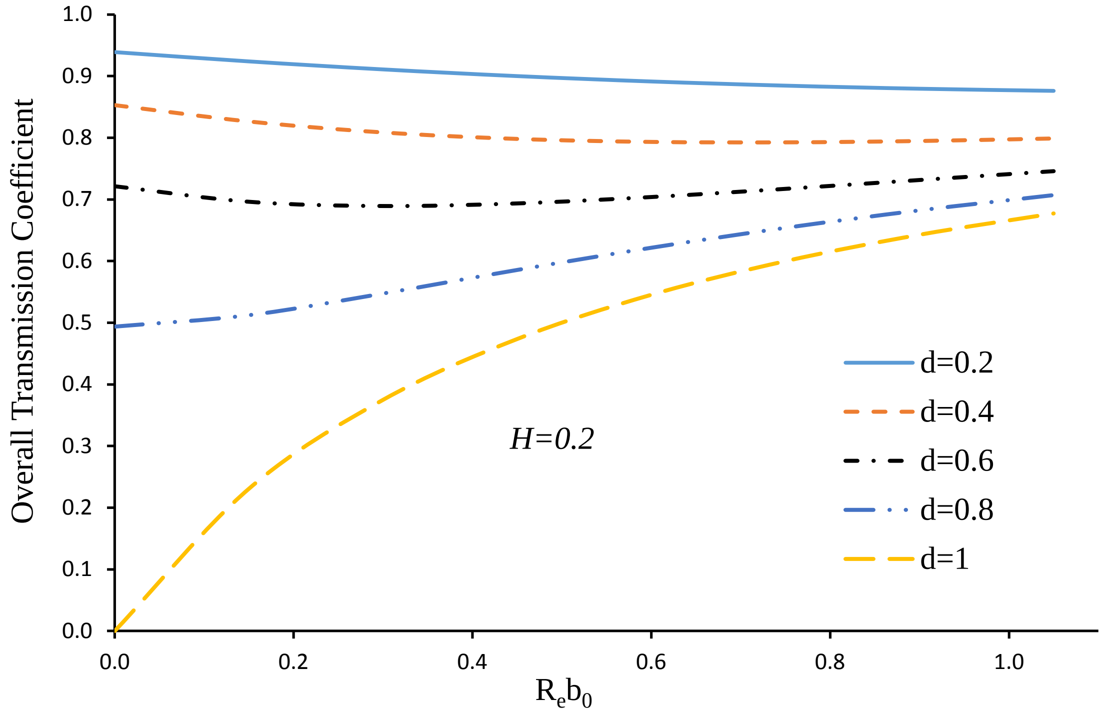

Figure 5-33: The overall transmission coefficient vs. the R_eb_0 with various d for a case of H=0.2.

5.3 Hydrodynamic Force on a Partially Submerged Porous Wall

Hydrodynamic force is also an important and a critical physical variable to be determined for the design consideration of the coastal and offshore engineering applications. Based on Eqn. (2-32), the horizontal hydrodynamic forces acting on the wall can be calculated. Figure 5-34 shows the comparison plot of the estimated maximum horizontal forces on a partially submerged solid wall by applying Eqn. (2-32) with $b_0 = 0$ versus the experimental data from Liu and Al-Banaa (2004)'s study, where 8 cases with different submerged depths and incident waves heights are included in the comparisons. The 45° line indicates the perfect fit. In general, the present analytical results agree reasonable well with the measurements. Since the analytical solution uses a linearized approximation of the velocity potential, it is more practical to be applied for smaller wave height waves, such as waves with $H \leq 0.3$. For waves with wave heights that are larger than 0.3, the errors for estimated forces become larger.

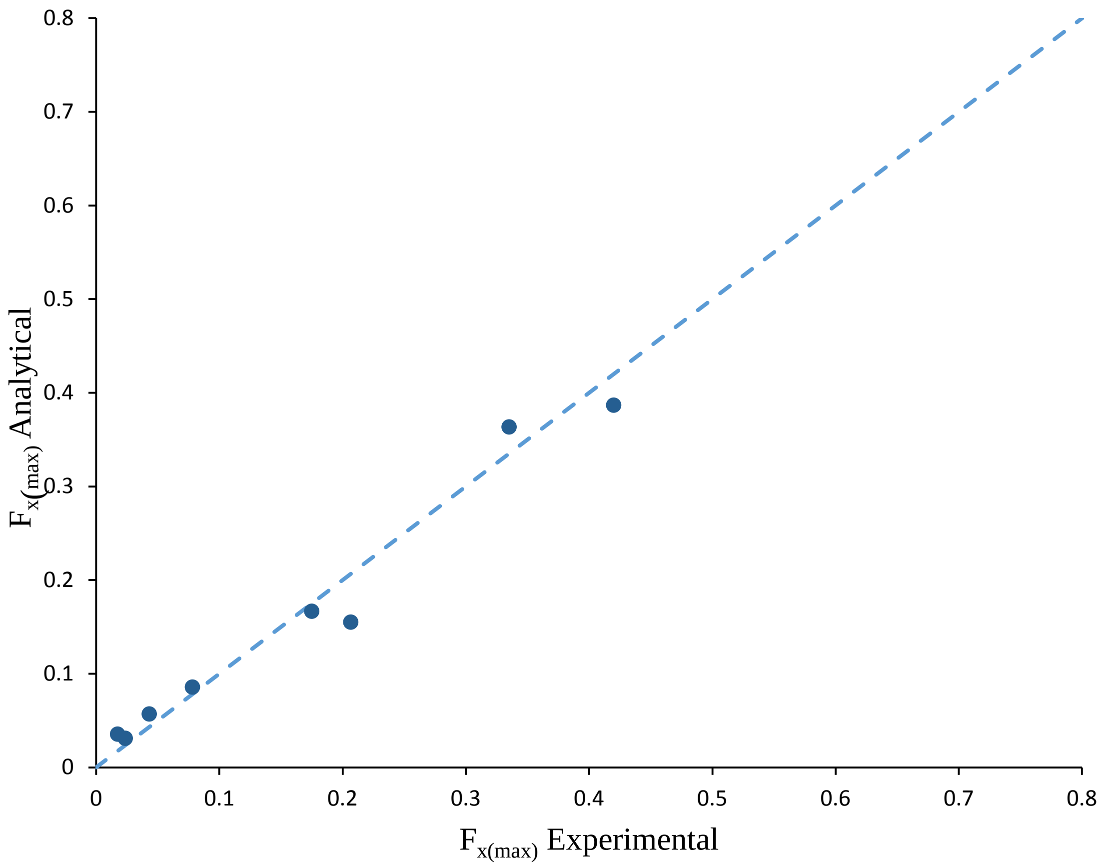

Figure 5-34: The Comparison of the analytical and experimental (Liu and Al-Banaa) results for maximum horizontal force (dashed line is 45 degree straight line).

Figure 5-35 and Figure 5-36 respectively display the time variations of the dimensionless horizontal force acting on a completely submerged (d=1) solid wall ($b_0 = 0$) with various incident wave heights. The results indicate that as the incident wave height increases the horizontal force increases and the impact time of the increased forces becomes shorter. For instance, the maximum horizontal force for the case of incident wave height H = 0.4 is larger than twice of the maximum horizontal force produced by an H =

0.2 wave. Comparing the results shown in Figure 5-35 and Figure 5-36, we notice that the forces on a completely submerged solid wall as expected are significantly larger than those on a partially submerged wall.

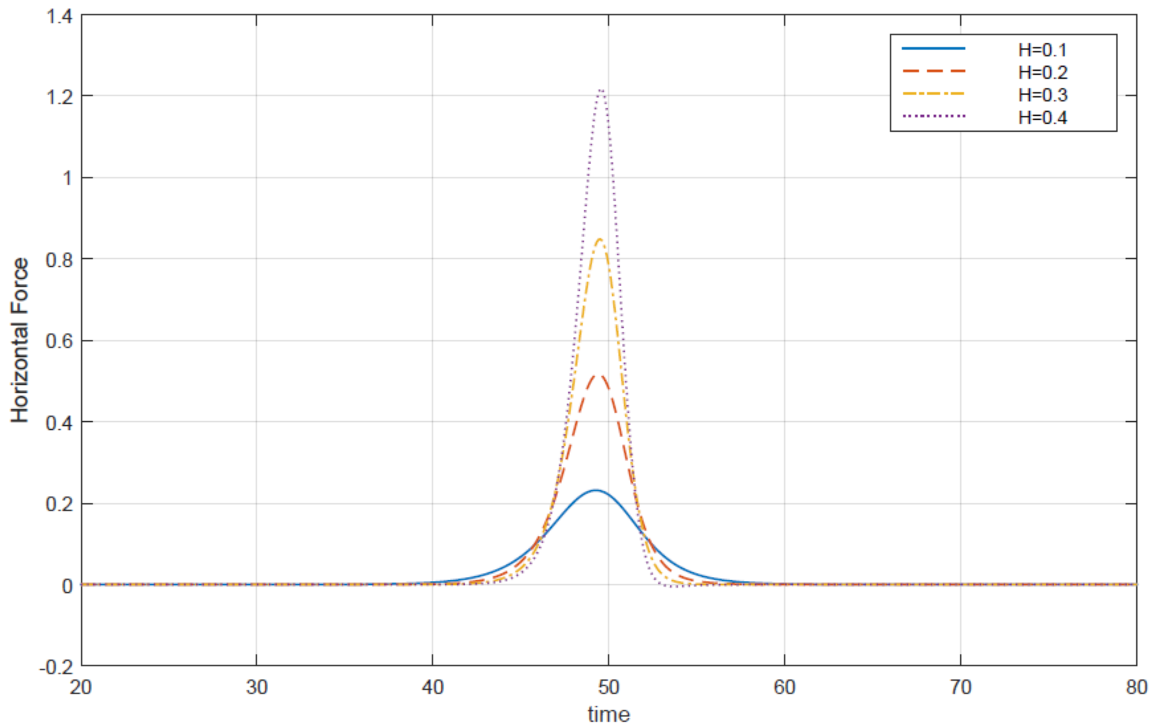

Figure 5-35: Comparison of horizontal forces on a completely submerged (d=1) solid wall with various H.

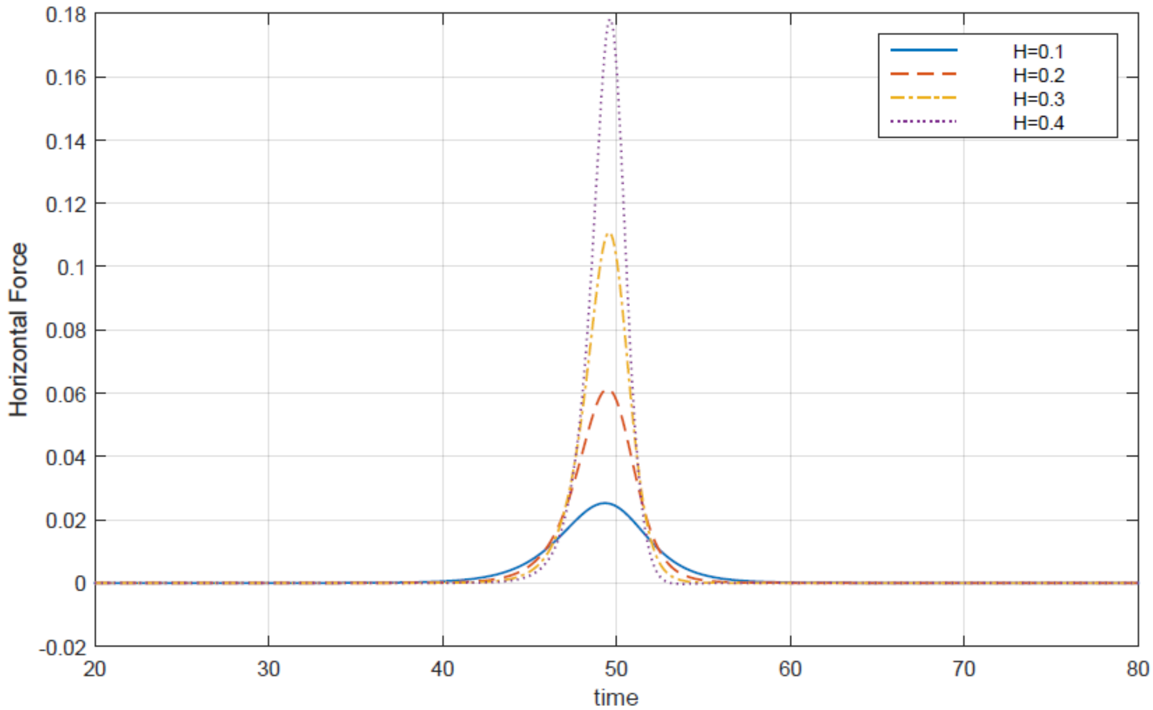

Figure 5-36: Comparison of horizontal forces on a partially submerged (*d*=0.5) solid wall with various *H*.

For porous wall conditions, Figure 5-37 and Figure 5-38 present the time variations of the horizontal force acting on a porous wall with $b_0 = 10^{-5}$ and respectively with the completely submerged (*d*=1) and partially submerged (*d*=0.5) conditions for various incident wave heights. Similar conclusions as those shown in Figure 5-35 and Figure 5-36 that the horizontal force increases as the incident wave height increases can be drawn for porous wall cases. Comparing Figure 5-37 with Figure 5-35, the significant decrease of the horizontal force can be seen when a completely submerged wall is applied. However, comparing Figure 5-38 with Figure 5-36, for a partially submerged wall (*d*=0.5), the horizontal forces in a porous condition is slightly larger than those in the solid wall case due to slightly larger wave run-ups.

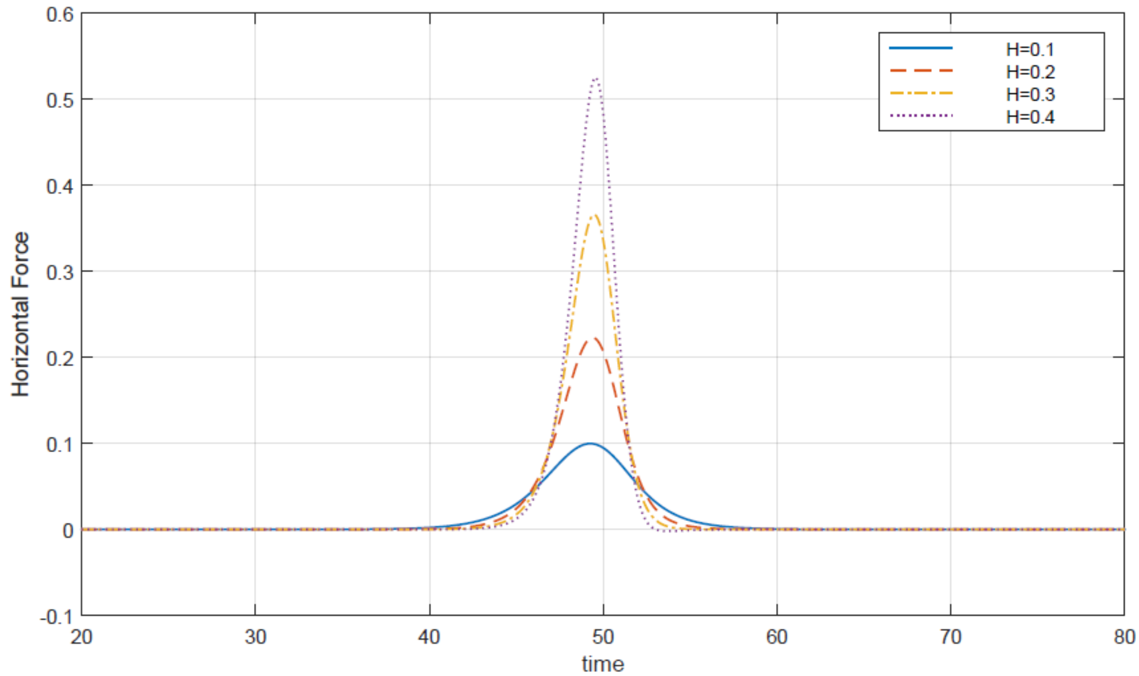

Figure 5-37: Comparison of horizontal forces on a completely submerged (d=1) porous wall $b_0 = 10^{-5}$ with various H.

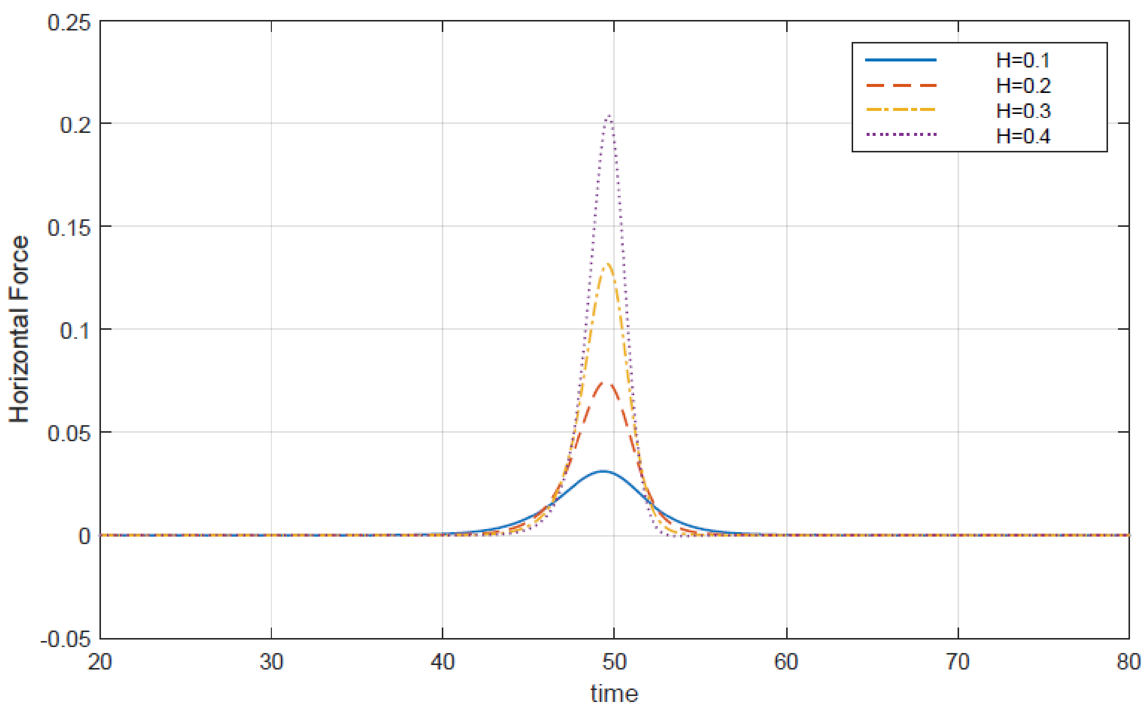

Figure 5-38: Comparison of horizontal forces on a partially submerged (d=0.5) porous wall $b_0 = 10^{-5}$ with various H.

Figure 5-39 shows the time variations of the horizontal force for cases with various submerged depths of solid walls when H= 0.2 and as a comparison Figure 5-40 displaces the results for porous wall cases by letting $b_0 = 10^{-5}$. By comparing these two figures, it can be concluded again that when the submerged depth is small, the maximum horizontal force for a solid case is slightly smaller than that for a porous wall with $b_0 = 10^{-5}$ whereas when the submerged depth becomes larger, the forces on porous walls are smaller than those on solid walls.

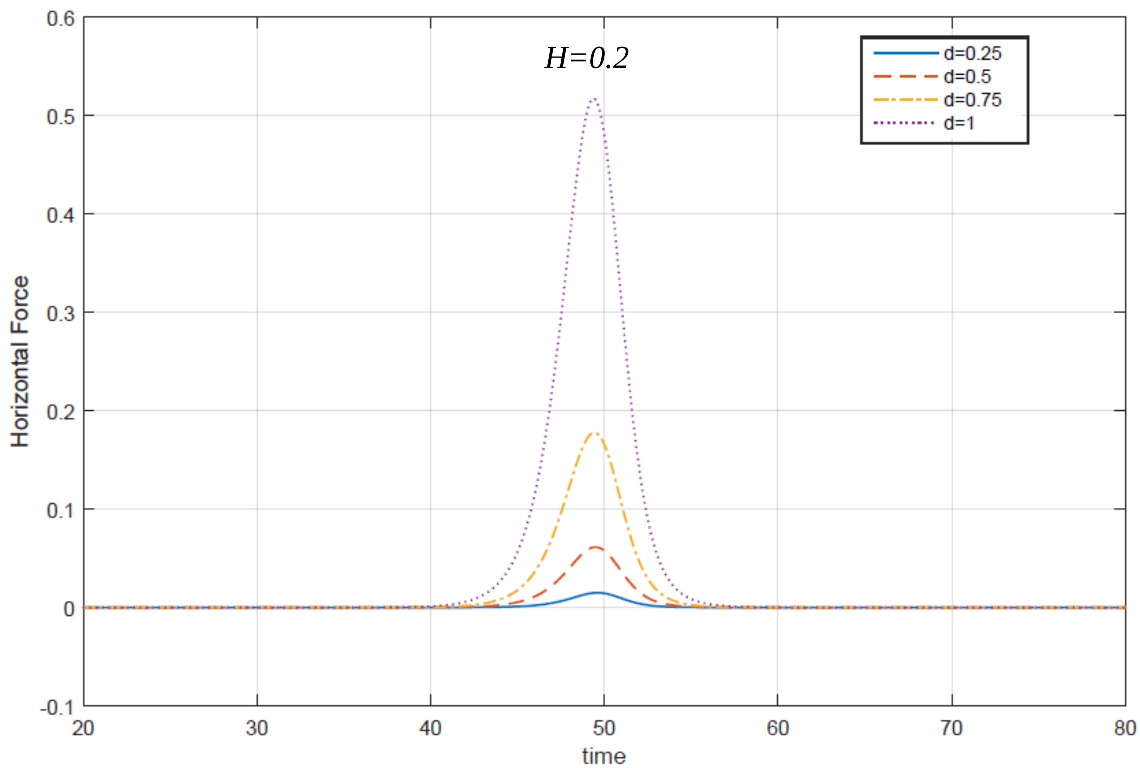

Figure 5-39: Comparison of horizontal forces on a solid wall with various *d* and a constant *H*=0.2.

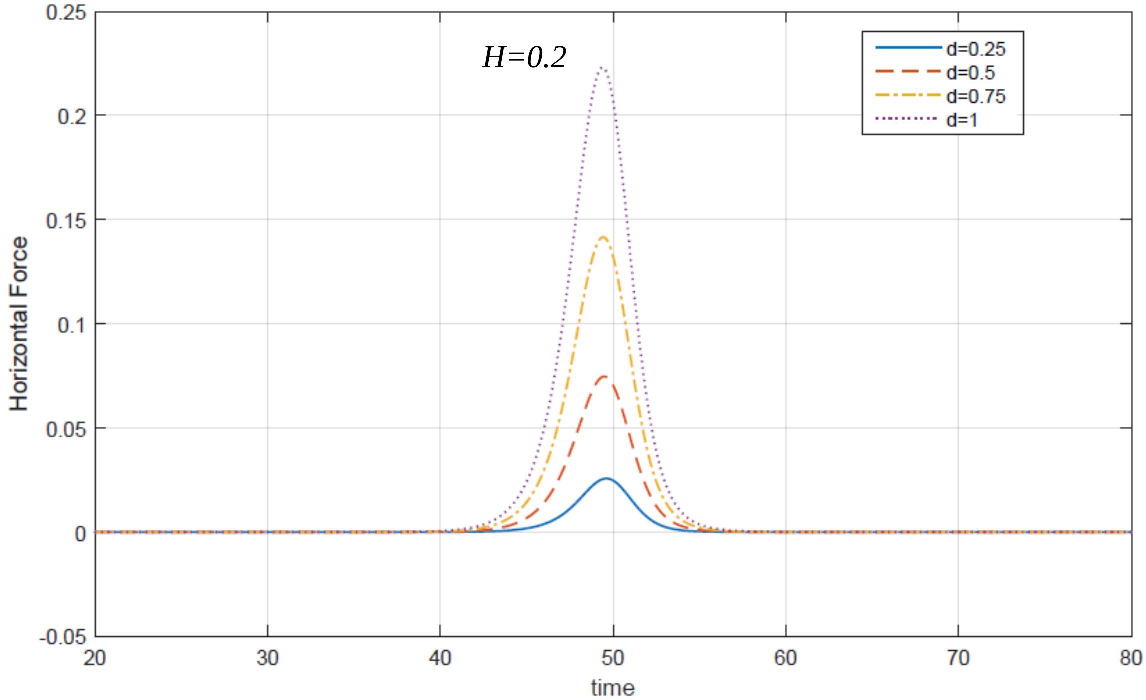

Figure 5-40: Comparison of horizontal forces on a porous wall ($b_0 = 10^{-5}$) with various d and a constant H=0.2.

The maximum force on a structure is a practical property that is widely required in the ocean and coastal engineering design consideration. Figure 5-41 illustrates the maximum horizontal force versus the incident wave height for various submerged depths of a solid wall. For a porous wall case with $b_0 = 10^{-5}$, the maximum horizontal force versus the incident wave height are presented in Figure 5-42. Basically, the maximum horizontal force is shown to increase as the incident wave height or submerged depth increases for both solid and porous wall cases. Again, for cases with larger submerged depths, the forces on a porous wall are much smaller than those on a solid wall.

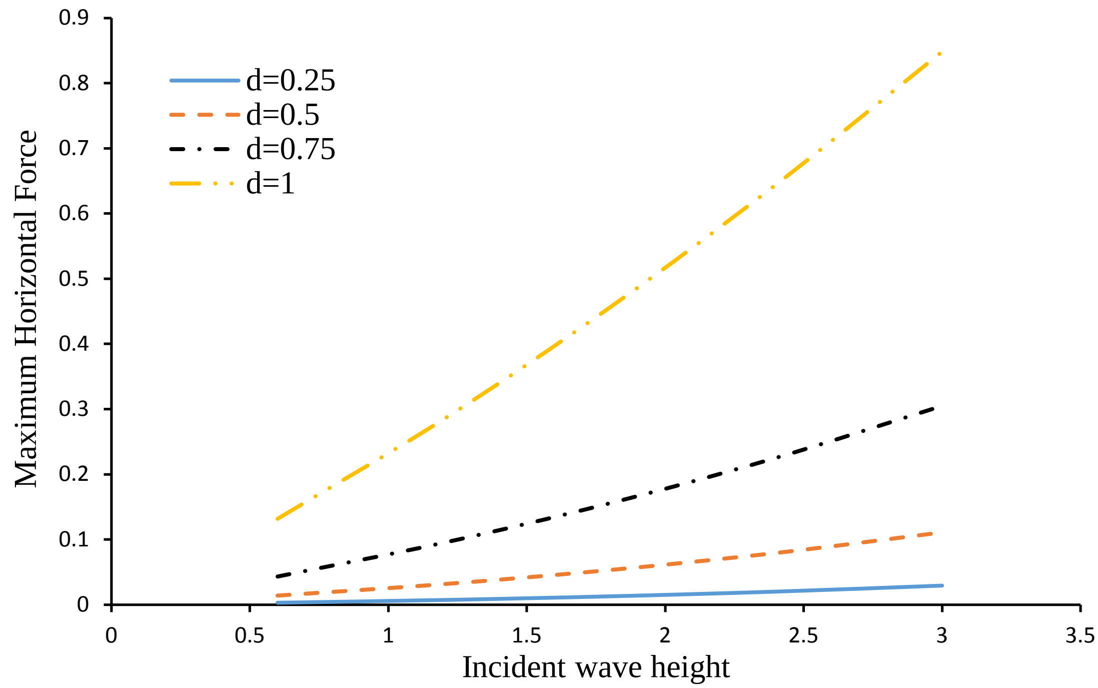

Figure 5-41: The maximum horizontal force vs. incident wave height with various *d* for solid wall case.

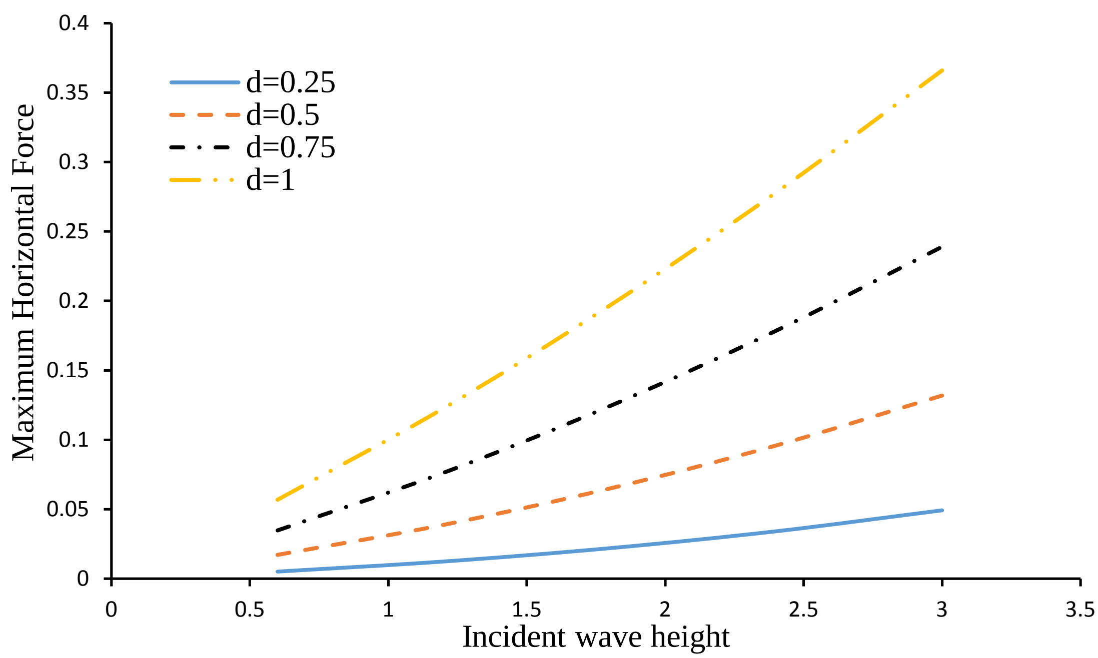

Figure 5-42: The maximum horizontal force vs. incident wave height with various *d* for porous wall case (b_0 = 10^{-5}).

In terms of the effect of the submerged depth of wall on the maximum horizontal force, the results showing the maximum horizontal force versus the submerged depth for various incident wave heights under a solid wall condition are presented in Figure 5-43 and the results for a porous wall case with $b_0 = 10^{-5}$ are plotted in Figure 5-44. The nonlinear increasing trends of the maximum horizontal forces as the submerged depth of either a solid wall or a porous wall increases can be noticed. For a solid wall case, the maximum horizontal force is much greater than the force under a porous wall condition when the submerged depth of wall becomes larger.

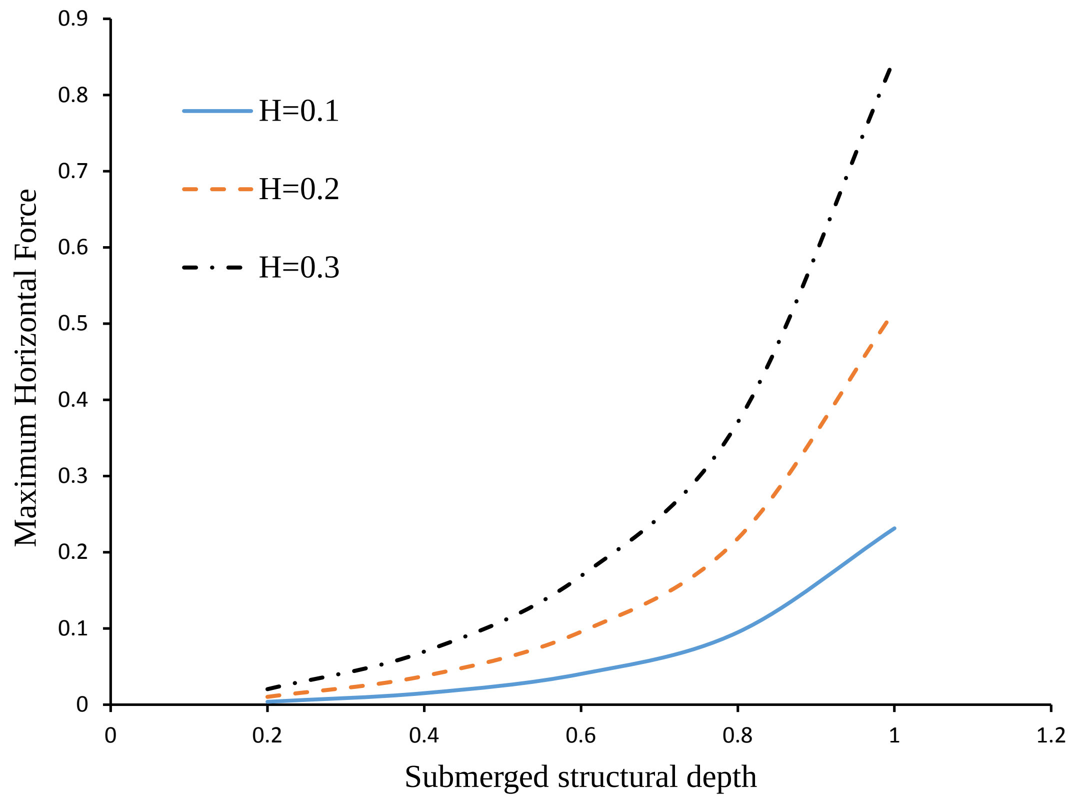

Figure 5-43: The maximum horizontal force vs. submerged structural depth with various H for solid wall case.

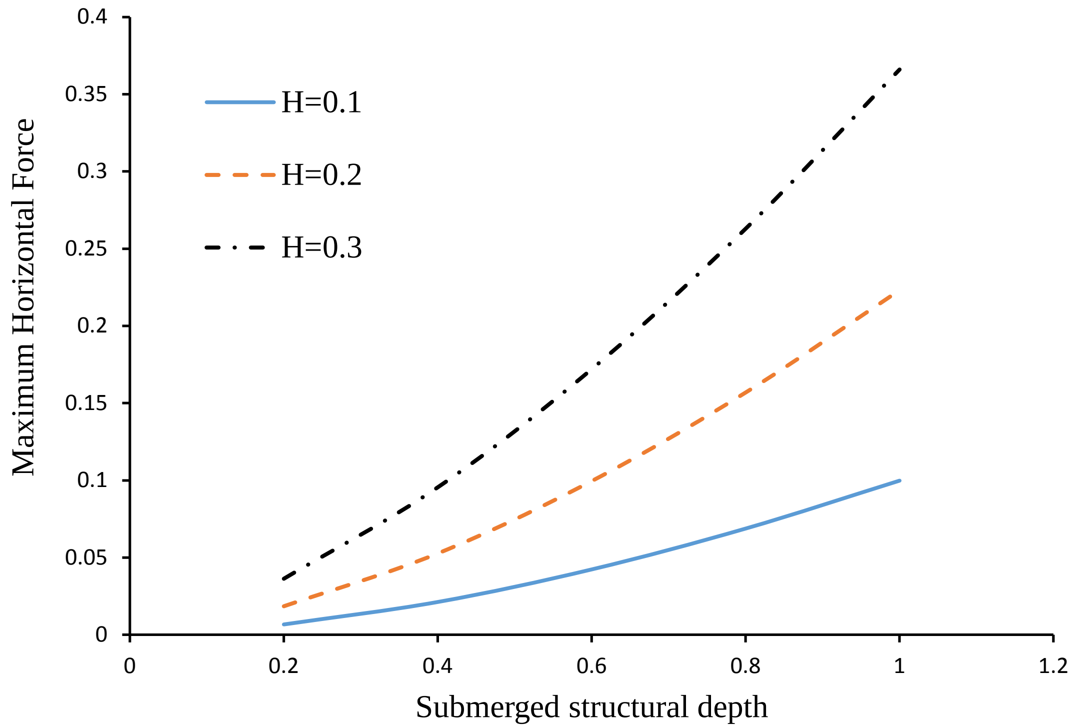

Figure 5-44: The maximum horizontal force vs. submerged structural depth with various *H* for porous wall case ($b_0 = 10^{-5}$).

Considering the effect of porous-effect parameter, Figure 5-45 presents the plot of the maximum horizontal force versus $R_e b_0$ with the uses of various incident wave heights for the condition of a completely submerged wall. Meanwhile, Figure 5-46 illustrates the maximum horizontal force versus $R_e b_0$ for a partially submerged (*d*=0.5) wall. Again, as the incident wave height increases, the maximum horizontal force increases. It can be seen that when the wall is completely submerged, the maximum horizontal force decreases as the $R_e b_0$ increases which indicates that a porous wall receives a smaller wave force than a solid wall does. However, for a partially submerged (*d*=0.5) wall, a concave down variation trend of the maximum horizontal force is noticed, and the maximum values can be found at a specific value of $R_e b_0$ under a porous wall condition.

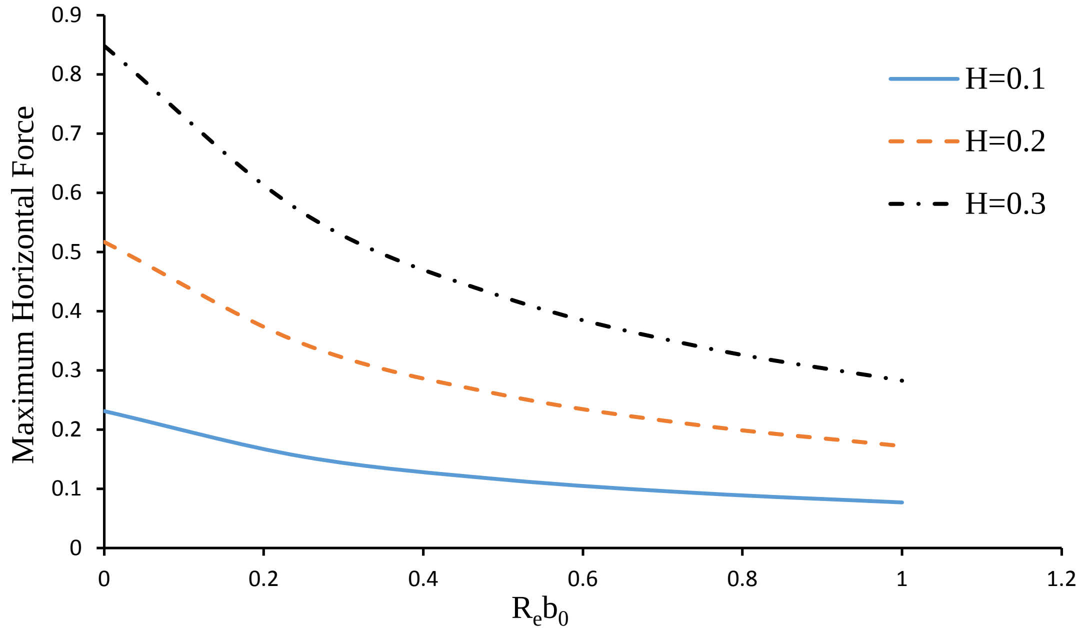

Figure 5-45: The maximum horizontal force vs. the $R_e b_0$ with various H for a completely submerged (d=1) wall case.

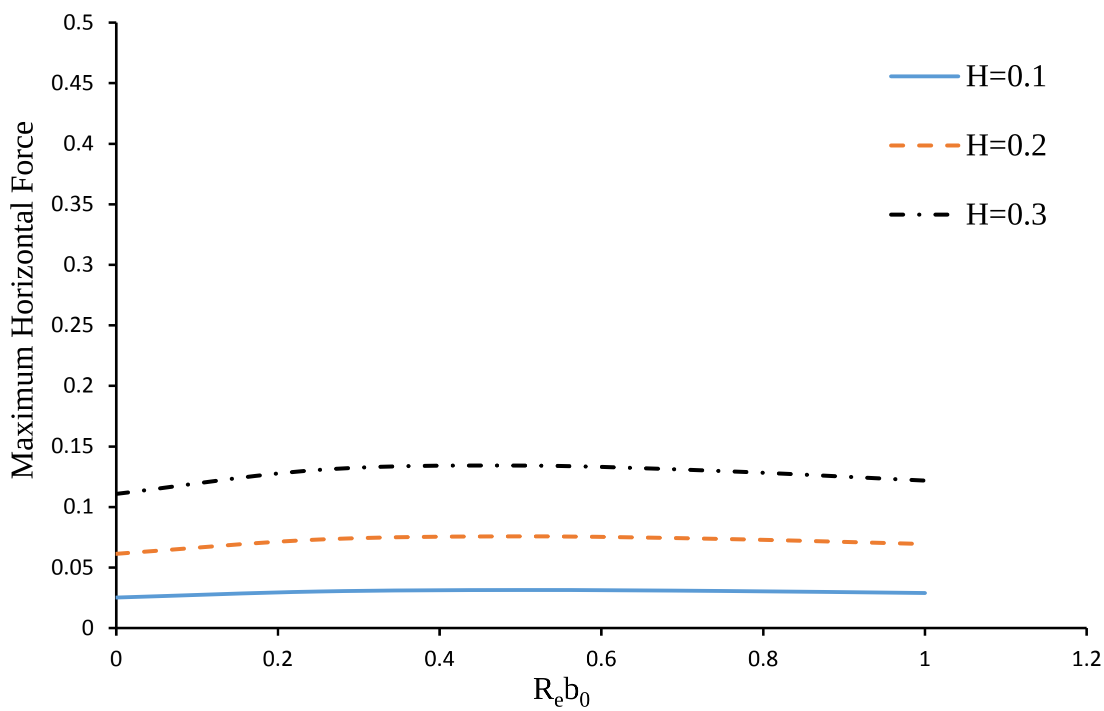

Figure 5-46: The maximum horizontal force vs. the $R_e b_0$ with various H for a partially submerged (d=0.5) wall case.

The combined effects of submerged depth of wall and porous-effect parameter $R_e b_0$ on the maximum horizontal force are shown in Figure 5-47 where the incident wave height is set to be 0.2. It is found that when the submerged depth is less than or equal to 0.5 (e.g. *d*=0.25 or *d*=0.5), the effect of $R_e b_0$ on the maximum horizontal force is insignificant. As the submerged depth become larger, the effect of $R_e b_0$ on the maximum horizontal force increases, especially for a complete submerged wall, the maximum horizontal force decreases as $R_e b_0$ increases.

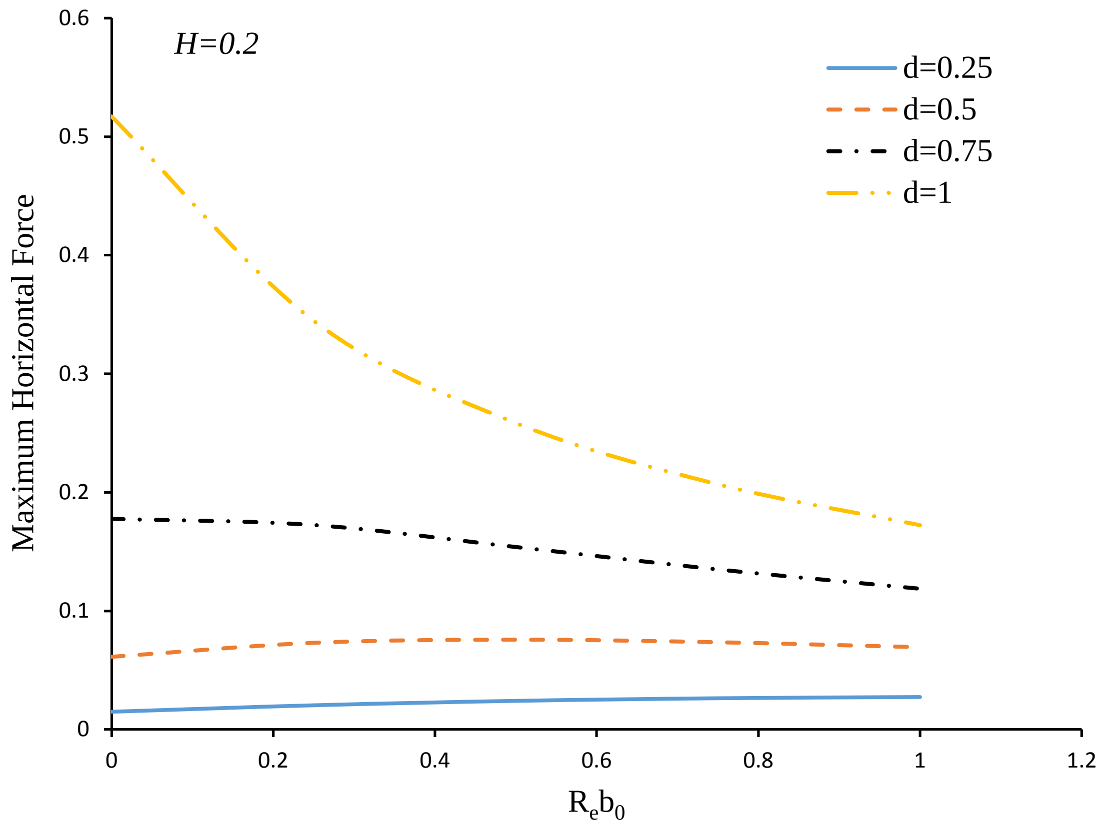

Figure 5-47: The maximum horizontal force vs. the $R_e b_0$ with various *d* for a case of *H*=0.2.

Chapter 6 Result for the Study of the Hydrodynamic Interactions between a Solitary Wave and a 2-D Finite-Length Body with Attached Dual Porous Walls

In this chapter, similar to Chapter 5, the results for the study of the hydrodynamic interactions between a solitary wave and a 2-D finite-length body with attached dual porous walls are presented. By applying the analytical solutions given in Chapter 3, the analytical results of the time variations of the free-surface elevations of the incident, reflected and transmitted waves during the process of wave-structure interactions can be obtained. The comparisons between the predicted free-surface elevations obtaining from the analytical solutions and the experimental data are conducted. With the analytical solutions, the effects of the parameters including incident wave height, 2-D body draft, submerged depth of porous wall, $R_e b_1$, $R_e b_2$ (all the cases or plots in this chapter use the same R_e value of 65882) and structural length on the reflection and transmission of an incident wave are also examined. Horizontal and vertical forces acting on the partially submerged body system under various wave and structural conditions are investigated.

6.1 Comparisons between the Analytical Results and Experimental Data

In order to verify the analytical solutions shown in Chapter 3, the free-surface elevations obtained by applying Eqns. (3-44) and (3-45) are compared with the experimental measurements. In this validation study, cases with various values of the incident wave height, 2-D body draft, submerged depth of porous wall, $R_e b_1$, $R_e b_2$, and the structural length are examined with comparison plots presented.

First, a comparison plot between the analytical results and Lu and Wang's (2015) experimental data for a case with $b=0.5$, $L=4$ and $H=0.23$ (without any porous conditions) is presented in Figure 6-1. The upper part of the figure shows the incident and reflected waves while the lower part reveals the transmitted waves. The analytical results agree well with the experimental data from Lu and Wang (2015) in magnitudes and phases for the incident and transmitted waves, however, slightly overestimated the peak of the reflected wave height. The present analytical model misses the predictions of the oscillatory tails as part of the reflected waves.

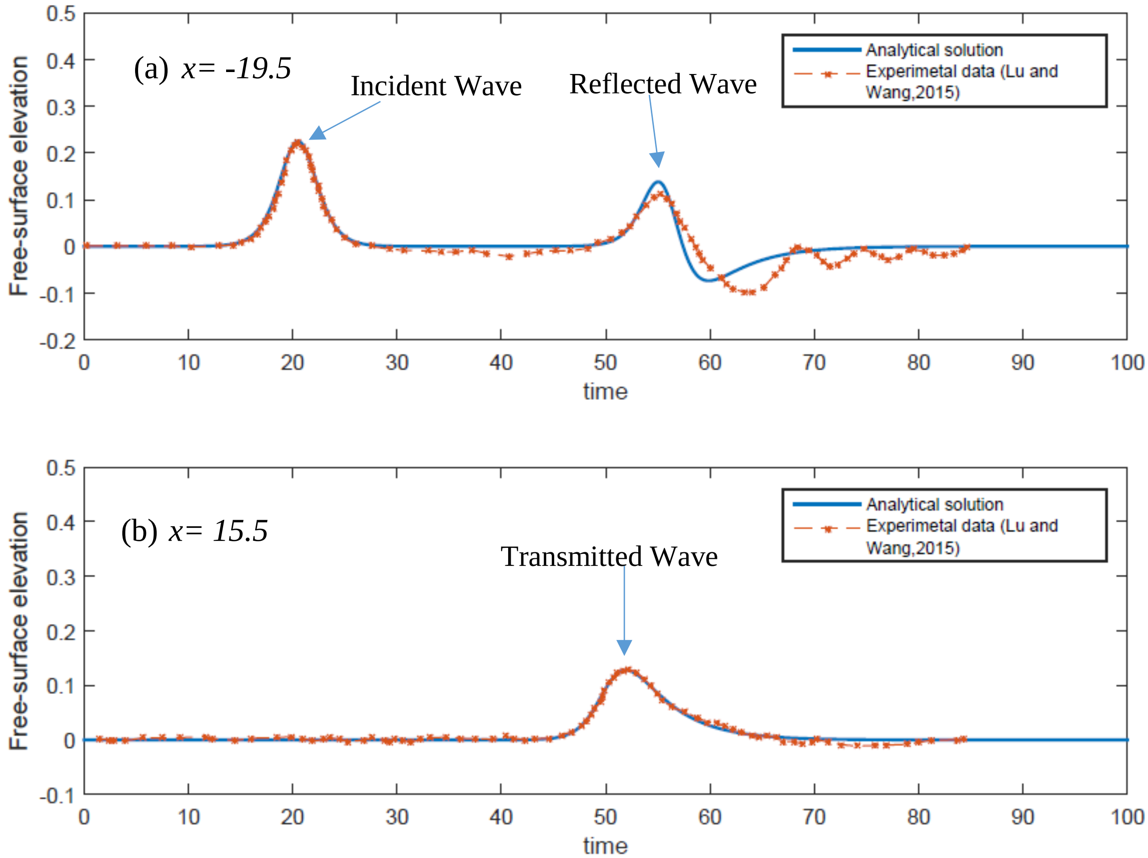

Figure 6-1: Comparisons of free surface elevation obtained from analytical solution and experimental data from Lu and Wang (2015) for a case with $b=d=0.5$(no porous conditions), $L=4$ and $H=0.23$: (a) incident and reflected wave; (b) transmitted wave.

Figure 6-2 shows the comparisons between the present analytical solutions and experimental measurements recorded by Gauges 1 and 2 for the case with $b=0.6$, $L=4$ and $H=0.294$ (without any porous conditions). As both the incident wave height and the body draft increase, the transmitted wave heights obtained from the analytical model still matches well with the measurements. For the reflected wave height, the difference between the analytical solutions and experimental data increases when comparing to the results shown in Figure 6-1. This may be caused by the nonlinear effect of the solitary wave, which is not completely retained in the analytical approach, where the linearized approximation is applied to each component of the integral forms of the solutions in velocity potentials and free-surface elevations. As a result, the solutions work better for waves with smaller incident wave heights. Also, as the body draft increases, experimentally, the enhanced energy dissipation effect may also cause the increase of comparison difference.

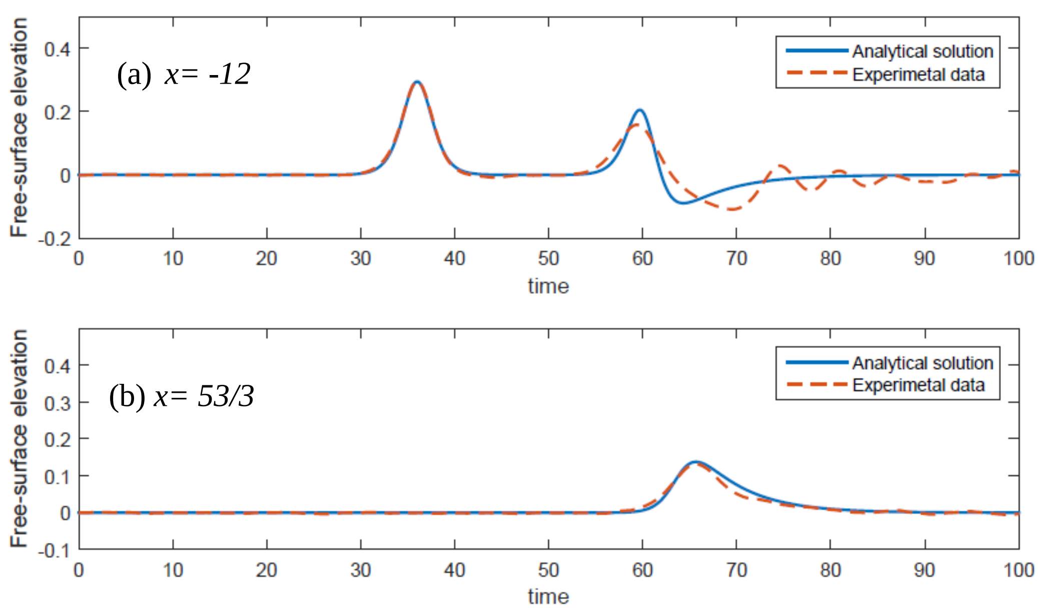

Figure 6-2: Comparisons of free surface elevation obtained from analytical solution and experimental data for a case with $b=d=0.6$ (no porous conditions), $L=4$ and $H=0.294$: (a) incident and reflected wave; (b) transmitted wave.

With further increase of the structural length, Figure 6-3 presents the comparisons between the present analytical and the experimental results for the case with *b=0.6*, *L=6* and *H=0.311* (without any porous conditions). Again, the transmitted wave height and varying trend obtained from the analytical solutions match well with the experimental data. The analytical model again over-estimates the reflected wav height, although predicts reasonably well on the phase and varying trend. As the structural length increases, the reflected wave height increases and the transmitted wave height decreases.

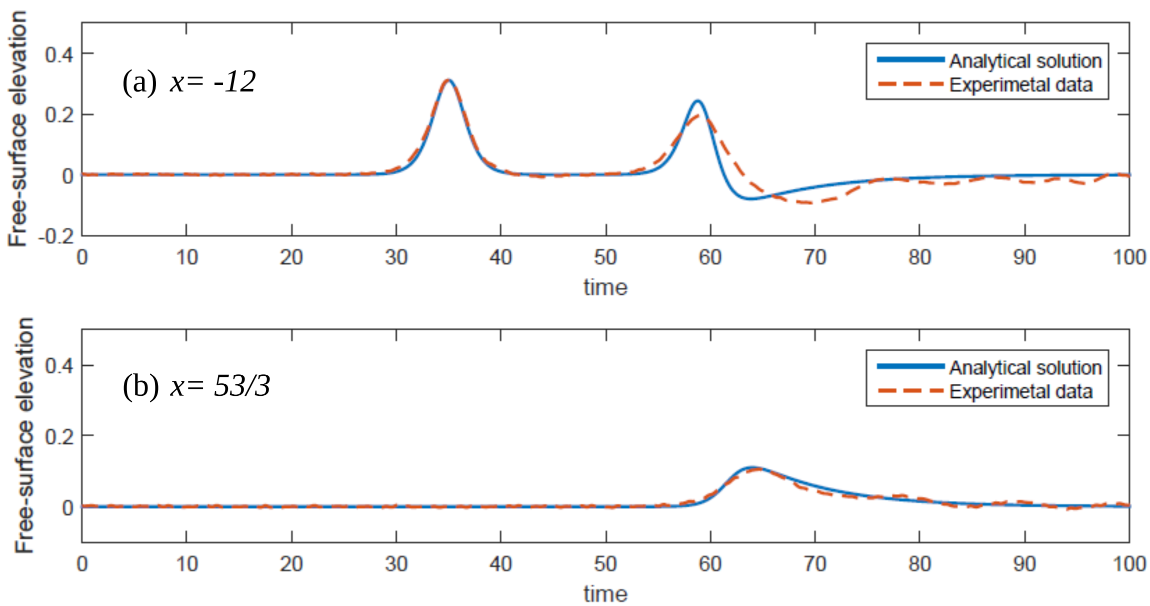

Figure 6-3: Comparisons of free surface elevation obtained from analytical solution and experimental data for a case with *b=d=0.6* (no porous conditions), *L=6* and *H=0.311*: (a) incident and reflected wave; (b) transmitted wave.

For the case with a smaller incident wave height, the comparison plots showing both the analytical solutions and the experimental results recorded by Gauges 1 and 2 for the case having *b=0.3*, *L=6* and *H=0.2* (without any porous conditions) are given in Figure 6-4. Again, comparing to the experimental measurements, the complete transmitted wave profile is well predicted by the present analytical model. In terms of wave peak, the reflected wave height obtained from the analytical solutions and experimental data agree reasonably well with each other even under this intermediate incident wave height (H=0.2) condition. Also, as the draft decreases, comparing with Figure 6-3, the error in the prediction of reflected wave height decreases. It should also be noticed that the smaller oscillatory tail following the main reflected wave is not completely captured by the present analytical solutions, which is again caused by the present approximated approach where the fully nonlinear interaction process is neglected in the solution procedure.

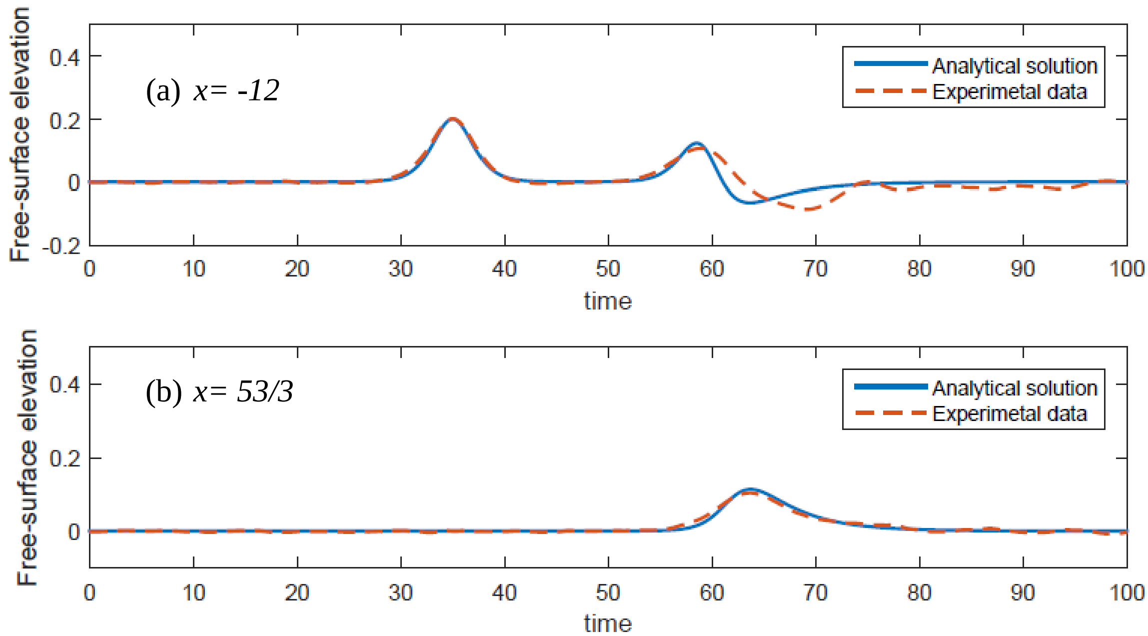

Figure 6-4: Comparisons of free surface elevation obtained from analytical solution and experimental data for a case with $b=d=0.3$ (no porous conditions), $L=6$ and $H=0.2$: (a) incident and reflected wave; (b) transmitted wave.

With the inclusion of the two attached porous walls, Figure 6-5 through Figure 6-7 present the comparisons between the results from the analytical solutions and the experimental measurements at the two gauge locations (Gauge 1 and Gauge 2) for the setting of $b=0.4$, $d=1$, $L=6$ and H = 0.2 with various porous conditions. For the results shown in Figure 6-5 to Figure 6-7, the value of $b_2 = 2.4 \times 10^{-5}$ is kept as a constant and the values of b_1 are respectively 2.4×10^{-5}, 1.0×10^{-5}, and 8×10^{-6}. The analytically obtained wave peaks for both the reflected and transmitted waves match closely with the experimental data. When comparing the reflected wave profiles, the depressions that follow the main reflected waves from the analytical solutions are found to be slightly higher than the measurements. Again, the predicted time varying free-surface profiles for transmitted waves fit fairly well with the measured profiles. Similar to the case presented in Figure 6-7, however with *H=0.285*, the comparison results are shown in Figure 6-8. The errors, especially for the predictions of the reflected wave peak, increase. In general, based on the comparisons for various wave and partially submerged body conditions, the analytical solutions are demonstrated to be able to predict well the transmitted wave height and the time varying profiles. For the reflected wave heights, the analytical solutions slightly overestimate the values when compared to the experimental data, and as the incident wave height or the draft of the partially submerged body system increases the prediction errors may become larger.

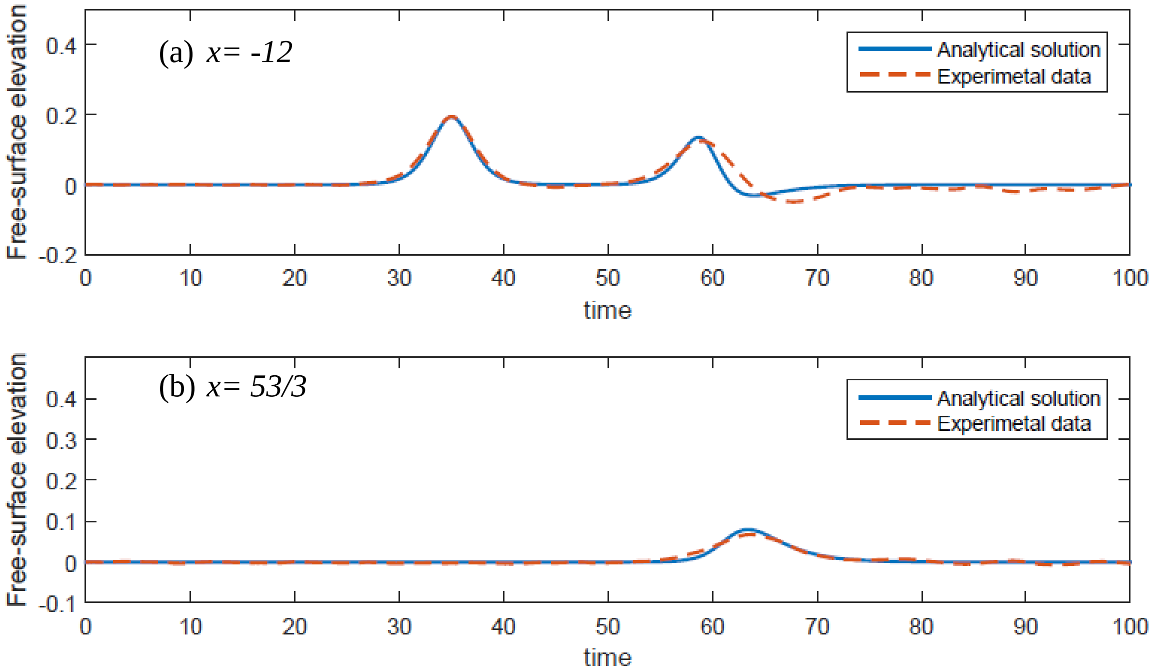

Figure 6-5: Comparisons of free surface elevation obtained from analytical solutions and experimental data for a case with b=0.4, d=1, L=6, H=0.193, b_1 =2.48×10^{-5} and b_2 =2.4×10^{-5}: (a) incident and reflected wave; (b) transmitted wave.

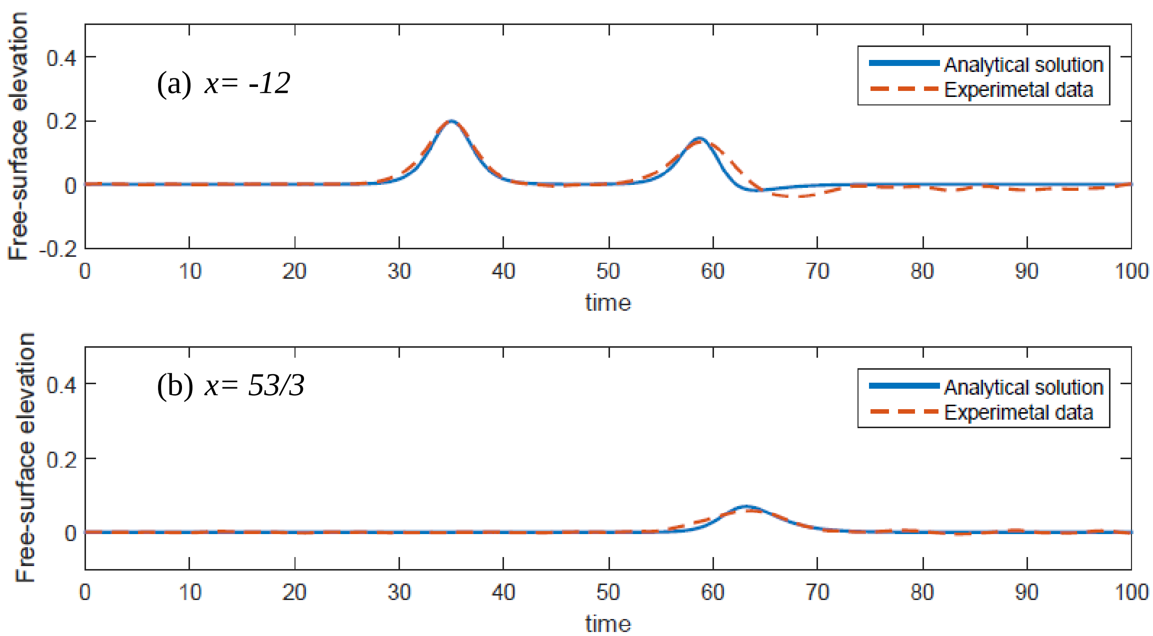

Figure 6-6: Comparisons of free surface elevation obtained from analytical solution and experimental data for a case with b=0.4, d=1, L=6, H=0.197, b_1 = 10^{-5} and b_2 = 2.4×10^{-5}: (a) incident and reflected wave; (b) transmitted wave.

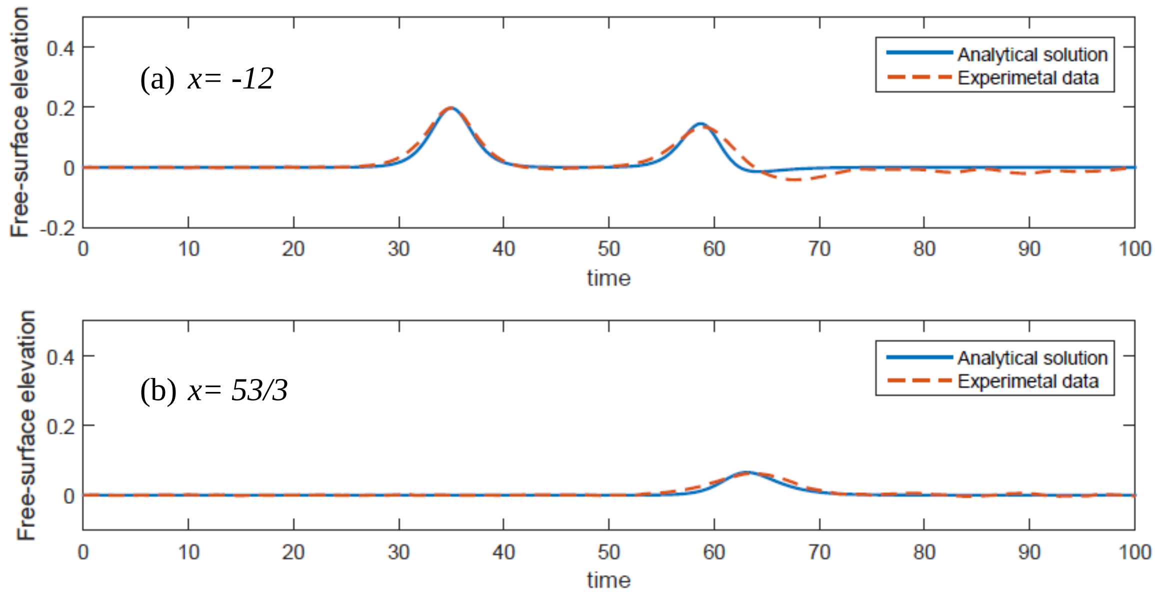

Figure 6-7: Comparisons of free surface elevation obtained from analytical solution and experimental data for a case with $b=0.4$, $d=1$, $L=6$, $H=0.197$, $b_1 = 8\times10^{-6}$ and $b_2 = 2.4\times10^{-5}$: (a) incident and reflected wave; (b) transmitted wave.

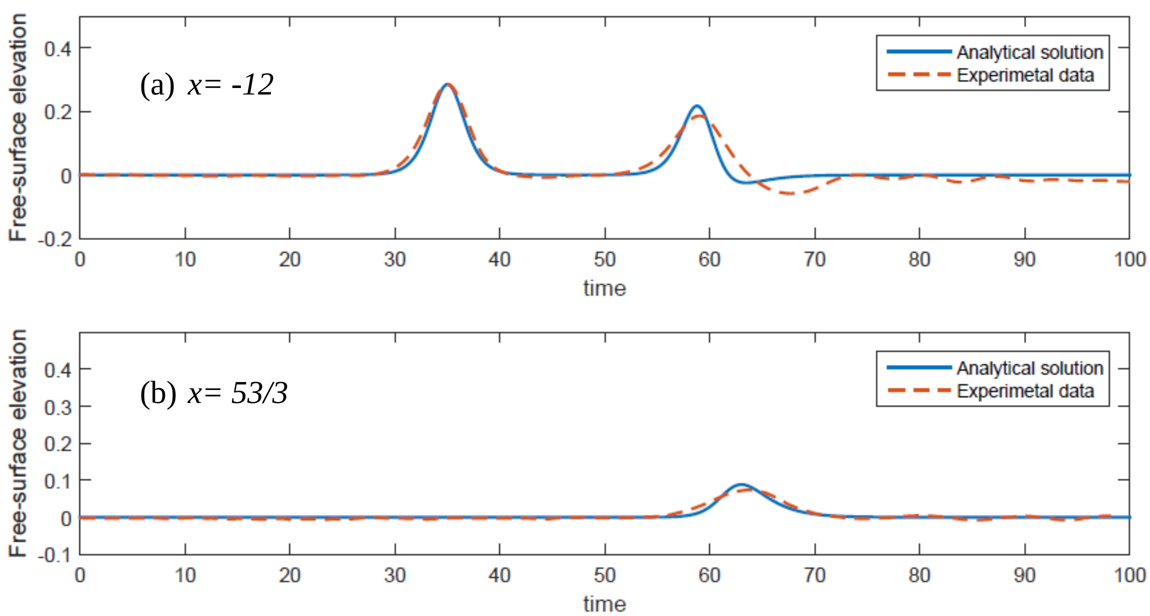

Figure 6-8: Comparisons of free surface elevation obtained from analytical solution and experimental data for a case with $b=0.4$, $d=1$, $L=6$, $H=0.284$, $b_1 = 8\times10^{-6}$ and $b_2 = 2.4\times10^{-5}$: (a) incident and reflected wave; (b) transmitted wave.

Various comparisons of the overall reflection and transmission coefficients obtained from the present analytical solutions and Lu and Wang's (2015) numerical results are shown through Figure 6-9 to Figure 6-12. Figure 6-9 and Figure 6-10 respectively present the comparisons of the overall reflection coefficients (defined as C_R in Chapter 5) obtained from the analytical solutions and Lu and Wang's (2015) numerical results versus incident wave height with various body drafts for cases with $L=6$ and $L=4$. In Lu and Wang's (2015) numerical study, only a 2-D partially submerged body was considered. Therefore, *d* is set to be equal to *b*, indicating the two porous walls are not included in the comparison study given in Figure 6-9 and Figure 6-10. It can be seen the difference in C_R from both the analytical and numerical approaches is small for cases of smaller incident wave height, however, it becomes larger due to the increased effect of nonlinearity as the incident wave height increases. The maximum difference is about 20%. The causes of the overestimation on the overall reflection coefficient may be explained as the present approximated approach does not include the fully nonlinear interaction process for capturing the small time delay on wave reflection.

Similar to the settings given in Figure 6-9 and Figure 6-10, Figure 6-11 and Figure 6-12 show the comparisons of the overall transmission coefficient (defined as C_T in Chapter 5) obtained from the present analytical solutions and Lu and Wang's (2015) numerical results for various incident wave heights. Different from the comparisons made to C_R, the results from the present analytical solutions match well with Lu and Wang's (2015) numerical results and the largest error is about 5%.

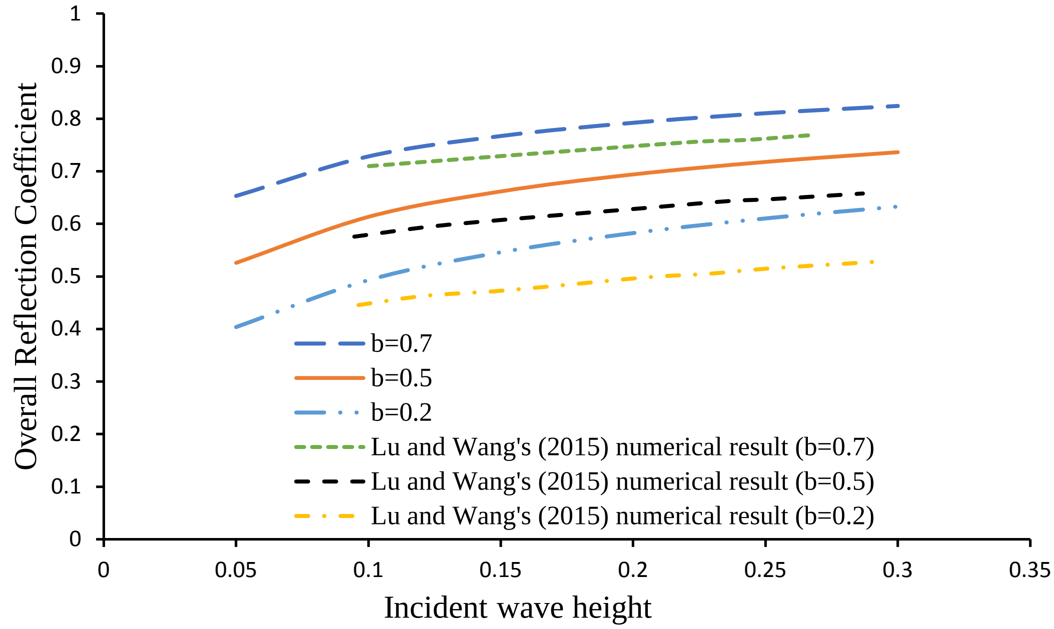

Figure 6-9: Comparisons of the overall reflection coefficient obtained from the analytical solutions and Lu and Wang’s (2015) numerical results for a case with $b=d$ (no porous conditions), and $L=6$.

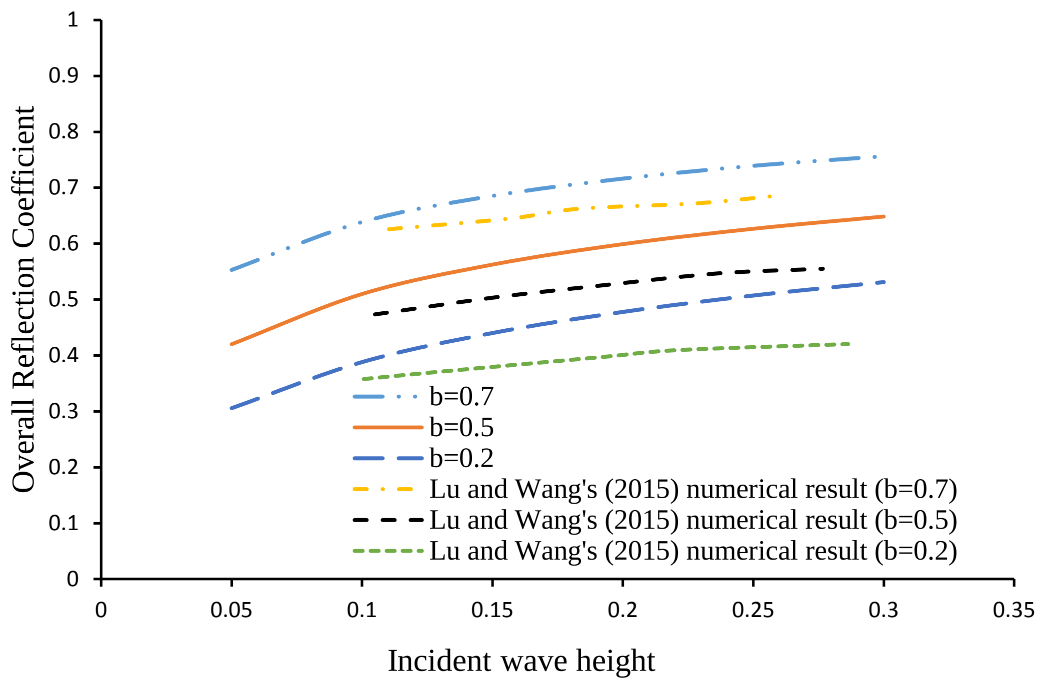

Figure 6-10: Comparisons of the overall reflection coefficient obtained from the analytical solutions and Lu and Wang’s (2015) numerical results for a case with $b=d$ (no porous conditions), and $L=4$.

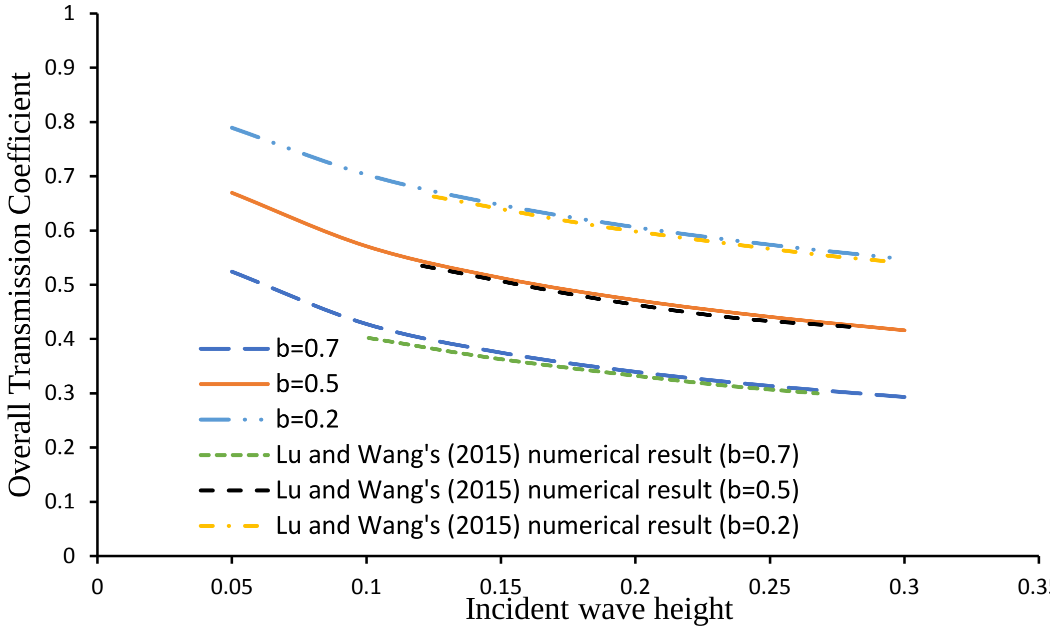

Figure 6-11: Comparisons of the overall transmission coefficient obtained from the analytical solutions and Lu and Wang's (2015) numerical results for a case with $b=d$ (no porous conditions), and $L=6$.

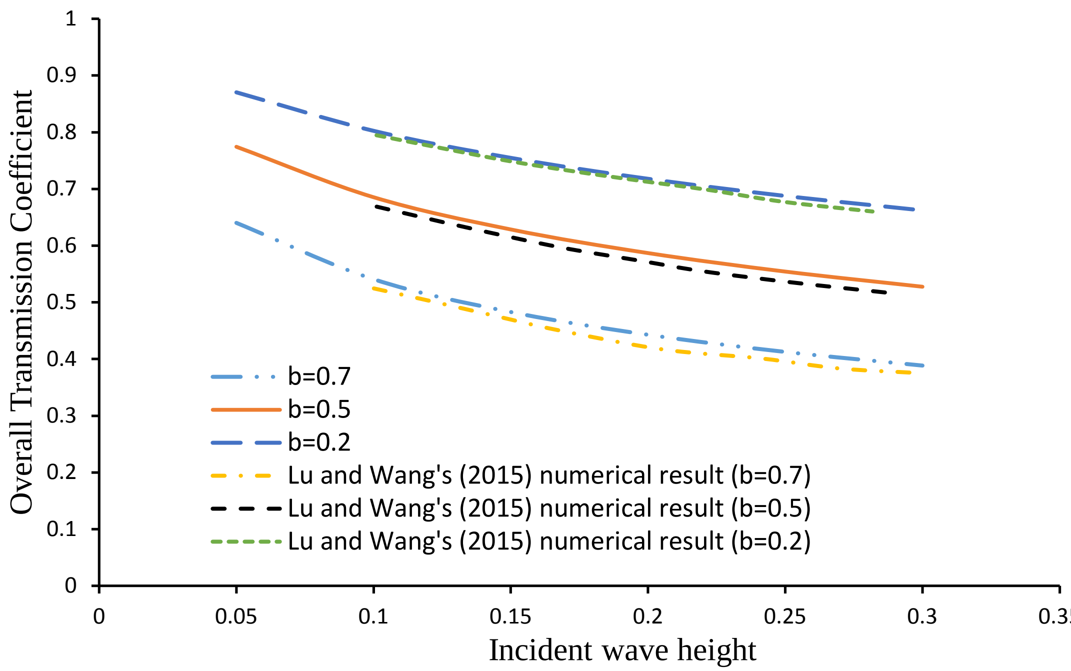

Figure 6-12: Comparisons of the overall transmission coefficient obtained from the analytical solutions and Lu and Wang's (2015) numerical results for a case with $b=d$ (no porous conditions), and $L=4$.

6.2 Parametric Study of the Effects of Physical Variables on the Reflection and Transmission of a Solitary Wave Interacting with a 2-D Finite-Length Body with Attached Dual Porous Walls

In this section, the influences of various affecting physical parameters including incident wave height, 2-D body draft, submerged depth of porous walls, $R_e b_1$, $R_e b_2$ and structural length on the reflection and transmission of the incident wave are examined. Results of examining the effects of the identified parameters on the physical variables of wave run-up on the encountering face of the body, time variation of the free-surface elevations in regions 1 and 3, and the overall reflection and transmission coefficients are presented in this section.

6.2.1 Effect of Incident Wave Height

The incident wave height is one of the important parameters affecting the reflection and transmission of a solitary wave interacting with a 2-D finite-length body with attached two porous walls. Figure 6-13 presents the variations of wave run-up versus the incident wave height for a 2-D finite-length body (L=*6*) with various body drafts, however, with no porous wall conditions, and Figure 6-14 shows the results of wave run-up under the similar conditions as described in Figure 6-13, but with dual porous walls applied, where d=*1* and $b_1 = b_2 = 10^{-5}$). It is found that as the incident wave height increases, the wave run-up on the encountering face of the body is shown to have a linearly increasing trend for both conditions with or without dual porous walls. When the body draft increases, the wave run-up also increases as expected. Comparing Figure 6-13 with Figure 6-14, the dual porous walls tend to increase slightly the wave run-ups for cases when the body draft is smaller. This is mainly caused by the added impacts on the additional porous wall structures. Also, as the body draft positions to a large value, the effect of the dual porous walls on the wave run-up becomes less important.

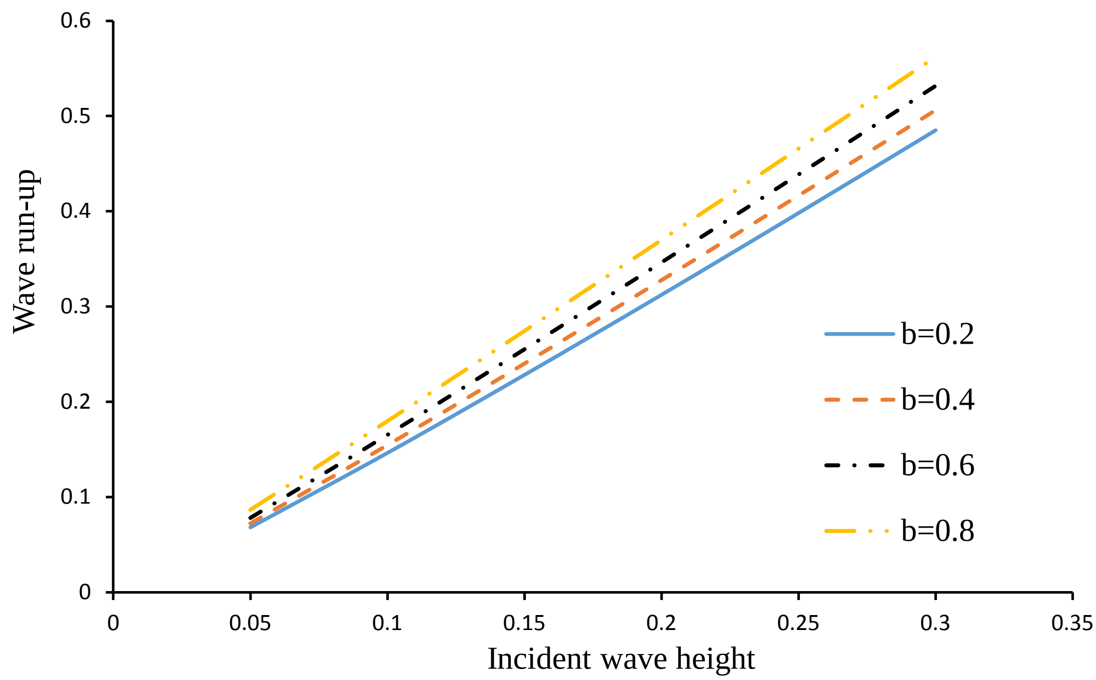

Figure 6-13: Wave run-up vs. incident wave height for a 2-D finite-length body ($L=6$) with various b (no porous conditions).

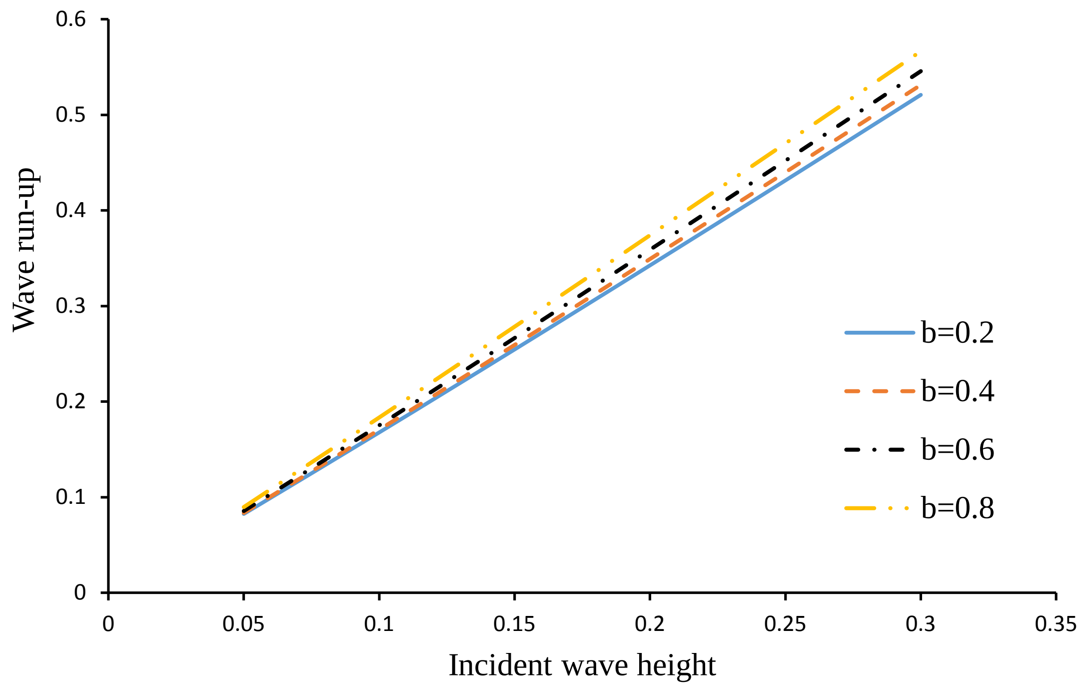

Figure 6-14: Wave run-up vs. incident wave height for a 2-D finite-length body (L=6) with various b (with porous conditions as d=1 and $b_1 = b_2 = 10^{-5}$).

When the body length is reduced from L=6 to L=4, the results of wave run-up versus the incident wave height for a 2-D finite-length body (L=4) for various body drafts (no porous conditions) are presented in Figure 6-15 while similar plots for the body system with additional dual porous walls (d=1 and $b_1 = b_2 = 10^{-5}$) are displayed in Figure 6-16. By comparing Figure 6-13 with Figure 6-15, we notice that as the structural length decreases, the wave run-up decreases. Also, as the body length decreases, the effect of the body draft on wave run-up increases. Similar results from Figure 6-14 and Figure 6-16 suggest that the dual porous walls decrease the effect of the structural length on the variation of wave run-up.

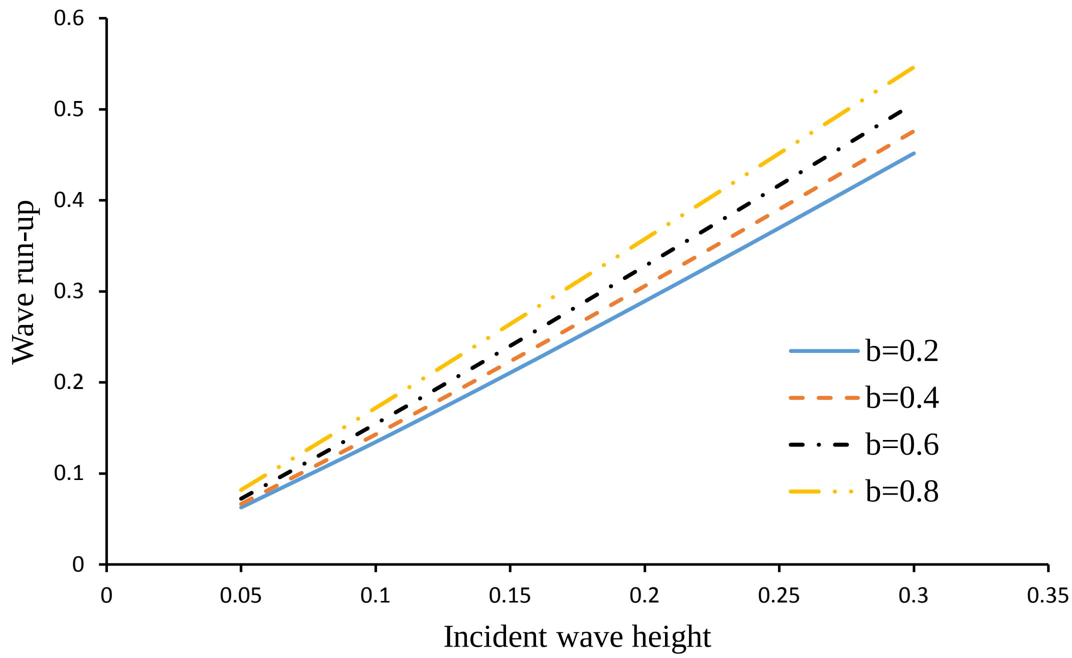

Figure 6-15: Wave run-up vs. incident wave height for a 2-D finite-length body ($L=4$) with various b (no porous conditions).

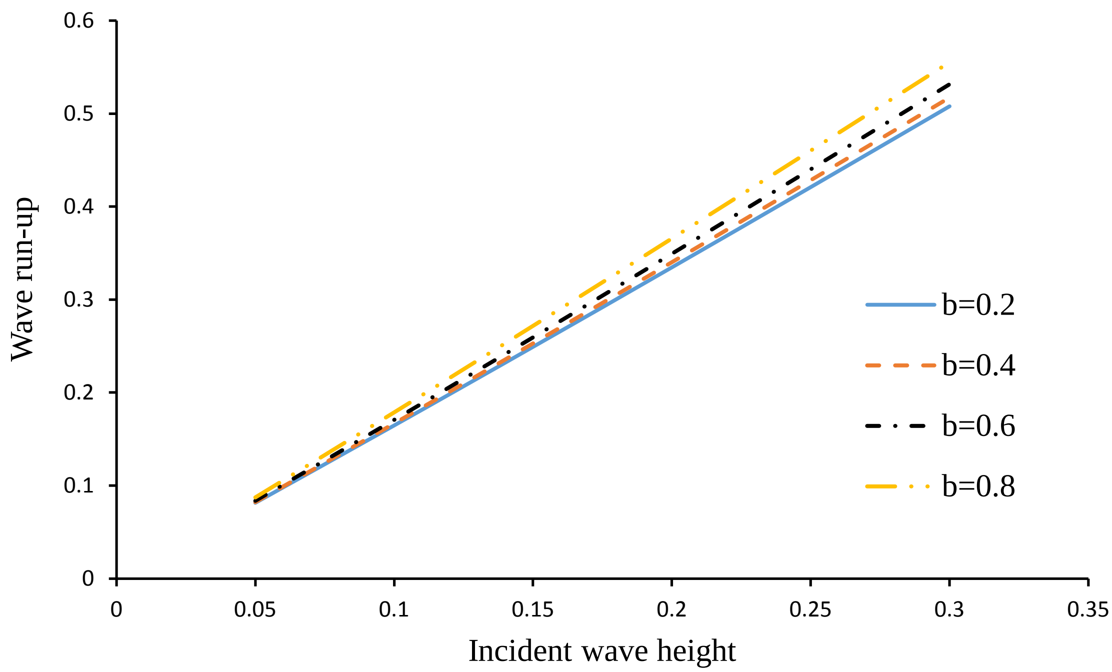

Figure 6-16: Wave run-up vs. incident wave height for a 2-D finite-length body ($L=4$) with various b (with porous conditions as $d=1$ and $b_1 = b_2 = 10^{-5}$).

Figure 6-17 presents the time variations of derived analytical solutions of free-surface elevation in regions 1 and 3 for solitary waves with various incident wave heights interacting with a partially submerged structure described above where its settings include *b=d=0.5* (no porous walls) and *L=6*. The location for plotting the results of incident and reflected wave profiles is set at *x=-12* in region 1 while the transmitted waves are presented at x=*53/3* in region 2. Throughout this chapter, the same setups in terms of locations of showing the free-surface profiles are used for all figures giving the results of the free-surface elevations. As expected, when the incident wave height increases, relatively, both the reflected and transmitted wave heights increase. Comparing Figure 6-17 with Figure 6-18 which is a plot of similar case with a smaller body draft (*b=d=0.2*), it can be seen as the body draft decreases, the reflected wave heights decrease while the transmitted wave heights increase.

Adding the effect of dual porous walls ($b_1 = b_2 = 10^{-5}$)Figure 6-19 to the partially submerged body with results shown in Figure 6-17, the free-surface elevations in regions 1 and 3 are presented in Figure 6-19. Comparing to Figure 6-17, we notice that the reflected wave heights increase and the transmitted wave heights decrease. This suggests that the added porous walls can enhance the reduction of the transmitted waves. Finally, Different from the case presented in Figure 6-19, Figure 6-20 illustrates the results of wave profiles using a smaller structural length, i.e. *L*=4. Again, the decreasing in structural length reflects a decrease in reflected wave height and accordingly an increase in transmitted wave height.

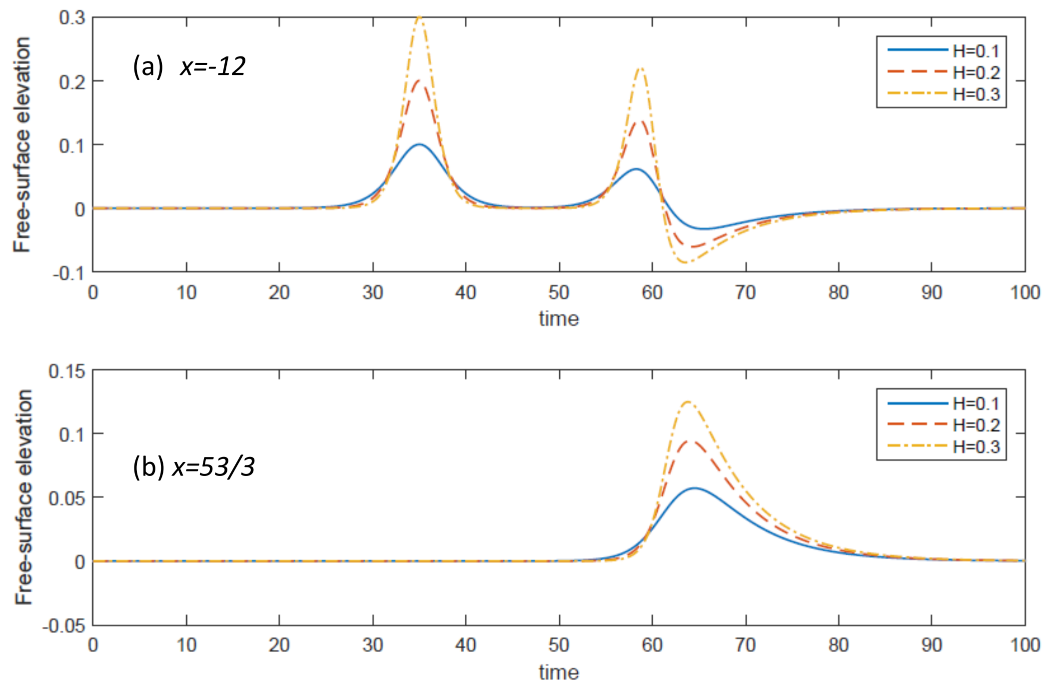

Figure 6-17: Time variations of derived analytical solutions of free-surface elevation for solitary waves with various H for a case with $b=d=0.5$ (no porous conditions) and $L=6$: (a) incident and reflected wave; (b) transmitted wave.

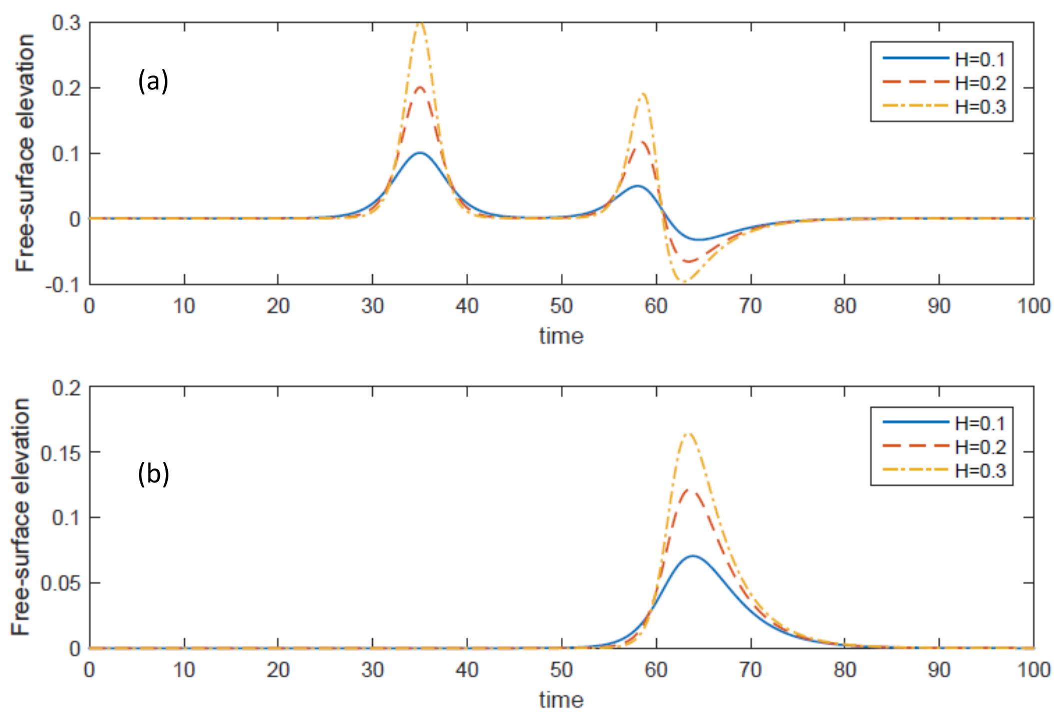

Figure 6-18: Time variations of derived analytical solutions of free-surface elevation for solitary waves with various H for a case with $b=d=0.2$ (no porous conditions) and $L=6$: (a) incident and reflected wave; (b) transmitted wave.

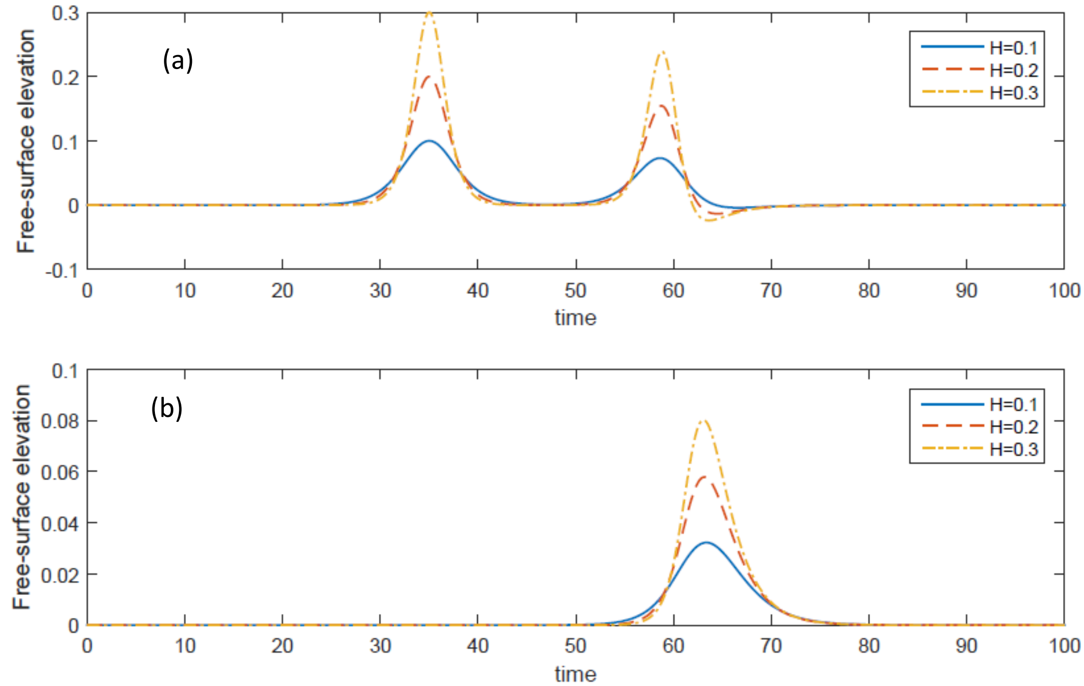

Figure 6-19: Time variations of derived analytical solutions of free-surface elevation for solitary waves with various H for a case with $b = 0.5$, $d=1$, $L=6$ and as $b_1 = b_2 = 10^{-5}$: (a) incident and reflected wave; (b) transmitted wave.

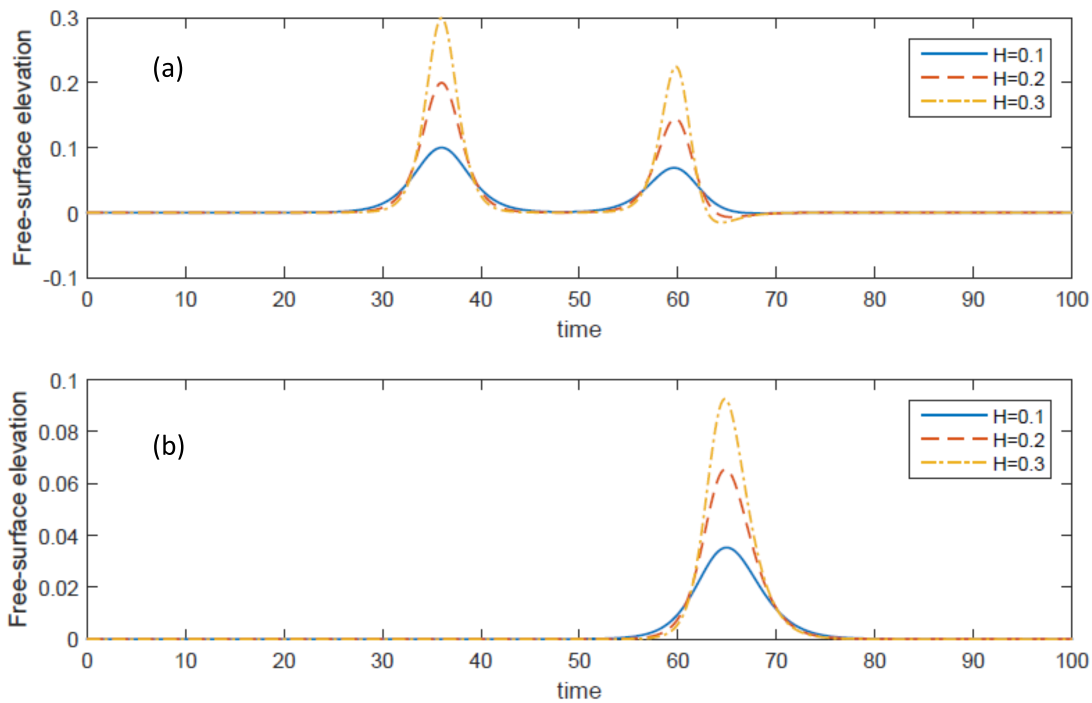

Figure 6-20: Time variations of derived analytical solutions of free-surface elevation for solitary waves with various H for a case with $b = 0.5$, $d=1$, $L=4$ and as $b_1 = b_2 = 10^{-5}$: (a) incident and reflected wave; (b) transmitted wave.

Additionally, the effect of incident wave height on the reflection coefficient (C_R) and transmission coefficient (C_T) for a solitary wave interacting with a 2-D finite-length body with attached dual porous walls under various body draft conditions is examined with results presented in Figure 6-21 to Figure 6-28. Figure 6-21 and Figure 6-22 give respectively the results of C_R for L=6 and conditions of without and with dual porous walls attached. The corresponding plots for C_T are shown in Figure 6-25 and Figure 6-26. For a smaller structural length, L=4, the results under the conditions of without and with dual porous walls are illustrated respectively in Figure 6-23 and Figure 6-24 for C_R and in Figure 6-27 and Figure 6-28 for C_T . It is noted from the comparisons that as the incident wave height or the body draft increases, the overall reflection coefficient increases while the overall transmission coefficient decreases. Adding the dual porous walls results in slightly increase in reflection coefficient when the body draft is small. However, the overall transmission coefficient is found to be significantly reduced, especially for cases with smaller incident wave height waves. Additionally, the dual porous walls are also found to have a greater influence on C_R and C_T for cases with smaller body draft than those with larger body draft. When the structural length decreases from 6 to 4, the variation trends of C_R and C_T verse the incident wave height are similar to those with L=6 case. It is also noted that the influence of structural length on C_R and C_T is shown to be stronger when the body draft is small.

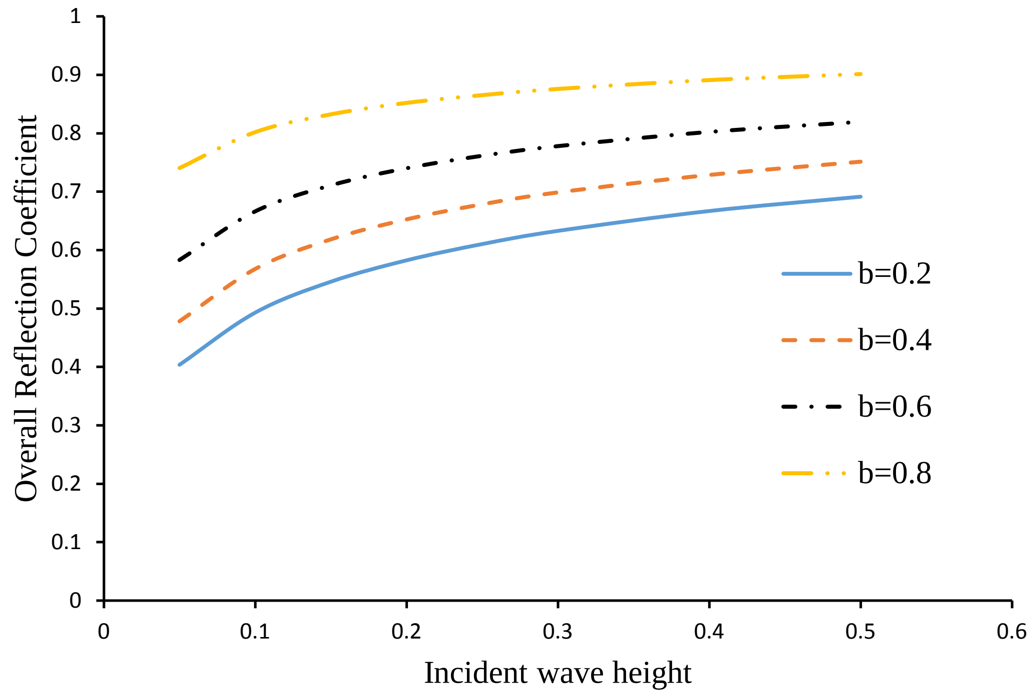

Figure 6-21: The overall reflection coefficient vs. incident wave height for various *b* for a case with $L=6$ and $d=b$ (no porous condition).

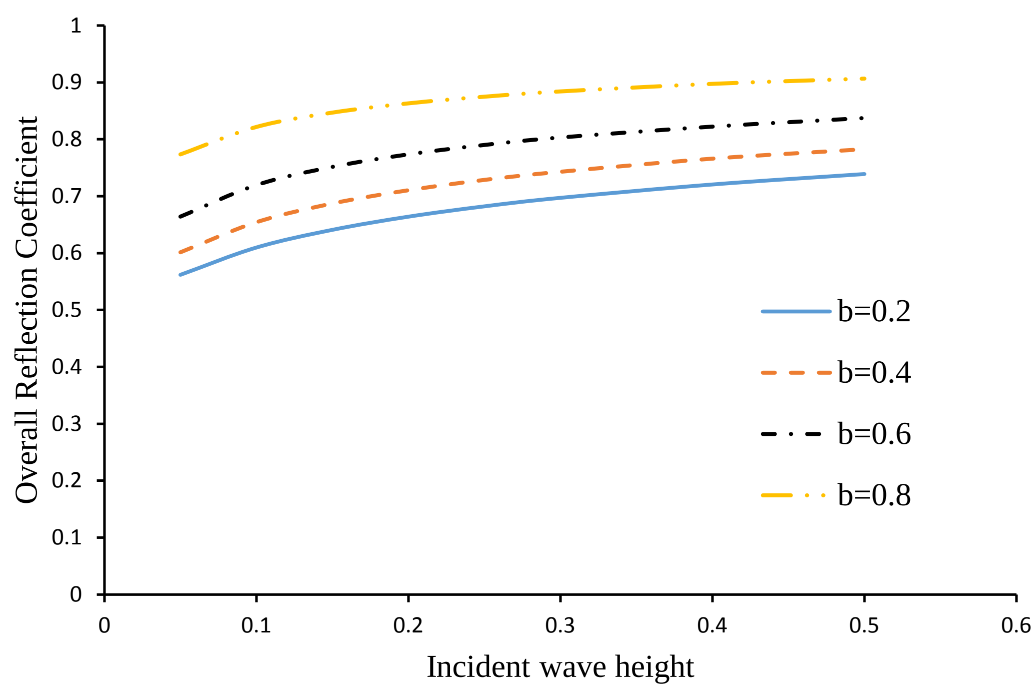

Figure 6-22: The overall reflection coefficient vs. incident wave height for various *b* for a case with $L=6$ and $d=1$ ($b_1 = 1.6\times10^{-5}$ and $b_2 = 2.4\times10^{-5}$).

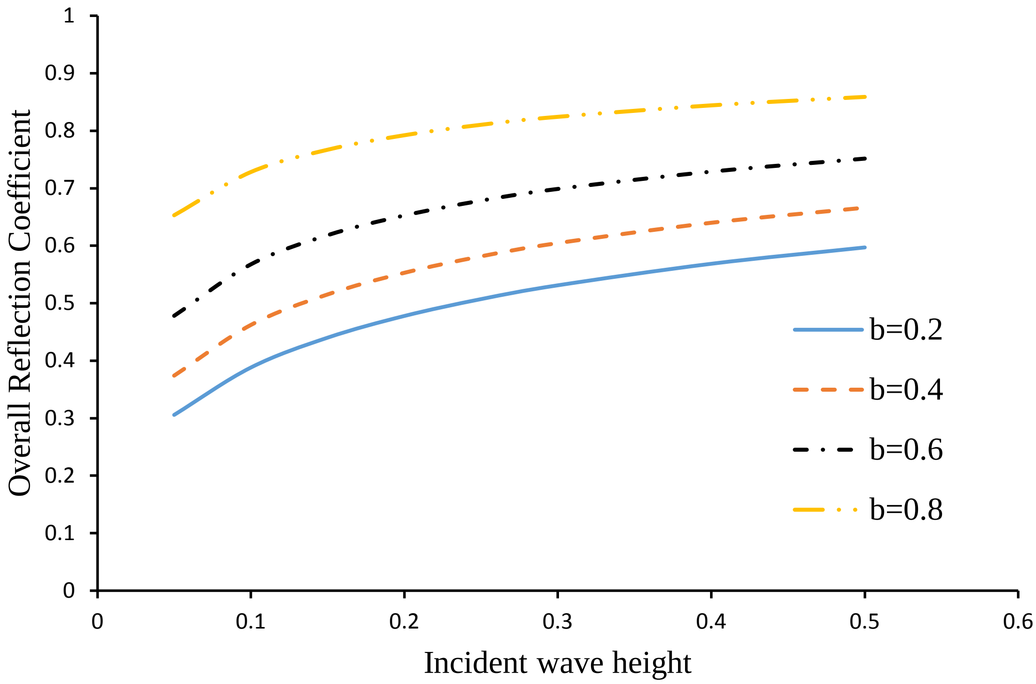

Figure 6-23: The overall reflection coefficient vs. incident wave height for various *b* for a case with $L=4$ and $d=b$ (no porous condition).

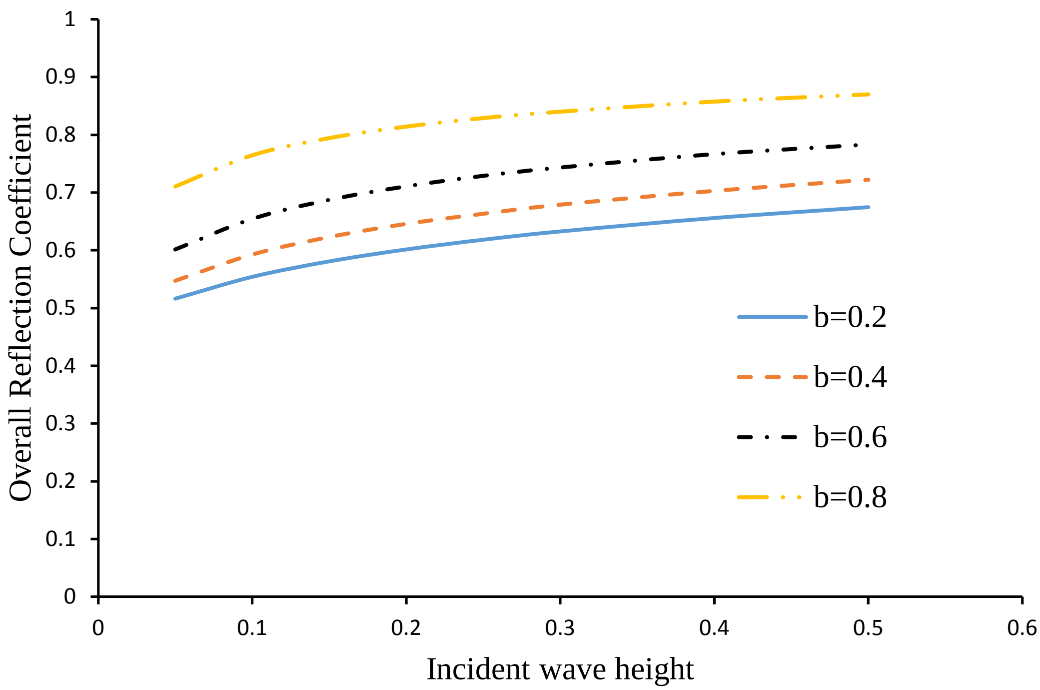

Figure 6-24: The overall reflection coefficient vs. incident wave height for various *b* for a case with $L=4$ and $d=1$ ($b_1 = 1.6\times10^{-5}$ and $b_2 = 2.4\times10^{-5}$).

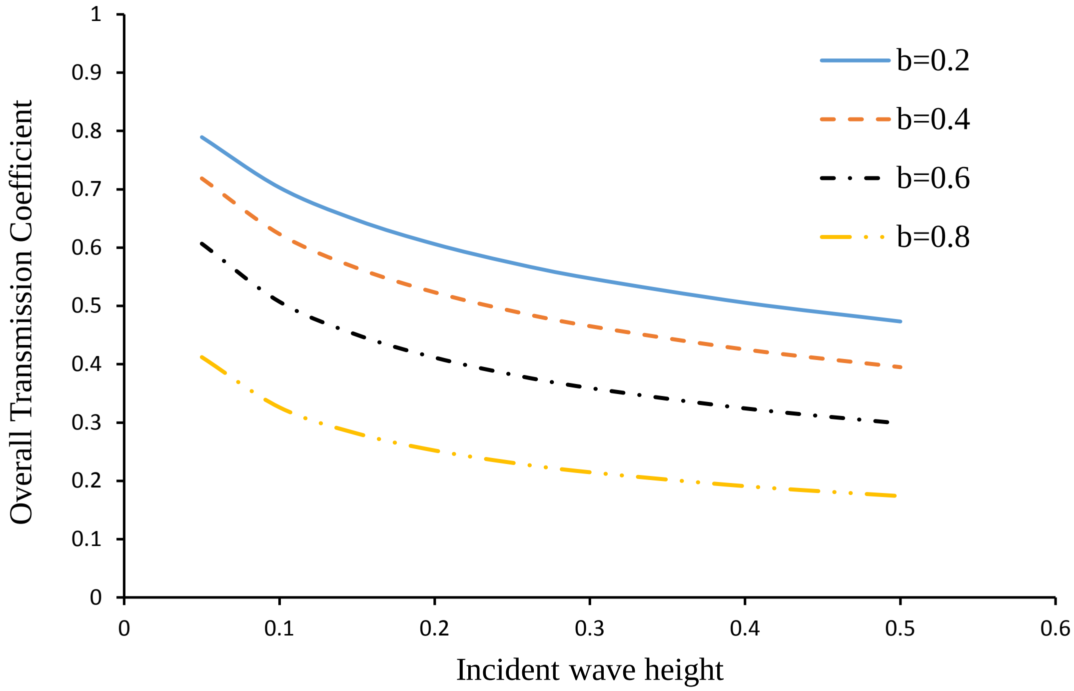

Figure 6-25: The overall transmission coefficient vs. incident wave height for various *b* for a case with $L=6$ and $d=b$ (no porous condition).

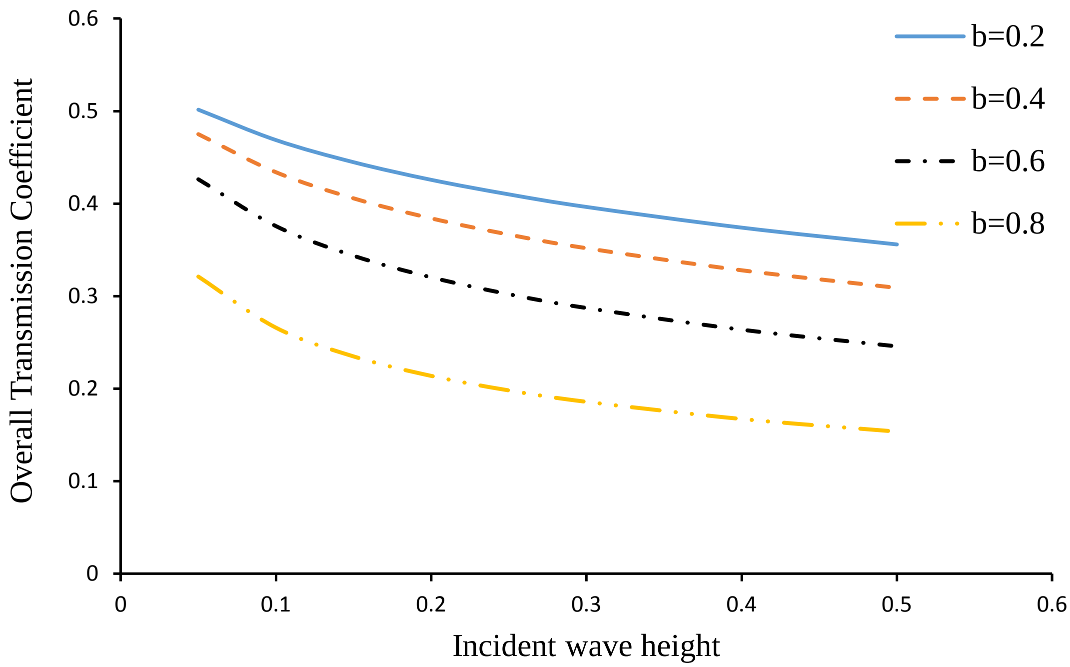

Figure 6-26: The overall transmission coefficient vs. incident wave height for various *b* for a case with $L=6$ and $d=1$ ($b_1 = 1.6\times10^{-5}$ and $b_2 = 2.4\times10^{-5}$).

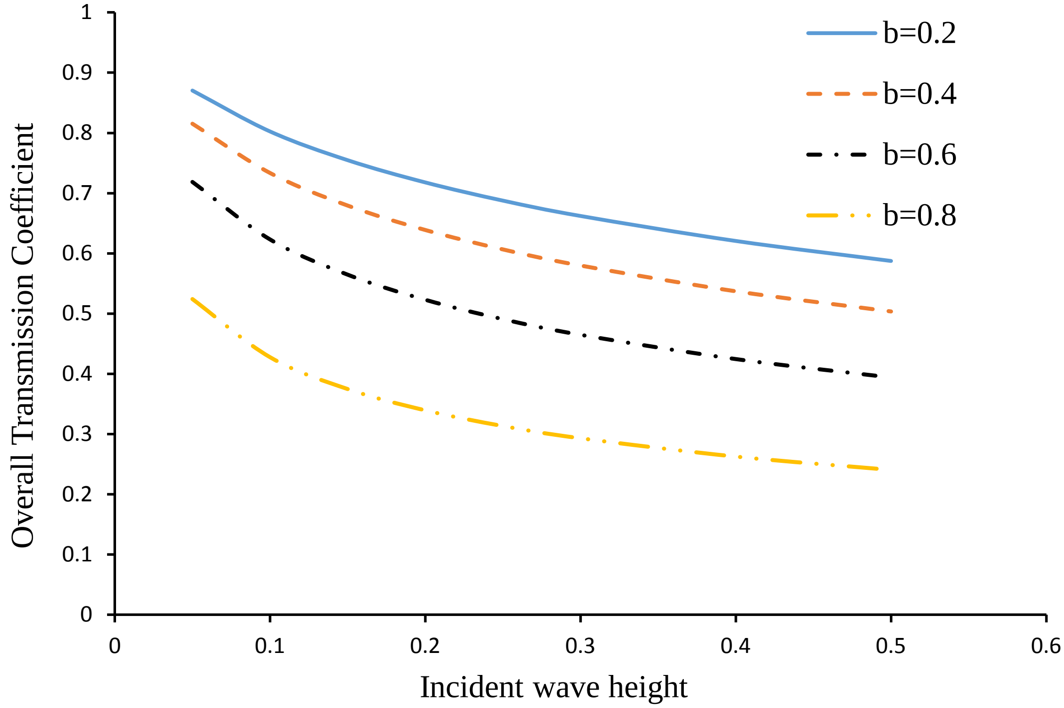

Figure 6-27: The overall transmission coefficient vs. incident wave height for various *b* for a case with *L=4* and *d=b* (no porous condition).

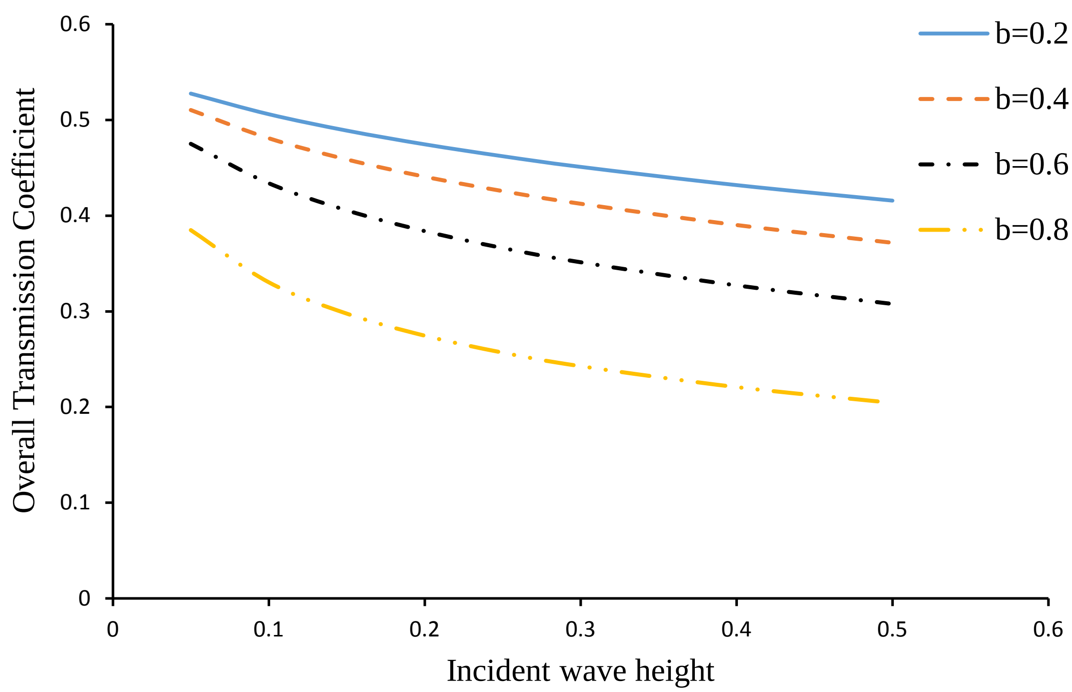

Figure 6-28: The overall transmission coefficient vs. incident wave height for various *b* for a case with *L=4* and *d=1* ($b_1 = 1.6\times10^{-5}$ and $b_2 = 2.4\times10^{-5}$).

6.2.2 Effect of 2-D Body Draft

Since the 2-D body draft is a very critical parameter in partially submerged barrier study, the effect of the draft of 2-D body on the physical variables, such as the wave run-up on the front face of the body, time variation of the free-surface elevations in regions 1 and 3, and the overall reflection and transmission coefficients is examined with the results plotted versus the body draft presented. For the variations of wave run-up versus the body draft for the cases of *L*=6 and various incident wave heights, Figure 6-29 and Figure 6-30 are shown for cases without porous walls and with porous walls (d=1 and $b_1 = b_2 = 10^{-5}$), respectively. The comparison cases for *L*=4 are presented in Figure 6-29 and Figure 6-32, respectively for not including the porous walls and including the porous walls. For all incident waves, with or without porous walls, the results indicate that when the body draft increases, the wave run-up shows a trend of gradual increase. Comparing Figure 6-29 with Figure 6-30, the additions of the dual porous walls increases slightly the wave run-up, and when the body draft is small, the differences between the wave run-ups under the conditions with or without porous walls are more noticeable. Also, decreasing the structural length from 6 to 4, as shown in Figure 6-31 and Figure 6-32, the general variation trends of the wave run-up are similar to those shown in Figure 6-29 and Figure 6-30.

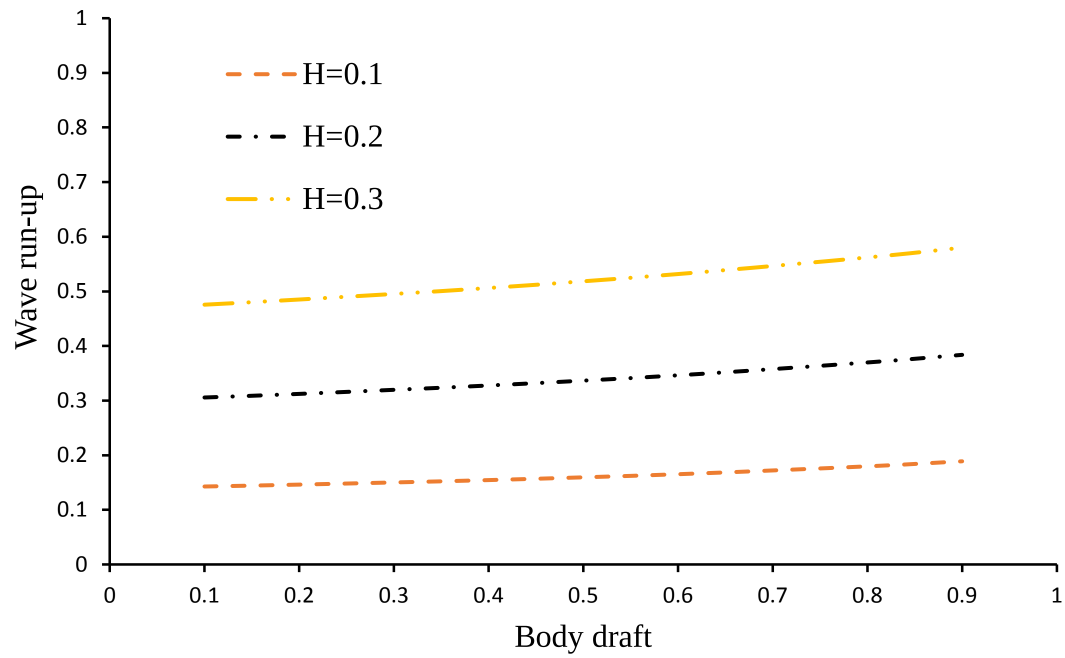

Figure 6-29: Wave run-up vs. the body draft ($L=6$) with various H (no porous conditions).

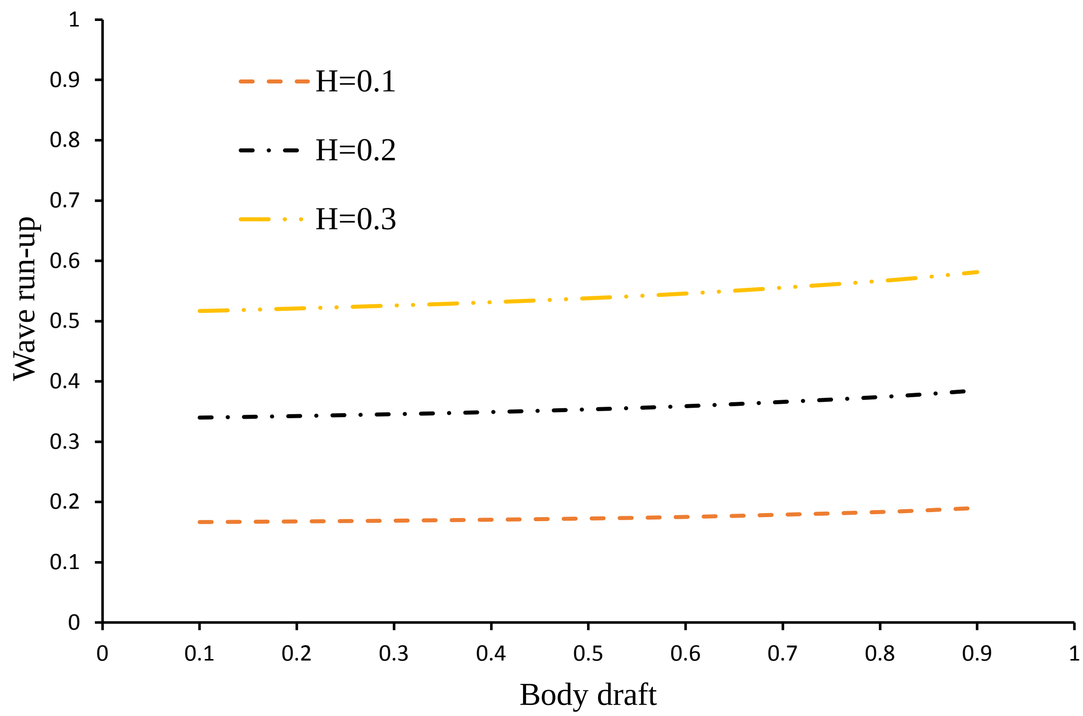

Figure 6-30: Wave run-up vs. the body draft ($L=6$) with various H (with porous conditions as $d=1$ and $b_1 = b_2 = 10^{-5}$).

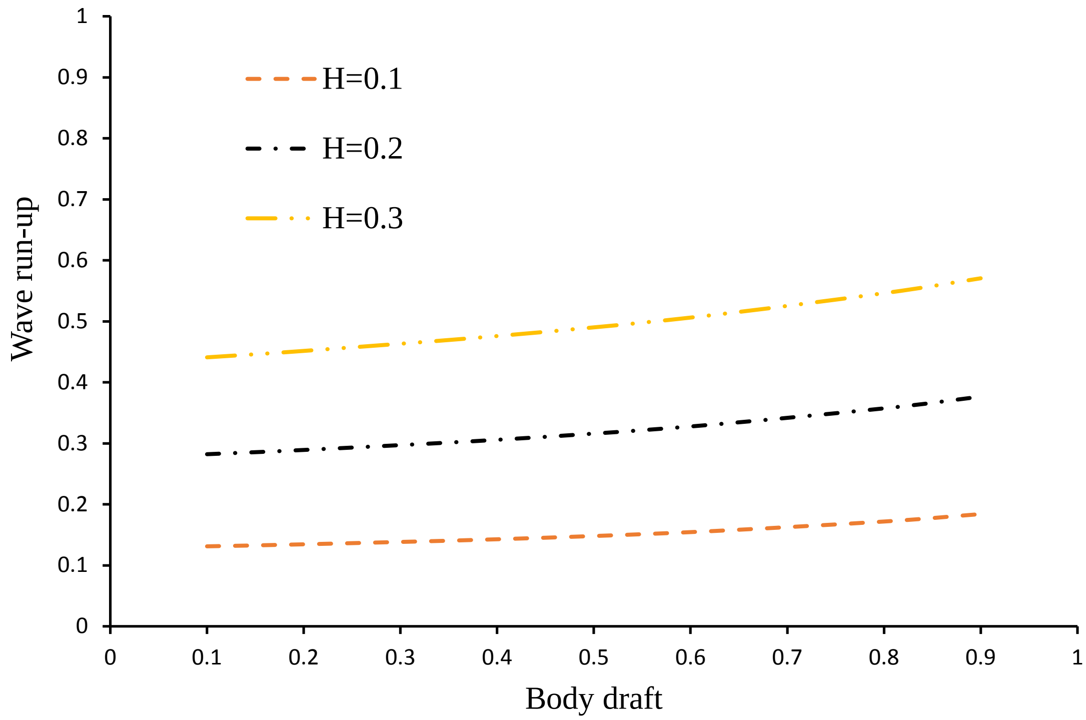

Figure 6-31: Wave run-up vs. the body draft ($L=4$) with various H (no porous conditions).

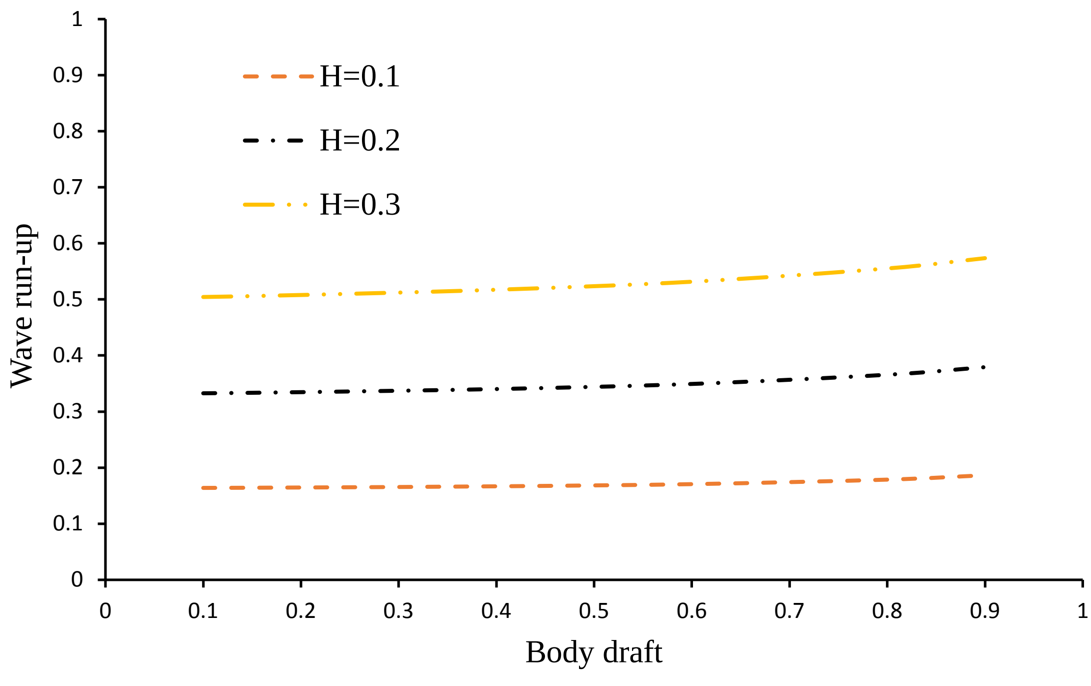

Figure 6-32: Wave run-up vs. the body draft ($L=4$) with various H (with porous conditions as $d=1$ and $b_1 = b_2 = 10^{-5}$).

Figure 6-33 through Figure 6-36 present the time variations of the free-surface elevations of a solitary wave (*H=0.2*) interacting with a 2-D finite-length body with or without dual porous walls under various body draft conditions. For the cases with dual porous walls, the porous property constants are $b_1 = b_2 = 10^{-5}$ and the submerged depth for positioning the porous walls is set as *d* =1. Again, as the body draft increases, the reflected wave height increases while the transmitted wave height decreases. From Figure 6-33 (without porous walls) and Figure 6-34 (with dual porous walls), the results again indicate that the additional porous wall structures result in slight increase in reflected wave height but greatly reduce the transmitted wave height. Figure 6-35 and Figure 6-36 are free-surface elevation plots for the corresponding results considering a smaller structural length, i.e. *L*=4. Similar conclusions can be made as the structural length decreases, the reflected wave height decreases and the transmitted wave height increases.

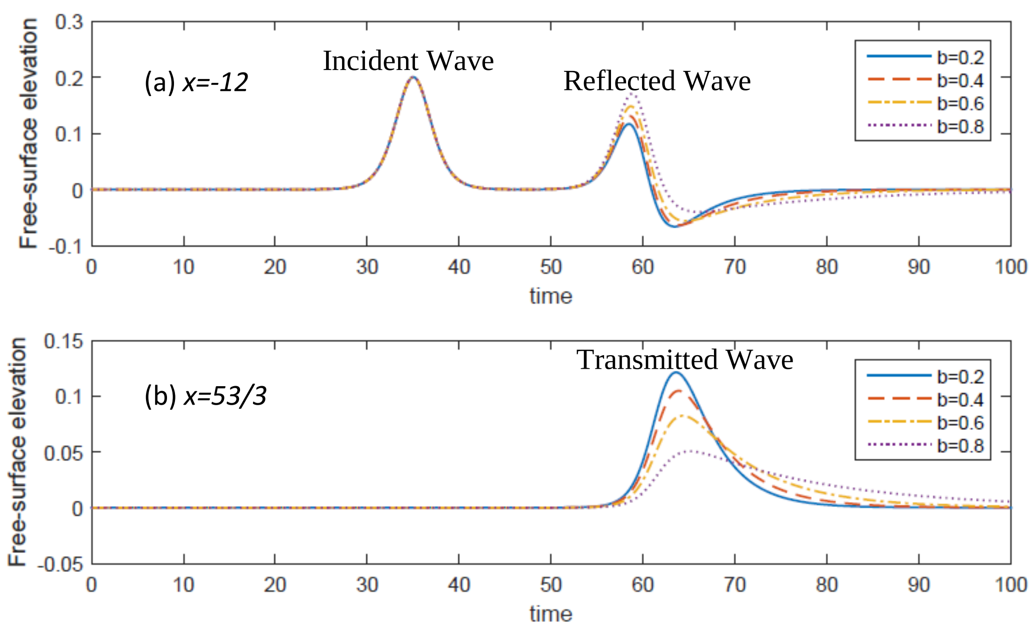

Figure 6-33: Time variations of derived analytical solutions of free-surface elevation with various *b* for a case with *H=0.2* and *L=6* (no porous conditions): (a) incident and reflected wave; (b) transmitted wave.

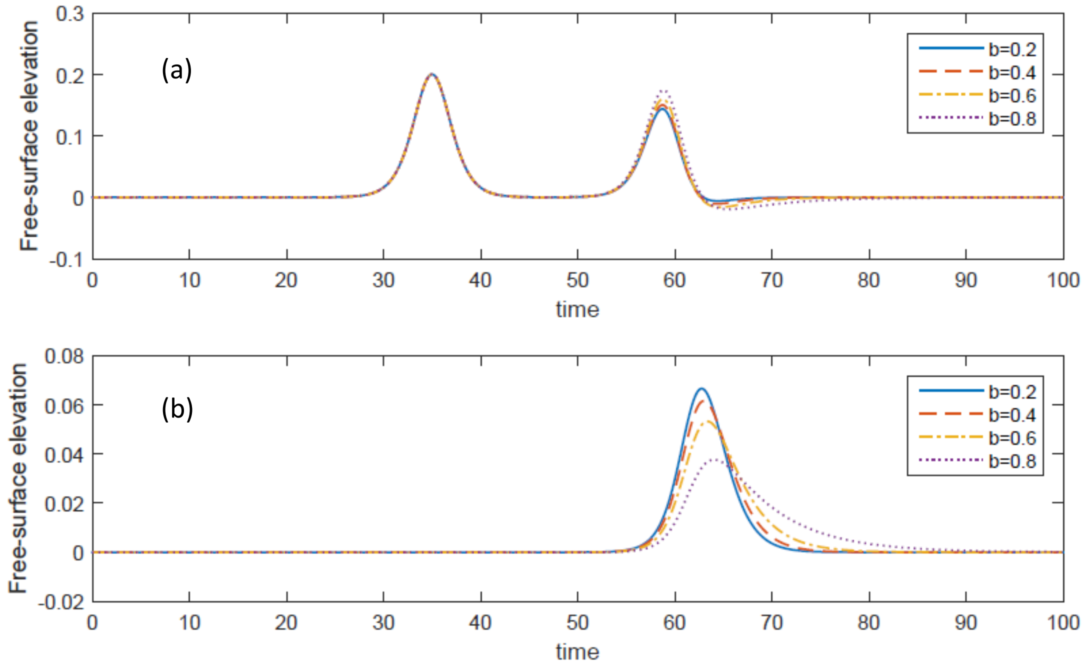

Figure 6-34: Time variations of derived analytical solutions of free-surface elevation with various b for a case with $H=0.2$, $L=6$, $d=1$ and $b_1 = b_2 = 10^{-5}$: (a) incident and reflected wave; (b) transmitted wave.

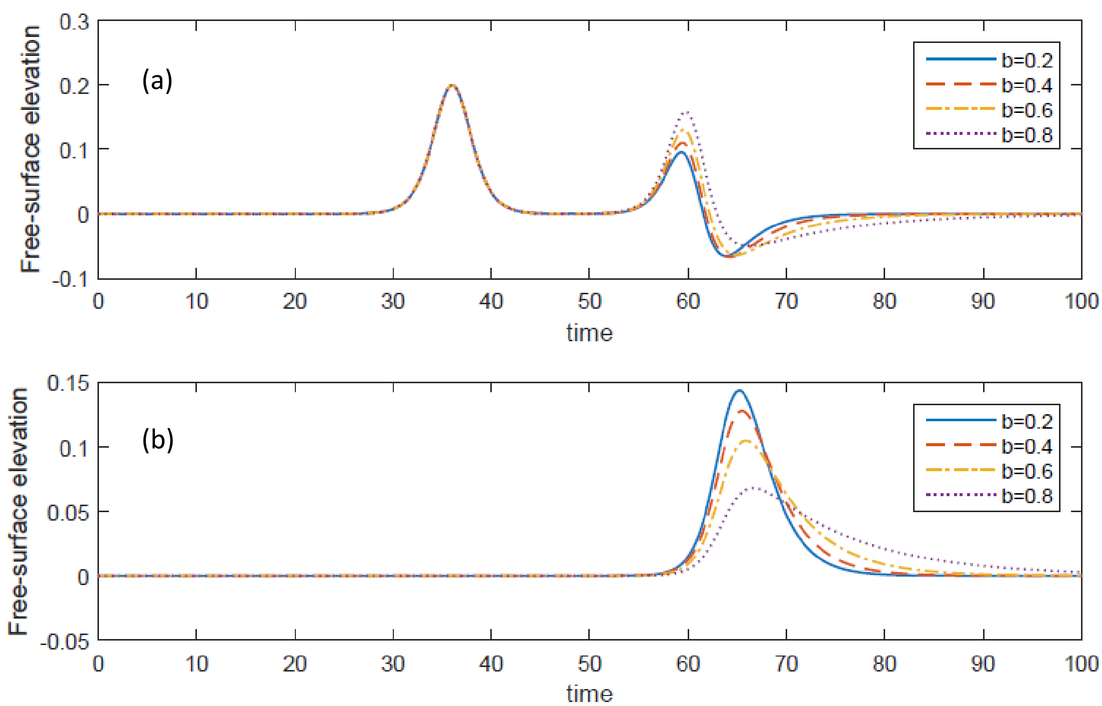

Figure 6-35: Time variations of derived analytical solutions of free-surface elevation with various b for a case with $H=0.2$ and $L=4$ (no porous conditions): (a) incident and reflected wave; (b) transmitted wave.

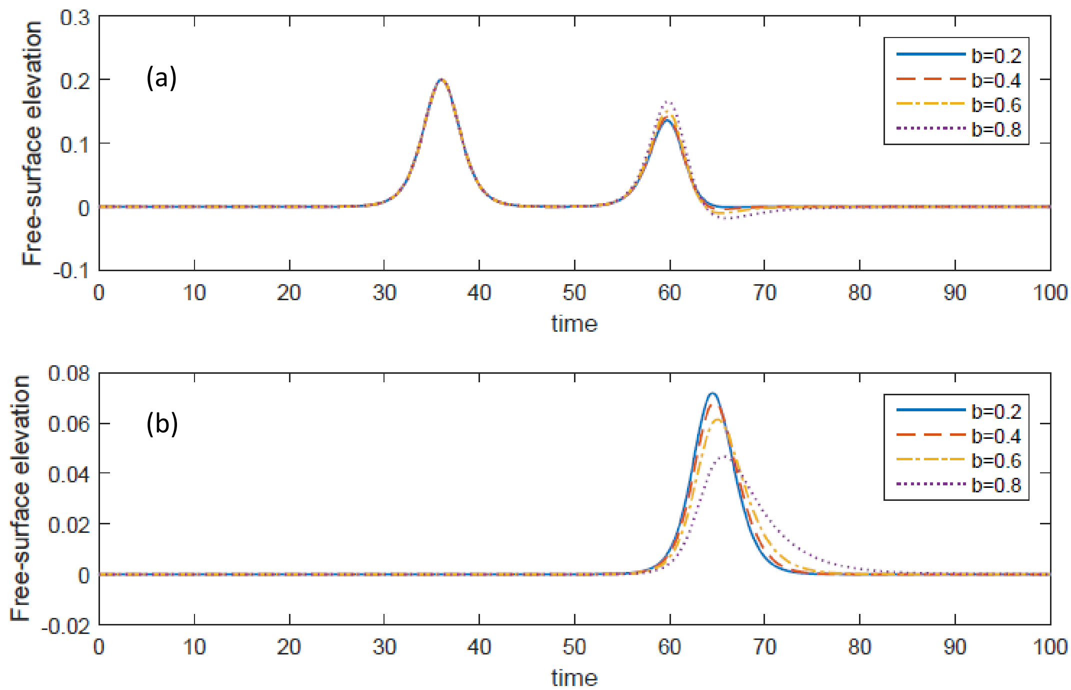

Figure 6-36: Time variations of derived analytical solutions of free-surface elevation with various b for a case with $H=0.2$, $L=4$, $d=1$ and $b_1 = b_2 = 10^{-5}$: (a) incident and reflected wave; (b) transmitted wave.

Figure 6-37 through Figure 6-44 present the overall reflection and transmission coefficients versus body draft for cases with various incident wave heights and the conditions without or with the porous walls. The body length is set as L=6. Similar to the results discussed in the free-surface profiles, the result show that when the body draft increases, the overall reflection coefficient increases and the overall transmission coefficient decreases. The added dual porous walls can effectively reduce the overall transmission coefficient for most body draft conditions. Its effectiveness is more significant when the body draft is small. Figure 6-39 to Figure 6-40 illustrate the corresponding results as given in Figure 6-37 to Figure 6-38 by means of a smaller structural length which is equal to 4. Similar to the conclusions mentioned above for the wave profiles, the decrease of the structural length causes the decrease of the overall reflection coefficient and accordingly the increase in overall transmission coefficient.

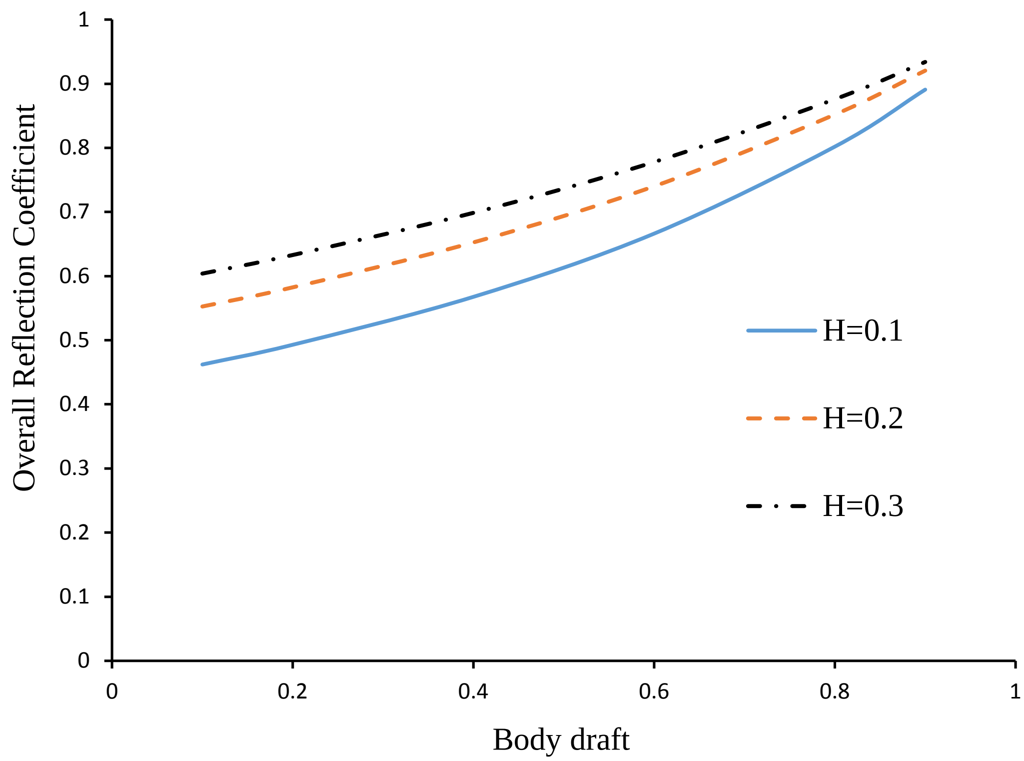

Figure 6-37: The overall reflection coefficient vs. body draft with various *H* for a case with *L=6* and *d=b* (no porous conditions).

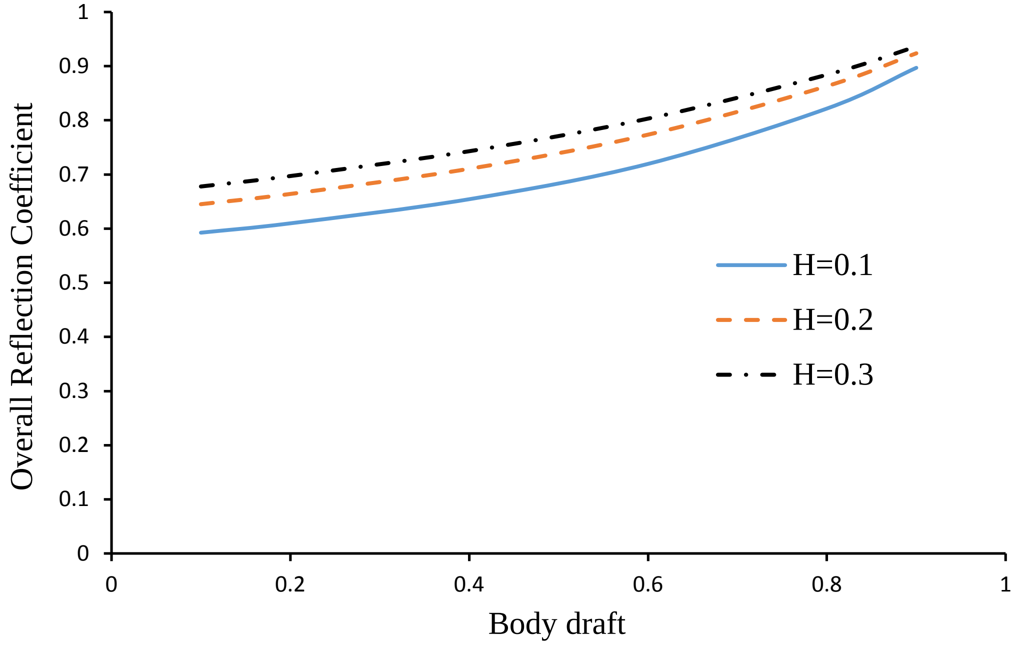

Figure 6-38: The overall reflection coefficient vs. body draft with various *H* for a case with $L=6$, $d=1$, $b_1 = 1.6*10^{-5}$ and $b_2 = 2.4*10^{-5}$.

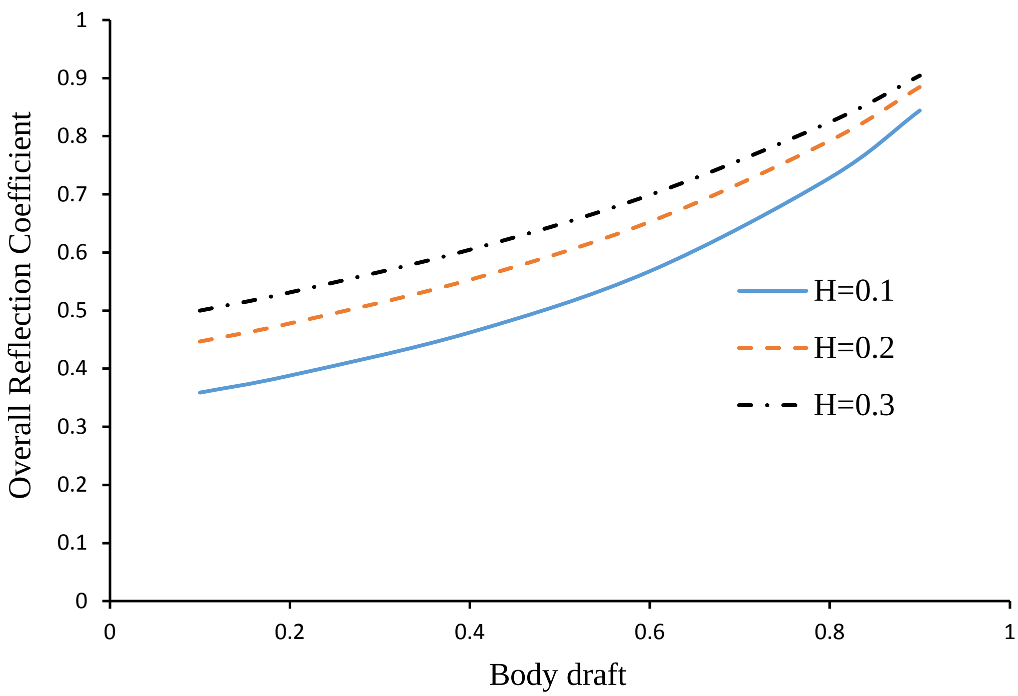

Figure 6-39: The overall reflection coefficient vs. body draft with various *H* for a case with $L=4$ and $d=b$ (no porous conditions).

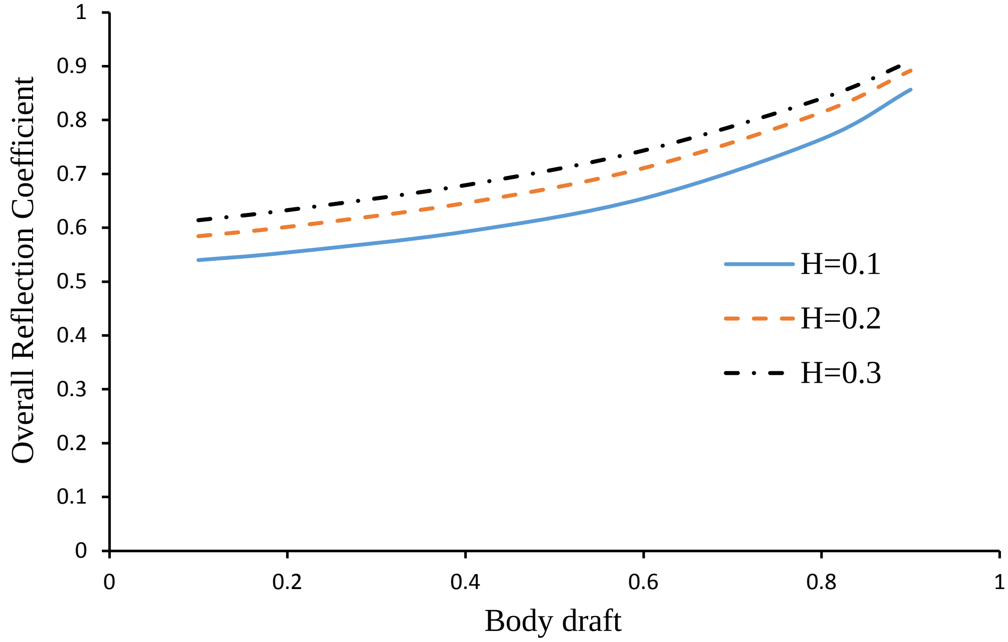

Figure 6-40: The overall reflection coefficient vs. body draft with various H for a case with $L=4$, $d=1$, $b_1 = 1.6\times10^{-5}$ and $b_2 = 2.4\times10^{-5}$.

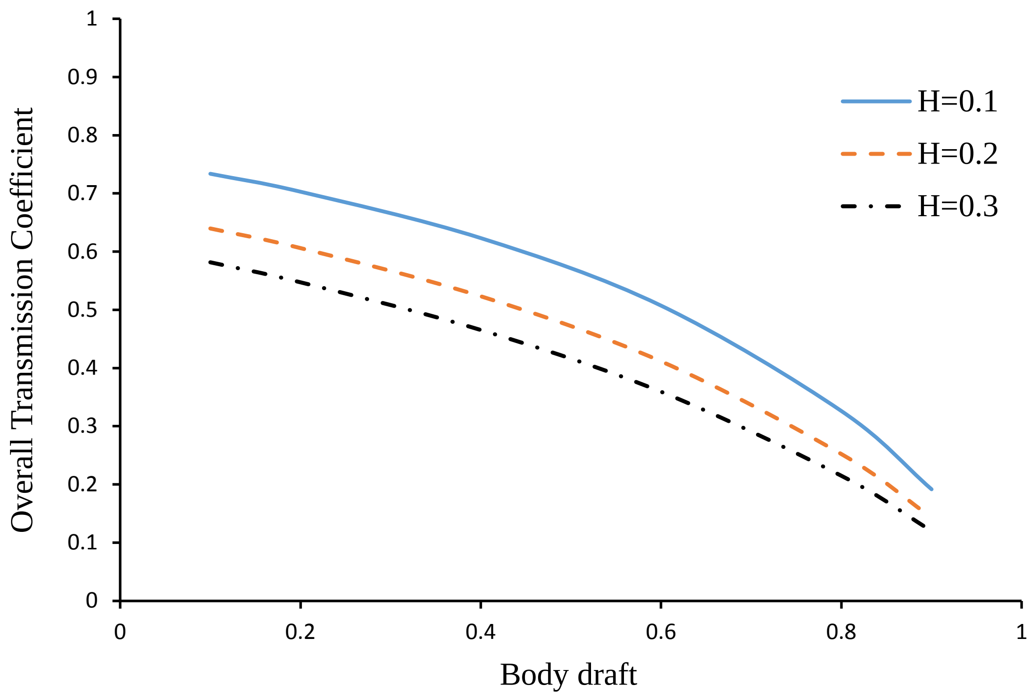

Figure 6-41: The overall transmission coefficient vs. body draft with various H for a case with $L=6$ and $d=b$ (no porous conditions).

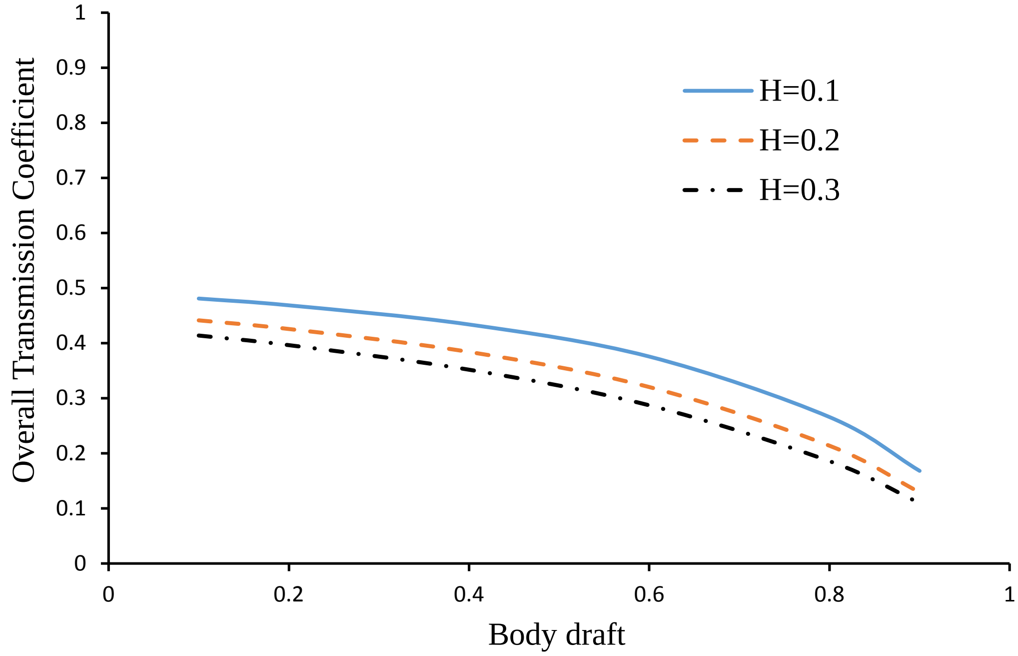

Figure 6-42: The overall transmission coefficient vs. body draft with various *H* for a case with $L=6$, $d=1$, $b_1 = 1.6\times10^{-5}$ and $b_2 = 2.4\times10^{-5}$.

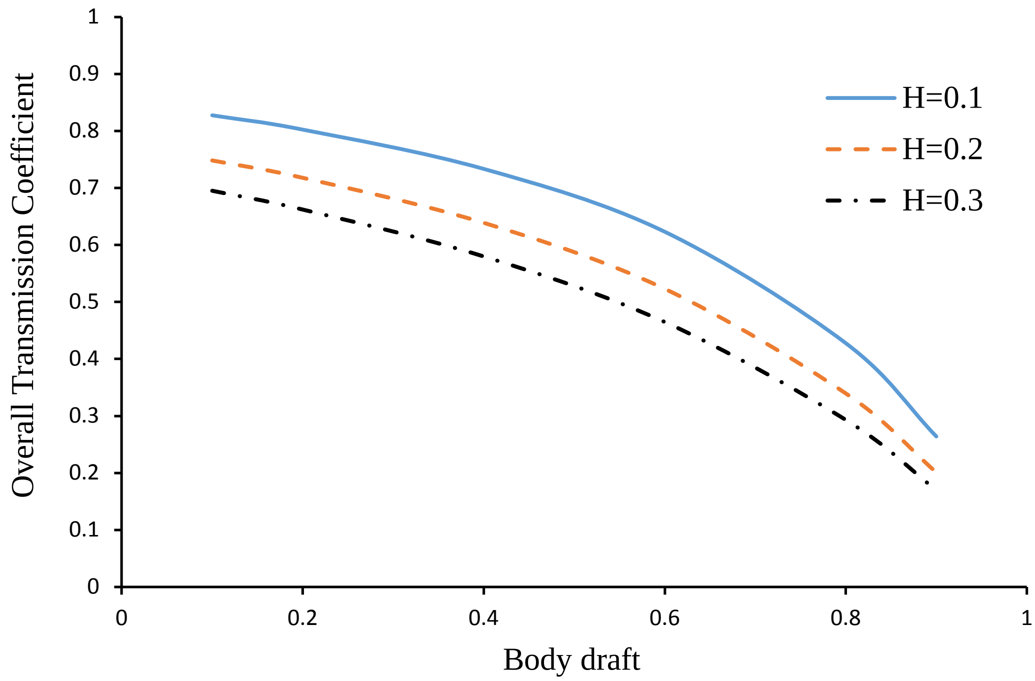

Figure 6-43: The overall transmission coefficient vs. body draft with various *H* for a case with $L=4$ and $d=b$ (no porous conditions).

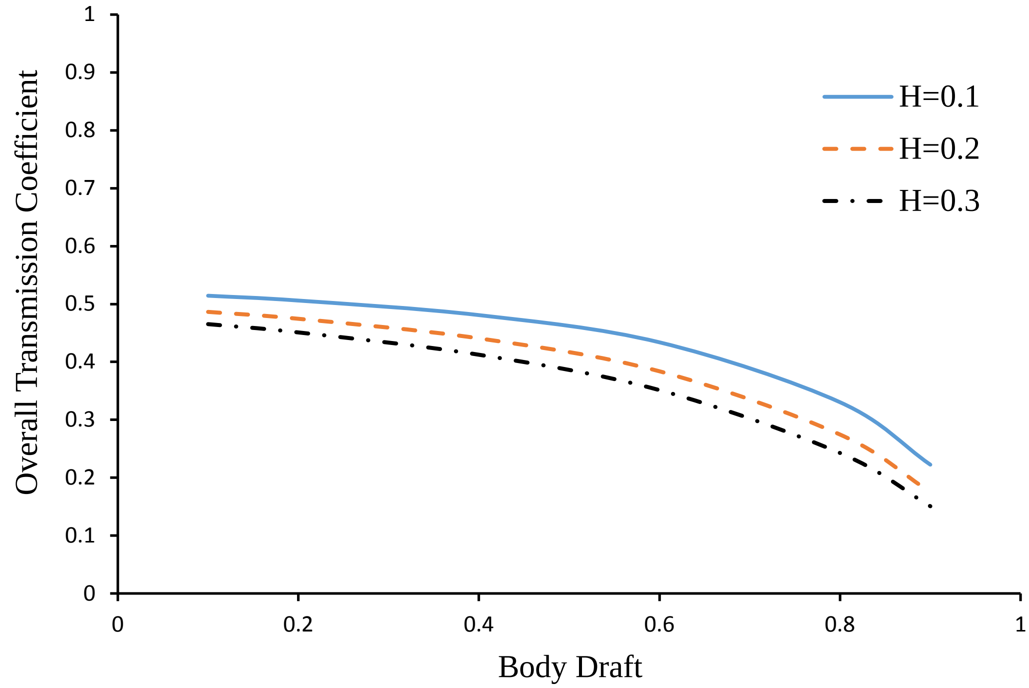

Figure 6-44: The overall transmission coefficient vs. body draft with various H for a case with $L=4$, $d=1$, $b_1 = 1.6\times10^{-5}$ and $b_2 = 2.4\times10^{-5}$.

6.2.3 Effect of Dual Porous Walls

The role played by dual porous walls in terms of their submerged depth and porous properties on the interactions between an incident solitary wave and a 2-D finite-length partially submerged body system with attached dual porous walls is investigated. Therefore, the results showing the effects of the submerged depth of porous walls and the porous-effect parameters $R_e b_1$ and $R_e b_2$ on different physical variables, including the wave run-up, time variation of the free-surface elevations in regions 1 and 3, and the overall reflection and transmission coefficients are presented and discussed in this section.

Figure 6-45 through Figure 6-47 present the wave run-ups versus the submerged depth of porous walls with various wave heights under different conditions. Figure 6-45 shows the variations of wave run-ups by varying the submerged depth of porous walls for cases with various incident wave heights and b=0.2, L=6, and $b_1 = b_2 = 10^{-5}$. Also, the R_e is set as 65882. The results indicate that when the submerged depth of porous walls increases, the wave run-up increases. Due to the effect of porous walls, a gradual increase is noticed. By varying the draft of partially submerged body, Figure 6-46 presents the results of wave run-up versus the submerged depth of porous walls for a case with H=0.2, L=6 and $b_1 = b_2 = 10^{-5}$. As the body draft increases, the opening area to cover with porous walls decreases. As a result, the wave run-up increases. When considering a shorter body length, i.e. L=4, it can be seen the variation trends of the wave run-up versus the submerged depth of porous walls that are similar to the results given in Figure 6-45 are shown in Figure 6-47.

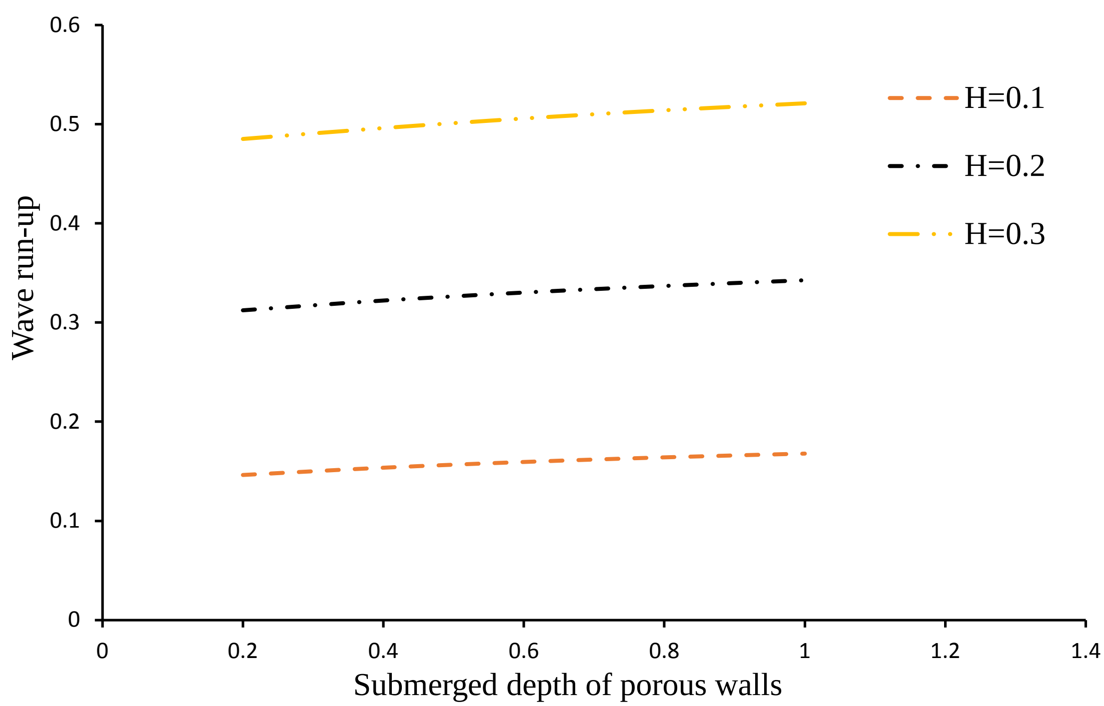

Figure 6-45: Wave run-up vs. the submerged depth of porous walls with various H for the case with b=0.2, L=6 and $b_1 = b_2 = 10^{-5}$.

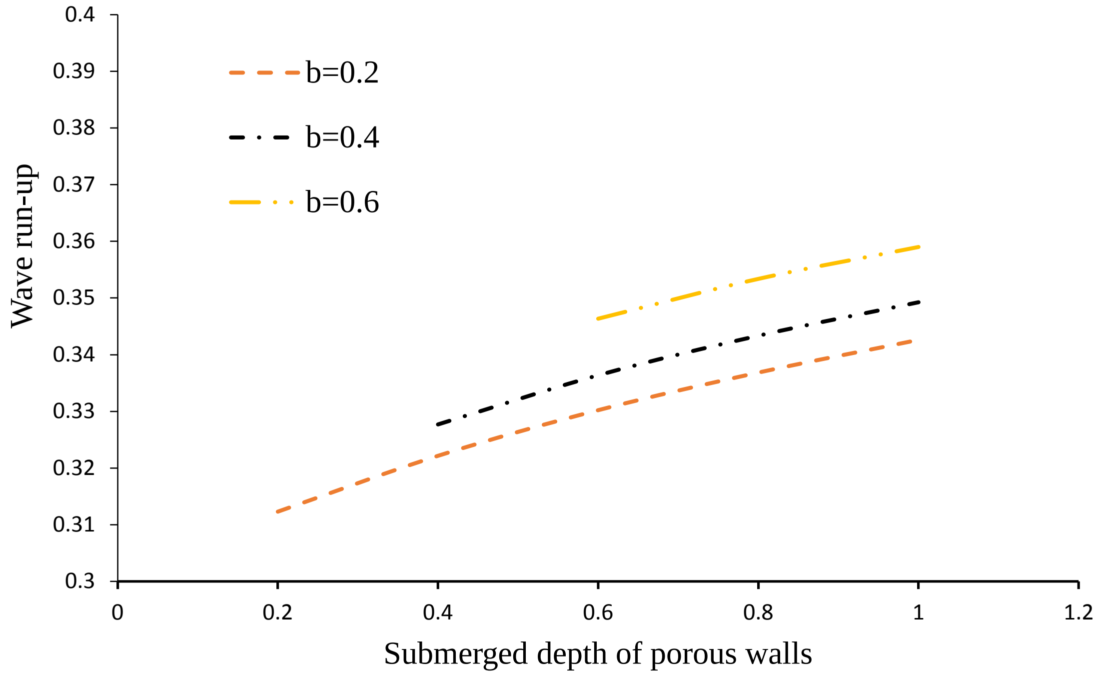

Figure 6-46: Wave run-up vs. the submerged depth of porous walls with various b for the case with $H=0.2$, $L=6$ and $b_1 = b_2 = 10^{-5}$.

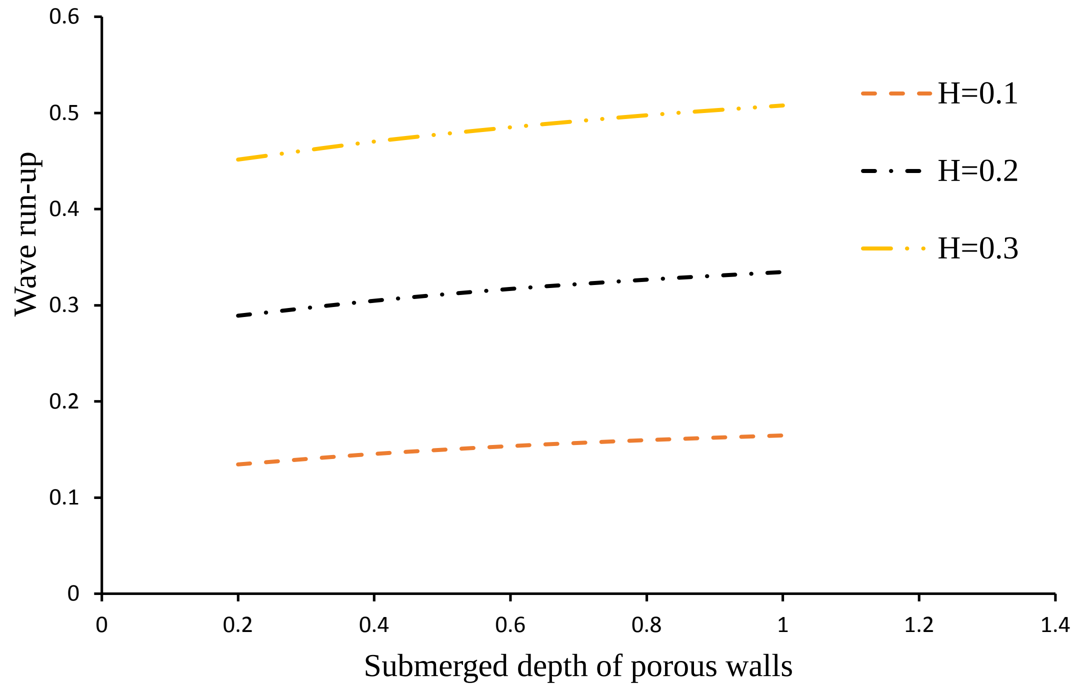

Figure 6-47: Wave run-up vs. the submerged depth of porous walls with various H for the case with $b=0.2$, $L=4$ and $b_1 = b_2 = 10^{-5}$.

The effects of porous property parameters, $R_e b_1$ and $R_e b_2$, on the variations of wave run-up are examined in Figure 6-48 through Figure 6-50. $R_e b_2$ is set to be equal to $R_e b_1$ for all the cases examined. The results of wave run-up are plotted versus $R_e b_1$. Here, we let R_e=65882 (using $h^* = 3$ inches). b_1 and b_2 are the material constants. Basically, the results suggest that when $R_e b_1$ increases, the wave run-up is shown to have a graduate decrease. Comparing results from Figure 6-48 (b=0.2) and Figure 6-49 (b=0.6), with an increase of the body draft, the effects of $R_e b_1$ and $R_e b_2$ on the rate of decreasing of the wave run-ups are reduced. Figure 6-50 presents the corresponding results for cases described for Figure 6-48 but with a smaller structural length *L*= 4. The results are shown to be similar to those illustrated in Figure 6-48.

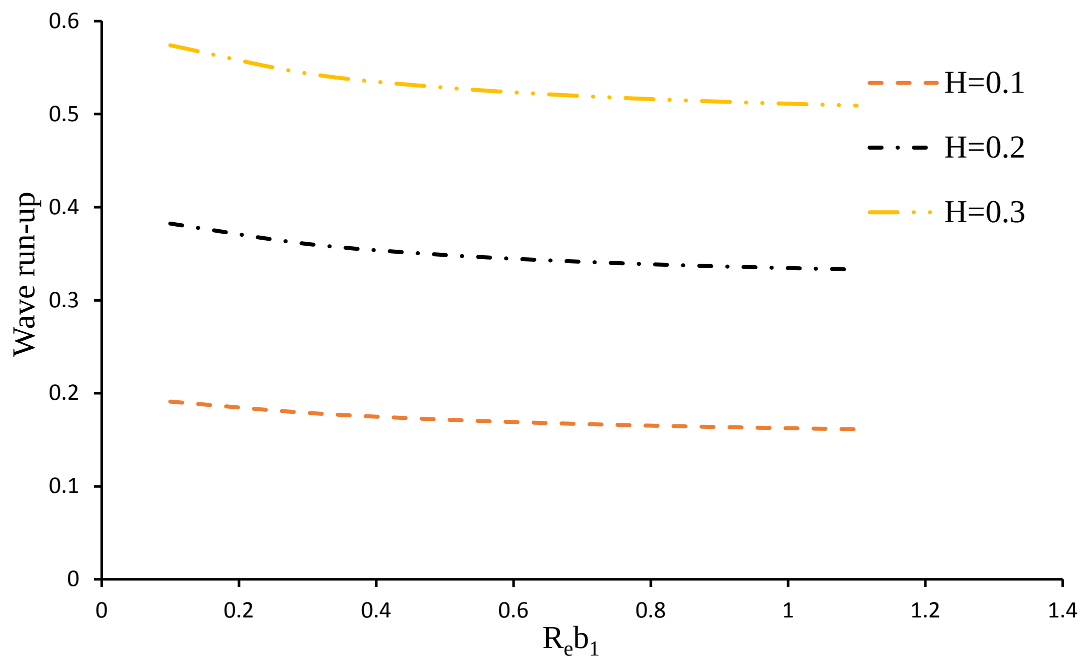

Figure 6-48: Wave run-up vs. the $R_e b_1$ with various *H* for the case with *b=0.2*, *d=1*, *L=6* and $R_e b_1 = R_e b_2$.

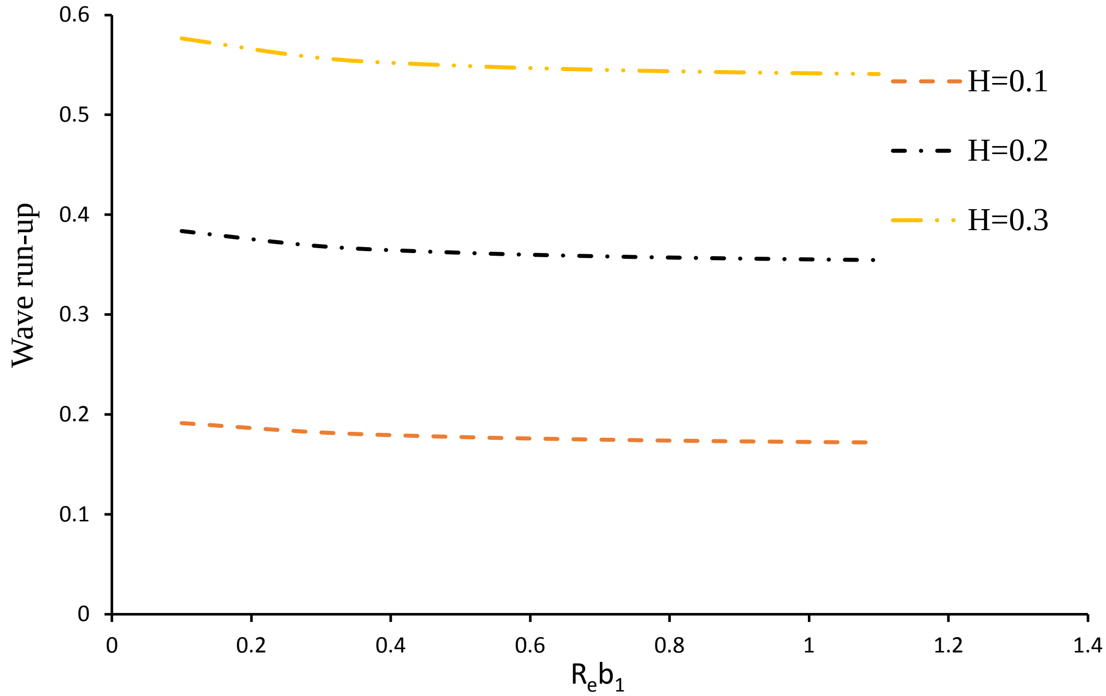

Figure 6-49: Wave run-up vs.$R_e b_1$ with various H for the case with $b=0.6$, $d=1$, $L=6$ and $R_e b_1 = R_e b_2$.

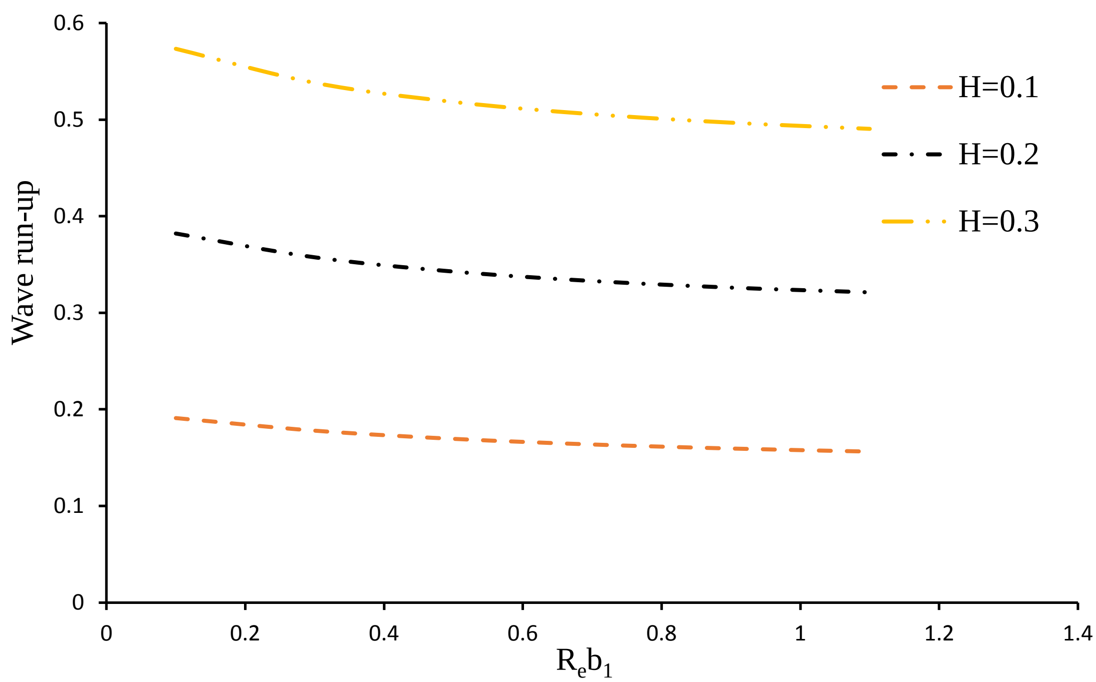

Figure 6-50: Wave run-up vs. the $R_e b_1$.with various H for the case with $b=0.2$, $d=1$, $L=4$ and $R_e b_1 = R_e b_2$.

Figure 6-51 and Figure 6-52 show the plots of time variations of the free-surface elevation with varying submerged depth of porous walls for cases of *H*= 0.2, *b*=0.2, and respective structural length *L*= 6 and *L*=4. The condition of the porous walls is set as $b_1 = b_2 = 10^{-5}$. When the submerged depth of porous walls increases, the reflected wave elevations increase slightly whereas the transmitted wave levels are subject to a greater rate of decreasing. Also, when the structural length decreases, again, the transmitted wave elevations show the increasing trend. Figure 6-53 through Figure 6-55 present the time variations of the free-surface elevations for cases with various values of $R_e b_1$. The settings for Figure 6-53 are *H=0.2*, *b=0.2*, *d=1*, *L=6* and $R_e b_2 = R_e b_1$ and for Figure 6-53 are *H=0.2*, *b=0.6*, *d=1*, *L=6* and $R_e b_2 = R_e b_1$.The results indicate that, for the structural setting conditions, when the porous-effect parameter $R_e b_1$ increases, the reflected wave elevations decrease and the transmitted wave elevations as expected increase. However, comparing with the incident wave profiles, the overall reflected and transmitted wave elevations are substantially reduced. By comparing results shown in Figure 6-53 and Figure 6-54, we find that when the body draft is larger, the effect of $R_e b_1$, as the portion of the porous walls is reduced, is less significant on varying the free-surface profiles. However, from Figure 6-53 and Figure 6-55, it is noticed that when the structural length is smaller, the effect of $R_e b_1$ becomes more important in affecting the reflected and transmitted wave elevations.

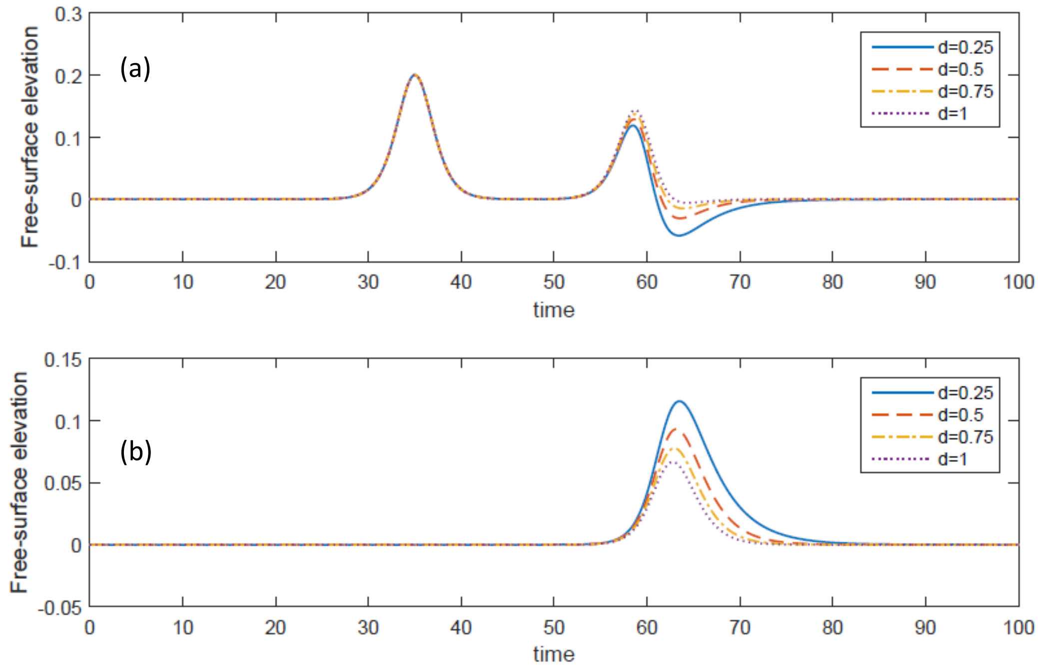

Figure 6-51: Time variations of derived analytical solutions of free-surface elevation with various submerged depth of porous walls for a case with $H=0.2$, $L=6$, $b=0.2$ and $b_1 = b_2 = 10^{-5}$: (a) incident and reflected wave; (b) transmitted wave.

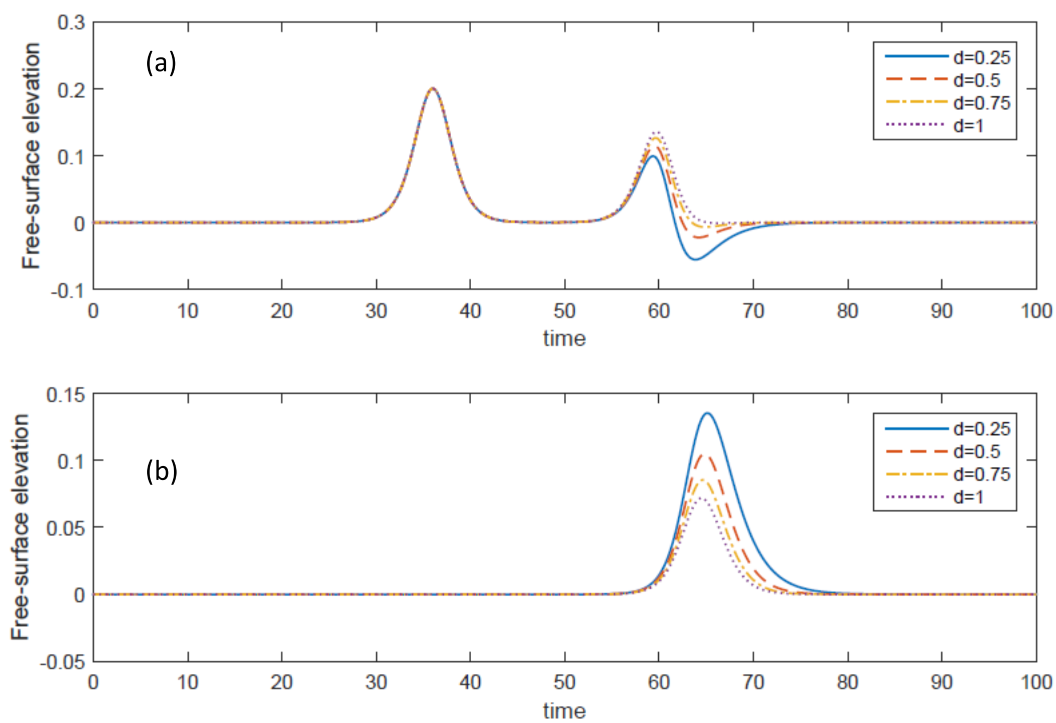

Figure 6-52: Time variations of derived analytical solutions of free-surface elevation with various submerged depth of porous walls for a case with $H=0.2$, $L=4$, $b=0.2$ and $b_1 = b_2 = 10^{-5}$: (a) incident and reflected wave; (b) transmitted wave.

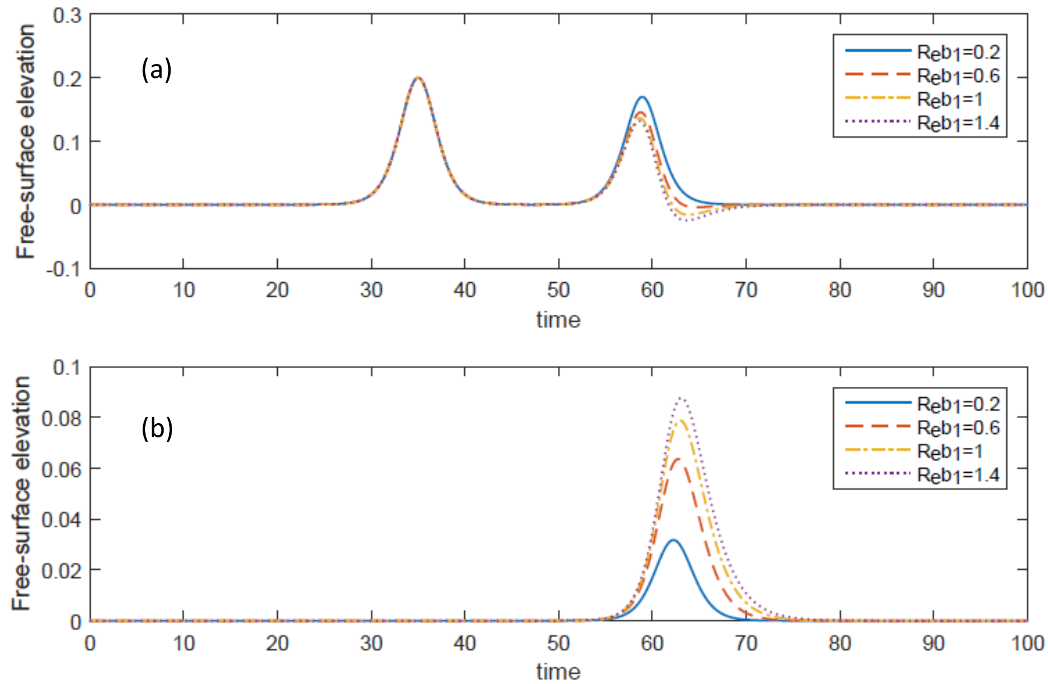

Figure 6-53: Time variations of derived analytical solutions of free-surface elevation with various R_eb_1 for a case with $H=0.2$, $b=0.2$, $d=1$, $L=6$ and $R_eb_1= R_eb_2$: (a) incident and reflected wave; (b) transmitted wave.

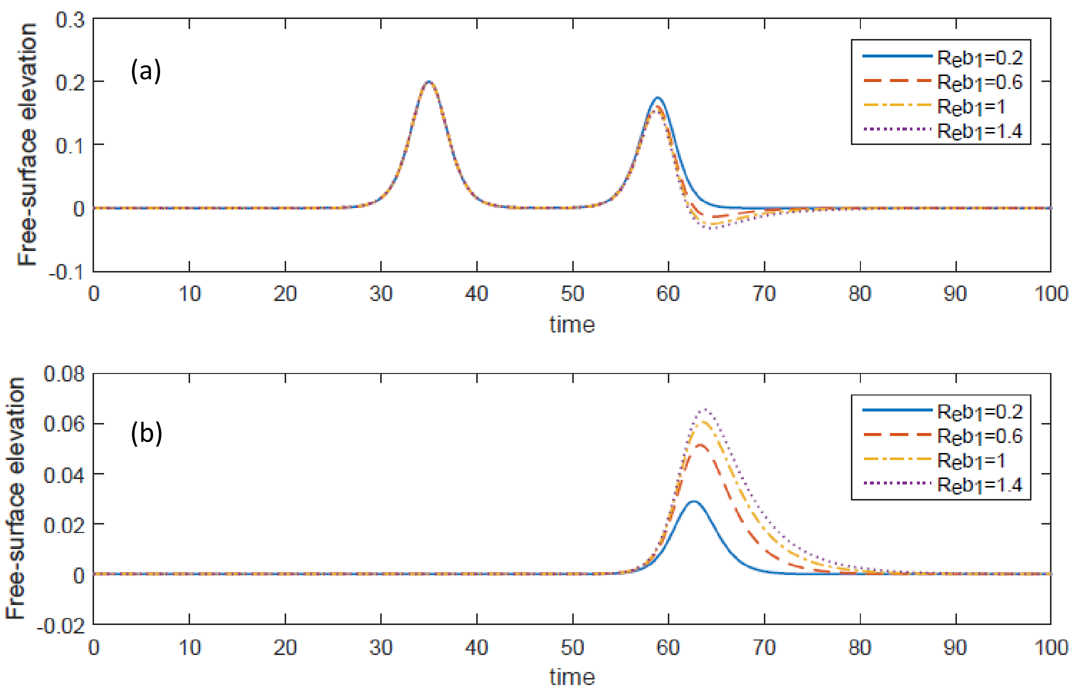

Figure 6-54: Time variations of derived analytical solutions of free-surface elevation with various R_eb_1 for a case with $H=0.2$, $b=0.6$, $d=1$, $L=6$ and $R_eb_1= R_eb_2$: (a) incident and reflected wave; (b) transmitted wave.

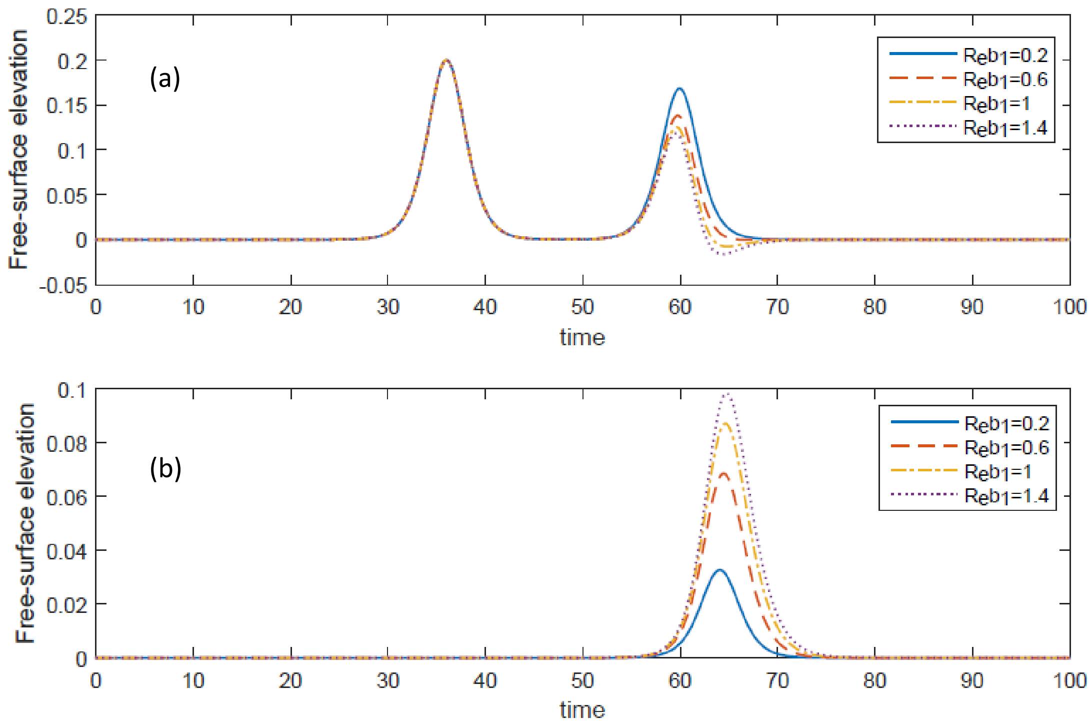

Figure 6-55: Time variations of derived analytical solutions of free-surface elevation with various R_eb_1 for a case with $H=0.2$, $b=0.2$, $d=1$, $L=4$ and $R_eb_1= R_eb_2$: (a) incident and reflected wave; (b) transmitted wave.

In terms of the overall reflection coefficients (C_R), they are plotted versus the submerged depth of porous walls with inputs of $b=0.2$, $b_1 = 1.6 \times 10^{-5}$, $b_2 = 2.4 \times 10^{-5}$ and various incident wave heights in Figure 6-56 for $L=6$ and Figure 6-57 for $L=4$. The results show that when the submerged depth of porous walls increases, the overall reflection coefficient increases and as the incident wave height increases, the effect of the submerged depth of porous walls decreases. Smaller structural length will lead to a smaller reflection coefficient for the same case. Figure 6-58 through Figure 6-60 show the plots of the overall reflection coefficients versus R_eb_1 with various incident wave heights and structural draft conditions. Again, it can be seen as R_eb_1 increases, the overall reflection coefficient decreases. When comparing the results shown in Figure 6-58 and Figure 6-59, we notice again as the body draft increases the effect of $R_e b_1$ on the overall reflection coefficient decreases.

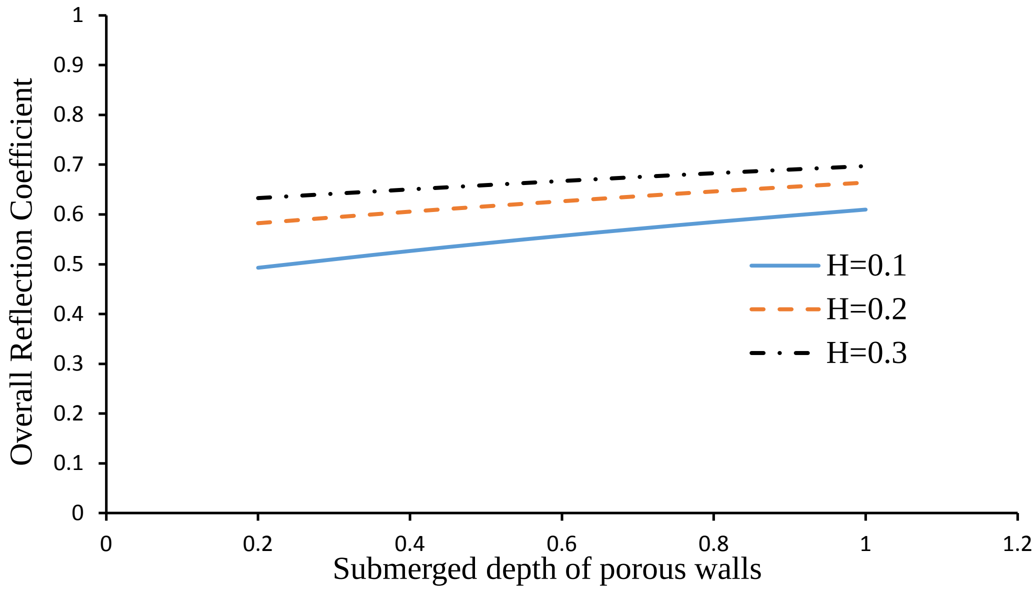

Figure 6-56: The overall reflection coefficient vs. submerged depth of porous walls with various H for a case with $L=6$, $b=0.2$, $b_1 = 1.6\times10^{-5}$ and $b_2 = 2.4\times10^{-5}$.

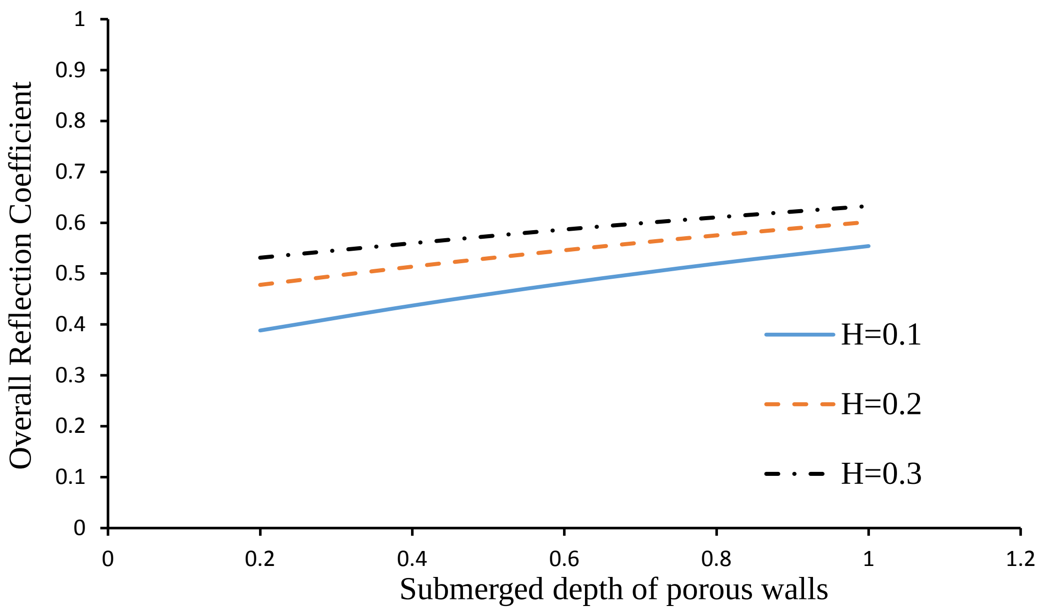

Figure 6-57: The overall reflection coefficient vs. submerged depth of porous walls with various H for a case with $L=4$, $b=0.2$, $b_1 = 1.6\times10^{-5}$ and $b_2 = 2.4\times10^{-5}$.

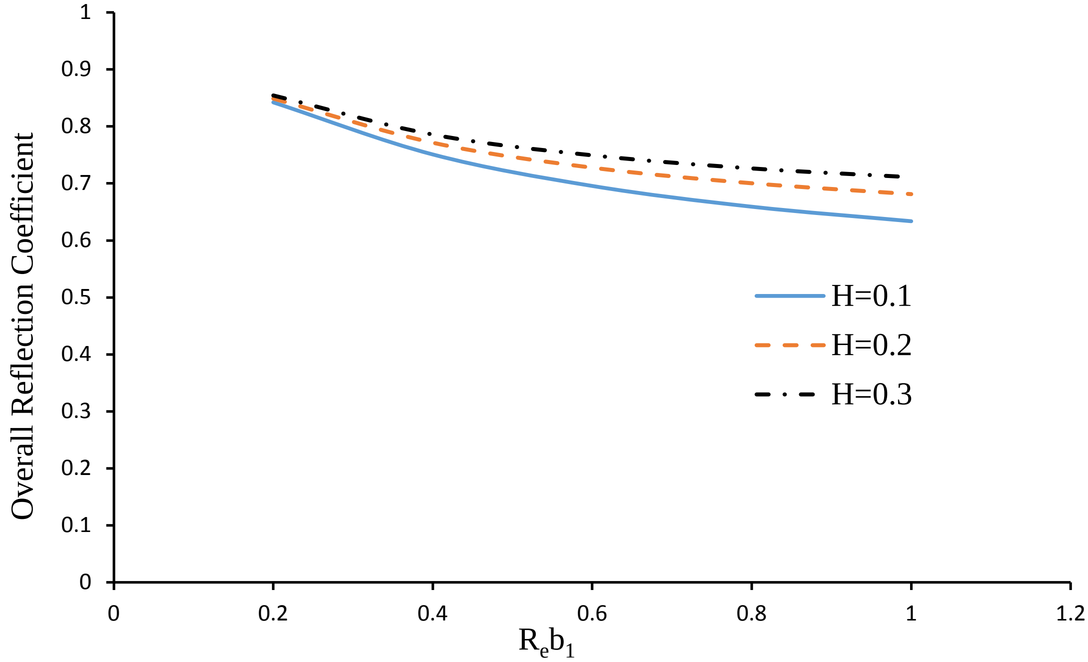

Figure 6-58: The overall reflection coefficient vs. R_eb_1 with various H for a case with $L=6$, $d=1$, $b=0.2$ and $R_eb_1= R_eb_2$.

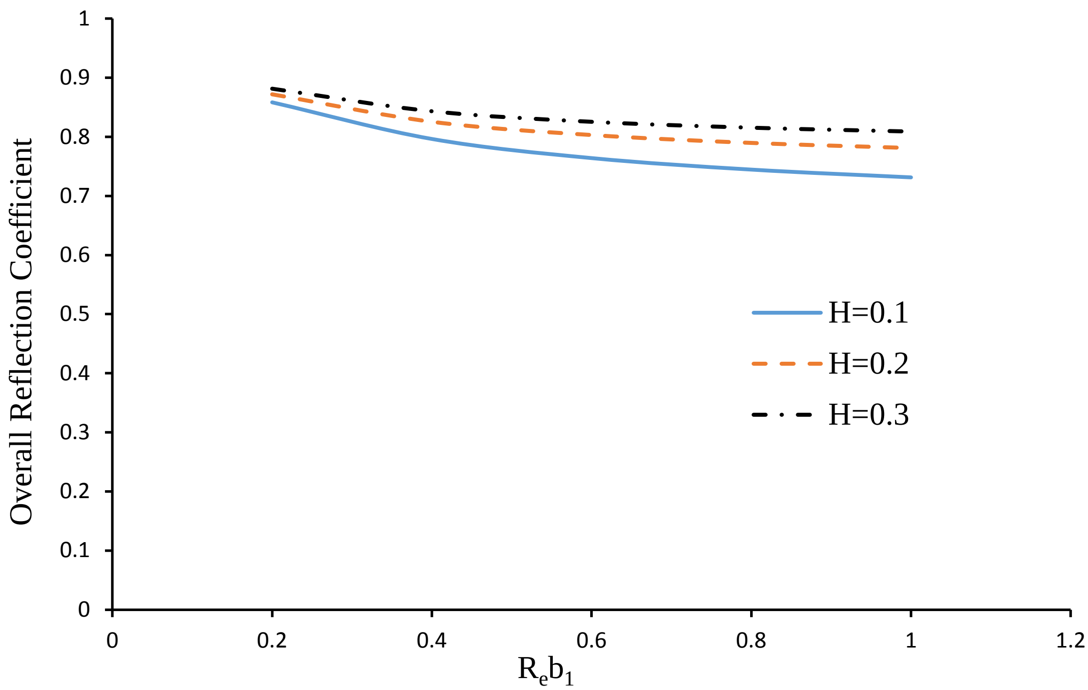

Figure 6-59: The overall reflection coefficient vs. R_eb_1 with various H for a case with $L=6$, $d=1$, $b=0.6$ and $R_eb_1= R_eb_2$.

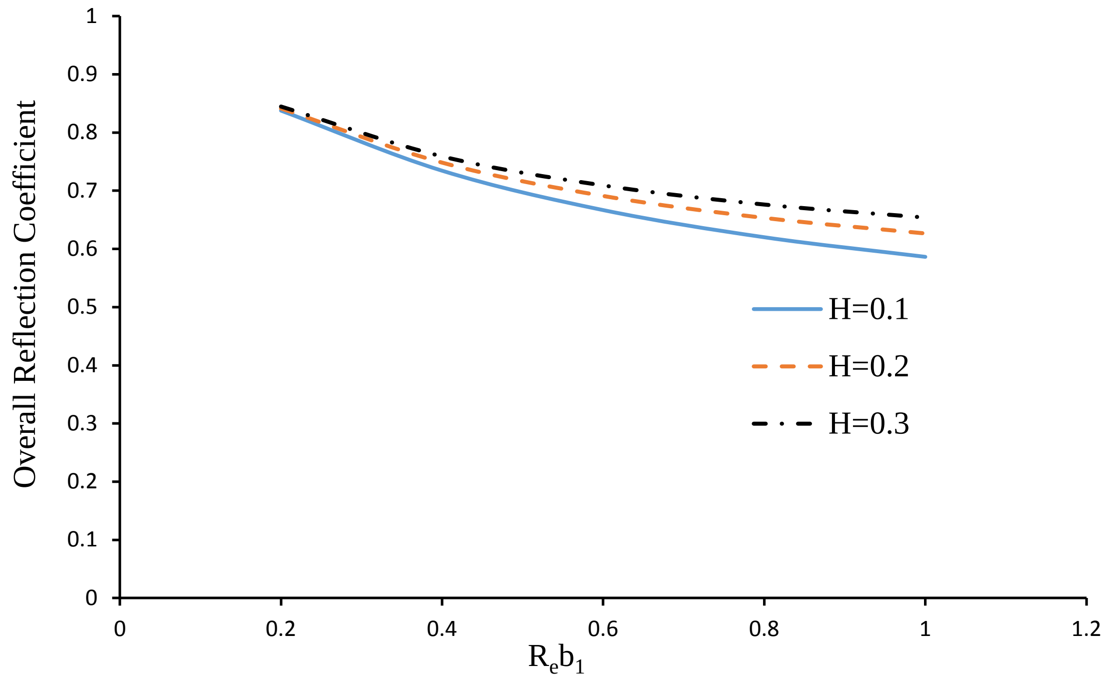

Figure 6-60: The overall reflection coefficient vs. R_eb_1 with various H for a case with $L=4$, $d=1$, $b=0.2$ and $R_eb_1= R_eb_2$.

Corresponding to the results of overall reflection coefficients shown in Figure 6-56 to Figure 6-60, the overall transmission coefficients (C_T) are presented in Figure 6-61 to Figure 6-62 where for Figure 6-61 and Figure 6-62, they are plotted versus the submerged depth of porous walls with b=0.2, $b_1 = 1.6 \times 10^{-5}$ and $b_2 = 2.4 \times 10^{-5}$ and respectively with L=6 and L=4. When the submerged depth of porous walls increases, the overall transmission coefficient decreases. Meanwhile, decreasing the structural length from 6 to 4 tends to cause an increase in the overall transmission coefficient, and when the incident wave height decreases, the effect of the submerged depth of porous walls on the overall transmission coefficient increases. In terms of the variations of C_T versus R_eb_1 , the results are presented in Figure 6-63 through Figure 6-65. As the values of R_eb_1 increases, the transmission coefficient increases. However, relatively to the incident waves, the overall transmission coefficient is considered to be reduced substantially. It can be noted from Figure 6-63 to Figure 6-65 that when the body draft or the structural length is larger, the overall transmission coefficient decreases.

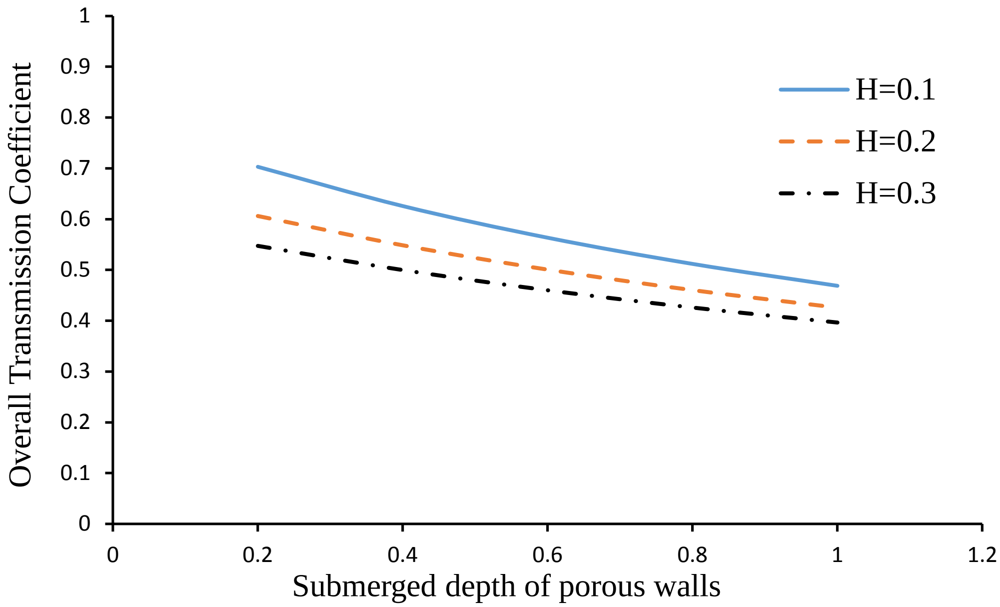

Figure 6-61: The overall transmission coefficient vs. submerged depth of porous walls with various H for a case with $L=6$, $b=0.2$, $b_1 = 1.6\times10^{-5}$ and $b_2 = 2.4\times10^{-5}$.

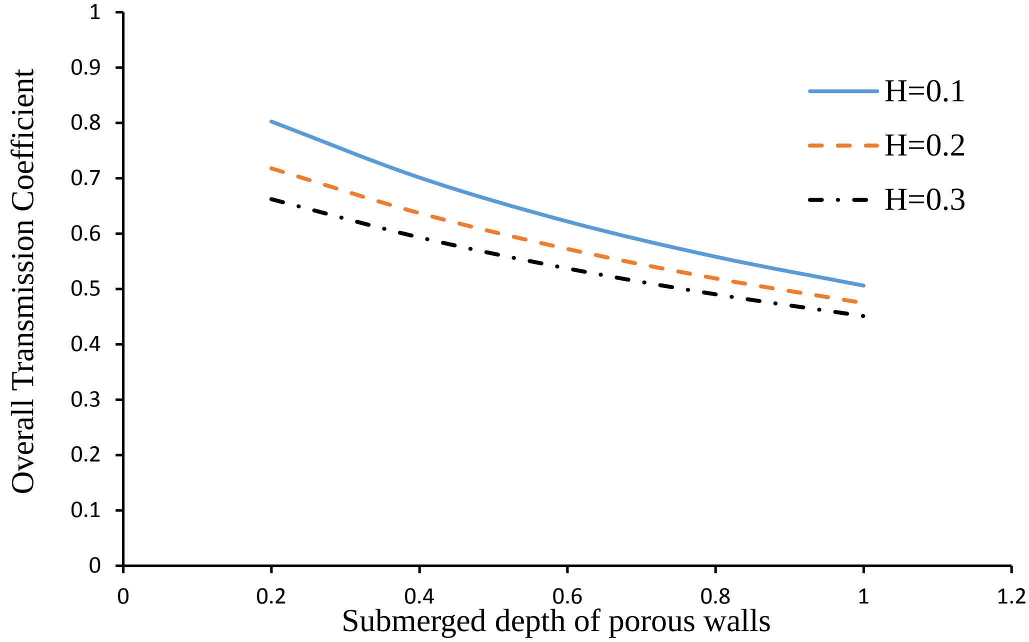

Figure 6-62: The overall transmission coefficient vs. submerged depth of porous walls with various H for a case with $L=4$, $b=0.2$, $b_1 = 1.6*10^{-5}$ and $b_2 = 2.4*10^{-5}$.

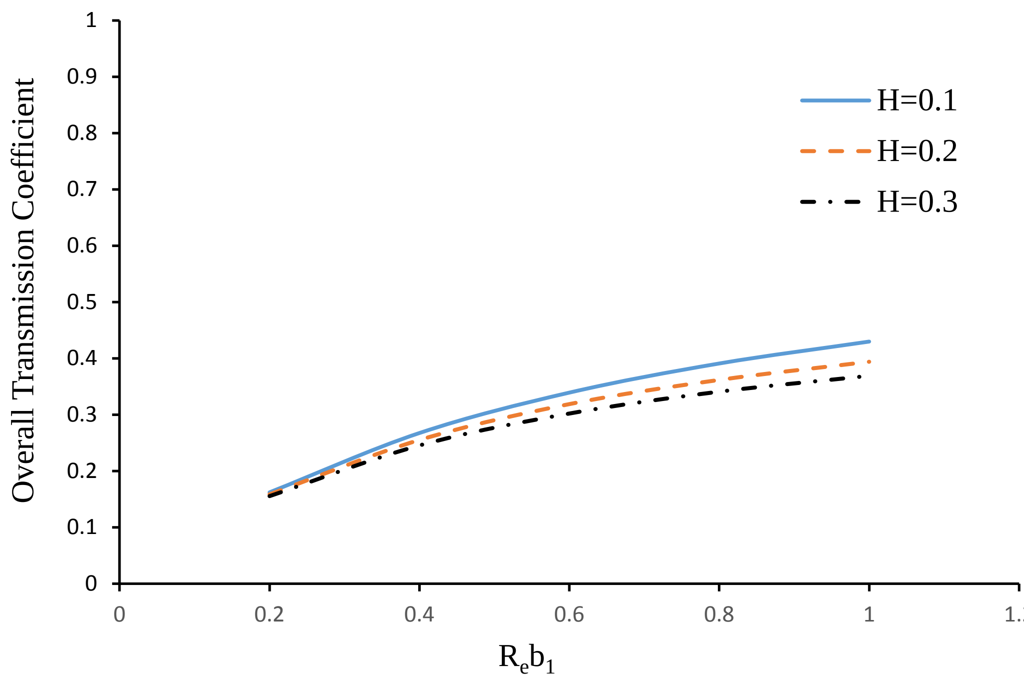

Figure 6-63: The overall transmission coefficient vs. $R_e b_1$ with various H for a case with $L=6$, $d=1$, $b=0.2$ and $R_e b_1 = R_e b_2$.

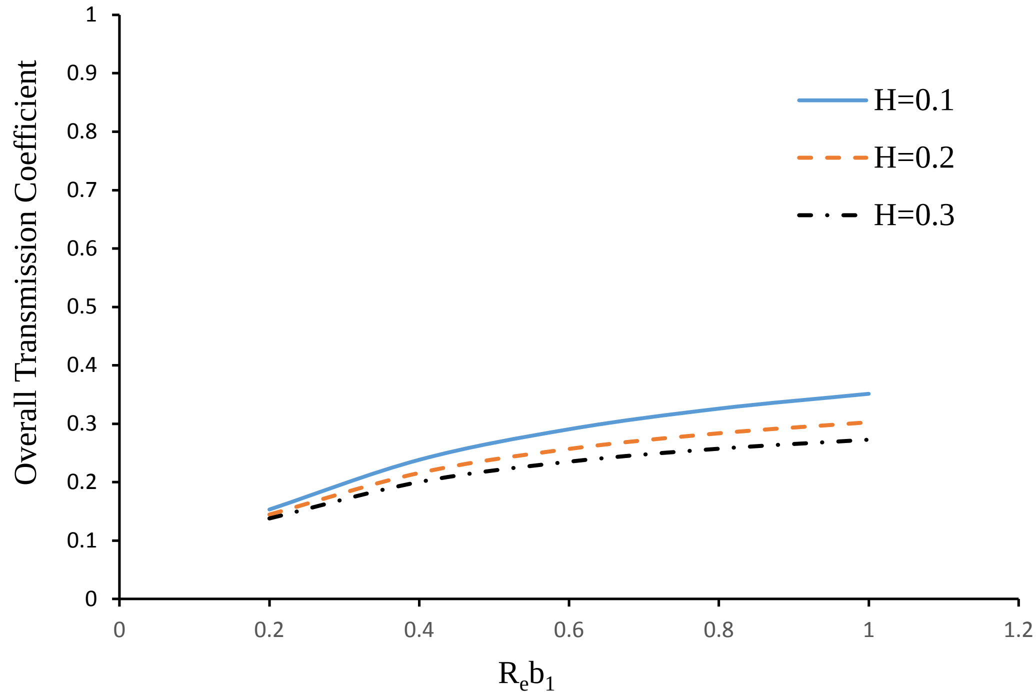

Figure 6-64: The overall transmission coefficient vs. $R_e b_1$ with various H for a case with $L=6$, $d=1$, $b=0.6$ and $R_e b_1 = R_e b_2$.

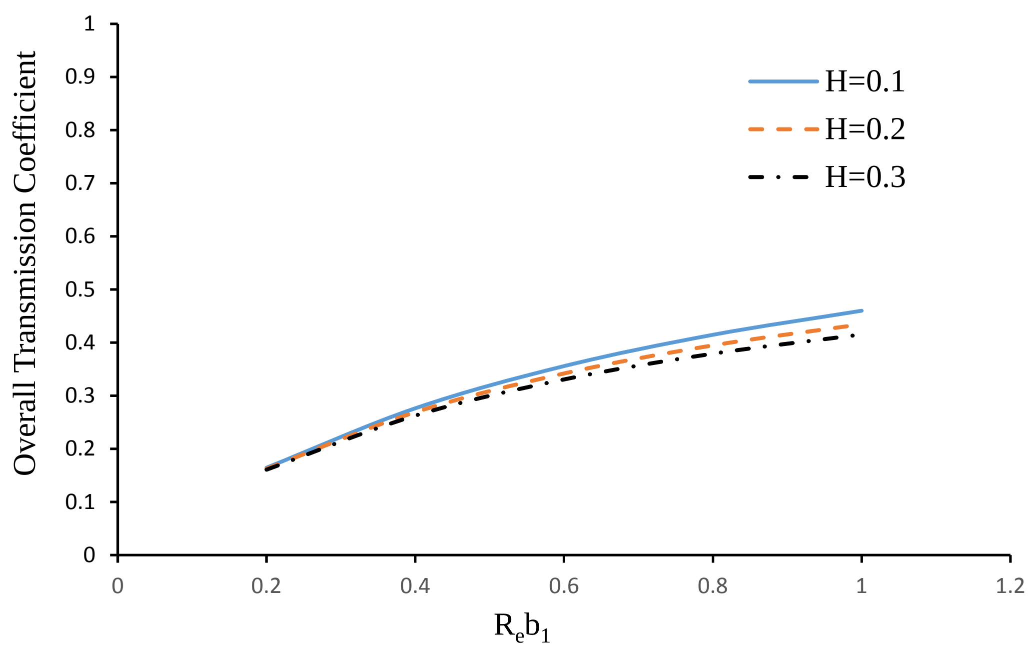

Figure 6-65: The overall transmission coefficient vs. $R_e b_1$ with various H for a case with $L=4$, $d=1$, $b=0.2$ and $R_e b_1 = R_e b_2$.

6.2.4 Effect of the Structural Length

The structural length of a 2-D partially submerged body with attached two porous walls system also affect the wave reflection and transmission after the interactions by an incident solitary wave. Here, only the results showing the effect of the structural length on the time variations of the free-surface elevations in regions 1 and 3 are presented in this section.

Figure 6-66 through Figure 6-68 present the time variations of the free-surface elevations with considerations of various structural lengths where for the results shown in Figure 6-66 and Figure 6-67, the porous walls are not included in the partially submerged body system and the other setting variables are respectively H=0.2, b=d=0.2 and are H=0.2, b=d=0.6. The free-surface plots by considering the effect of dual porous wall with $b_1 = b_2 = 10^{-5}$ are presented in Figure 6-68. It can be seen when the structural length is larger, the reflected wave height is larger and the transmitted wave height is smaller. Also, with the increase of the body draft b or the application of the dual porous walls, the reflected wave height increases and the transmitted wave height decreases. However, with the increase of the structural length and use of the dual porous walls, both the reflected and transmitted wave elevations can be effectively reduced. Meanwhile, the effect of the structural length on the reflected and transmitted wave elevations is less significant when the body draft increases or the dual porous walls are applied.

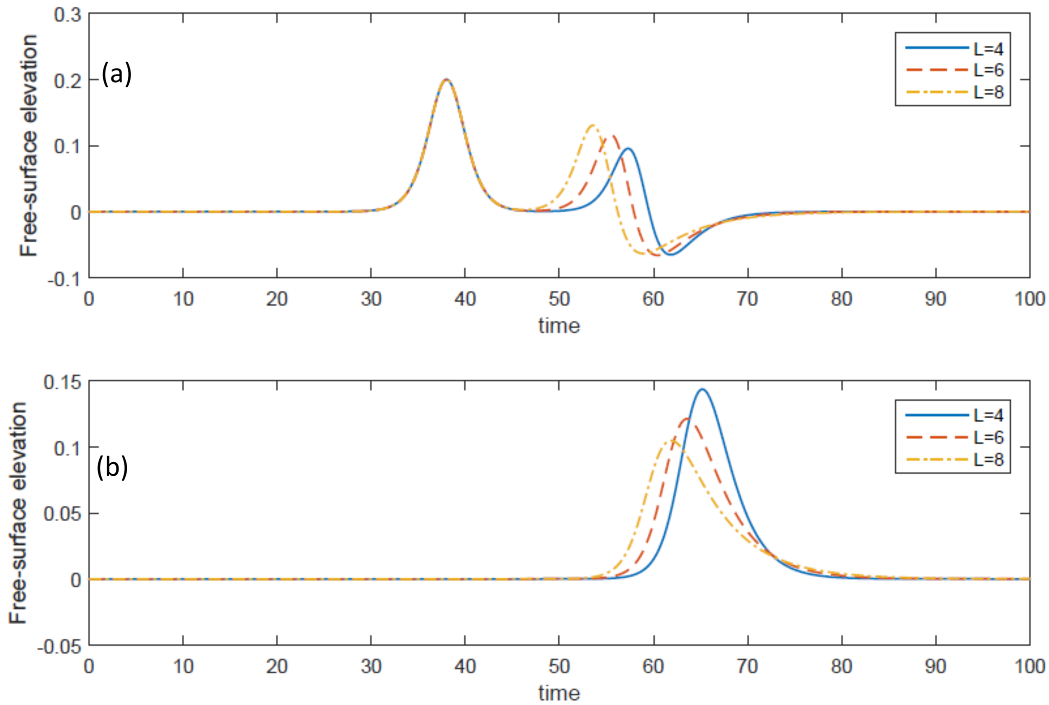

Figure 6-66: Time variations of derived analytical solutions of free-surface elevation with various structural lengths for a case with *H=0.2*, *b= d=0.2* (no porous conditions): (a) incident and reflected wave; (b) transmitted wave.

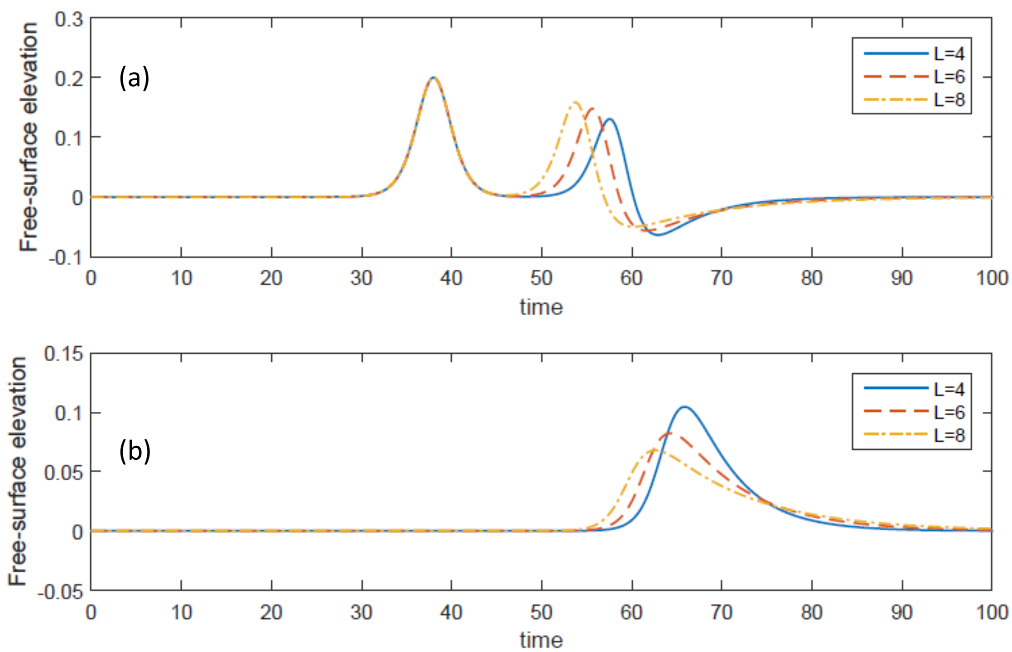

Figure 6-67: Time variations of derived analytical solutions of free-surface elevation with various structural lengths for a case with *H=0.2*, *b= d=0.6* (no porous conditions): (a) incident and reflected wave; (b) transmitted wave.

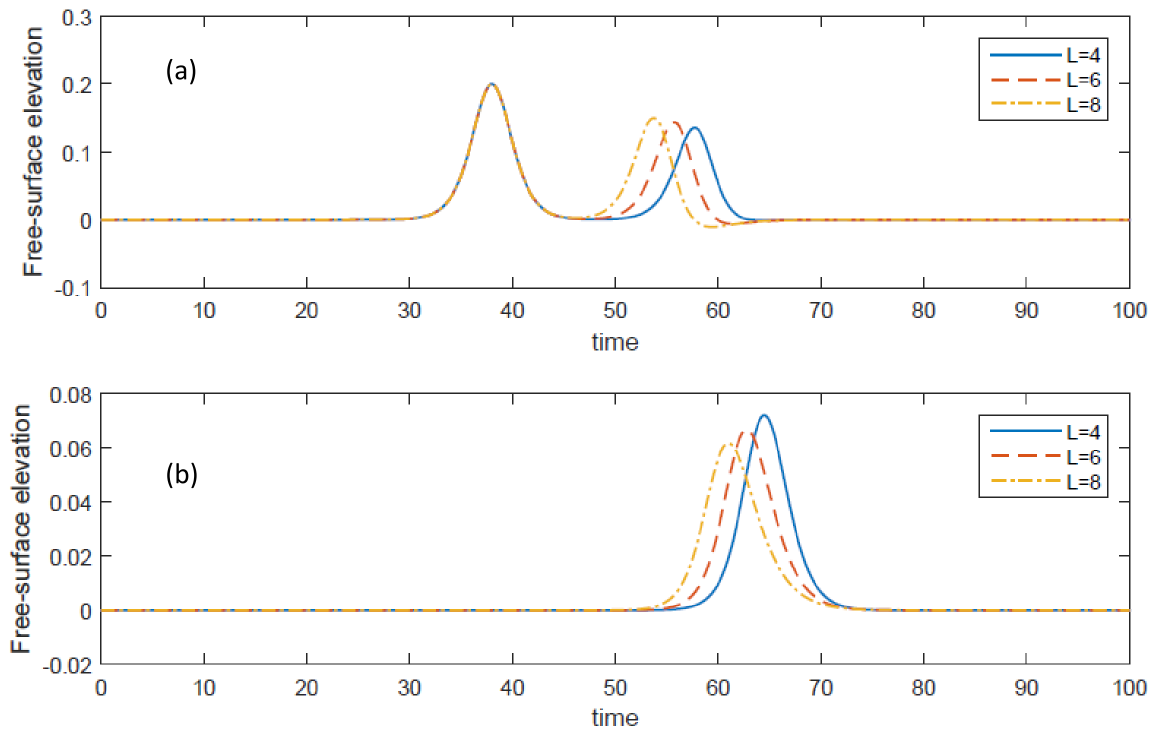

Figure 6-68: Time variations of derived analytical solutions of free-surface elevation with various structural lengths for a case with $H=0.2$, $b=0.2$, $d=1$ and $b_1 = b_2 = 10^{-5}$: (a) incident and reflected wave; (b) transmitted wave.

6.3 Hydrodynamic Forces on a 2-D Partially submerged Body with Attached Dual Porous Walls

The hydrodynamic forces acting at various directions are important physical variables required in the design of coastal and offshore structures. By applying Eqns. (3-46) and (3-47), separately, the horizontal force acting on a 2-D partially submerged body with two attached porous walls and the vertical force acting on the bottom of the structural system can be obtained .

For horizontal forces, Figure 6-69 through Figure 6-76 present the time variations of the horizontal forces under various setting conditions. Figure 6-69 shows the time variations of the horizontal forces with various incident wave heights for a case with

$b=d=0.2$ and $L=4$ (without porous walls). The force results with consideration of two porous walls with $b_1 = b_2 = 10^{-5}$ are given in Figure 6-70. When the wave height increases, the positive horizontal forces increase. The results in Figure 6-69 and Figure 6-70 indicate that with the additions of the porous structures the positive horizontal forces increase, however, the negative forces (forces acting on the negative x direction) are greatly reduced as a result of the reduction of the transmitted wave heights. As a comparison, Figure 6-71 shows plots of the time variations of the horizontal forces with a greater body draft (b=0.6), which is equal to 0.6, for various incident wave heights and without the attached porous walls. When comparing to the results given in Figure 6-69, it is noted as the body draft increases, the positive horizontal force increases. The negative horizontal force also increases when the body draft increases. The structural length also affects the horizontal force, where in Figure 6-72 plots of horizontal forces similar to the cases for results shown in Figure 6-69 but with a larger structural length (L= 6) are presented. As the structural length increases, the horizontal force also increases.

Figure 6-73 illustrates the time variations of the horizontal forces with various body draft for a case with $H=0.2$, $b=d$ (with porous walls) and $L=6$. As the body draft increases, due to the increased body surface subject to wave impact, the maximum positive horizontal force increases and the time period for the partially submerged body experiencing the negative forces is also increases. With setting of various porous-effect parameter R_eb_1, Figure 6-74 shows the time variations of the horizontal forces for a case with $H=0.2$, $b=0.2$, $d=1$, $L=6$ and $R_eb_1= R_eb_2$. When R_eb_1 increases, the maximum horizontal force decreases and the negative horizontal force affected with a slightly increasing trend. The plots of time variations of horizontal forces with various submerged depth of porous walls are presented in Figure 6-75. As the submerged depth of porous walls increases, the maximum horizontal force increases and the negative force decreases. In terms of the effect of structural length, Figure 6-76 gives the results of time varying horizontal force for cases with various structural lengths. As the structural length increases, the positive horizontal force increases, but the negative maximum force basically maintains at the similar level.

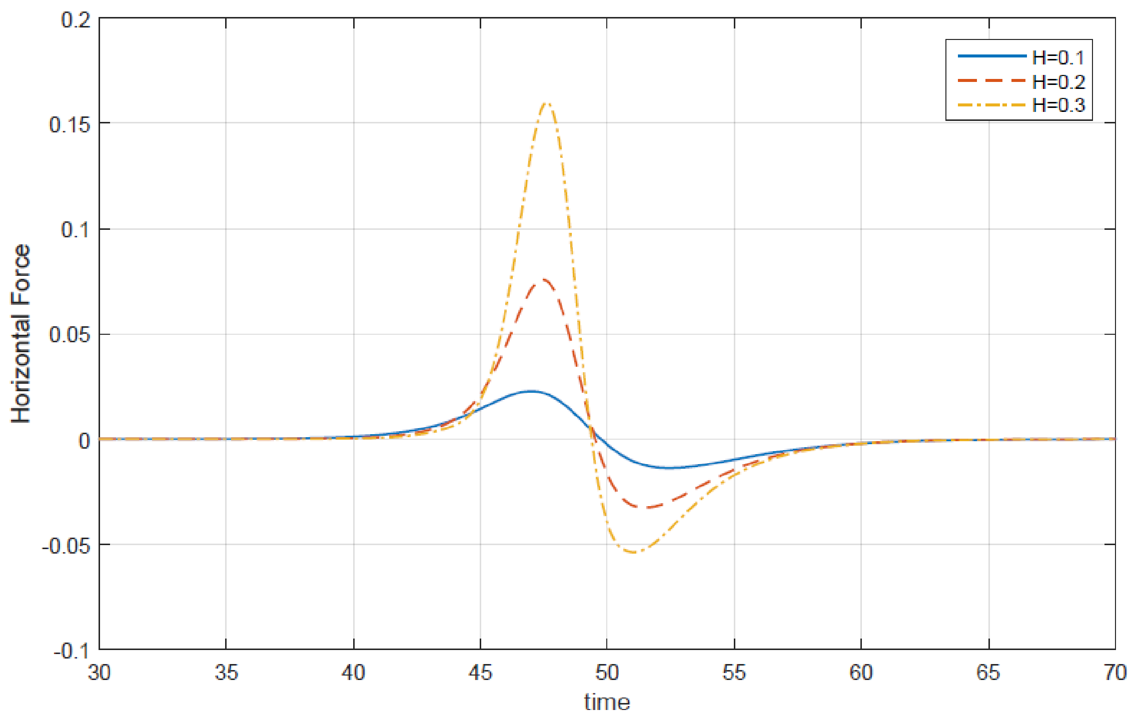

Figure 6-69: Comparison of horizontal forces with various H for a case with *d=b=0.2* (no porous conditions) and *L=4*.

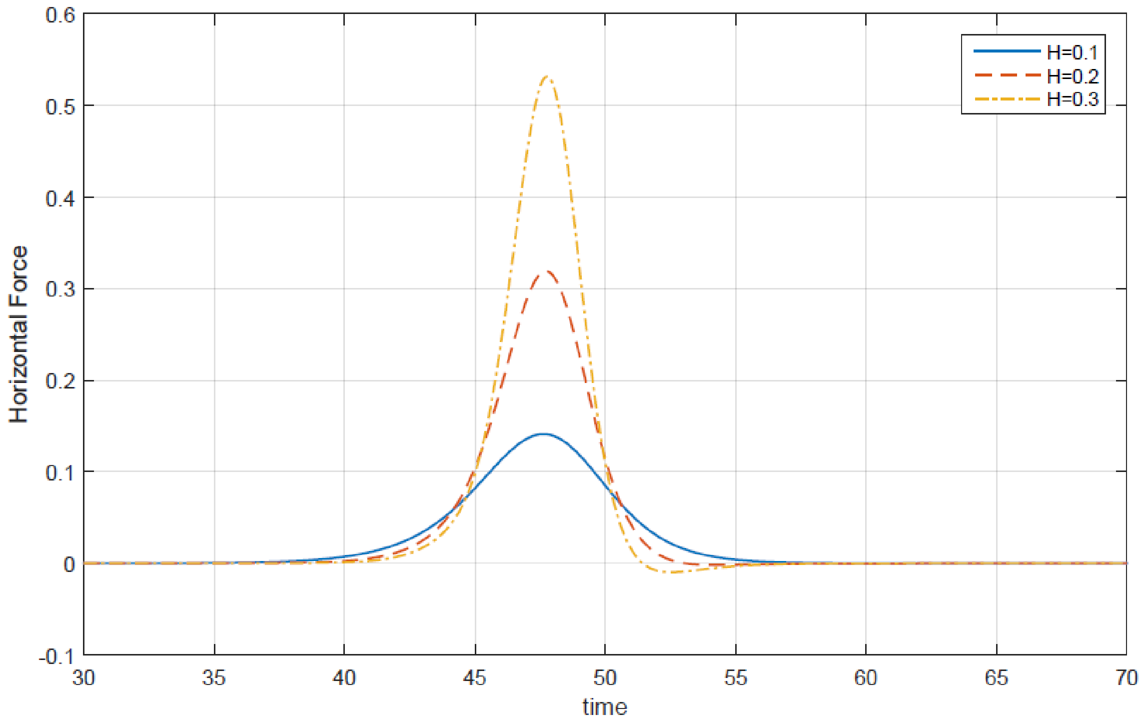

Figure 6-70: Comparison of horizontal forces with various H for a case with *d=1*, *b=0.2*, *L=4* and $b_1 = b_2 = 10^{-5}$.

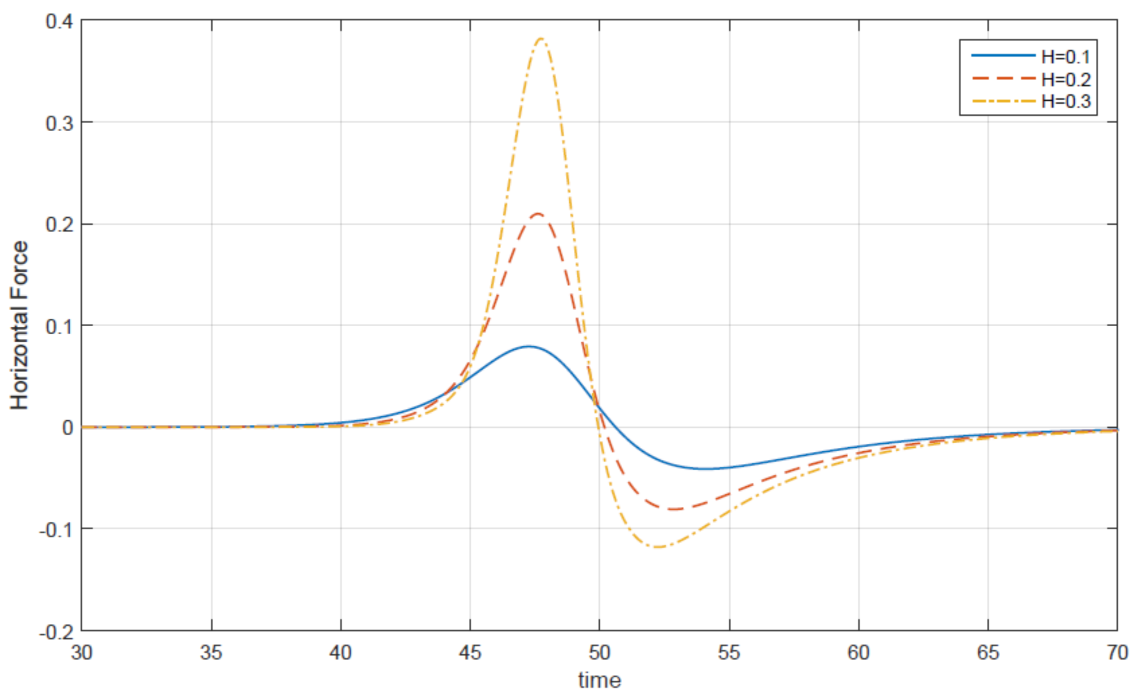

Figure 6-71: Comparison of horizontal forces with various H for a case with *b=d=0.6* (no porous conditions) and *L=4*.

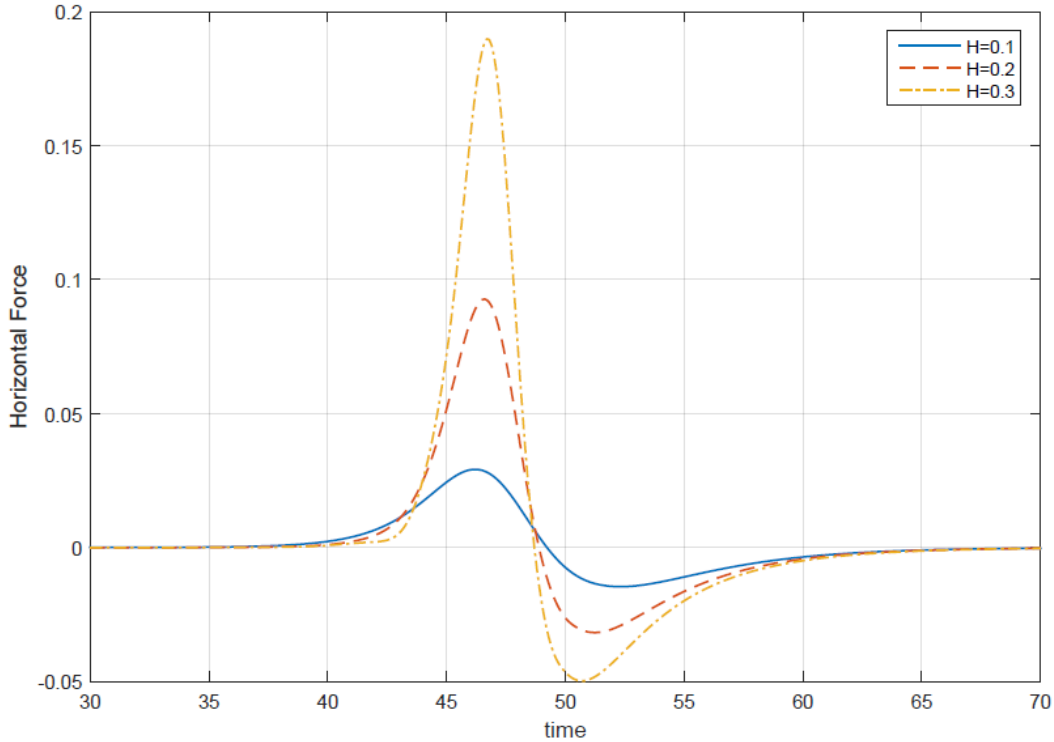

Figure 6-72: Comparison of horizontal forces with various H for a case with *d=b=0.2* (no porous conditions) and *L=6*.

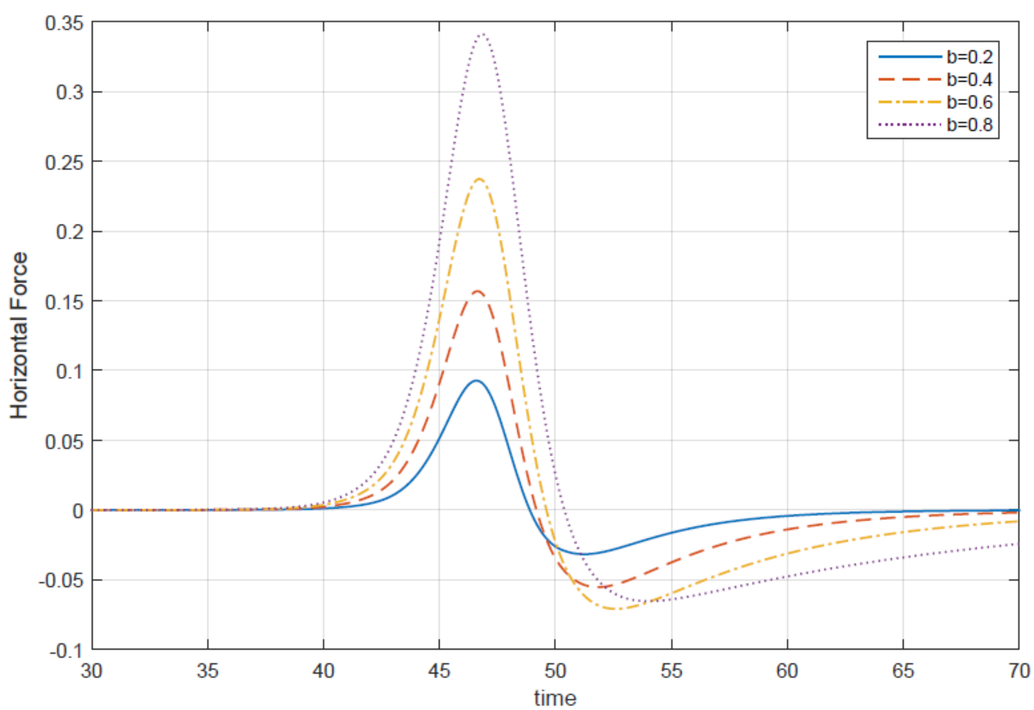

Figure 6-73: Comparison of horizontal forces with various b for a case with *H=0.2*, *b=d* (no porous conditions) and *L=6*.

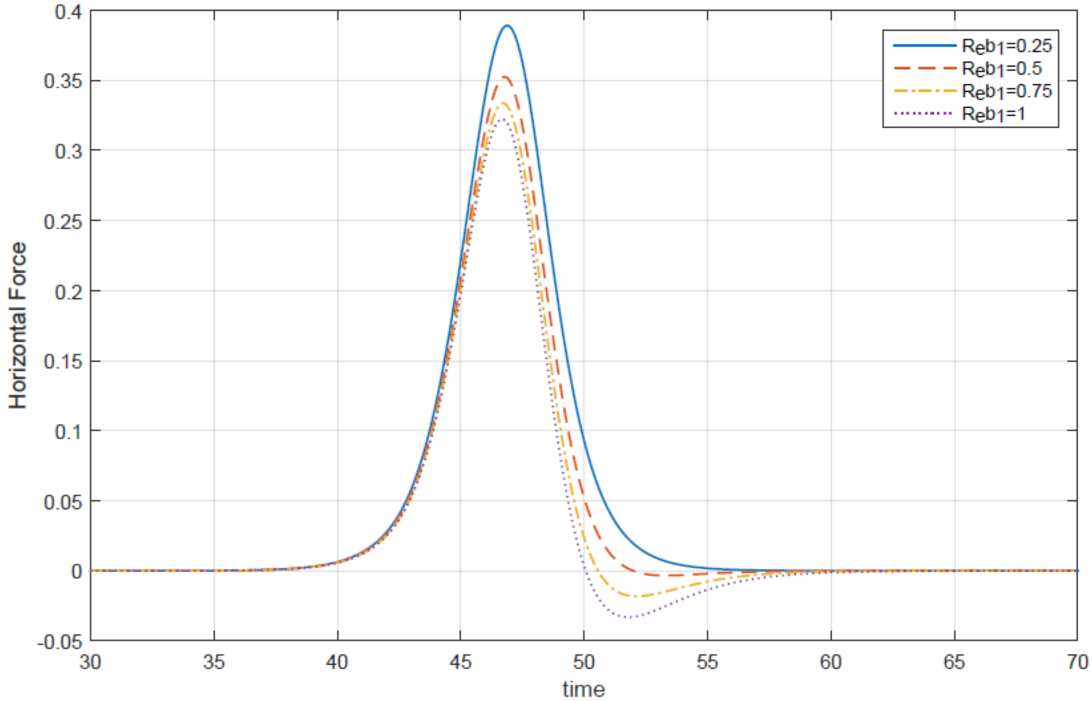

Figure 6-74: Comparison of horizontal forces with various $R_e b_1$ for a case with $H=0.2$, $b=0.2$, $d=1$, $L=6$ and $R_e b_1 = R_e b_2$.

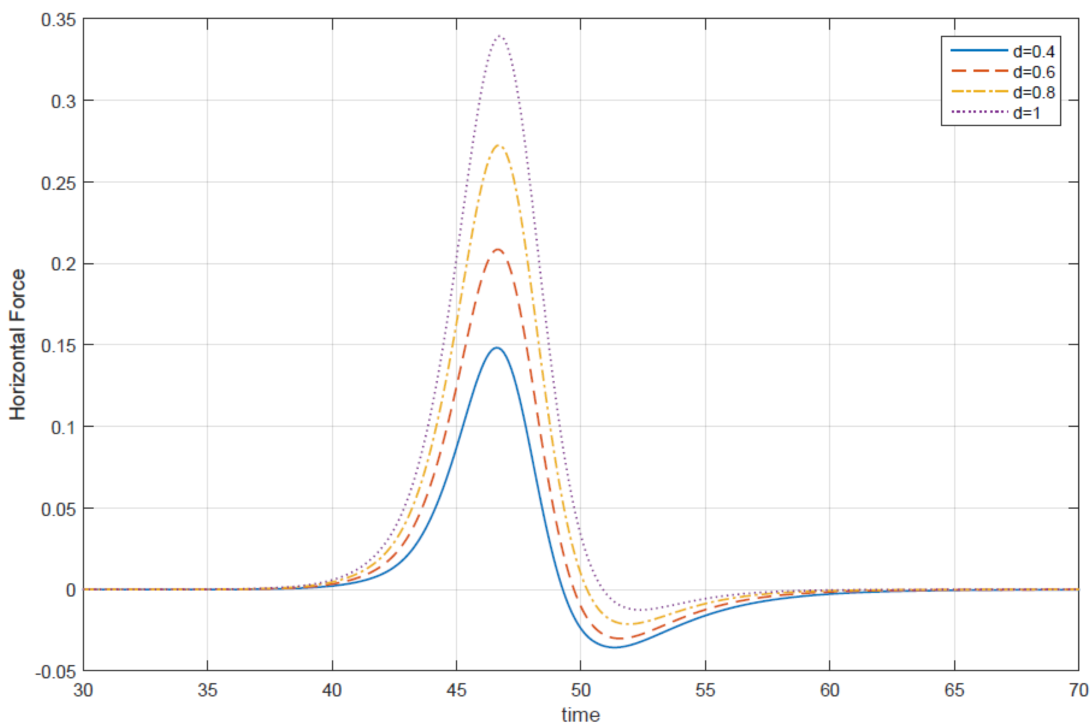

Figure 6-75: Comparison of horizontal forces with various d for a case with $H=0.2$, $b=0.2$, $L=6$ and $b_1 = b_2 = 10^{-5}$.

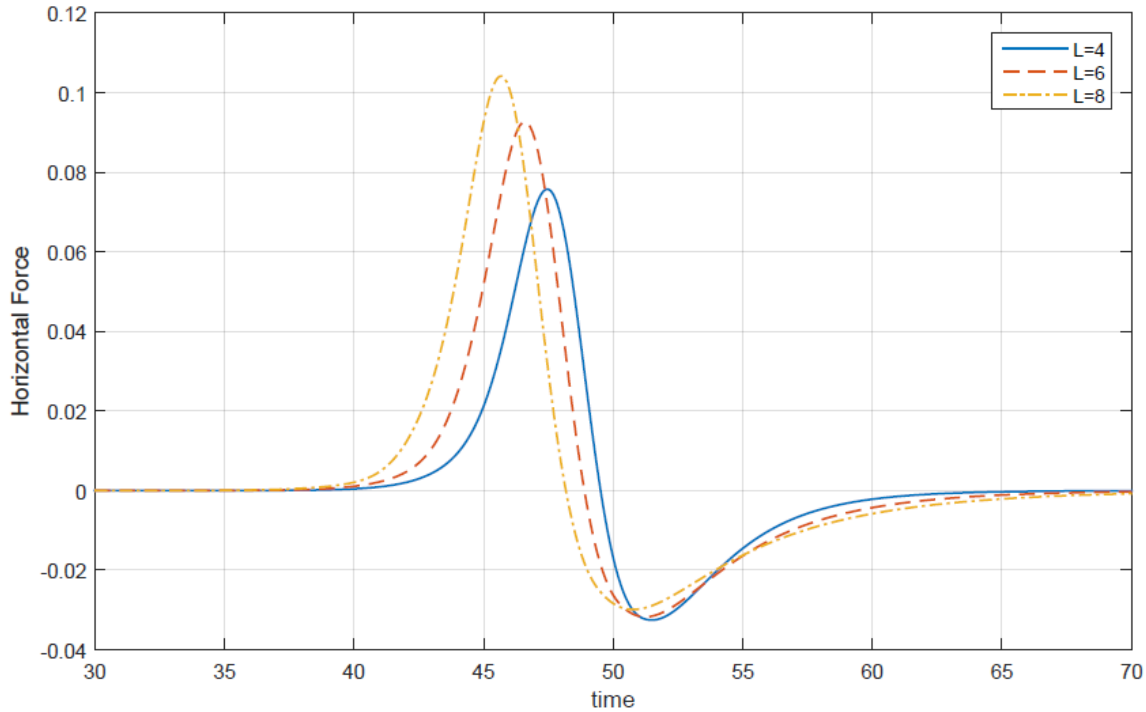

Figure 6-76: Comparison of horizontal forces with various L for a case with *H=0.2*, and *b=d=0.2* (no porous conditions).

For the vertical or uplift forces, Figure 6-77 through Figure 6-81 present the time variations of the vertical forces acting on the bottom of a 2-D partially submerged structure with or without attached dual porous walls under various setting conditions. It should be noticed that all the forces presented here are hydrodynamic forces, and no hydrostatic force is considered. Figure 6-77 shows the time variations of the vertical forces with vary incident wave heights for a case with d=b=0.2 and L=6 without any dual porous walls applied. As the results indicated, when the wave height increases, the maximum vertical force increases. Meanwhile, Figure 6-78, Figure 6-79, and Figure 6-80 present the time variations of the vertical forces under various conditions with changing body draft, submerged depth of porous walls, and R_eb_1, respectively. All the results show that the body draft, submerged depth of porous walls and R_eb_1 have negligible effects on the vertical forces. On the contrary of the body draft, submerged depth of porous walls and R_eb_1, the structural length, by examining the results of vertical forces presented in Figure 6-81, is one critical parameter in affecting the vertical forces. As expected, when the structural length increases, the maximum vertical force increases and the time period that the structure system experiences the vertical force becomes larger.

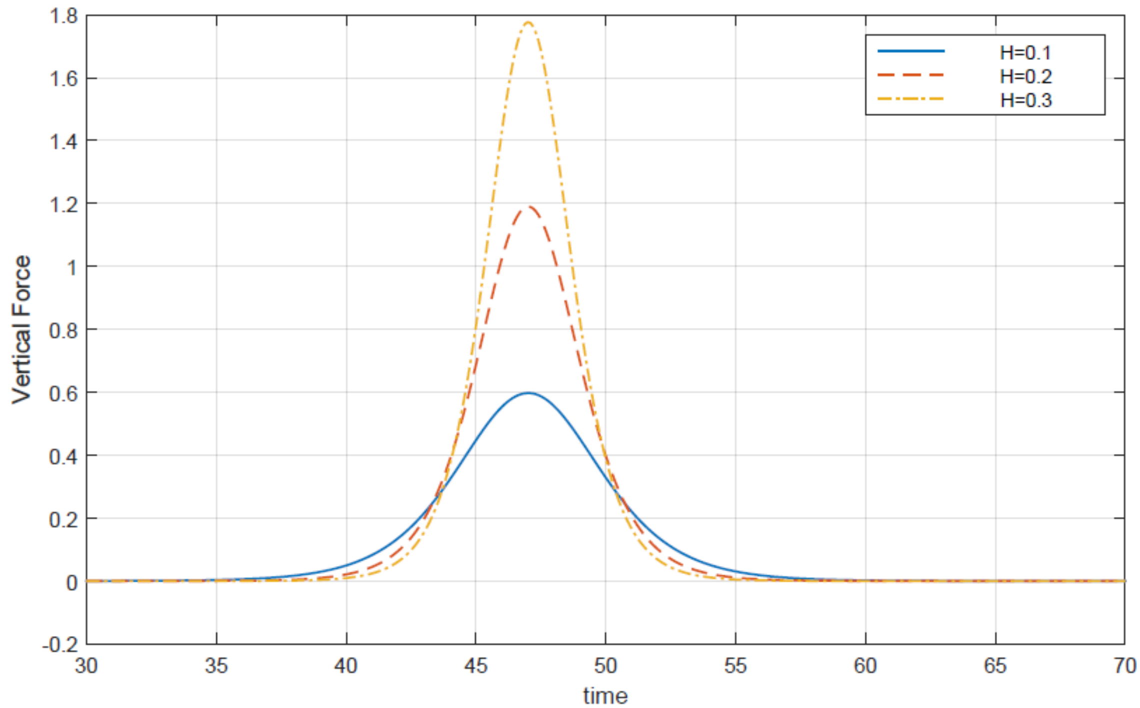

Figure 6-77: Comparison of vertical forces with various H for a case with *d=b=0.2* (no porous conditions) and *L=6.*

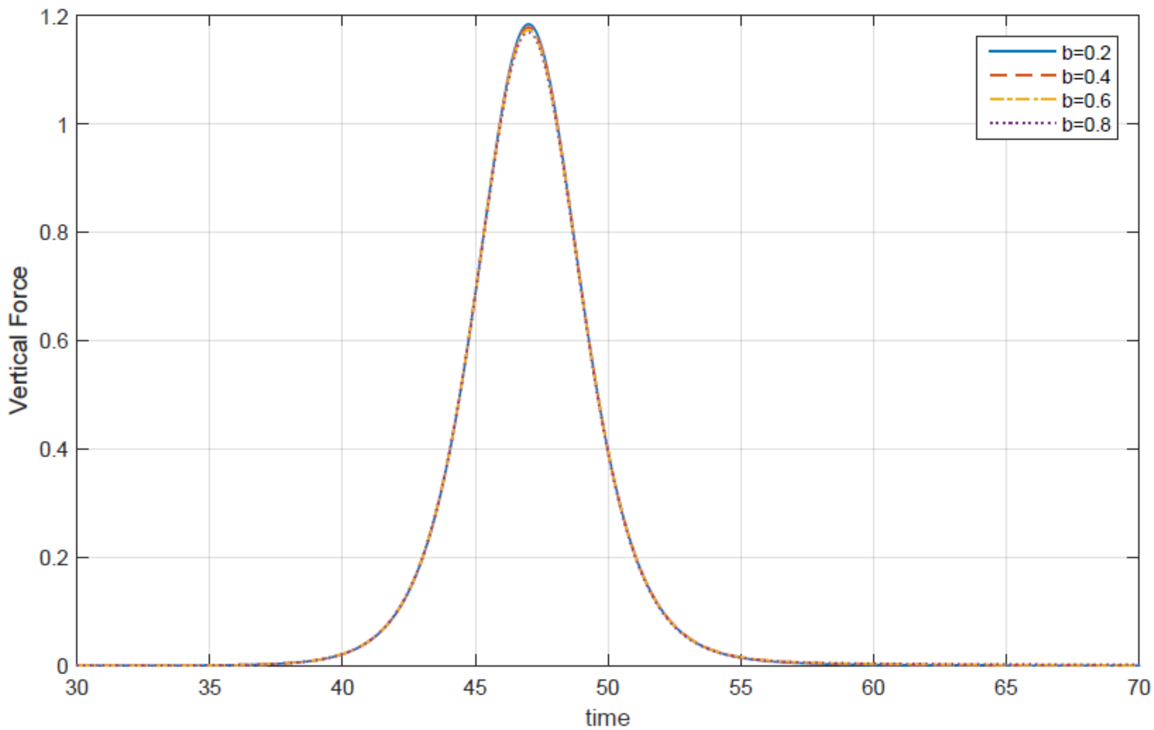

Figure 6-78: Comparison of vertical forces with various b for a case with *H=0.2*, *d=b* (no porous conditions) and *L=6*.

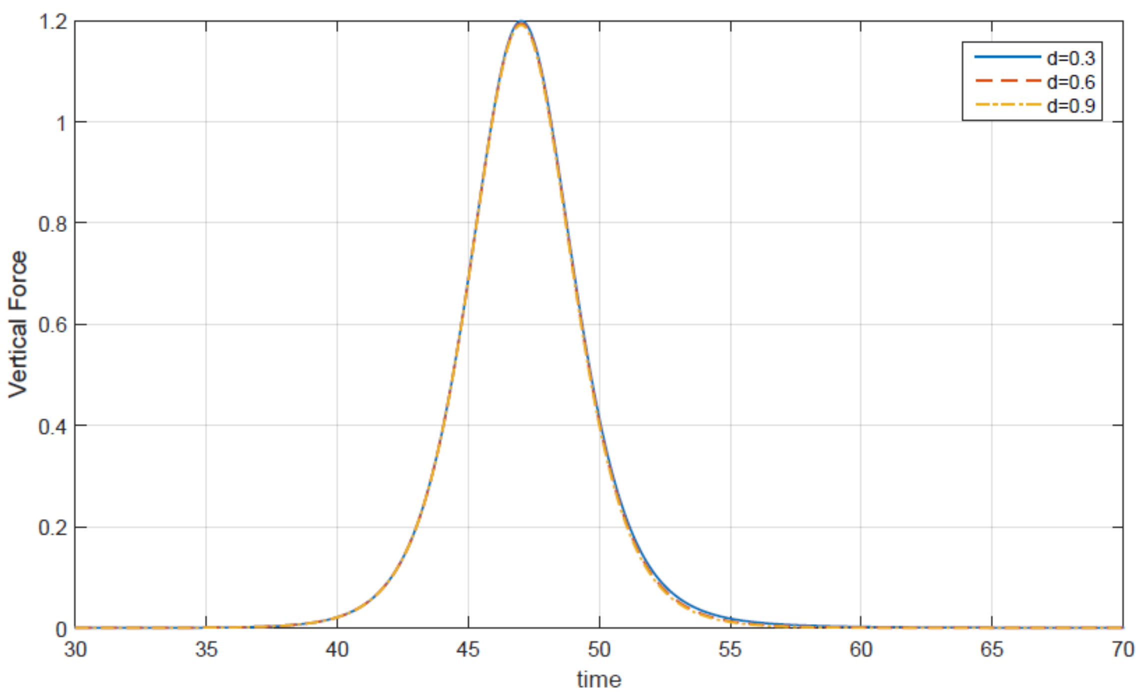

Figure 6-79: Comparison of vertical forces with various d for a case with *H=0.2*, *b=0.2*, *L=6* and $b_1 = b_2 = 10^{-5}$.

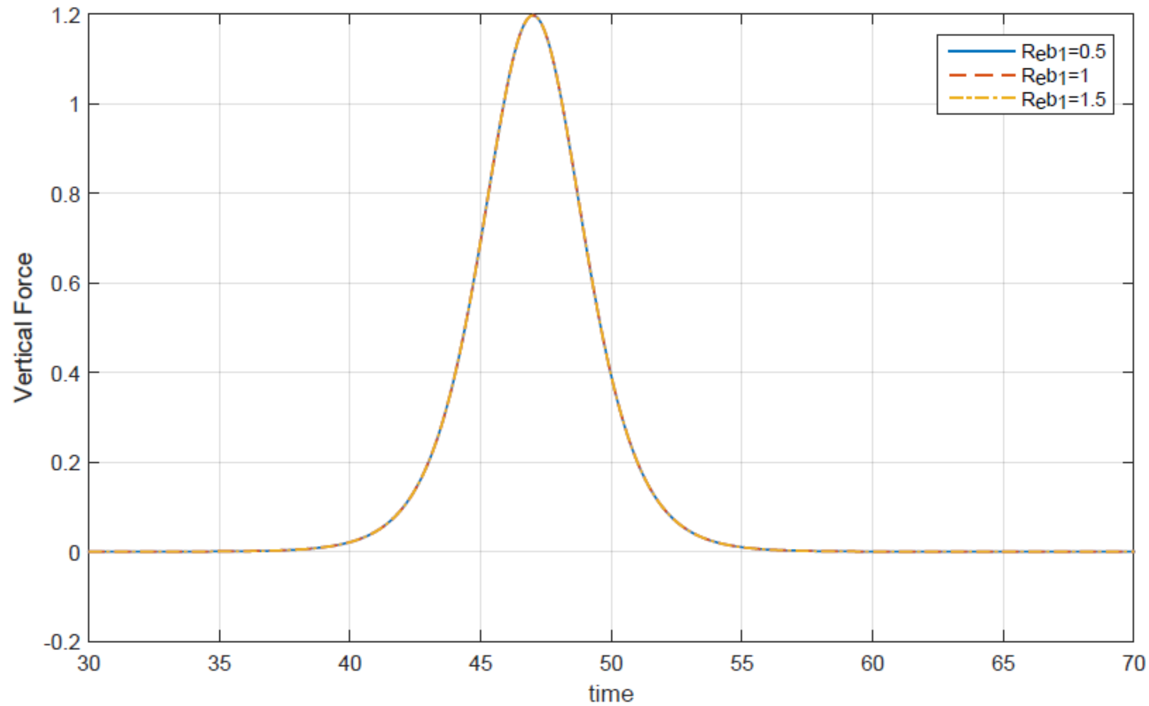

Figure 6-80: Comparison of vertical forces with various R_eb_1 for a case with *H=0.2*, *b=0.2*, *d=1* and *L=6*.

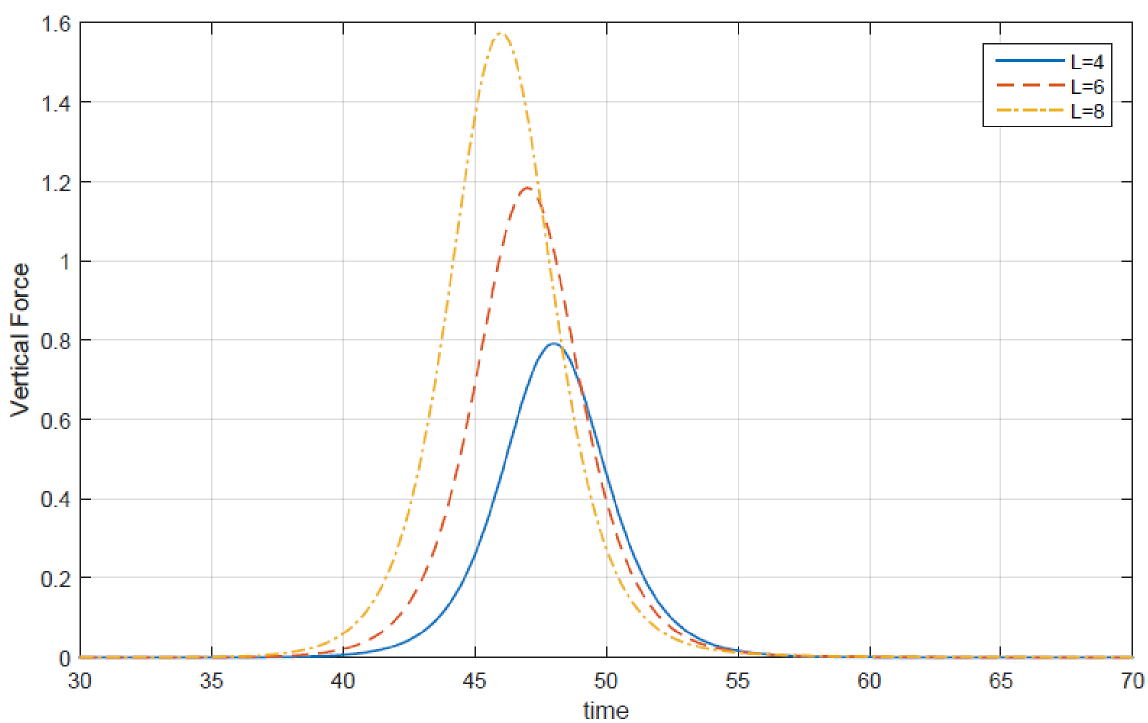

Figure 6-81: Comparison of vertical forces with various L for a case with *H=0.2*, and *d=b=0.2* (no porous conditions).

Chapter 7 Conclusions

In this dissertation, the hydrodynamic interactions between a solitary wave and a partially submerged structure considering either a thin porous wall or a 2-D finite-length body with attached dual porous walls are studied with proposed solution procedures and laboratory verifications. According to the defined fluid domains, analytical solutions of the velocity potentials, wave elevations and hydrodynamic forces in terms of reflection and transmission related coefficients are derived by assuming the fluid is viscid and incompressible and the flow is irrotational. Since the reflection and transmission related coefficients are time-independent, the present analytical solutions provide an easier and more efficient way to estimate the reflected and transmitted wave profiles and hydrodynamic forces on the structures.

The interactions of a solitary wave with a thin porous wall are firstly investigated analytically and experimentally. The analytical solutions of the velocity potentials and free-surface elevations of incident, reflected and transmitted wave are derived by applying the Fourier integral method and solution superposition procedure proposed by Isaacson (1983) and Zhong and Wang (2006). The formulations of the porous-wall boundary conditions are included by using Chwang's (1983) porous flow equations and Zhong and Wang's (2006) work based on the Darcy's law. To derive the reflection and transmission related coefficients, the least squares method is applied to the mixed boundary conditions at the interface of porous wall. By substituting the derived coefficients back to the equations of velocity potentials and free-surface elevations, the free-surface profiles for both reflected and transmitted waves and their corresponding velocity potentials can be determined. Using the nonlinear Bernoulli equation, the pressure can be calculated and the hydrodynamic forces acting on the porous wall can be estimated by integrating the pressure distribution on the wall surfaces.

Laboratory experiments under various conditions are conducted to collect the free-surface elevations with two resistance-type wave gauges at locations of upstream (for incident and reflected waves) and downstream (for transmitted waves) of a thin porous wall. The experimental measurements are plotted to verify the analytical solutions of the free-surface elevations. As the results shown, the incident and transmitted waves predicted by the present analytical solutions in magnitudes and phases match well with the experimental data, and for the reflected waves, in general, the analytical solutions tends to overestimate the reflected wave height. The over-estimation of the reflected waves may be caused by the energy dissipation and damping effect that are not included in the analytical solutions.

The parametric study is also performed to examine the effects of various physical variables, such as the incident wave height, submerged structural depth, and properties of porous wall, on the reflected/transmitted waves and hydrodynamic forces after an incident solitary wave encountering a partially submerged porous wall. For both solid wall ($b_0 = 0$) and porous wall ($b_0 \neq 0$) cases, the linearly increased trend of the wave run-up as the incident wave height increases is observed. Similar conclusions can be made that the wave run-up increases with an increase in submerged depth of porous wall and by extending a porous wall to near the sea bottom, the wave run-up can be substantially reduced. For a completely submerged (d=1) case, as the incident wave height increases, stronger nonlinear decreasing trends of the wave run-up as $R_e b_0$ increases can be noticed and for a partially submerged case (e.g. d=0.5), the effect of $R_e b_0$ on the wave run-ups is not significant. As expected, the submerged depth of porous wall is a dominant parameter on affecting the variations of the overall transmission coefficient; as the submerged depth of porous wall increases, the transmission coefficient (C_T) decreases and the decreasing rate of C_T appears more substantial for a solid wall with a larger submerged depth case, however, becomes a nearly linear trend for a porous wall case. In contrast, as $R_e b_0$ increases, the overall transmission coefficient increases for a completely submerged wall and the increasing trend of the overall transmission coefficient versus $R_e b_0$ is nonlinear. For a porous wall with a relatively smaller draft, the variation of $R_e b_0$ has a limit effect on the overall transmission coefficient. The incident wave height also has negligible effects on the variation of the overall transmission coefficient for all cases. In terms of the maximum horizontal hydrodynamic forces on a partially submerged solid wall ($b_0 = 0$), the present analytical results match reasonably well with the experimental measurements from Liu and Al-Banaa (2004)'s study. Since the analytical solutions use a linearized approximation of the velocity potentials, they are more practical to be applied for waves with smaller incident wave heights, such as waves with $H \leq 0.3$. Both incident wave height and submerged depth of porous wall have dominant effects on the variation of the horizontal hydrodynamic forces, and the $R_e b_0$ will have significant effect on the hydrodynamic forces when the submerged depth of porous wall is large. When the wall is completely submerged, the maximum horizontal force decreases as the $R_e b_0$ increases which indicates that a porous wall receives a smaller wave force than a solid wall does. However, for a partially submerged wall (e.g. d=0.5), a concave down variation trend of the maximum horizontal force is noticed, and the maximum values can be found at a specific value of $R_e b_0$ under a porous wall condition.

Similarly, the analytical and experimental approaches are utilized to study the interactions between a solitary wave and a partially submerged 2-D finite-length body with attached dual porous walls. The analytical solutions of the velocity potentials outside of the 2-D body are similar to those derived for the reflected and transmitted regions of the first topic considering a thin porous wall, and the velocity potential in region 2 underneath a partially submerged structure is derived by solving the Laplace equation with the kinematic boundary conditions on solid surfaces based on Lu and Wang's (2015) work. The unknown coefficients can be derived by applying the matching conditions and the orthogonality property of solution based eigenfunctions at the interfaces of the inner and outer domains. By substituting the derived unknown coefficients into the solutions of physical variables, the free-surface elevations in regions 1 (upstream) and 3 (downstream), the horizontal hydrodynamic forces and the vertical hydrodynamic forces in region 2 can be determined. Experimental data collected in the lab and from Lu and Wang's (2015) work are used to verify the derived analytical solutions of the free-surface elevations. The incident and transmitted waves predicted by the present analytical solutions in magnitudes and phases match well with the experimental measurements whereas the theoretically estimated reflected wave heights are higher than the experimental data. Additionally, the overall transmission coefficients from the present analytical solutions agree reasonably well with the numerical results from Lu and Wang (2015), but the overall reflection coefficients obtained from the analytical solutions are greater than Lu and Wang's numerical results. The differences between the compared overall reflection coefficients may be caused by the linearized approximations applied to express the free-surface elevation and the damping effect of the 2-D body, which is not included in the present analytical approach. The results indicate that the reflection process happens immediately in the analytical solutions, however, potentially, there will be a small time delay related to the wave run-up before the formation of the reflected waves. This immediate reflection process will narrow the shape of the reflected wave profile and accordingly with the amount of reflected fluid mass and energy allow the reflected wave height predicted by the present analytical solutions to be higher. Meanwhile, neglecting the damping effect may also physically cause slightly more wave energy reflected back and as a result increases the reflected wave height.

It is found the wave run-up on the encountering face of the body is shown to have a linearly increasing trend for both conditions with or without dual porous walls attached to a partially submerged 2-D finite-length body as the incident wave height increases. When the body draft, submerged depth of the porous wall, or structural length increases, the wave run-up also increases. In contrast, as $R_e b_1$ increases, the wave run-up decreases. With the dual porous walls applied, the effects of incident wave height, body draft, or structural length on the variation of the wave run-up become less significant. As the results indicated, with an increase of the incident wave height or body draft, the overall reflection coefficient increases and the overall transmission coefficient decreases. Similarly, when the submerged depth of the porous walls and the structural length increase, the overall reflection coefficient increases while the overall transmission coefficient decreases. On the contrary, the overall reflection coefficient decreases and the overall transmission coefficient increases as the R_eb_1 increases. Meanwhile, when the body draft or the structural length is smaller, the effects of the dual porous wall become more important in affecting the overall reflection and transmission coefficients. An increase of the incident wave height, body draft, submerged porous-wall depth or structural length and a decrease of R_eb_1 will cause an increase in the positive horizontal hydrodynamic force acting on the 2-D body system. The negative horizontal force also increases when the body draft increases. With the application of the dual porous walls, the negative horizontal forces become smaller. The incident wave height and the structural length are two dominant parameters on the variations of the vertical hydrodynamic forces. As the incident wave height or the structural length increases, the vertical hydrodynamic force increases. The body draft, submerged depth of the porous walls and R_eb_1 have negligible effects on the variations of the vertical hydrodynamic forces.

In summary, through the comparisons between the derived analytical solutions and the present experimental measurements or other published results, the proposed analytical models presented in this study are demonstrated to be able to serve as efficient and reasonably accurate engineering tools to investigate the hydrodynamic interactions between a solitary wave and either a partially submerged thin porous wall or a 2-D finite-length partially submerged body with attached dual porous walls in terms of the transmitted waves and the wave forces on the structures, although the models tend to slightly overestimate the overall reflection coefficients. For the design considerations, the present models can provide reasonable estimations on the solitary waves induced hydrodynamic forces on the two proposed partially submerged structures as breakwaters.

For future studies, the present analytical approaches may be modified by adding a term with damping effect or time-delay factor to improve the accuracy on estimating the reflected wave height. For more practical usages, extended laboratory experiments can be carried out to estimate the damping coefficients or time-delay factor for various cases, which potentially can be used to improve the predictions of the reflected waves. Also, due to the lack of the related data, laboratory measurements or numerical simulations on the reflected and transmitted wave heights (or the reflection and transmission coefficients) for the interactions between a solitary wave and a partially submerged ($d < 1$) thin solid wall are recommended to provide additional data or results for comparisons with model predictions. Furthermore, the laboratory experiments on the hydrodynamic forces are also very limited. It is recommended in the future study to carry out laboratory tests to measure the wave induced hydrodynamic forces on the proposed structures of the present studies that include either a partially submerged thin porous wall or a partially submerged 2-D finite-length body with attached dual porous walls.

References

Abul-Azm, A. (1993). "Wave Diffraction Through Submerged Breakwaters." *Journal of Waterway, Port, Coastal, and Ocean Engineering*, 119(6), pp. 587-605.

Beji, S., and Battjes, J.A. (1993). "Experimental Investigation of Wave Propagation over a Bar." *Journal of Coastal Engineering*, 19, pp. 151-162.

Boussinesq, M. J. (1871). "Theorie Generale des Mouvements qui Sout Propages Dans un Canal Retangulaire Horizontal." *Comtes Rendus, Acad. Sci.*, vol. 73, pp. 256-260.

Chu, T. (2014). "Part 1- Geostatistical Interpolation of Rain Fields using Radar Estimates and Gauge Observations: Algorithm Design and Automation and Part 2-Energy Dissipation in Fluid Flows and Wave Transformation by Porous Barriers and Submerged Cavities." Houston, Tx: University of Houston.

Chwang, A. (1983). "A Porous-wavemaker Theory." *J. Fluid Mech.*, 132, pp. 395-406.

Chwang, A. T. and Wu, J. (1994). "Wave Scattering by Submerged Porous Disk." J. *Eng. Mech.*, 120(12), pp. 2575-2587.

Chwang, A.T. and Li, W. (1983). "A Piston-type Porous Wavemaker Theory." *J. Engrg. Mathematics*, 17. pp. 301-313.

Dalrymple, R.A., and Martin, P.A. (1990). "Wave Diffraction Through Offshore Breakwaters." *Journal of Waterway, Port Coastal, Ocean Engineering*, ASCE, 116(6), 727-741.

De, S. C. (1955). "Contributions to the Theory of Stokes Waves." *Proc. Cambridge Phil. Soc.*, 51, 713–736.

Dick, T.M. and Brebner, A. (1968). "Solid and Permeable Submerged Breakwaters." Proceedings 11th Conference on Coastal Engineering, ASCE, (pp. II, 1141-1158). New York, NY.

Dong, G.H., Zheng, Y.N., Li, Y.C., Teng, B., Guan, C.T., and Lin, D.F. (2008). "Experiments on Wave Transmission Coefficients of Floating Breakwaters." *Ocean Engineering*, 35, pp. 931-938.

Drimer, N., Agnon, Y., and Stiassnie, M. (1992). "A Simplified Analytical Model for a Floating Breakwater in Water of Finite Depth." *Applied Ocean Research*, 14, pp. 33-41.

Friedrichs, K. O. (1948). "On the Derivation of the Shallow Water Theory. Appendix to the Formation of Breakers and Bores by Stoker. J. J." *Comm. Pure Appl. Math*, 1,pp.81-85.

Gobbi, M. F., Kirby, J. T., and Wei, G. (2000). "A Fully Nonlinear Boussinesq Model for Surface Waves, Part 2. Extension to 0(kh)4." *J. Fluid Mech.*, 405, pp. 181-210.

Goring, D.G. (1978). "Tsunamis-The Propagation of Long Waves onto a Shelf." Pasadena, California: California Institute of Technology.

Hu, H., and Wang, K. H. (2005). "Damping Effect on Waves Propagating Past a Submerged Horizontal Plate and a Vertical Porous Wall." *J. Eng. Mech.*, 131(4), pp. 427-437.

Isaacson, M. (1977). "Shallow Wave Diffraction around Large Cylinder." *Journal of the Waterway, Port, Coastal and Ocean Engineering*, 103(WW1), pp.69-82.

Isaacson, M. (1978). "Wave Runup around Large Circular Cylinder." *Journal of the Waterway, Port, Coastal and Ocean Engineering*, 104(WW1), pp. 69-79.

Isaacson, M. (1982). "Nonlinear-wave Effects on Fixed and Floating Bodies." *J. Fluid Mech.*, 120, pp. 267-281.

Isaacson, M. (1983). "Solitary Wave Diffraction around Large Cylinder." *Journal of Waterway Port, Coastal, Ocean Engineering*, ASCE 109(1), pp. 121-127.

Jaf, J. M., and Wang, K. H. (2015). "Interaction of Solitary Waves with a Submerged Impermeable Breakwater." *Journal of Engineering Mechanics*, 141.9 (2015): 04015030.

Korteweg, D. J. and De Vries, G. (1895). "On the Change of Form of Long Wave Advancing in a Rectangular Canal and on a New Type of Long Stationary Waves." *Phil. Mag.*, 5, pp. 422-430.

Koutandos, E., Prinos, P. and Gironella, X. . (2005). "Floating Breakwaters under Regular and Irregular Wave Forcing: Reflection and Tranmission Characteristics." *J. of Hydraulic Research*, 43, pp.174-188.

Laitone, E. V. . (1960). "The Second Approximation to Cnoidal and Solitary Waves." *J.Fluid Mech.*, 9, pp. 430-444.

Laitone, E. V. . (1962). "Limiting Conditions for Cnoidal and Stokes Waves." *J. Geophys.Res.*, 67, pp. 1555-1564.

Laitone, E. V. . (1965). "Series Solutions for Shallow Water Waves." *J. Geophys. Res.*, 70, pp. 995-998.

Li, W. (1999). "Modeling Nonlinear Shallow Water Waves in Irregular Basins and Through a Porous Breakwater." Houston, TX: University of Houston.

Lin, P. (2004). "A Numerical Study of Solitary Wave Interaction with Rectangular Obstacles." *Coastal Engineering*, 51, pp. 35-51.

Lin, P. (2006). "A Multiple-layer a -coordinate Model for Simulation of Wave-structure Interaction." *Computers & Fluids*, 35, pp. 147-167.

Liu, H., Luo, J., Lin, P. and Liu, R. (2013). "Analytical Solution for Long-Wave Reflection by a General Breakwater or Trench with Curvilinear Slopes." *Journal of Engineering Mech.*, 139(2), pp. 229-245.

Liu, P. L.-F. (1994). "Model Equations for Wave Propagation from Deep to Shallow Water." *Advances in Coastal Engineering*, 1, pp. 125-157.

Liu, Philip L.-F and Al-Banaa, Khaled. (2004). "Solitary Wave Runup and Force on a Vertical Barrier." *J. Fluid Mech.*, vol. 505, pp. 225-233.

Liu, Philip L-F., and Wen, J. (1997). "Nonlinear Diffusive Surface Waves in Porous Media." *Journal of Fluid Mechanics*, 347, pp. 119-139.

Liu, Y., and Li, H. (2012). "Analysis of Wave Interaction with Submerged Perforated Semi-circular Breakwaters Through Multiple Method." *Applied ocean Research*, 34, pp. 164-172.

Losada I.J, Silva, R., and Losada, M.A. (1996). "Interaction of Non-Breaking Directional Random Waves with Submerged Breakwaters." *Journal of Coastal Engineering*, 28, pp. 249-266.

Lu, X. and Wang, K. H. (2015). "Modeling a Solitary Wave Interaction with a Fixed Floating Body Using an Integrated Analytical–numerical Approach." *Ocean Engineering*, 109, pp. 691-704.

Lynett, P. J., Liu, P. L. F., Losada, I. J., and Vidal, C. (2000). "Solitary Wave Interaction with Porous Breakwaters." *Journal of Waterway, Port, Coastal, and Ocean Engineering*, 126(6), pp. 314-322.

MacCamy, R.C., Fuchs, R.A. (1954). "Wave Forces on Piles: A Diffraction Theory." Technical Memorandum No.69 Beach Erosion Board.

Madsen, O. S. (1974). "Wave Transmission Through Porous Structures." *J. Wtrwy., Harb. and Coast. Engrg. Div.*, ASCE, 100(3), 169–188.

Madsen, P. A., Murray, R., Sarensen, O. R. . (1991). "A New Form of the Boussinesq Equations with Improved Linear Dispersion Characteristics: Part I." *Coastal Eng.*, 15, pp. 371-388.

Mccartney, B.L. (1985). "Floating Breakwater Design." *J. of Waterways, Port, Coastal and Ocean Engng.*, ASCE, 111, pp. 304-318.

Mei, C. and LeMehaute, B. (1966). "Note on the Equation of Long Waves over an Uneven Bottom." *J. Geophys. Res.*, 71, pp. 393-400.

Mei, C.C. and Black, J.L. (1969). "Scattering of Surface Waves by Rectangular Obstacles in Water of Finite Depth." *J. of Fluid Mech.*, 38(3), pp. 499-511.

Murali, K. and Mani, J.S. (1997). "Performance of Cage Floating Breakwater." *J. of Waterway, Port, Coastal, and Ocean Engng.*, ASCE, 123,pp.172-179.

Nwogu, O. (1993). "Alternative Form of Boussinesq Equations for Near-shore Wave Propagation." *J. Waterw., Port, Coastal, Ocean Eng.*, ASCE 119(6), pp. 618.

Ohyama, K. (1991). "Numerical Method of Solitary Forces Acting on a Large Vertical Cylinder." Proceedings of the Coastal Engineering Conference, (pp. 1, 840-852).

Patarapanich, M. and Cheong, H. F. (1989). "Reflection and Transmission Characteristics of Regular and Random Waves from a Submerged Horizontal Plate." *Coastal Engineering*, 13(2), pp. 161-182.

Peregrine, D. H. (1967). "Long Waves on a Beach." *J. Fluid Mech.*, 27, pp. 815-882.

Power, H., and Chwang, A. T. (1984). "On Reflection of a Planar Solitary Wave." Wave Motion, 6, pp. 183-195.

Ren, X. and Wang, K.H. (1994). "Mooring Lines Connected to Floating Porous Breakwaters." *Int. J. Engng. Sci.*, 32, pp. 1511-1530.

Russell, J. S. (1845). "Report on Waves." *Rep.Meet.Brit.Assoc.Adv.Sci.14th*, vol.1844, pp. 311-390.

Russell, J.S. (1838). "Report of the Committee on Waves." *Rep.Meet.Brit.Assoc.Adv.Sci. 7th*, vol.1837, pp. 417-496.

Silva, R., Losada, I.J., and Losada M.A. (2000). "Reflection and Transmission of Tsunami Waves by Coastal Structures." *Applied Ocean Research*, 22, pp. 215-223.

Sneddon, I. (1966). "Mixes Boundary Value Problems in Potential Theory." Amsterdam, The Netherlands: North Holland Publishing Co.

Sogimoto N., Hosokawa K., and Kakutani T. (1987). "Reflection and Transmission of a Shallow Water Soliton Over a Barrier." *Journal of the Physical society of Japan*, 56(8), pp. 2744-2754.

Sollitt, C. K., and Cross, R. H. (1972). "Wave Transmission Through Permeable Breakwaters." *Proc., 13rd Int. Conf. Coast. Engrg*, (pp. ASCE, pp. 1827–1846). New York.

Stephan, T.G., Miguel, A.L., and Francisco, M. (1994). "Characteristics of Solitary Wave Breaking Induced by Breakwaters." *Journal of Waterway, Port, Coastal, and Ocean Engineering*, 120(1), pp. 74-92.

Taylor, G. (1956). "Fluid Flow in Regions Bounded by Porous Surface." *Proc. Royal Society of London*, Series A, 234, pp. 456-475.

Ursell, F. (1947). "The Effect of a Fixed Vertical Barrier on Surface Waves in Deep Water." *Proc. Cambridge Philosophical Soc.*, 43(3), pp. 374-382.

Vidal C., Losada M., Medina R., and Rubio J. (1988). "Solitary Wave Transmission Through Porous Breakwater." *International Coastal Engineering Conference*, ASCE, pp. 73-83.

Wang, K. H. and Jiang, L. (1994). "Interactions of Solitary Waves with Cylinder Arrays." *Proceedings of the International Conference on Offshore Mechanics and Arctic*, (pp. OMAE, 1, pp. 99-107).

Wang, K.H. and Ren, X. (1993). "Water Waves on Flexible and Porous Breakwaters." *J. of Engineering Mechanics*, ASCE, 119, pp. 1025-1047.

Wang, K.H., and Ren, X. (1994). "Wave Interaction with a Concentric Porous Cylinder System." *Ocean Engineering*, 21(4), pp. 343–360.

Wang, K.H., Wu, T.Y., and Yates, G.T. (1992). "Three Dimensional Scattering of Solitary Waves by Vertical Cylinder." *Journal of Waterway, Port, Coastal, and Ocean Engineering*, 118(5), pp. 551-566.

Wei, G., Kirby, J. T. (1995). "A Time-dependent Numerical Code for the Extended Boussinesq Equations." *J. Waterw., Port, Coastal, Ocean Eng.*, ASCE 121(5), pp. 251-161.

Wei, G., Kirby, J. T., Grilli, S., and Subramanya, R. (1995). "A Fully Nonlinear Boussinesq Model for Surface Waves, Part 1. Highly Nonlinear Unsteady Waves." *J. Fluid Mech.*, 294, pp. 71-92.

Williams, A.N., and Li, W. (2000). "Water Wave Interaction with an Array of Bottom-mounted Surface-piercing Porous Cylinders." *Ocean Engineering*, 27 (8), pp. 841–866.

Williams, A.N., Lee, H.S., and Huang, Z. (2000). "Floating Pontoon Breakwaters." *Ocean Engineering*, 27(3), pp. 221-240.

Wu, J., Wan, Z. and Fang, Y. (1998). "Wave Reflection by a Vertical Wall with a Horizontal Submerged Porous Plate." *Ocean Engineering*, 25(9), pp. 767-779.

Wu, T. Y. (1981). "Long Waves in Ocean and Coastal Waters." *J. Engrg. Mech. Div.*, ASCE, 107, pp. 501-522.

Wu, T. Y. (2001). "On Theoretical Modeling of Aquatic and Aerial Animal Locomotion." *Adv. Appl. Mech.*, 38, pp. 291-353.

Wu, Y. T., Yeh, C. L., and Hsiao, S. C. (2014). "Three-dimensional Numerical Simulation on The Interaction of Solitary Waves and Porous Breakwaters." *Coastal Engineering*, 85, pp. 12-29.

Wu, Y., Hsiao. Sh., Huang, Z., and Hwang, K. (2012). "Propagation of Solitary Waves over a Bottom-mounted Barrier." *Journal of Coastal Engineering*, 62, pp. 31-47.

Xie, J., Liu, H., and Lin, P. (2011). "Analytical Solution for Long-Wave Reflection by a Rectangular Obstacle with Two Scour Trenches." *Journal of Engineering Mech.*, 137(12), pp. 919-930.

Yates, G.T., and Wang, K.H. (1994). "Solitary Wave Scattering by Vertical Cylinder: Experimental Study." *Proceedings of the International Offshore and Polar Engineering Conference*, (pp. 3, 118-124).

Yu, X. and Chwang, A.T. (1994). "Water Waves above Submerged Porous Plate." *Journal of Engineering Mechanics*, ASCE, 120, 1270-1282.

Yu, X., and Chwang, A. T. (1993). "Analysis of Wave Scattering by Submerged Disk." *J. Engineering Mechanics*, 119(9), pp. 1804-1817.

Zabusky, N. J. and Kruskal, M. D. (1965). "Interaction of "Solitons" in a Collisionless Plasma and the Recurrence of Initial States." *Phys. Rev. Lett.*, vol 15, pp. 240-243.

Zheng, Y.H., You, Y.G., and Shen, Y.M.,. (2004). "On the Radiation and Diffraction of Water Waves by a Rectangular Buoy." *Ocean Engineering*, 31, pp. 1063-1082.

Zhong, Z and Wang, K. H. (2006). "Solitary Wave Interaction with a Concentric Porous Cylinder System." *Ocean Engineering*, 33, pp. 927-929.

Zhong, Z. and Wang, K. H. (2009). "Modeling Fully Nonlinear Shallow-water Waves and Their Interactions with Cylindrical Structures." *Computers & Fluids*, 38(5), pp. 1018-1025.

Appendix A Derivation of the Analytical Solutions of a Solitary Wave Interacting with a Partially Submerged Porous Wall

As shown in the Chapter 2, the velocity potentials in region 1 and 3 can be expressed as

$$\phi_1 = \int_{-\infty}^{\infty} \{(-iq)[e^{ik(x)} + R_0 e^{-ik(x)}] + \alpha k^2 \left(\frac{1}{3} + z + \frac{z^2}{2}\right)(-iq)[e^{ik(x)} + R_0 e^{-ik(x)}]\} e^{-ikct} dk \quad and \tag{A-1}$$

$$\phi_3 = \int_{-\infty}^{\infty} \{(-iq)[T_0 e^{ik(x)}] + \alpha k^2 \left(\frac{1}{3} + z + \frac{z^2}{2}\right)(-iq)[T_0 e^{ik(x)}]\} e^{-ikct} dk, \tag{A-2}$$

and the boundary conditions can be written as

$$\left(\frac{\partial \phi_1}{\partial x}\right)_{x=0} = \left(\frac{\partial \phi_3}{\partial x}\right)_{x=0} \quad @-1 \le z \le 0, \tag{A-3}$$

$$\left(\frac{\partial \phi_1}{\partial x}\right)_{x=0} = \left(\frac{\partial \phi_3}{\partial x}\right)_{x=0} = (ik)R_e b_0(\phi_1 - \phi_3) \quad @-d \le z \le 0, and \tag{A-4}$$

$$\phi_1 = \phi_3 \quad @-1 \le z \le -d. \tag{A-5}$$

Based on the velocity potentials in region 1 and 3, we can derive the velocity in x-axis in region 1 and 3 as

$$\frac{\partial \phi_1}{\partial x} = \int_{-\infty}^{\infty} \{(-iq)[(ik)e^{ik(x)} + (-ik)R_0 e^{-ik(x)}] + \alpha k^2 \left(\frac{1}{3} + z + \frac{z^2}{2}\right)(-iq)[(ik)e^{ik(x)} + (-ik)R_0 e^{-ik(x)}]\} e^{-ikct}\, dk \quad and \tag{A-6}$$

$$\frac{\partial \phi_3}{\partial x} = \int_{-\infty}^{\infty} \{(-iq)[(ik)T_0 e^{ik(x)}]$$

$$+ \alpha k^2 \left(\frac{1}{3} + z + \frac{z^2}{2}\right)(-iq)[(ik)T_0 e^{ik(x)}]\} e^{-ikct}\, dk. \tag{A-7}$$

Substituting Eqns. (A-1), (A-2), (A-6) back into Eqn. (A-4) with the condition of $T_0 = 1 - R_0$, and take the integration off, we can have

$$\left\{(-iq)\left[(ik)e^{ik(x)} + (-ik)R_0 e^{-ik(x)}\right]\right.$$

$$\left. + \alpha k^2 \left(\frac{1}{3} + z + \frac{z^2}{2}\right)(-iq)\left[(ik)e^{ik(x)} + (-ik)R_0 e^{-ik(x)}\right]\right\} e^{-ikct}$$

$$= (ikc)R_e b_0 \left\{\left\{(-iq)\left[e^{ik(x)} + R_0 e^{-ik(x)}\right]\right.\right.$$

$$\left. + \alpha k^2 \left(\frac{1}{3} + z + \frac{z^2}{2}\right)(-iq)\left[e^{ik(x)} + R_0 e^{-ik(x)}\right]\right\} e^{-ikct}$$

$$- \left\{(-iq)\left[(1 - R_0)e^{ik(x)}\right]\right.$$

$$\left.\left. + \alpha k^2 \left(\frac{1}{3} + z + \frac{z^2}{2}\right)(-iq)\left[(1 - R_0)e^{ik(x)}\right]\right\} e^{-ikct}\right\}$$

$$@x = 0. \tag{A-8}$$

At x equals to 0, taking off the e^{-ikct} on both side, we will have

$$\left\{[1-R_0]+\alpha k^2\left(\frac{1}{3}+z+\frac{z^2}{2}\right)[1-R_0]\right\}$$

$$=R_e b_0 c\{\{[1+R_0]+\alpha k^2\left(\frac{1}{3}+z+\frac{z^2}{2}\right)[1+R_0]\}-\{[(1-R_0)]$$

$$+\alpha k^2\left(\frac{1}{3}+z+\frac{z^2}{2}\right)[(1-R_0)\}\}. \quad \text{(A-9)}$$

Then, it can be rewritten as

$$1-R_0-2GR_0+\alpha k^2\left(\frac{1}{3}+z+\frac{z^2}{2}\right)[1-R_0-2GR_0]=0 \quad @-d\leq z\leq 0. \quad \text{(A-10)}$$

Substituting Eqns. (A-1) and (A-2) into Eqn. (A-5) the condition of $T_0=1-R_0$, we have

$$\int_{-\infty}^{\infty}\{(-iq)[e^{ik(x)}+R_0e^{-ik(x)}]+\alpha k^2\left(\frac{1}{3}+z+\frac{z^2}{2}\right)(-iq)[e^{ik(x)}+R_0e^{-ik(x)}]\}e^{-ikct}dk$$

$$=\int_{-\infty}^{\infty}\{(-iq)[(1-R_0)e^{ik(x)}]+\alpha k^2\left(\frac{1}{3}+z+\frac{z^2}{2}\right)(-iq)[(1$$

$$-R_0)e^{ik(x)}]\}e^{-ikct}dk\}. \quad \text{(A-11)}$$

And taking the integration off, we can get

$$\left\{\left\{(-iq)\left[e^{ik(x)}+R_0e^{-ik(x)}\right]+\alpha k^2\left(\frac{1}{3}+z+\frac{z^2}{2}\right)(-iq)\left[e^{ik(x)}+R_0e^{-ik(x)}\right]\right\}\right.$$

$$\left.-\left\{(-iq)\left[(1-R_0)e^{ik(x)}\right]+\alpha k^2\left(\frac{1}{3}+z+\frac{z^2}{2}\right)(-iq)\left[(1-R_0)e^{ik(x)}\right]\right\}\right\}$$

$$=0. \quad \text{(A-12)}$$

At x equals to 0, we can rewrite it as

$$\left\{ \begin{array}{l} \left\{[1+R_0]+\alpha k^2\left(\frac{1}{3}+z+\frac{z^2}{2}\right)[1+R_0]\right\} - \\ \left\{[(1-R_0)]+\alpha k^2\left(\frac{1}{3}+z+\frac{z^2}{2}\right)[(1-R_0)]\right\} \end{array} \right\} = 0. \tag{A-13}$$

And we can simplify it as

$$2R_0+\alpha k^2\left(\frac{1}{3}+z+\frac{z^2}{2}\right)(2R_0)=0 \quad -1\le z\le -d. \tag{A-14}$$

Applying lease-square method, we can get

$$H_0 = \begin{cases} 1+(-1-2G)R_0+\alpha k^2\left(\frac{1}{3}+z+\frac{z^2}{2}\right)[1+(-1-2G)R_0] & -d\le z\le 0 \\ 2R_0+\alpha k^2\left(\frac{1}{3}+z+\frac{z^2}{2}\right)(2R_0) & -1\le z\le -d \end{cases}. \tag{A-15}$$

As we discussed, the lease-square method should satisfy the condition that

$$\int_{-1}^{0} H_0(z)\frac{\partial H_0}{\partial R_0}dz=0, \tag{A-16}$$

where $\frac{\partial H_0}{\partial R_0}$ can be expressed as

$$\frac{\partial H_0}{\partial R_0} = \begin{cases} (-1-2G)+\alpha k^2\left(\frac{1}{3}+z+\frac{z^2}{2}\right)[(-1-2G)] & -d\le z\le 0 \\ 2+\alpha k^2\left(\frac{1}{3}+z+\frac{z^2}{2}\right)(2) & -1\le z\le -d \end{cases}. \tag{A-17}$$

So that Eqn. (A-16) can be rewritten as

$$\int_{-1}^{0} H_0(z)\frac{\partial H_0}{\partial R_0}dz$$

$$= \int_{-d}^{0}\left\{1 + BR_0 + C\left(\frac{1}{3} + z + \frac{z^2}{2}\right)[1 + BR_0]\right\}\left\{B + C\left(\frac{1}{3} + z + \frac{z^2}{2}\right)[B]\right\}dz$$

$$+ \int_{-1}^{-d}\left\{2R_0 + C\left(\frac{1}{3} + z + \frac{z^2}{2}\right)(2R_0)\right\}\left\{2 + C\left(\frac{1}{3} + z + \frac{z^2}{2}\right)(2)\right\}dz$$

$$= 0, \tag{A-18}$$

where

$$B = -1 - 2G\ and \tag{A-19}$$

$$C = \alpha k^2. \tag{A-20}$$

Then, we have

$$\int_{-d}^{0}\left\{1 + BR_0 + C\left(\frac{1}{3} + z + \frac{z^2}{2}\right)[1 + BR_0]\right\}\left\{B + C\left(\frac{1}{3} + z + \frac{z^2}{2}\right)[B]\right\}dz$$

$$= \frac{Bd\{9C^2d^4 - 45C^2d^3 + (80C^2 + 60C)d^2 + (-60C^2 - 180C)d + 20C^2 + 120C + 180\}(BR_0 + 1)}{180}$$

$$= \frac{B\{9C^2d^5 - 45C^2d^4 + (80C^2 + 60C)d^3 + (-60C^2 - 180C)d^2 + (20C^2 + 120C + 180)d\}(BR_0 + 1)}{180}$$

$$= \frac{B\{E\}(BR_0 + 1)}{180}.$$

(A-21)

where

$$E = 9C^2d^5 - 45C^2d^4 + (80C^2 + 60C)d^3 + (-60C^2 - 180C)d^2 + (20C^2 + 120C + 180)d, \tag{A-22}$$

and

$$\int_{-1}^{-d}\left\{2R_0+C\left(\frac{1}{3}+z+\frac{z^2}{2}\right)(2R_0)\right\}\left\{2+C\left(\frac{1}{3}+z+\frac{z^2}{2}\right)(2)\right\}dz$$

$$=-\frac{R_0\{9C^2d^5-45C^2d^4+(80C^2+60C)d^3+(-60C^2-180C)d^2+(20C^2+120C+180)d-4C^2-180\}}{45}$$

$$=-\frac{R_0\{E-4C^2-180\}}{45}.$$

(A-23)

Substituting Eqns. (A-21) and (A-23) back to Eqn. (A-18), we will get

$$-\frac{R_0\{E-4C^2-180\}}{45}+\frac{B\{E\}(BR_0+1)}{180}=0, \tag{A-24}$$

so that

$$R_0=\frac{-\frac{BE}{180}}{\frac{B^2E}{180}-\frac{\{E-4C^2-180\}}{45}}=\frac{-BE}{B^2E-4(E-4C^2-180)}. \tag{A-25}$$

Appendix B Derivation of the Analytical Solutions of a Solitary Wave Interacting with a 2-D Finite-Length Body with Attached Dual Porous Walls

As shown in Chapter 3, at the interface between region 1 and 2 ($x = -x_1$), we have

$$\int_{-1}^{-d} \phi_1^p \, dz = \int_{-1}^{-d} \phi_2^p \, dz \ @ -1 \leq z \leq -d \ \ and \tag{B-1}$$

$$\frac{\partial \phi_1^p}{\partial x} = -R_e b_1 \left(\frac{\partial \phi_1^p}{\partial t} - \frac{\partial \tilde{\phi}_2}{\partial t} \right) \ @ -d \leq z \leq -b, \tag{B-2}$$

where Eqn. (B-2) can be rewritten as

$$\frac{\partial \tilde{\phi}_2}{\partial t} = \frac{\partial \phi_1^p}{\partial t} + \frac{\partial \phi_1^p}{\partial x} \left(\frac{1}{R_e b_1} \right) \ @ -d \leq z \leq -b. \tag{B-3}$$

Eqns. (B-4) through (B-8) show the detail terms in Eqns. (B-1) and (B-3) shown above

$$\phi_1^p = \left\{ (-iq)\left[e^{ik(x)} + R_1 e^{-ik(x)}\right] + \alpha k^2 \left(\frac{1}{3} + z + \frac{z^2}{2} \right) (-iq)\left[e^{ik(x)} + R_1 e^{-ik(x)}\right] \right\} e^{-ikct}, \tag{B-4}$$

$$\phi_2^p = \left\{ \sum_{j=1}^{\infty} \left(A_j \cosh\left(m_j(x)\right) + B_j \sinh\left(m_j(x)\right) \right) \cos\left(m_j(z+1)\right) + C(x) + D \right\} e^{-ikct}, \tag{B-5}$$

$$\frac{\partial \phi_1^p}{\partial x} = \left\{(-iq)\left[(ik)e^{ik(x)} + (-ik)R_1 e^{-ik(x)}\right]\right.$$

$$+ \alpha k^2 \left(\frac{1}{3} + z + \frac{z^2}{2}\right)(-iq)\left[(ik)e^{ik(x)}\right.$$

$$\left.\left. + (-ik)R_1 e^{-ik(x)}\right]\right\} e^{-ikct}, \qquad \text{(B-6)}$$

$$\frac{\partial \phi_1^p}{\partial t} = (-ikc)\left\{(-iq)\left[e^{ik(x)} + R_1 e^{-ik(x)}\right]\right.$$

$$\left. + \alpha k^2 \left(\frac{1}{3} + z + \frac{z^2}{2}\right)(-iq)\left[e^{ik(x)} + R_1 e^{-ik(x)}\right]\right\} e^{-ikct}, and \qquad \text{(B-7)}$$

$$\frac{\partial \tilde{\phi}_2}{\partial t} = (-ikc)\left\{\sum_{j=1}^{\infty}\left(A_j\, cosh\left(m_j(x)\right) + B_j\, sinh\left(m_j(x)\right)\right) cos\left(m_j(z+1)\right) + C(x)\right.$$

$$\left. + D\right\} e^{-ikct} = (-ikc)\tilde{\phi}_2. \qquad \text{(B-8)}$$

By substituting the equations shown above back into Eqn. (B-3), we have

$$(-ikc)\tilde{\phi}_2$$

$$= (-ikc)\left\{(-iq)\left[e^{ik(x)} + R_1 e^{-ik(x)}\right]\right.$$

$$\left. + \alpha k^2 \left(\frac{1}{3} + z + \frac{z^2}{2}\right)(-iq)\left[e^{ik(x)} + R_1 e^{-ik(x)}\right]\right\} e^{-ikct}$$

$$+ \left(\frac{1}{R_e b_1}\right)\left\{(-iq)\left[(ik)e^{ik(x)} + (-ik)R_1 e^{-ik(x)}\right]\right.$$

$$\left. + \alpha k^2 \left(\frac{1}{3} + z + \frac{z^2}{2}\right)(-iq)\left[(ik)e^{ik(x)} + (-ik)R_1 e^{-ik(x)}\right]\right\} e^{-ikct}. \qquad \text{(B-9)}$$

Rearrange Eqn. (B-9), we have

$$\tilde{\phi}_2 = \Bigg\{(-iq)\left[e^{ik(x)} + R_1 e^{-ik(x)}\right]$$

$$+ \alpha k^2\left(\frac{1}{3} + z + \frac{z^2}{2}\right)(-iq)\left[e^{ikx} + R_1 e^{-ikx}\right]\Bigg\} e^{-ikct}$$

$$+ \left(\frac{1}{R_e b_1}\right)\left(\frac{-1}{c}\right)\Bigg\{(-iq)\left[e^{ikx} - R_1 e^{-ikx}\right]$$

$$+ \alpha x^2\left(\frac{1}{3} + z + \frac{z^2}{2}\right)(-iq)\left[e^{ikx} - R_1 e^{-ikx}\right]\Bigg\} e^{-ikct}$$

$$= \phi_1^p + \left(\frac{1}{R_e b_1}\right)\left(\frac{-1}{c}\right)\tilde{\phi}_1, \qquad \text{(B-10)}$$

where

$$\tilde{\phi}_1 = \Bigg\{(-iq)\left[e^{ikx} - R_1 e^{-ikx}\right]$$

$$+ \alpha k^2\left(\frac{1}{3} + z + \frac{z^2}{2}\right)(-iq)\left[e^{ikx} - R_1 e^{-ikx}\right]\Bigg\} e^{-ikct}. \qquad \text{(B-11)}$$

Eqn. (B-3) can be expressed as

$$\int_{-1}^{-d} \phi_1^p \, dz + \int_{-d}^{-b} \tilde{\phi}_2 dz = \int_{-1}^{-b} \phi_2^p \, dz. \qquad \text{(B-12)}$$

By multiplying the orthogonality property of eigenfunctions, $cos\left(m_j(z+1)\right)$, we have

$$\int_{-1}^{-d} \phi_1^p \; cos\left(m_j(z+1)\right) dz + \int_{-d}^{-b} \tilde{\phi}_2 \, cos\left(m_j(z+1)\right) dz$$

$$= \int_{-1}^{-b} \phi_2^p \, cos\left(m_j(z+1)\right) \, dz \qquad @\; x = -x_1, j = 1,2, \dots.. \qquad \text{(B-13)}$$

By rearranging Eqn. (B-13), we have

$$\int_{-1}^{-d} \phi_1^p \; cos\left(m_j(z+1)\right) dz + \int_{-d}^{-b} (\phi_1^p$$

$$+ \left(\frac{1}{R_e b_1}\right)\left(\frac{-1}{c}\right)\tilde{\phi}_1 \;) \; cos\left(m_j(z+1)\right) dz$$

$$= \int_{-1}^{-b} \phi_2^p \, cos\left(m_j(z+1)\right) \; dz \qquad @ \; x = -x_1, j = 1,2, \ldots.., \qquad \text{(B-14)}$$

and then combining terms with ϕ_1^p, we can get

$$\int_{-1}^{-b} \phi_1^p \; cos\left(m_j(z+1)\right) dz +$$

$$+ \int_{-d}^{-b} \left(\frac{1}{R_e b_1}\right)\left(\frac{-1}{c}\right)\tilde{\phi}_1 \, cos\left(m_j(z+1)\right) dz$$

$$= \int_{-1}^{-b} \phi_2^p \, cos\left(m_j(z+1)\right) \; dz. \qquad \text{(B-15)}$$

Each of the term in Eqn. (B-15) can be expressed as

$$\int_{-1}^{-b} \phi_1^p \; cos\left(m_j(z+1)\right) dz$$

$$= \int_{-1}^{-b} \{(-iq)[e^{ik(x)} + R_1 e^{-ik(x)}] + \alpha k^2 \left(\frac{1}{3} + z + \frac{z^2}{2}\right)(-iq)[e^{ik(x)}$$

$$+ R_1 e^{-ik(x)}]\} e^{-ikct} \; cos\left(m_j(z+1)\right) dz$$

$$= \frac{(1-b)cos(j\pi)}{(m_j)^2}(-iq)\alpha k^2 [e^{ik(x)} + R_1 e^{-ik(x)}]\} e^{-ikct}$$

$$= C_a(-iq)\alpha k^2 [e^{ik(x)} + R_1 e^{-ik(x)}]\} e^{-ikct}, \qquad \text{(B-16)}$$

$$\int_{-d}^{-b}\left(\frac{1}{R_e b_1}\right)\left(\frac{-1}{c}\right)\tilde{\phi}_1 \cos\left(m_j(z+1)\right)dz$$

$$=\left(\frac{1}{R_e b_1}\right)\left(\frac{-1}{c}\right)\int_{-d}^{-b}\{(-iq)[e^{ik(x)}-R_1e^{-ik(x)}]+\alpha k^2\left(\frac{1}{3}+z+\frac{z^2}{2}\right)(-iq)[e^{ik(x)}$$

$$-R_1e^{-ik(x)}]\}e^{-ikct}\cos\left(m_j(z+1)\right)dz$$

$$=\left(\frac{1}{R_e b_1}\right)\left(\frac{-1}{c}\right)\Bigg\{(-iq)\left(1+\frac{1}{3}\alpha k^2\right)\left[e^{ik(x)}-R_1e^{-ik(x)}\right]\left(-\frac{1}{m_j}\sin\left(m_j(1-d)\right)\right)$$

$$+(-iq)(\alpha k^2)\Big[e^{ik(x)}$$

$$-R_1e^{-ik(x)}\Big]\left(\frac{\left((d^2-2d){m_j}^2-2\right)\sin\left(m_j(d-1)\right)+(2d-2)m_j\cos\left(m_j(d-1)\right)}{2\left(m_j\right)^3}\right.$$

$$\left.+\frac{(-2b+2)\cos\left(m_j(b-1)\right)}{2\left(m_j\right)^2}\right)\Bigg\}e^{-ikct}$$

$$=\left(\frac{1}{R_e b_1}\right)\left(\frac{-1}{c}\right)\Big\{(-iq)\left(1+\frac{1}{3}\alpha k^2\right)\left[e^{ik(x)}-R_1e^{-ik(x)}\right]C_b$$

$$+(-iq)(\alpha k^2)\left[e^{ik(x)}-R_1e^{-ik(x)}\right]C_c\Big\}e^{-ikct}, \qquad \text{(B-17)}$$

where

$$C_a=\frac{(1-b)\cos(j\pi)}{(m_j)^2}, \qquad \text{(B-18)}$$

$$C_b=-\frac{1}{m_j}\sin\left(m_j(1-d)\right), and \qquad \text{(B-19)}$$

$$C_c = \frac{\left((d^2 - 2d){m_j}^2 - 2\right) sin\left(m_j(d-1)\right) + (2d-2)m_j\, cos\left(m_j(d-1)\right)}{2\left(m_j\right)^3}$$

$$+ \frac{(-2b+2)\, cos\left(m_j(b-1)\right)}{2\left(m_j\right)^2}. \tag{B-20}$$

$$\int_{-1}^{-b} \phi_2^p \, cos\left(m_j(z+1)\right)\, dz$$

$$= \int_{-1}^{-b} \{\sum_{j=1}^{\infty} \left(A_j\, cosh\left(m_j(x)\right) + B_j\, sinh\left(m_j(x)\right)\right) cos\left(m_j(z+1)\right)$$

$$+ C(x) + D\} e^{-ikct} cos\left(m_j(z+1)\right)\, dz$$

$$= \left\{\left(A_j\, cosh\left(m_j(x)\right)\right.\right.$$

$$\left.\left. + B_j\, sinh\left(m_j(x)\right)\right) \frac{sin\left(2m_j(1-b)\right) + 2m_j(1-b)}{4m_j}\right\} e^{-ikct}$$

$$= \left(A_j\, cosh\left(m_j(x)\right) + B_j\, sinh\left(m_j(x)\right)\right) \frac{(1-b)}{2} e^{-ikct}. \tag{B-21}$$

By substituting these equations back into Eqn. (B-15), we have

$$C_a(-iq)\alpha k^2 [e^{ik(x)} + R_1 e^{-ik(x)}]\} e^{-ikct}$$

$$+ \left(\frac{1}{R_e b_1}\right)\left(\frac{-1}{c}\right)\left\{(-iq)\left(1 + \frac{1}{3}\alpha k^2\right)\left[e^{ik(x)} - R_1 e^{-ik(x)}\right] C_b\right.$$

$$\left. + (-iq)(\alpha k^2)\left[e^{ik(x)} - R_1 e^{-ik(x)}\right] C_c\right\} e^{-ikct}$$

$$= (A_j\, cosh\left(m_j(x)\right) + B_j\, sinh\left(m_j(x)\right)) \frac{(1-b)}{2} e^{-ikct}. \tag{B-22}$$

By canceling e^{-ikct}, we have

$$
\begin{aligned}
&C_a(-iq)\alpha k^2[e^{ik(x)} + R_1 e^{-ik(x)}]\}\\
&\qquad + \left(\frac{1}{R_e b_1}\right)\left(\frac{-1}{c}\right)\left\{(-iq)\left(1+\frac{1}{3}\alpha k^2\right)\left[e^{ik(x)} - R_1 e^{-ik(x)}\right]C_b\right.\\
&\qquad \left. + (-iq)(\alpha k^2)\left[e^{ik(x)} - R_1 e^{-ik(x)}\right]C_c\right\}\\
&\qquad = (A_j\, cosh\left(m_j(x)\right) + B_j\, sinh\left(m_j(x)\right))\frac{(1-b)}{2}. \qquad \text{(B-23)}
\end{aligned}
$$

Applying the similar approach for the interface of region 2 and region 3, we have

$$
\begin{aligned}
&\int_{-1}^{-d} \phi_3^p\ cos\left(m_j(z+1)\right)dz + \int_{-d}^{-b} \hat{\phi}_2\, cos\left(m_j(z+1)\right)dz\\
&\qquad = \int_{-1}^{-b} \phi_2^p\, cos\left(m_j(z+1)\right)\ dz. \qquad \text{(B-24)}
\end{aligned}
$$

Since

$$\frac{\partial\hat{\phi}_2}{\partial t} = \frac{\partial\phi_3^p}{\partial t} - \frac{\partial\phi_3^p}{\partial x}\left(\frac{1}{R_e b_2}\right), \qquad \text{(B-25)}$$

similarly, we have

$$\hat{\phi}_2 = \phi_3^p - \left(\frac{1}{R_e b_2}\right)\left(\frac{-1}{c}\right)\phi_3^p. \qquad \text{(B-26)}$$

By substituting Eqn. (B-26) back into Eqn. (B-24), we have

$$\int_{-1}^{-d} \phi_3^p \ cos\left(m_j(z+1)\right) dz + \int_{-d}^{-b} (\phi_3^p - \left(\frac{1}{R_e b_2}\right)\left(\frac{-1}{c}\right)\phi_3^p) \, cos\left(m_j(z+1)\right) dz$$

$$= \int_{-1}^{-b} \phi_2^p \, cos\left(m_j(z+1)\right) \ dz, \qquad \text{(B-27)}$$

so that

$$\int_{-1}^{-b} \phi_3^p \ cos\left(m_j(z+1)\right) dz$$

$$- \int_{-d}^{-b} \left(\frac{1}{R_e b_2}\right)\left(\frac{-1}{c}\right)\phi_3^p \, cos\left(m_j(z+1)\right) dz$$

$$= \int_{-1}^{-b} \phi_2^p \, cos\left(m_j(z+1)\right) \ dz. \qquad \text{(B-28)}$$

Each term in the Eqn. (B-28) can be expressed as

$$\int_{-1}^{-b} \phi_3^p \ cos\left(m_j(z+1)\right) dz$$

$$= \int_{-1}^{-b} \{(-iq)[T_1 e^{ik(x)}]$$

$$+ \alpha k^2 \left(\frac{1}{3} + z + \frac{z^2}{2}\right)(-iq)[T_1 e^{ik(x)}]\} e^{-ikct} \ cos\left(m_j(z+1)\right) dz$$

$$= \alpha k^2 \left(\frac{(1-b)cos(j\pi)}{(m_j)^2}\right)(-iq)[T_1 e^{ik(x)}]\} e^{-ikct}$$

$$= \alpha k^2 (C_a)(-iq)[T_1 e^{ik(x)}]\} e^{-ikct}, \qquad \text{(B-29)}$$

$$\int_{-d}^{-b}\left(\frac{1}{R_e b_2}\right)\left(\frac{-1}{c}\right)\phi_3^p \cos\left(m_j(z+1)\right)dz$$

$$=\int_{-d}^{-b}\left(\frac{1}{R_e b_2}\right)\left(\frac{-1}{c}\right)\{(-iq)[T_1 e^{ik(x)}]$$

$$+\alpha k^2\left(\frac{1}{3}+z+\frac{z^2}{2}\right)(-iq)[T_1 e^{ik(x)}]\}e^{-ikct}\cos\left(m_j(z+1)\right)dz$$

$$=\left(\frac{1}{R_e b_2}\right)\left(\frac{-1}{c}\right)\left\{(-iq)\left[T_1 e^{ik(x)}\right]\left(1+\frac{1}{3}\alpha k^2\right)\left(-\frac{1}{m_j}\sin\left(m_j(1-d)\right)\right)\right.$$

$$+\alpha k^2(-iq)\left(\frac{\left((d^2-2d){m_j}^2-2\right)\sin\left(m_j(d-1)\right)+(2d-2)m_j\cos\left(m_j(d-1)\right)}{2\left(m_j\right)^3}\right.$$

$$\left.\left.+\frac{(-2b+2)\cos\left(m_j(b-1)\right)}{2\left(m_j\right)^2}\right)\left[T_1 e^{ik(x)}\right]\right\}e^{-ikct}$$

$$=\left(\frac{1}{R_e b_2}\right)\left(\frac{-1}{c}\right)\left\{(-iq)\left[T_1 e^{ik(x)}\right]\left(1+\frac{1}{3}\alpha k^2\right)(C_b)\right.$$

$$\left.+\alpha k^2(-iq)(C_c)\left[T_1 e^{ik(x)}\right]\right\}e^{-ikct}, and \qquad \text{(B-30)}$$

$$\int_{-1}^{-b} \phi_2^p \cos\left(m_j(z+1)\right)\, dz$$

$$= \int_{-1}^{-b} \{\sum_{j=1}^{\infty} \left(A_j \cosh\left(m_j(x)\right) + B_j \sinh\left(m_j(x)\right)\right) \cos\left(m_j(z+1)\right)$$

$$+ C(x) + D\} e^{-ikct} \cos\left(m_j(z+1)\right)\, dz$$

$$= \left\{\left(A_j \cosh\left(m_j(x)\right)\right.\right.$$

$$\left.\left. + B_j \sinh\left(m_j(x)\right)\right) \frac{\sin\left(2m_j(1-b)\right) + 2m_j(1-b)}{4m_j}\right\} e^{-ikct}$$

$$= \left(A_j \cosh\left(m_j(x)\right) + B_j \sinh\left(m_j(x)\right)\right) \frac{(1-b)}{2} e^{-ikct}. \qquad \text{(B-31)}$$

By substituting these equations back into Eqn. (B-28), we have

$$\alpha k^2 (C_a)(-iq)[T_1 e^{ik(x)}]\} e^{-ikct}$$

$$- \left(\frac{1}{R_e b_2}\right)\left(\frac{-1}{c}\right)\left\{(-iq)\left[T_1 e^{ik(x)}\right]\left(1 + \frac{1}{3}\alpha k^2\right)(C_b)\right.$$

$$\left. + \alpha k^2 (-iq)(C_c)\left[T_1 e^{ik(x)}\right]\right\} e^{-ikct}$$

$$= (A_j \cosh\left(m_j(x)\right) + B_j \sinh\left(m_j(x)\right)) \frac{(1-b)}{2} e^{-ikct}. \qquad \text{(B-32)}$$

After canceling the e^{-ikct}, we can get

$$\alpha k^2(C_a)(-iq)[T_1e^{ik(x)}]\}e^{-ikct}$$

$$-\left(\frac{1}{R_eb_2}\right)\left(\frac{-1}{c}\right)\left\{(-iq)\left[T_1e^{ik(x)}\right]\left(1+\frac{1}{3}\alpha k^2\right)(C_b)\right.$$

$$\left.+\alpha k^2(-iq)(C_c)\left[T_1e^{ik(x)}\right]\right\}$$

$$=(A_j\,cosh\left(m_j(x)\right)+B_j\,sinh\left(m_j(x)\right))\frac{(1-b)}{2}. \qquad \text{(B-33)}$$

Since Eqn. (B-23) is at $x=-x_1$ and Eqn. (B-33) is at $x=x_1$, we can rewrite them into

$$C_a(-iq)\alpha k^2\left[e^{ik(-x_1)}+R_1e^{-ik(-x_1)}\right]$$

$$+\left(\frac{1}{R_eb_1}\right)\left(\frac{-1}{c}\right)\left\{(-iq)\left(1+\frac{1}{3}\alpha k^2\right)\left[e^{ik(-x_1)}-R_1e^{-ik(-x_1)}\right]C_b\right.$$

$$\left.+(-iq)(\alpha k^2)\left[e^{ik(-x_1)}-R_1e^{-ik(-x_1)}\right]C_c\right\}$$

$$=\left(A_j\,cosh\left(m_j(-x_1)\right)+B_j\,sinh\left(m_j(-x_1)\right)\right)\frac{(1-b)}{2}$$

$$=\left(A_j\,cosh\left(m_j(x_1)\right)-B_j\,sinh\left(m_j(x_1)\right)\right)\frac{(1-b)}{2}\ and \qquad \text{(B-34)}$$

$$\alpha k^2(C_a)(-iq)\left[T_1e^{ik(x_1)}\right]$$

$$-\left(\frac{1}{R_eb_2}\right)\left(\frac{-1}{c}\right)\left\{(-iq)\left[T_1e^{ik(x_1)}\right]\left(1+\frac{1}{3}\alpha k^2\right)(C_b)\right.$$

$$\left.+\alpha k^2(-iq)(C_c)\left[T_1e^{ik(x_1)}\right]\right\}$$

$$=\left(A_j\,cosh\left(m_j(x_1)\right)+B_j\,sinh\left(m_j(x_1)\right)\right)\frac{(1-b)}{2}. \qquad \text{(B-35)}$$

By solving these two equations, we can get A_j and B_j as

$$A_j = \frac{\{C_a(-iq)\alpha k^2 + G_1\left\{(-iq)\left(1+\frac{1}{3}\alpha k^2\right)C_b + (-iq)\left(\alpha k'^2\right)C_c\right\}\}[I_2]}{(1-b)\,cosh\left(m_j(x_1)\right)} + \frac{\{C_a(-iq)\alpha k^2 + G_1\left\{(-iq)\left(1+\frac{1}{3}\alpha k^2\right)(-C_b) + (-iq)(\alpha k^2)(-C_c)\right\}\}R_1[I_1]}{(1-b)\,cosh\left(m_j(x_1)\right)} + \frac{\{\alpha k^2(C_a)(-iq) - G_2\left\{(-iq)\left(1+\frac{1}{3}\alpha k^2\right)(C_b) + \alpha k^2(-iq)(C_c)\right\}\}T_1[I_3]}{(1-b)\,cosh\left(m_j(x_1)\right)}\ and \quad \text{(B-36)}$$

$$B_j = \frac{\{\alpha k^2(C_a)(-iq) - G_2\left\{(-iq)\left(1+\frac{1}{3}\alpha k^2\right)(C_b) + \alpha k^2(-iq)(C_c)\right\}\}T_1[I_3]}{(1-b)sinh\left(m_j(x_1)\right)} - \frac{\{C_a(-iq)\alpha k^2 + G_1\left\{(-iq)\left(1+\frac{1}{3}\alpha k^2\right)C_b + (-iq)(\alpha k^2)C_c\right\}\}I_2}{(1-b)sinh\left(m_j(x_1)\right)} - \frac{\left\{C_a(-iq)\alpha k^2 + G_1\left\{(-iq)\left(1+\frac{1}{3}\alpha k^2\right)(-C_b) + (-iq)(\alpha k^2)(-C_c)\right\}\right\}R_1 I_1}{(1-b)sinh\left(m_j(x_1)\right)}, \quad \text{(B-37)}$$

where

$$G_1 = \left(\frac{1}{R_e b_1}\right)\left(\frac{-1}{c}\right), \quad \text{(B-38)}$$

$$G_2 = \left(\frac{1}{R_e b_2}\right)\left(\frac{-1}{c}\right), \quad \text{(B-39)}$$

$$I_1 = I_3 = e^{ik(x_1)}, and \quad \text{(B-40)}$$

$$I_2 = e^{ik(-x_1)}. \quad \text{(B-41)}$$

To solve C and D, each of the terms in Eqn. (B-14) without the orthogonality property of eigenfunctions, $cos\left(k_j(z+1)\right)$, can be expressed as

$$\int_{-1}^{-b} \phi_1^p \, dz = \int_{-1}^{-b} \{(-iq)[e^{ik(x)} + R_1 e^{-ik(x)}] + \alpha k^2 \left(\frac{1}{3} + z + \frac{z^2}{2}\right)(-iq)[e^{ik(x)}$$

$$+ R_1 e^{-ik(x)}]\} e^{-ikct} \, dz$$

$$= \left\{(-iq)\left[e^{ik(x)} + R_1 e^{-ik(x)}\right](1-b)\right.$$

$$\left. + \alpha k^2 \left(-\frac{b^3 - 3b^2 + 2b}{6}\right)(-iq)\left[e^{ik(x)} + R_1 e^{-ik(x)}\right]\right\} e^{-ikct}, \qquad \text{(B-42)}$$

$$\int_{-d}^{-b} \left(\frac{1}{R_e b_1}\right)\left(\frac{-1}{c}\right) \tilde{\phi}_1 dz$$

$$= \left(\frac{1}{R_e b_1}\right)\left(\frac{-1}{c}\right) \int_{-d}^{-b} \{(-iq)[e^{ik(x)} - R_1 e^{-ik(x)}]$$

$$+ \alpha k^2 \left(\frac{1}{3} + z + \frac{z^2}{2}\right)(-iq)[e^{ik(x)} - R_1 e^{-ik(x)}]\} e^{-ikct} dz$$

$$= \left(\frac{1}{R_e b_1}\right)\left(\frac{-1}{c}\right)\left\{(-iq)\left[e^{ik(x)} - R_1 e^{-ik(x)}\right](d-b)\right.$$

$$+ \alpha k^2 \left(\frac{(d^3 - b^3) - 3(d^2 - b^2) + 2(d-b)}{6}\right)(-iq)\left[e^{ik(x)}\right.$$

$$\left.\left. - R_1 e^{-ik(x)}\right]\right\} e^{-ikct}, and \qquad \text{(B-43)}$$

$$\int_{-1}^{-b} \phi_2^p \, dz = \int_{-1}^{-b} \{\sum_{j=1}^{\infty} \left(A_j \, cosh\left(m_j(x)\right) + B_j \, sinh\left(m_j(x)\right)\right) cos\left(m_j(z+1)\right) + C(x)$$

$$+ D\} e^{-ikct} \, dz = \left(C(x)(1-b) + D(1-b)\right) e^{-ikct}. \qquad \text{(B-44)}$$

Therefore, we have

$$
\begin{aligned}
&\Bigg\{(-iq)\left[e^{ik(x)} + R_1 e^{-ik(x)}\right](1-b) \\
&\qquad + \alpha k^2\left(-\frac{b^3 - 3b^2 + 2b}{6}\right)(-iq)\left[e^{ik(x)} + R_1 e^{-ik(x)}\right]\Bigg\} e^{-ikct} \\
&\qquad + \left(\frac{1}{R_e b_1}\right)\left(\frac{-1}{c}\right)\Bigg\{(-iq)\left[e^{ik(x)} - R_1 e^{-ik(x)}\right](d-b) \\
&\qquad + \alpha k^2\left(\frac{(d^3 - b^3) - 3(d^2 - b^2) + 2(d-b)}{6}\right)(-iq)\Big[e^{ik(x)} \\
&\qquad - R_1 e^{-ik(x)}\Big]\Bigg\} e^{-ikct} = \big(C(x)(1-b) + D(1-b)\big)e^{-ikct}. \qquad \text{(B-45)}
\end{aligned}
$$

Since it is at $x = -x_1$, it can be rewritten as

$$
\begin{aligned}
&\Bigg\{(-iq)\left[e^{ik(-x_1)} + R_1 e^{-ik(-x_1)}\right](1-b) \\
&\qquad + \alpha k^2\left(-\frac{b^3 - 3b^2 + 2b}{6}\right)(-iq)\left[e^{ik(-x_1)} + R_1 e^{-ik(-x_1)}\right]\Bigg\} \\
&\qquad + \left(\frac{1}{R_e b_1}\right)\left(\frac{-1}{c}\right)\Bigg\{(-iq)\left[e^{ik(-x_1)} - R_1 e^{-ik(-x_1)}\right](d-b) \\
&\qquad + \alpha k^2\left(\frac{(d^3 - b^3) - 3(d^2 - b^2) + 2(d-b)}{6}\right)(-iq)\Big[e^{ik(-x_1)} \\
&\qquad - R_1 e^{-ik(-x_1)}\Big]\Bigg\} = C(-x_1)(1-b) + D(1-b). \qquad \text{(B-46)}
\end{aligned}
$$

Similarly, for the interface of region 2 and region 3, the terms can be expressed as

$$\int_{-1}^{-b} \phi_3^p \, dz = \int_{-1}^{-b} \{(-iq)[T_1 e^{ik(x)}] + \alpha k^2 \left(\frac{1}{3} + z + \frac{z^2}{2}\right)(-iq)[T_1 e^{ik(x)}]\} e^{-ikct} \, dz$$

$$= \Big\{(-iq)\big[T_1 e^{ik(x)}\big](1-b)$$

$$+ \alpha k^2 \left(-\frac{b^3 - 3b^2 + 2b}{6}\right)(-iq)\big[T_1 e^{ik(x)}\big]\Big\} e^{-ikct}, \tag{B-47}$$

$$\int_{-d}^{-b} \left(\frac{1}{R_e b_2}\right)\left(\frac{-1}{c}\right) \phi_3^p dz$$

$$= \left(\frac{1}{R_e b_2}\right)\left(\frac{-1}{c}\right) \int_{-d}^{-b} \{(-iq)[T_1 e^{ik(x)}] + \alpha k^2 \left(\frac{1}{3} + z + \frac{z^2}{2}\right)(-iq)[T_1 e^{ik(x)}]\} e^{-ikct} dz$$

$$= \left(\frac{1}{R_e b_2}\right)\left(\frac{-1}{c}\right) \Big\{(-iq)\big[T_1 e^{ik(x)}\big](d-b)$$

$$+ \alpha k^2 \left(\frac{(d^3 - b^3) - 3(d^2 - b^2) + 2(d-b)}{6}\right)(-iq)\big[T_1 e^{ik(x)}\big]\Big\} e^{-ikct}, and \tag{B-48}$$

$$\int_{-1}^{-b} \phi_2^p \, dz \; = \int_{-1}^{-b} \{\sum_{j=1}^{\infty} \Big(A_j \cosh\big(m_j(x)\big) + B_j \sinh\big(m_j(x)\big)\Big) \cos\big(m_j(z+1)\big) + C(x)$$

$$+ D\} e^{-ikct} \, dz \; = \big(C(x)(1-b) + D(1-b)\big) e^{-ikct}. \tag{B-49}$$

By substituting these equations back, we have

$$\left(\frac{1}{R_e b_2}\right)\left(\frac{-1}{c}\right) \Big\{(-iq)\big[T_1 e^{ik(x)}\big](d-b)$$

$$+ \alpha k^2 \left(\frac{(d^3 - b^3) - 3(d^2 - b^2) + 2(d-b)}{6}\right)(-iq)\big[T_1 e^{ik(x)}\big]\Big\} e^{-ikct}$$

$$= \big(C(x)(1-b) + D(1-b)\big) e^{-ikct}, \tag{B-50}$$

and by canceling e^{-ikct} and $x = x_1$, we have

$$\left\{(-iq)\left[T_1 e^{ik(x_1)}\right](1-b) + \alpha k^2 \left(-\frac{b^3 - 3b^2 + 2b}{6}\right)(-iq)\left[T_1 e^{ik(x_1)}\right]\right\}$$

$$-\left(\frac{1}{R_e b_2}\right)\left(\frac{-1}{c}\right)\left\{(-iq)\left[T_1 e^{ik(x_1)}\right](d-b)\right.$$

$$\left.+\alpha k^2 \left(\frac{(d^3 - b^3) - 3(d^2 - b^2) + 2(d-b)}{6}\right)(-iq)\left[T_1 e^{ik(x_1)}\right]\right\}$$

$$= C(x_1)(1-b) + D(1-b). \tag{B-51}$$

Solving Eqns. (B-46) and (B-51), we can get C and D as

$$-C(x_1)(1-b) - D(1-b) + \big(C(-x_1)(1-b) + D(1-b)\big) = -2Cx_1(1-b)$$

$$= \left\{(-iq)\left[e^{ik(-x_1)} + R_1 e^{-ik(-x_1)}\right](1-b)\right.$$

$$\left.+\alpha k^2 \left(-\frac{b^3 - 3b^2 + 2b}{6}\right)(-iq)\left[e^{ik(-x_1)} + R_1 e^{-ik(-x_1)}\right]\right\}$$

$$+\left(\frac{1}{R_e b_1}\right)\left(\frac{-1}{c}\right)\left\{(-iq)\left[e^{ik(-x_1)} - R_1 e^{-ik(-x_1)}\right](d-b)\right.$$

$$\left.+\alpha k^2 \left(\frac{(d^3 - b^3) - 3(d^2 - b^2) + 2(d-b)}{6}\right)(-iq)\left[e^{ik(-x_1)} - R_1 e^{-ik(-x_1)}\right]\right\}$$

$$-\left\{\left\{(-iq)\left[T_1 e^{ik(x_1)}\right](1-b) + \alpha k^2 \left(-\frac{b^3 - 3b^2 + 2b}{6}\right)(-iq)\left[T_1 e^{ik(x_1)}\right]\right\}\right.$$

$$-\left(\frac{1}{R_e b_2}\right)\left(\frac{-1}{c}\right)\left\{(-iq)\left[T_1 e^{ik(x_1)}\right](d-b)\right.$$

$$\left.\left.+\alpha k^2 \left(\frac{(d^3 - b^3) - 3(d^2 - b^2) + 2(d-b)}{6}\right)(-iq)\left[T_1 e^{ik(x_1)}\right]\right\}\right\} \; and \tag{B-52}$$

$$C(x_1)(1-b) + D(1-b) + \big(C(-x_1)(1-b) + D(1-b)\big) = 2D(1-b)$$

$$= \Bigg\{(-iq)\big[e^{ik(-x_1)} + R_1 e^{-ik(-x_1)}\big](1-b)$$

$$+ \alpha k^2 \left(-\frac{b^3 - 3b^2 + 2b}{6}\right)(-iq)\big[e^{ik(-x_1)} + R_1 e^{-ik(-x_1)}\big]\Bigg\}$$

$$+ \left(\frac{1}{R_e b_1}\right)\left(\frac{-1}{c}\right)\Bigg\{(-iq)\big[e^{ik(-x_1)} - R_1 e^{-ik(-x_1)}\big](d-b)$$

$$+ \alpha k^2 \left(\frac{(d^3 - b^3) - 3(d^2 - b^2) + 2(d-b)}{6}\right)(-iq)\big[e^{ik(-x_1)} - R_1 e^{-ik(-x_1)}\big]\Bigg\}$$

$$+ \Bigg\{\Bigg\{(-iq)\big[T_1 e^{ik(x_1)}\big](1-b) + \alpha k^2 \left(-\frac{b^3 - 3b^2 + 2b}{6}\right)(-iq)\big[T_1 e^{ik(x_1)}\big]\Bigg\}$$

$$- \left(\frac{1}{R_e b_2}\right)\left(\frac{-1}{c}\right)\Bigg\{(-iq)\big[T_1 e^{ik(x_1)}\big](d-b)$$

$$+ \alpha k^2 \left(\frac{(d^3 - b^3) - 3(d^2 - b^2) + 2(d-b)}{6}\right)(-iq)\big[T_1 e^{ik(x_1)}\big]\Bigg\}\Bigg\}. \qquad \text{(B-53)}$$

So that C and D can be written as

$$C = \frac{1}{-2x_1(1-b)}\{\{(-iq)[I_2 + R_1 I_1 - T_1 I_3](1-b) + C_1(-iq)[I_2 + R_1 I_1 - T_1 I_3]\}$$

$$+ \{(-iq)[G_1(I_2 - R_1 I_1) + G_2 T_1 I_3](d-b)$$

$$+ C_2(-iq)[G_1(I_2 - R_1 I_1) + G_2 T_1 I_3]\}\} \; and \qquad \text{(B-54)}$$

$$D = \frac{1}{2(1-b)}\{\{(-iq)[I_2 + R_1 I_1 + T_1 I_3](1-b) + C_1(-iq)[I_2 + R_1 I_1 + T_1 I_3]\}$$

$$+ \{(-iq)[G_1(I_2 - R_1 I_1) - G_2 T_1 I_3](d-b)$$

$$+ C_2(-iq)[G_1(I_2 - R_1 I_1) - G_2 T_1 I_3]\}\}. \qquad \text{(B-55)}$$

where

$$C_1 = \alpha k^2 \left(-\frac{b^3 - 3b^2 + 2b}{6}\right) \ and \tag{B-56}$$

$$C_2 = \alpha k^2 \left(\frac{(d^3 - b^3) - 3(d^2 - b^2) + 2(d - b)}{6}\right). \tag{B-57}$$

In order to solve R_1 and T_1, we have the condition on the interface of region 1 and 3 as

$$\int_{-1}^{-0} \frac{\partial \phi_1^p}{\partial x}\, dz = \int_{-1}^{-b} \frac{\partial \phi_2^p}{\partial x}\, dz. \tag{B-58}$$

For each term in the equation above, we have

$$\int_{-1}^{-0} \frac{\partial \phi_1^p}{\partial x}\, dz = \int_{-1}^{-0} \{(-iq)[(ik)e^{ik(x)} - (ik)R_1 e^{-ik(x)}]$$

$$+ \alpha k^2 \left(\frac{1}{3} + z + \frac{z^2}{2}\right)(-iq)[(ik)e^{ik(x)} - (ik)R_1 e^{-ik(x)}]\} e^{-ikct}\, dz$$

$$= (-iq)\left[(ik)e^{ik(-x_1)} - (ik)R_1 e^{-ik(-x_1)}\right] e^{-ikct}$$

$$= (-iq)[(ik)I_2 - (ik)R_1 I_1] e^{-ikct} \ and \tag{B-59}$$

$$\int_{-1}^{-b} \frac{\partial \phi_2^p}{\partial x}\, dz = C(1 - b)$$

$$= \frac{1}{-2x_1}\big\{\{(-iq)[I_2 + R_1 I_1 - T_1 I_3](1 - b) + C_1(-iq)[I_2 + R_1 I_1 - T_1 I_3]\}$$

$$+ \{(-iq)[G_1(I_2 - R_1 I_1) + G_2 T_1 I_3](d - b)$$

$$+ C_2(-iq)[G_1(I_2 - R_1 I_1) + G_2 T_1 I_3]\}\big\} e^{-ikct}. \tag{B-60}$$

So that, we can get

$$(ik)I_2 - (ik)R_1I_1$$

$$= \frac{1}{-2x_1}\left\{\{[I_2 + R_1I_1 - T_1I_3](1-b) + C_1[I_2 + R_1I_1 - T_1I_3]\}\right.$$

$$+ \{[G_1(I_2 - R_1I_1) + G_2T_1I_3](d-b)$$

$$\left.+ C_2[G_1(I_2 - R_1I_1) + G_2T_1I_3]\}\right\}. \tag{B-61}$$

Similarly, for the interface of region 2 and 3, we have

$$\int_{-1}^{-0} \frac{\partial \phi_3^p}{\partial x}\, dz = \int_{-1}^{-0} \left\{(-iq)\left[(ik)T_1e^{ik(x)}\right]\right.$$

$$\left. + \alpha k^2\left(\frac{1}{3} + z + \frac{z^2}{2}\right)(-iq)\left[(ik)T_1e^{ik(x)}\right]\right\} e^{-ikct}\, dz$$

$$= (-iq)(ik)\left[T_1e^{ik(x)}\right]e^{-ikct} = (-iq)(ik)[T_1I_3]e^{-ikct} \; and \tag{B-62}$$

$$\int_{-1}^{-b} \frac{\partial \phi_2^p}{\partial x}\, dz = C(1-b)$$

$$= \frac{1}{-2x_1}\left\{\{(-iq)[I_2 + R_1I_1 - T_1I_3](1-b) + C_1(-iq)[I_2 + R_1I_1 - T_1I_3]\}\right.$$

$$+ \{(-iq)[G_1(I_2 - R_1I_1) + G_2T_1I_3](d-b)$$

$$\left.+ C_2(-iq)[G_1(I_2 - R_1I_1) + G_2T_1I_3]\}\right\}e^{-ikct}. \tag{B-63}$$

So that, we can get

$$(ik)[T_1I_3] = \frac{1}{-2x_1}\left\{\{[I_2 + R_1I_1 - T_1I_3](1-b) + C_1[I_2 + R_1I_1 - T_1I_3]\}\right.$$

$$+ \{[G_1(I_2 - R_1I_1) + G_2T_1I_3](d-b)$$

$$\left.+ C_2[G_1(I_2 - R_1I_1) + G_2T_1I_3]\}\right\}. \tag{B-64}$$

Combining Eqns. (B-61) and (B-64), we have

$$T_1 I_3 = I_2 - R_1 I_1. \tag{B-65}$$

So, T_1 can be written as a function of R_0

$$T_1 = \frac{I_2}{I_3} - \frac{R_1 I_1}{I_3}. \tag{B-66}$$

Substituting Eqn. (B-66) back into Eqn. (B-61), we can get

$$\begin{aligned}
&(ik)I_2 - (ik)R_1 I_1 \\
&\qquad = \frac{1}{-2x_1}\Big\{\{[I_2 + R_1 I_1 - (I_2 - R_1 I_1)](1-b) \\
&\qquad + C_1[I_2 + R_1 I_1 - (I_2 - R_1 I_1)]\} \\
&\qquad + \{[G_1(I_2 - R_1 I_1) + G_2(I_2 - R_1 I_1)](d-b) \\
&\qquad + C_2[G_1(I_2 - R_1 I_1) + G_2(I_2 - R_1 I_1)]\}\Big\}.
\end{aligned} \tag{B-67}$$

Rearrange the equation, we have

$$\begin{aligned}
&(ik)I_2 - (ik)R_1 I_1 \\
&\qquad = \frac{1}{-2x_1}\Big\{\{[2R_1 I_1](1-b) + C_1[2R_1 I_1]\} \\
&\qquad + \{[(G_1 + G_2)I_2 - (G_1 + G_2)R_1 I_1](d-b) \\
&\qquad + C_2[(G_1 + G_2)I_2 - (G_1 + G_2)R_1 I_1]\}\Big\}.
\end{aligned} \tag{B-68}$$

So that

$$\begin{aligned}\{(ik)R_1I_12x_1 - [2R_1I_1](1-b) + C_1[2R_1I_1]\\ + \{(G_1+G_2)R_1I_1(d-b) + (G_1+G_2)R_1I_1C_2\}\}\\ = 2x_1(ik)I_2 + (G_1+G_2)I_2(d-b) + (G_1+G_2)I_2C_2. \qquad \text{(B-69)}\end{aligned}$$

Taking R_1 out on the left, we have

$$\begin{aligned}\{(ik)I_12x_1 - [2I_1](K_1) + \{(G_1+G_2)I_1(K_2)\}\}R_1\\ = 2x_1(ik)I_2 + (G_1+G_2)I_2(K_2), \qquad \text{(B-70)}\end{aligned}$$

where

$$K_1 = 1 - b + C_1 \; and \qquad \text{(B-71)}$$

$$K_2 = d - b + C_2. \qquad \text{(B-72)}$$

Finally, we can solve R_1 as

$$\mathrm{R_1} = \frac{2\mathrm{x_1(ik)I_2} + (\mathrm{G_1}+\mathrm{G_2})\mathrm{I_2(K_2)}}{\{\mathrm{(ik)I_1 2x_1} - [2\mathrm{I_1}](\mathrm{K_1}) + \{(\mathrm{G_1}+\mathrm{G_2})\mathrm{I_1(K_2)}\}\}}. \qquad \text{(B-73)}$$